AD-A057 139 CALIFORNIA UNIV LIVERMORE LAWRENCE LIVERMORE LAB F/G 6/6
ANNUAL REPORT OF LAWRENCE LIVERMORE LABORATORY TO THE HIGH ALTI--ETC(U)
MAY 78 F M LUTHER DOT-FA76WA1-653

UNCLASSIFIED FAA-EQ-78-09 NL

1 OF 2
AD A057 139

LEVEL II

Report No. FAA-EQ-78-09

11 NW

ANNUAL REPORT OF LAWRENCE LIVERMORE LABORATORY TO THE HIGH ALTITUDE POLLUTION PROGRAM- 1977

Frederick M. Luther,
Principal Investigator

MAY 1978

Annual Report

Prepared for

HIGH ALTITUDE POLLUTION PROGRAM

U.S. DEPARTMENT OF TRANSPORTATION
FEDERAL AVIATION ADMINISTRATION
Office of Environmental Quality
Washington, D.C. 20591

Technical Report Documentation Page

1. Report No.	2. Government Accession No.	3. Recipient's Catalog No.
FAA-EQ-78-09		

4. Title and Subtitle
Annual Report of Lawrence Livermore Laboratory to the High Altitude Pollution Program - 1977

5. Report Date
May 1978

6. Performing Organization Code

8. Performing Organization Report No.

7. Author(s)
Frederick M. Luther, Principal Investigator

9. Performing Organization Name and Address
Lawrence Livermore Laboratory
University of California
Livermore, California 94550

92 p.

10. Work Unit No. (TRAIS)

11. Contract or Grant No.
DOT-FA76WA1-653 new

13. Type of Report and Period Covered
Annual Report

12. Sponsoring Agency Name and Address
Department of Transportation
Federal Aviation Administration
High Altitude Pollution Program
Washington, D.C. 20591

14. Sponsoring Agency Code

15. Supplementary Notes

NO sub X

16. Abstract

The Lawrence Livermore Laboratory's one-dimensional chemical kinetics-transport model was extended to include full diurnal averaging and used to re-examine the effects of NO_x injections and other perturbations on ozone. The model was also used to test the sensitivity of species concentrations to atmospheric multiple scattering and to changes in stratospheric water vapor.

Radiative transfer calculations were made to study the effect of receiver orientation on erythemal dose.

A description of the processing, archiving, and analysis of the Block 5-D satellite multifilter radiometer sensor data on total ozone is given.

17. Key Words	18. Distribution Statement
Ozone Perturbations, Total Ozone, NO_x Injections, Stratospheric Model, Erythema Dose, Anthropogenic Activities and Ozone.	Available to the public through National Technical Information Service, Springfield, Virginia 22161

19. Security Classif. (of this report)	20. Security Classif. (of this page)	21. No. of Pages	22. Price
UNCLASSIFIED	UNCLASSIFIED	98	

Form DOT F 1700.7 (8-72) Reproduction of completed page authorized

page 2

390 999 LB

PREFACE

Since July 1, 1975, Lawrence Livermore Laboratory (LLL) has been participating in the High Altitude Pollution Program sponsored by the U.S. Department of Transportation's Federal Aviation Administration. This report describes the major accomplishments and significant findings during the fiscal year ending September 30, 1977, for work performed at LLL under Reimbursable Agreement DOT-FA76WAI-653. There are two major research areas covered by this agreement: (1) numerical modeling of the atmospheric response to stratospheric perturbations, and (2) the processing, archiving, and analysis of satellite ozone data. Each of these research areas has been divided into a number of subtasks, and the successful accomplishment of these subtasks has required contributions and cooperation from many participants. The work reported here should be considered the collective effort of all those listed below.

Scientific Administration
Joseph B. Knox, Division Leader
Frederick M. Luther

Numerical Modeling
Frederick M. Luther, Principal Investigator
James E. Burt
Julius S. Chang
William H. Duewer
Hugh W. Ellsaesser
Joyce E. Penner
Raymond L. Tarp
Donald J. Wuebbles

Satellite Ozone Data Analysis
James E. Lovill, Principal Investigator
James S. Ellis
John-Gilbert Huebel
John A. Korver
Freda A. Phelps
Thomas J. Sullivan
Patrick P. Weidhaas
Roger L. Weichel

CONTENTS

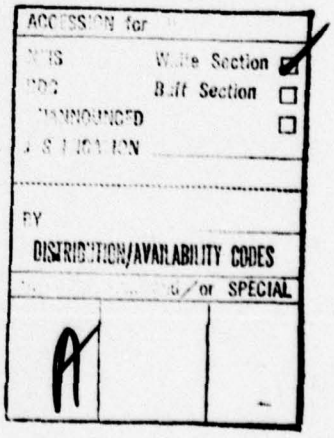

ANNUAL REPORT OF LAWRENCE LIVERMORE LABORATORY TO THE HIGH ALTITUDE POLLUTION PROGRAM—1977

1. INTRODUCTION

The High Altitude Pollution Program (HAPP) was initiated by the Federal Aviation Administration to ensure that aircraft engine emissions in the stratosphere will not result in unacceptable effects on the biosphere. Lawrence Livermore Laboratory (LLL) has participated in HAPP since July 1975. The primary research emphasis at LLL is on numerical modeling of the atmospheric response to stratospheric perturbations. The modeling effort at LLL covers four major research areas: photochemical kinetics, coupled kinetics and transport, radiative transfer, and meteorological analysis.

A fundamental tool in the LLL effort has been the one-dimensional transport-kinetics model. This model, which includes as complete a set of the important chemical and photochemical reactions as is feasible, is designed for time-dependent perturbation and sensitivity studies. The model includes 28 chemical species and 83 chemical and photochemical reactions. Species concentrations are computed at 44 levels in the atmosphere, extending from the ground to an altitude of 55 km. The model uses an accurate numerical method for solving stiff systems of differential equations. Vertical transport is parameterized using a one-dimensional diffusion formulation which describes hemispheric-average net vertical transport by an altitude-dependent diffusion coefficient. The model can include temperature coupling between changes in composition and reaction rate coefficients.

During the past year we improved this one-dimensional model by adding multiple scattering effects to the photodissociation rate calculation and by developing a more accurate method for incorporating diurnal averaging. We also directed considerable attention to the problem of evaluating the effect that changes in key chemical rate coefficients (as a result of new measurements) have on the model's sensitivity.

In addition to the one-dimensional model, we are in the process of developing a two-dimensional transport-kinetics model.

Support for model development is shared between HAPP and another project at LLL involving assessment of the chemical and climatic effects of atmospheric nuclear explosions. The latter project is funded by the Division of Military Application (DMA) of the Department of Energy. Although the same numerical models are used for both studies, the applications of the models are quite different. For example, the study of the climatic effect of nuclear explosions is primarily concerned with the time-dependent response of the atmosphere to pulse injections of NO_x, whereas the HAPP study is concerned with steady-state injections of NO_x. Work relating to model development or refinement benefits both projects, and consequently such work has been divided between the two projects. In this way each project's sponsor benefits from the participation of the other sponsor.

In August 1976, LLL's participation in HAPP was extended to include the processing, archiving, and analysis of global ozone data derived from a new series of Air Force meteorological-satellite sensors: the cross-track-scanning multifilter radiometer sensors. The Satellite Ozone Analysis Center (SOAC) was formed at LLL for the purpose of producing high-quality total-ozone data based on radiance measurements made with the new satellite sensors. The goal is to develop a capability for producing daily maps of total global ozone that can be made readily available to the scientific community. Our initial task is to demonstrate the feasibility of obtaining good ozone data from the satellite measurements. To do this we must first develop a satisfactory method for converting the satellite measurements to total ozone data. We plan to assess the quality of the resultant ozone data by comparing it in detail against corresponding Dobson ozone data obtained at selected stations in the world surface network of Dobson observatories. This feasibility study is scheduled for completion by June 1978.

In this annual report we describe LLL's major accomplishments and findings in HAPP studies since July 1, 1976. Earlier HAPP work is described in our First Annual Report (Luther et al. 1976). In the present report we emphasize the results in the atmospheric modeling area and limit our discussion

of the SOAC project to a description of the satellite multifilter radiometer sensor and a summary of the major tasks and objectives. The results of the SOAC feasibility study will be described in a later report.

2. RESEARCH ACTIVITIES: TRANSPORT KINETICS MODELING, PHOTOCHEMICAL KINETICS, AND RADIATIVE TRANSFER

Because of the complex nature of the work, most of the research tasks represent the combined effort of several scientists rather than individual contributions. It is not possible to separate the tasks by research area or scientific discipline because of the team approach. Most of the work described below has been or is in the process of being submitted for publication in technical journals.

2.1 A Fully Diurnal-Averaged Model of the Stratosphere

An outstanding question in the formulation of stratospheric chemical kinetics models is the proper averaging procedure for photochemical reaction rates involving diurnally varying chemical species. We have developed a fully diurnal-averaged model (DAM) that is consistent with our diurnal model (DM). By definition, these two models are consistent if the average tracer concentration from the diurnal-averaged model is the same as the diurnal average of the time-dependent solution from the diurnal model, and if all the corresponding averaged photochemical reaction rates are also identical. With the DM model we can calculate relevant details and compare the results with atmospheric measurements, and with the DAM model we can study the long-term atmospheric response to any perturbation. To study this latter class of problems with the DM model would not be economical. A computation procedure has been devised to assure the total consistency between these two models under all given conditions.

Model Description

We shall limit our discussion to the one-dimensional model since this is our current development. The procedure described is directly applicable to two-dimensional models. In a one-dimensional model of the stratosphere, the continuity equation for a specific trace species i is

$$\frac{\partial n_i}{\partial t} = -\frac{\partial}{\partial z} F(n_i) + P_i - L_i n_i + S_i \ , \qquad (1\text{-}1)$$

where n_i is the concentration of species i at time t and altitude z, $F(n_i)$ is the net vertical transport flux, P_i and $L_i n_i$ are the nonlinear chemical and photochemical production and loss rates, and S_i is the net production or loss rate due to any other process. If Eq. (1-1) is averaged over a time period T (here assumed to be 24 hours) which is very small compared to the time scale of the problem of interest, then

$$\frac{\partial \bar{n}_i}{\partial t} = -\frac{\partial}{\partial z}\overline{F(n_i)} + \overline{P_i} - \overline{L_i n_i} + \overline{S_i} \ . \qquad (1\text{-}2)$$

with the bar representing the following averaging process:

$$\bar{\phi} = \frac{1}{T} \int_{t-T/2}^{t+T/2} \phi(z,t')\, dt' \ .$$

The net vertical flux $F(n_i)$ is usually represented by

$$F(n_i) = -K_z \rho \frac{\partial}{\partial z}(n_i/\rho) \ ,$$

where K_z is the one-dimensional diffusion coefficient and ρ is the air density. Because K_z and ρ are independent of n_i in this approximation,* the net vertical flux $F(n_i)$ is a linear function of n_i. Furthermore, since K_z and ρ are assumed to be independent of time, i.e., to have no variation over the averaging period, we have

$$\overline{F(n_i)} = -K_z \rho \frac{\partial}{\partial z}(n_i/\rho) = -K_z \rho \frac{\partial}{\partial z}(\bar{n}_i/\rho) = F(\bar{n}_i) \ .$$

The source function S_i is usually well defined, hence $\bar{S}_i$ is easily computed. Equation (1-2) will be self-consistent if we can express the nonlinear expressions in $\bar{P}_i$ and $\overline{L_i n_i}$ in terms of $\bar{n}_i$. Fortunately, P_i and $L_i n_i$ are both linear sums of terms in the form of the typical two-body chemical kinetics reactions

*It is true that K_z may be derived from some known n_i distributions. But once it is derived the 1-D model assumes K_z as a fixed input variable.

$K_{ij}n_in_j$ or the photodissociation reaction J_in_i. The kinetics reaction rate coefficient K_{ij} may be a function of ρ but not of n_i or n_j. We define the diurnal weighting factors $\alpha_{ij}(z)$ and $\beta_i(z)$ by

$$\overline{K_{ij}n_in_j} = \alpha_{ij}\,\overline{K_{ij}}\,\bar{n}_i\,\bar{n}_j$$

and

$$\overline{J_in_i} = \beta_i\,\bar{J}_i\,\bar{n}_i \ .$$

Since K_{ij} is defined and is independent of time, we have

$$\alpha_{ij} = \overline{n_in_j} \,/\, \bar{n}_i\,\bar{n}_j$$

and

$$\beta_i = \overline{J_in_i} \,\Big/\, \bar{J}_i\,\bar{n}_i \ .$$

The computation of photodissociation rates has always been an expensive part of stratospheric model calculation, hence $\bar{J}_i$'s are expensive to evaluate in the DAM model. If we define β_i by

$$\beta_i = \overline{J_in_i} \,\Big/\, \left(J_i^{noon}\,\bar{n}_i\right) \ ,$$

then the computation in the DAM model will be significantly simplified. Using the results from a diurnal model we can determine $\overline{n_in_j}$, $\overline{J_in_i}$, $\bar{n}_i$, $\bar{n}_j$, J_i^{noon} so that α_{ij} and β_i can be obtained for every chemical and photochemical reaction in the model.

Using the α's and β's evaluated from the diurnal model, we can now write Eq. (1-2) in terms of the diurnal-averaged concentrations $\bar{n}_i$.

$$\frac{\partial \bar{n}_i}{\partial t} = -\nabla\cdot F(\bar{n}_i) + P(\alpha,\beta,\bar{n}_j,\bar{n}_k,K_{ij},J_j^{noon}) - L_i(\alpha,\beta,K_{mi},J_i^{noon},\bar{n}_m)\bar{n}_i + \bar{S}_i \ , \qquad (1\text{-}3)$$

where j, k, m are taken to represent species usually different from i. Formally, Eqs. (1-1) and (1-3) are identical in form except that every reaction rate in Eq. (1-3) is multiplied by an α or β factor determined from the solutions of Eq. (1-1).

The DM consists of Eq. (1-1) and its associated boundary and initial conditions. In this model the photodissociation rate coefficients vary throughout the day and vanish at night, and the local concentrations of many trace species such as $O(^1D)$, $O(^3P)$, NO, HO_2, Cl, ClO, HO, HO_2, etc. also have strong diurnal variations. For the DAM, i.e., Eq. (1-3) and the appropriate averaged initial and boundary conditions, all the photodissociation rates are constant on the diurnal time scale. All solutions of Eq. (1-3) represent averaged concentrations, i.e., they exhibit no diurnal variations. As such, solutions of Eq. (1-3) are not directly comparable to many atmospheric measurements. Most atmospheric data are taken under daytime conditions or during sunset or sunrise. For the present model it is quite simple to recover the time-dependent solution (DM model) from the averaged solution (DAM model). In the derivation of α's and β's a third set of variables γ_i's can be defined,

$$n_i^{noon} = \gamma_i\,\bar{n}_i \ .$$

Consequently, given any n_i from the DAM model, the corresponding noontime concentrations can be obtained through a simple multiplication, and this n_i^{noon} can be used as the input condition to the DM model to obtain the corresponding time-dependent diurnal solution.

In this formulation of the DAM model, it is implicitly assumed that the diurnal weighting factors are essentially constant even though the individual concentrations $\bar{n}_i$, hence the corresponding n_i, may vary considerably in magnitude. This assumption is valid if the functional shapes, i.e., the periodic functions representing the individual diurnal trace-species concentrations, are not sensitive to variations in the absolute magnitude of the concentrations. This simple fact can be directly verified with the DM model through the iteration procedure outlined in Fig. 1. Given initial estimates of α's and β's, we can use the DAM and DA models alternatively to assure that the α's and β's and $\bar{n}$'s are indeed consistent for any given atmospheric condition. Since this only involves a few diurnal cycles with the DM model at a judiciously chosen juncture of the calculation, the full iteration procedure is rather economical. In fact, in the present calculations involving the study of potential NO_x and ClX perturbations in the stratosphere, we have found that two or at most three iterations are sufficient to assure constancy of better than a few percent over most of the stratosphere for every trace species. The only exceptions are NO_3 and N_2O_5 above 40 km. At this altitude these species play such an insignificant role in stratospheric chemical balances that even major errors in their local concentrations have no significant impact. Purely for the sake of theoretical consistency, a study is still proceeding to understand the interesting diurnal behavior of N_2O_5 so that a

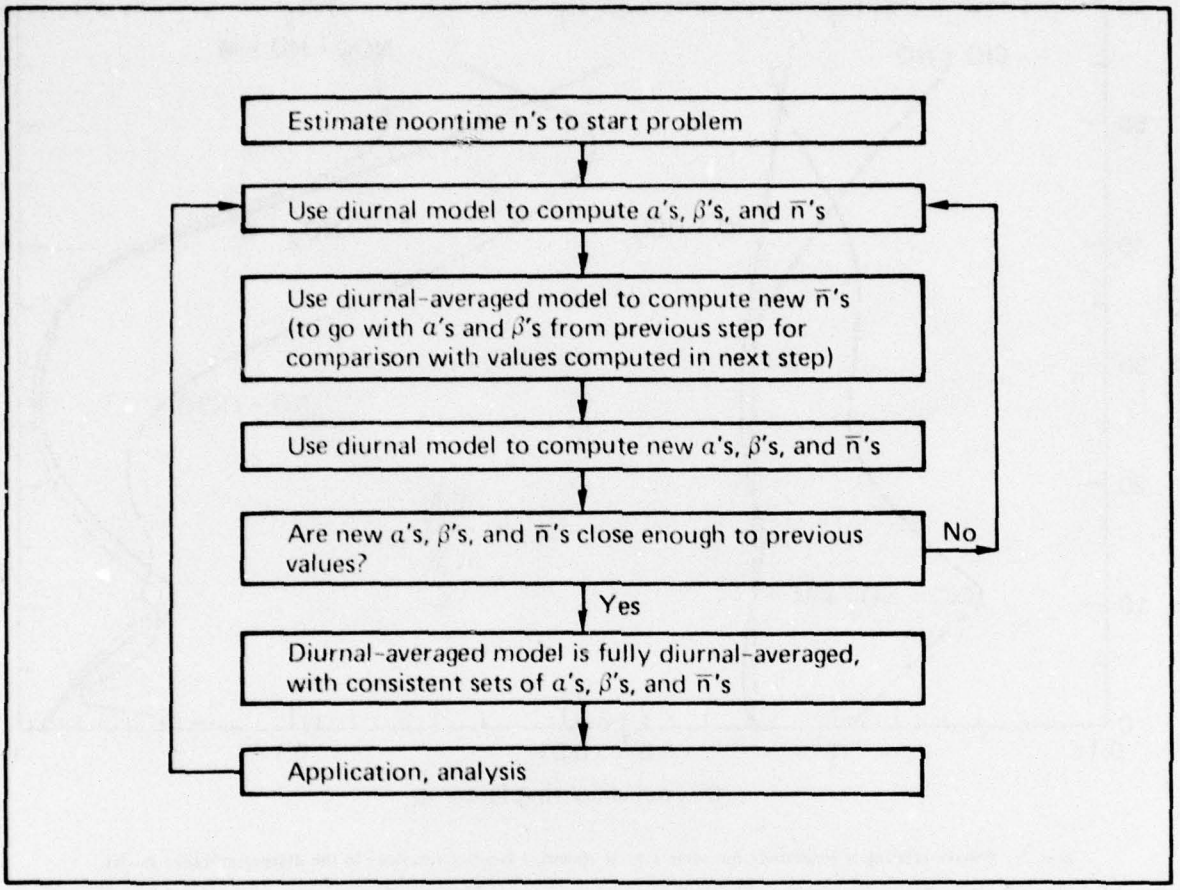

Figure 1 **Iteration procedure followed in the diurnal-averaged model (DAM).**

better averaging procedure can be defined specifically for N_2O_5 to reduce this local variation in diurnal weighting factors.

Discussion of Results

The α's and β's calculated from the diurnal model for some of the reactions in the model are shown in Figs. 2 and 3. These reactions were selected not because they are the more important ones in the model but because they represent some of the interesting features found in the derived multipliers for kinetic rates to be used in a diurnal-averaged model.

If a reaction involves a species that does not have a diurnal variation (i.e., the concentration is essentially constant over a 24-hour period), then the α's for that reaction will be 1.0. Therefore, if a reaction involves HNO_3 or HCl, for example, the weighting factor will not change the original reaction rate. However, if both reactants in a two-body reaction have diurnal variations, the value for α will be different from 1.0. For instance, for reactions involving two species whose diurnal variations are in phase and predominantly determined by photolysis (i.e., both having extremely small concentrations at night relative to their daytime values or vice versa), the expected values for α would be approximately 2. Thus, as shown in Fig. 2, the α's for the reactions ClO + NO and HO + HO_2 are both approximately 2 in the lower stratosphere. In the upper stratosphere ClO does not decrease much at night, and the value for α falls off sharply. Above 45 km ClO actually increases at night, hence it is out of phase with NO. On the other hand, the weighting factor for the $ClONO_2$ formation reaction ClO + NO_2 + M varies exactly in the opposite manner as compared with ClO + NO. In the lower stratosphere ClO and NO_2 are out of phase while above 45 km they are in phase (Fig. 4). For other important reactions such as NO_2 + O and NO_2 + HO + M, this variation in phase relation is again different. The diurnal variations of the reactants involved are very much out of phase both in the lower and upper stratosphere. These few examples show quite clearly

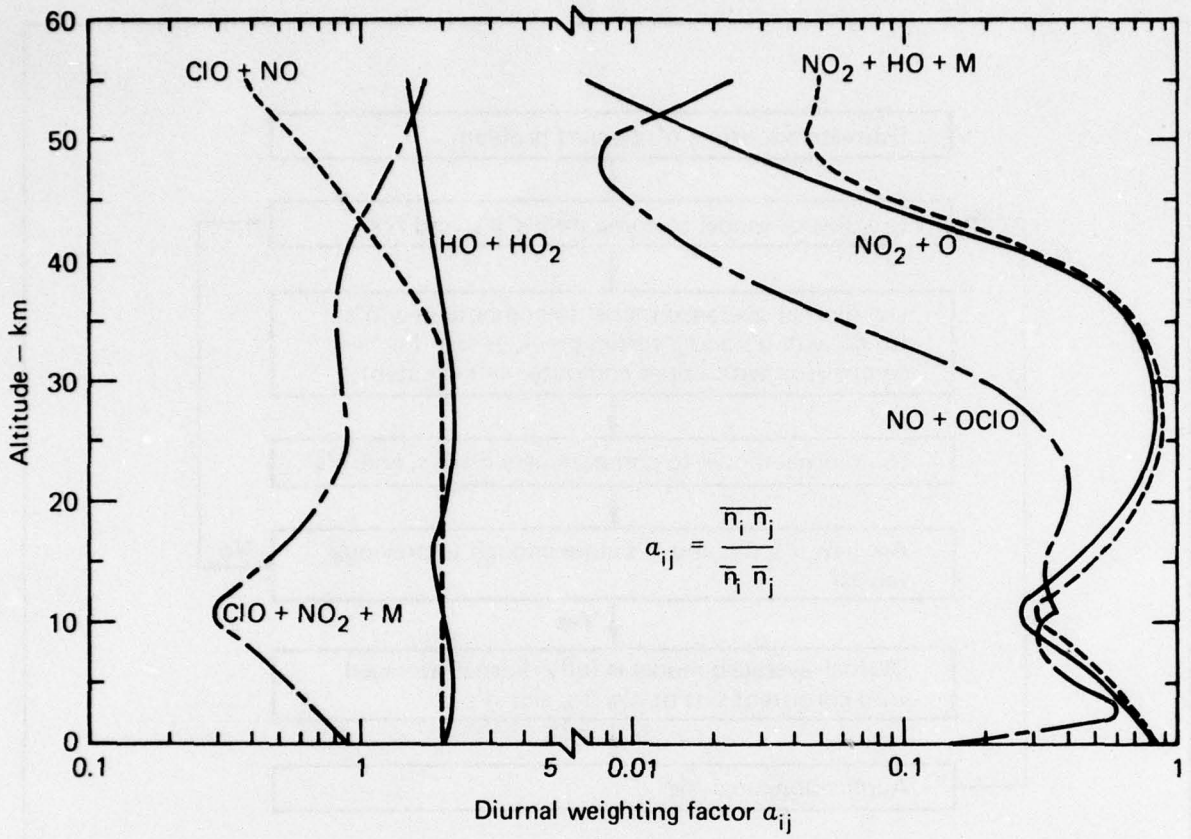

Figure 2. Curves relating α to altitude for some typical chemical kinetics reactions in the diurnal-averaged model.

that although the phase relationship in diurnal variations can be used as a qualitative guide in appreciating the diurnal effect on net reaction rates, it is by no means adequate. Due to the complexity of the chemical system only detailed calculations such as are used in our current procedure can provide the proper balanced evaluation. It is to be noted that when diurnally averaged concentrations are used in the rate expressions, the weighting factors (or correction factors) can have a very large effect on some of the reaction rate coefficients, increasing them by more than a factor of 2 or decreasing them by several orders of magnitude.

Figure 3 shows similar results for the photodissociation rate weighting factor β. Again there is a phase relationship between the variation of photodissociation rates and the individual trace-species concentrations. In fact from Fig. 3 it is quickly apparent that above 35 km photolysis is a dominant mechanism in determining the local concentrations of $ClONO_2$, NO_2, and N_2O_5, although this is not the case for HO_2. A strong out-of-phase relation with the photodissociation coefficient, J, shows that photolysis is the dominant loss mechanism. From this small sample of values for β, it is clear that no single averaged solar zenith angle or simple averaged photolysis rate coefficients can approximate the loss rates corresponding to even this small sample of photodissociation rates.

The computation procedure in the limit (i.e., infinite iteration) is actually the full diurnal model. Current experience indicates that a uniform local accuracy of better than a few percent deviation can be achieved with two or three iteration cycles. For such information as total ozone column or total NO_y, ClX, etc., one iteration would be sufficient.

2.2 Analysis of Selected Chemical Rate Data*

Our earlier work (Duewer et al. 1977b) identified several reactions for which variations in the rate coefficients have a significant effect on model sensitivity. Reduction of the uncertainties associated

*See Duewer et al. (1977c).

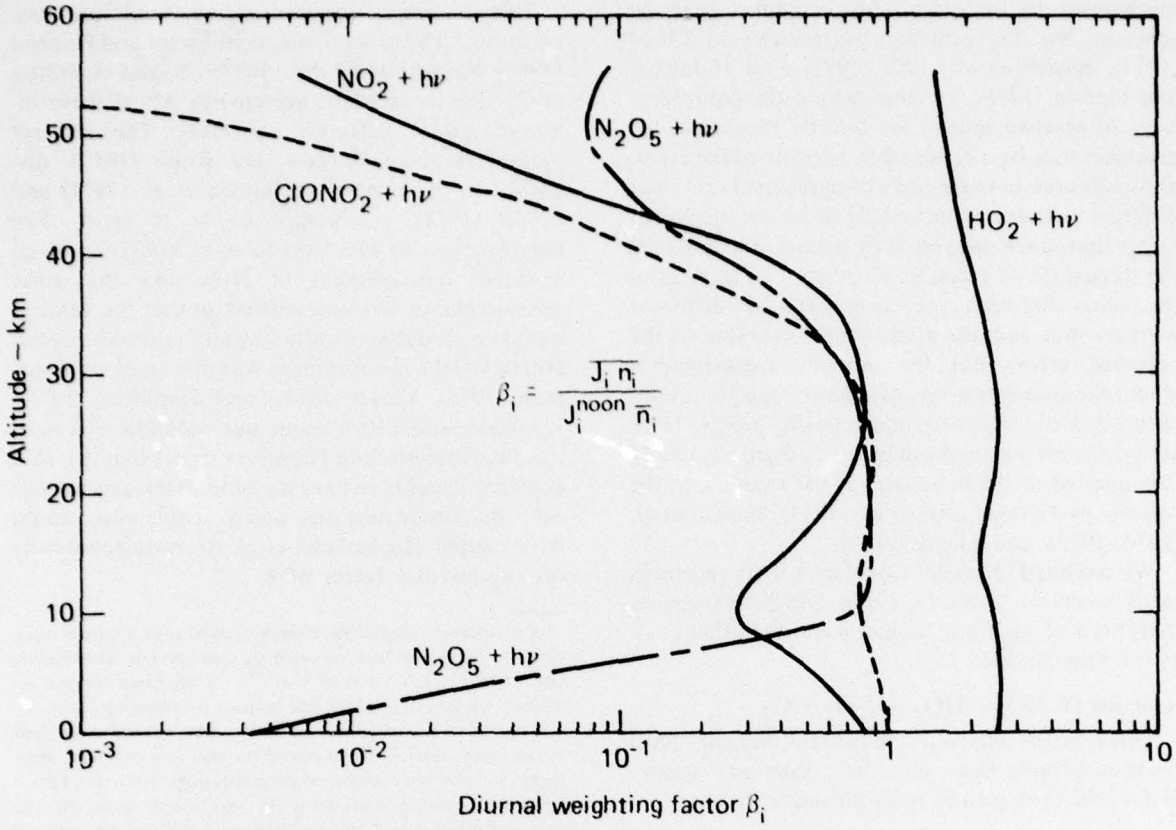

Figure 3. **Curves relating β to altitude for some typical photodissociation reactions in the diurnal-averaged model.**

with these rate coefficients would in turn reduce the uncertainty associated with the model assessments of the atmospheric response to stratospheric perturbations. For this reason we have carefully analyzed the chemical rate data for these reactions, taking into account recent laboratory measurements conducted at other laboratories. Our analyses for these reactions are given below.

In evaluating an experimental measurement, one normally takes the precision-based standard deviation of the measurement as a lower limit to the expected error. Historically, precision has often been a very unrealistic basis for estimating the experimental error in chemical rate data, especially when the measurements are indirect (that is, based on inferred concentrations using an assumed kinetic

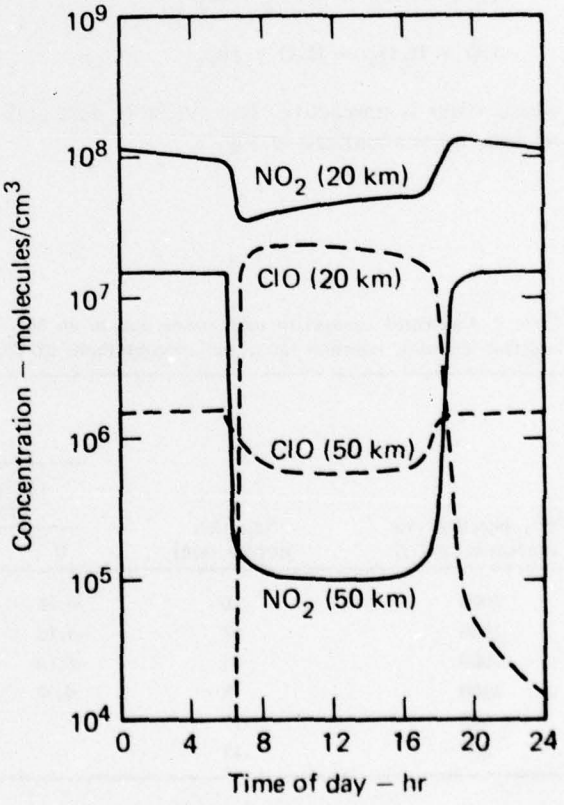

Figure 4. **Diurnal variation of NO_2 and ClO concentrations in the atmosphere at altitudes of 20 and 50 km.**

mechanism in an often fairly complex reaction scheme). See for example the reviews of Lloyd (1974), Baulch et al. (1972, 1973), and Hampson and Garvin (1975). In cases where the concentrations of reactive species are directly measured, the precision may be a reasonable estimate of the error, although even in these cases disagreements between different workers, while usually small, are also often larger than those suggested by precision alone. (See the discussion of reaction 12 below.) In such cases the error between measurements by different workers may provide a reasonable estimate of the expected error. But for indirect measurements where the concentrations of reactive species are inferred from a multistep mechanistic model, large systematic errors are more likely, and are frequently encountered in the literature, as for example in the reviews by Dixon-Lewis et al. (1974), Baulch et al. (1972, 1973), and Lloyd (1974).

We analyzed chemical rate data for six reactions in all: reactions 18, 14, 12, 19, 26, and 20 as specified in Table 1 of our First Annual Report (Luther et al. 1976). Our analyses follow.

Reaction 18. $HO_2 + HO_2 \cdot H_2O_2 + O_2$

This reaction acts as a sink for HO_x radicals, both by transforming them into the "reservoir" species H_2O_2 and through the reaction sequence

$$HO_2 + HO_2 \rightarrow H_2O_2 + O_2 ,$$

$$HO + H_2O_2 \rightarrow H_2O + HO_2 ,$$

where water is unreactive. The available data and reviews are summarized in Fig. 5.

This reaction has been measured at only one temperature.* The measurements of Foner and Hudson (1962), Paukert and Johnston (1972), and Hamilton (1975) are in excellent agreement. All of these involved direct detection of HO_2. The indirect measurement of Burgess and Robb (1957), discussed in the reviews of Baulch et al. (1972) and Lloyd (1974), is thought to be in error. The measurement by Hochanadel et al. (1972) involved a direct measurement of HO_2, like the other measurements, but was indirect in that the value is based on modeling a fairly complex reaction system. Hochanadel's measurement was discussed by Kaufman (1975), Lloyd (1974), and Hamilton (1975). Kaufman and Lloyd point out probable errors in the data analysis, and Hamilton shows that this rate constant appears to have an anomalous dependence on water concentrations, and that this effect could have caused Hochanadel et al. to overestimate the rate by about a factor of 3.

*A preliminary unpublished measurement over a narrow temperature range has been reported by Cox (private communication, 1977)(i.e., $k = 1.4 \times 10^{-14} e^{+1651/T}$). The large negative activation energy obtained for this reaction is surprising; it may involve some of the complications responsible for the anomalous water-vapor dependence observed for this rate constant, since these incompletely understood processes might very well have a strong temperature dependence. In any case, it seems obvious that measurements of this reaction over a broad temperature range are urgently needed. If Cox's expression is even approximately valid, a novel complex mechanism is implied for this reaction. This type of mechanism had been suggested as a plausible occurrence long before experimental data supporting it were available (H. S. Johnston, private communication, 1976). At present we prefer the NASA panel's recommendation (Hudson 1977), but we believe the uncertainty to exceed a factor of 3.

Table 1. **Calculated changes in total ozone due to an NO_x injection as NO_2 in a 1-km-thick layer of air for various injection altitudes, injection rates, and concentrations of ClO_x.**

NO_x injection rate (molecules/cm^3·s)	Injection altitude (km)	Percent change in total ozone calculated with following assumptions: Chang (1976) K_z profile, ClO_x concentration of: 0	1 ppb	2 ppb	4 ppb	Hunten (1975) K_z profile, ClO_x concentration of: 0	1 ppb	2 ppb
2000	20	−4.20	−3.26	−2.61	−1.27	−10.64	−8.76	−8.06
2000	17	−1.15	−0.70	−0.40	0.23	−4.06	−2.79	−2.33
2000	13	−0.10	0.01	0.09	0.24	0.08	0.16	0.20
2000	9	0.07	0.08	0.09	0.11	−0.10	0.12	0.12
600	17	–	−0.19	−0.09	0.12	–	−0.79	−0.39
200	17	–	−0.06	−0.03	0.04	–	−0.16	−0.10

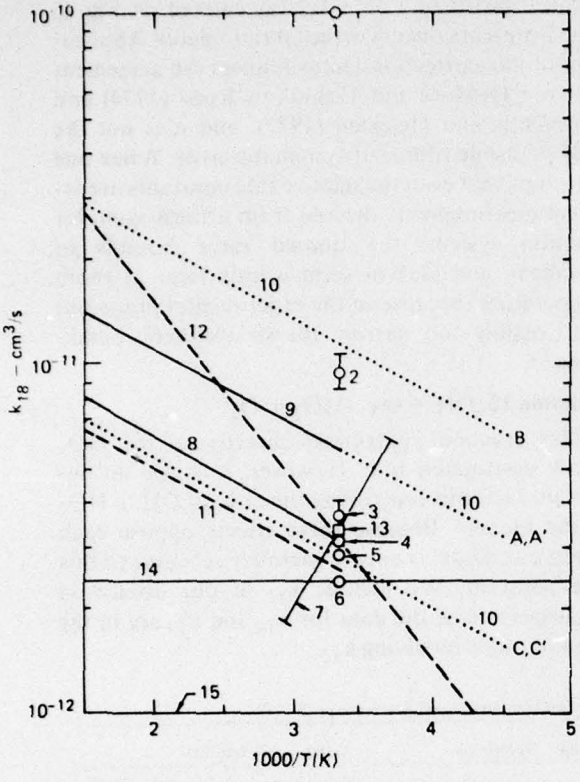

Experimental data (1–7) and reviews (8–15)

Symbol	Reference	T (K)	k (cm^3/s)
1	Burgess and Robb (1957)[a,b]	300	1×10^{-10}
2	Hochanadel et al. (1972)[a]	300	9.5×10^{-12}
3	Paukert and Johnston (1972)	300	3.6×10^{-12}
4	Hamilton (1975)	300	3.2×10^{-12}
5	Foner and Hudson (1962)	300	3.0×10^{-12}
6	Hamilton and Liu (1976)	300	2.5×10^{-12}
7	Cox (1977)	273–338	$1.4 \times 10^{-14} e^{1651/T}$
8	Lloyd (1974)	300–1000	$1.7 \times 10^{-11} e^{-500/T}$
9	Hampson and Garvin (1974)	300–1000	$3 \times 10^{-11} e^{-500/T}$
10	Models (this work)	–	–
11	Lloyd (1971)[b]	300–800	$1.4 \times 10^{-11} e^{-500/T}$
12	Nicolet (1964)	Not given	$5 \times 10^{-12} T^{1/2} e^{-1000/T}$
13	Baulch et al. (1972)	300	$(3.3 \pm 0.3) \times 10^{-12}$
14	Hudson (1977)	200–300	2.5×10^{-12}
15	Stolarski (1977)	200–300	1×10^{-12}

[a] Thought to be unreliable; see Lloyd (1974), Baulch et al. (1972), Hamilton (1975), and Kaufman (1975).

[b] From table of Baulch et al. (1972).

Figure 5. **Summary of available data for k_{18} ($HO_2 + HO_2 \rightarrow H_2O_2 + O_2$).**

There are few data on the temperature dependence of this reaction.* In his early review, Nicolet (1964) assumed a temperature-dependent rate coefficient of $5 \times 10^{-12} T^{1/2} e^{-1000/T}$. Lloyd (1974) assumed a temperature-dependent rate constant of $1.7 \times 10^{-11} e^{-500/T}$ based on the room-temperature measurements of Paukert and Johnston (1972) and Foner and Hudson (1962) and theoretical expectations for the high-temperature rate. Hampson and Garvin (1975) averaged the measurements of Paukert and Johnston and Hochanadel et al. and adopted Lloyd's temperature dependence in recommending the expression $k = 3 \times 10^{-11} e^{-500/T}$, uncertain by a factor of 2.

The assumed temperature dependence is arrived at by combining the room-temperature rate coefficient with a plausible theoretical estimate of the high-temperature rate coefficient. In our opinion, the room-temperature rate coefficient is fairly well known and should be based on the average of the rate constants reported by Paukert and Johnston (1972), Foner and Hudson (1962), and Hamilton (1975) with a subjectively estimated uncertainty of a factor of 1.5. However, the temperature dependence is effectively unknown. The rate constant could be nearly independent of temperature, or its temperature dependence might be as strong as $e^{\pm 1000/T}$.

We accept the preferred value for k_{18} recommended by Lloyd (1974), but we believe the rate constant to be uncertain by roughly a factor of 4 at stratospheric temperatures.

*See previous footnote.

Reaction 14. $HO_2 + O_3 \rightarrow OH + 2O_2$

This reaction effectively controls the efficiency of the HO_x ozone destruction cycle in the lower stratosphere and shifts the ratio $OH:HO_2$ toward OH.

This rate coefficient has never been measured directly, but there are three pertinent indirect

measurements (see Fig. 6). Anderson and Kaufman (1973) determined an upper limit for k_{14} relative to k_{12}, and DeMore (1973), DeMore and Tschuikow-Roux (1974), and Simonaitis and Heicklen (1973) measured the ratio of k_{14} to the square root of k_{18} (R_1). The various measurements are all roughly consistent with each other and with the recommended rate given by Hampson and Garvin (1975).* Indeed, as demonstrated by Johnston and Nelson (1977), at room temperature the agreement between different measurements of R_1 seems to suggest that R_1 provides an additional constraint on k_{14} more severe than the estimated error in the rate constant. However, DeMore and Tschuikow-Roux identified a systematic error (resulting from the finite optical depth of their system) that causes their ratio to be low by an amount that we estimate to be about a factor of 1.25 ± 0.2 (as entered on Fig. 6; Fig. 7 presents the uncorrected ratio data). Application of this correction factor reduces the agreement between DeMore and Tschuikow-Roux (1974) and Simonaitis and Heicklen (1973), and it is not the only plausible source of systematic error. When one considers that even the relative rate constants are indirect measurements derived from a fairly complex reaction system, the quoted error bounds of Hampson and Garvin seem a little large at room temperature (because of the experimental precision) but possibly too narrow for stratospheric conditions.

*If the preliminary value for k_{18} determined by Cox (1977) is used in the estimation of k_{14}, a very different expression is obtained for k_{14} than has been used earlier. At present we do not favor an expression based on Cox (1977) but recommend that it be considered as a possibility.

Reaction 12. $OH + O_3 \rightarrow HO_2 + O_2$

This reaction contributes directly to the HO_x ozone destruction rate. However, it is also an important factor in controlling the ratio of OH to HO_2 in the models. Because these effects oppose each other, our model is only moderately sensitive to this rate constant. We include k_{12} in our discussion because some of the data for k_{14} and k_{19} are in the form of ratios involving k_{12}.

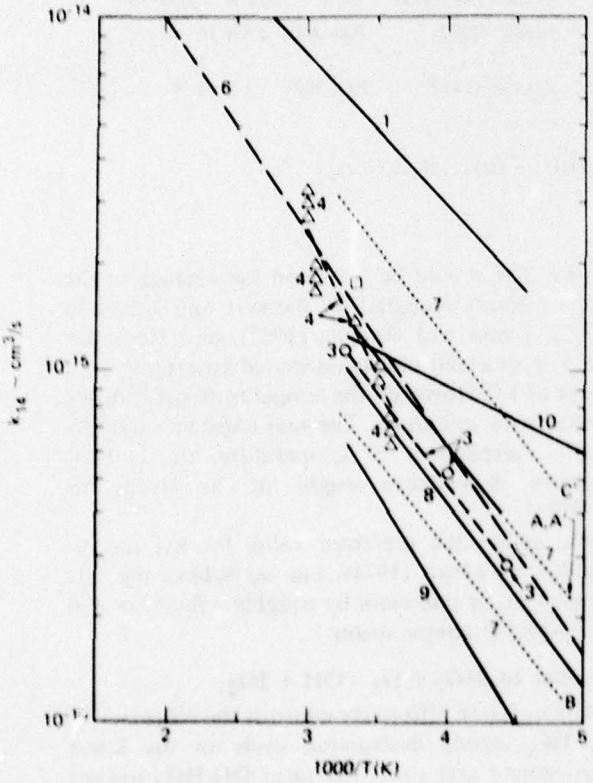

Experimental data (1–4) and reviews (5–10)

Symbol	Reference	T (K)	k (cm^3/s)
1	Anderson and Kaufman (1973)[a]	220–450	$1.6 \times 10^{-13} e^{-1000/T}$
2	DeMore (1973)[b,c]	300	1.7×10^{-13}
3	Simonaitis and Heicklen (1973)[b,c]	225–298	$7.7 \times 10^{-14} e^{-1250/T}$
4	DeMore and Tschuikow-Roux (1974)[b,c,d]	273–332	$5.7 \times 10^{-13} e^{-1800/T}$
5	Garvin and Hampson (1974)[e]	225–298	$1 \times 10^{-13} e^{-1250/T}$
6	Lloyd (1974)	200–500	$1.7 \times 10^{-13} e^{-1400/T}$
7	*Models (this work)*	200–300	
8	Hudson (1977)	200–300	$7.3 \times 10^{-14} e^{-1275/T}$
9	Stolarski (1977)	200–300	$1 \times 10^{-13} e^{-1525/T}$
10	Implications of Cox (1977)	–	$5.48 \times 10^{-19} e^{449/T}$

[a] Upper limit based on ratio to k_{12}.

[b] Ratio to $(k_{18})^{1/2}$.

[c] Recalculated using k_{18} from Lloyd (1974).

[d] Corrected by a factor of 1.25 to allow for a systematic error discussed by the authors.

[e] Used a higher value of k_{18} (average of Hochanadel et al. 1972 and Paukert and Johnston 1972).

Figure 6. **Summary of available data for k_{14} ($HO_2 + O_3 \rightarrow HO + 2O_2$).**

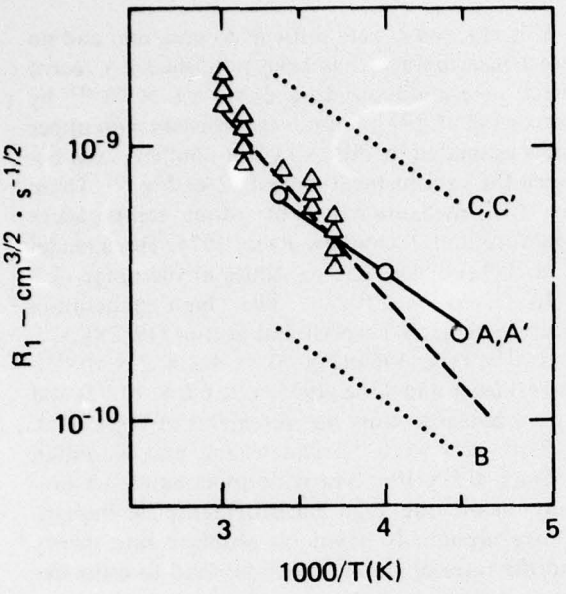

Figure 7. **The uncorrected ratio $R_1 = k_{14}/(k_{18})^{1/2}$. Circles are experimental data of Simonaitis and Heicklen (1974), triangles are data of DeMore and Tschuikow-Roux (1974). Our models A and A' are represented by the solid line, and models B, C, and C' by the dotted lines.**

Values for k_{12} have been independently measured by four research groups as summarized in Fig. 8. The room-temperature measurements of Davis (1974) and of Kurylo (1973) were made using the flash-photolysis resonance fluorescence technique. Accordingly they are both very direct and very precise measurements. (Both quoted values are averages of large numbers of separate determinations.) The error quoted by Kurylo (1973) was ±8%; Davis' (1974) error was ±4%. These two measurements differ by more than the precision bounds, although the agreement is very good by any other standard. The measurements of Anderson and Kaufman (1973) are also direct and precise, but they were made using resonance fluorescence detection in a flow system. Flow irregularities are always a potential problem in flow system measurements, and the measurement is probably slightly less accurate than the flash photolysis measurements.

The measurement of DeMore (1975) was also rather precise but was indirect, being based on a measurement of ozone in a photolysis system involving O_2, water, and CO_2.

We would use the average of the Davis, Kurylo, and Anderson and Kaufman measurements to establish a room-temperature rate constant and then

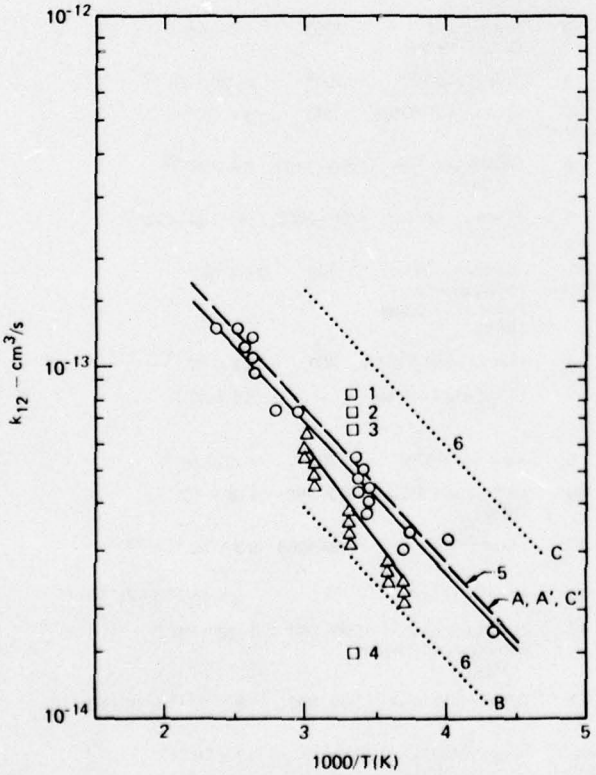

Experimental data (1, Δ, O, 2–4) and reviews (5, 6)

Symbol	Reference	T (K)	k (cm^3/s)
1	DeMore (1973)[a]	300	8×10^{-14}
Δ	DeMore (1975)[a,b]	271–333	$2.4 \times 10^{-12} e^{-1230/T}$
O	Anderson and Kaufman (1973)[c]	220–450	$1.3 \times 10^{-12} e^{-956/T}$
2	Davis (1974)[d]	300	$(7.5 \pm 0.3) \times 10^{-14}$
3	Kurylo (1973)[d]	248	$(6.5 \pm 0.5) \times 10^{-14}$
4	Simonaitis and Heicklen (1973)[a]	300	$\sim 1.5 \times 10^{-14}$
5	Hampson (1973), quoted by Hampson and Garvin (1974), and models A, A', and C' (this work)	220–450	$1.6 \times 10^{-12} e^{-1000/T}$
6	Models B, C (this work)	–	–
(Not plotted)	Hudson (1977)	–	$1.5 \times 10^{-12} e^{-1000/T}$

[a] Indirect measurement.

[b] Individual determinations are plotted as triangles.

[c] Individual determinations are plotted as circles.

[d] Very precise measurements. Plotted points are averages of many individual determinations.

Figure 8. **Summary of available data for k_{12} ($OH + O_3 \rightarrow HO_2 + O_2$).**

apply the activation energy measured by Anderson and Kaufman to provide a temperature-dependent rate constant. In our appraisal, an appropriate expected error would be a factor of 1.2 at room temperature, increasing to a factor of about 2.5 at 200 K. For the purposes of stratospheric modeling, our estimate is only trivially different from Hampson and Garvin's (1975) recommendation for this reaction.*

Reaction 19. $HO + HO_2 \rightarrow H_2O + O_2$

If the faster of the quoted rates for reaction 19 is correct, then this reaction is the major sink for stratospheric HO_x radicals. If the slower rates are correct, it is still a major sink for HO_x radicals.

This reaction is very difficult to measure, and no direct measurement has been published. (A recent direct determination does exist, 5.1×10^{-11} by Burrows et al. 1977, but it is inconsistent with upper limits estimated by others.) Clear conflicts exist between the various measurements (see Fig. 9). There are two measurements at room temperature (DeMore and Tschuikow-Roux 1974, Hochanadel et al. 1972) which lead to values in the range of 2×10^{-11} to 6×10^{-11}. The high-temperature measurements of Friswell and Sutton (1972)($k = 2 \times 10^{-11}$), Tröe (1969)($2 \times 10^{-12} \leq k \leq 2 \times 10^{-11}$), and Glänzer and Tröe (1975)($k \leq 6.6 \times 10^{-11}$) and the room-temperature measurements of Hack et al. (1975)($k \leq 3 \times 10^{-11}$) and Chang and Kaufman (1976)($k \leq 5 \times 10^{-11}$) provide upper limits substantially below the high measurements. Semiquantitative arguments based on absolute rate theory and the rates of similar reactions lead to estimates

*The NASA panel (Hudson 1977) recommends that this rate constant be lowered by 8% because of an error in the O_3 absorption coefficients used in reducing the experimental data. We would concur.

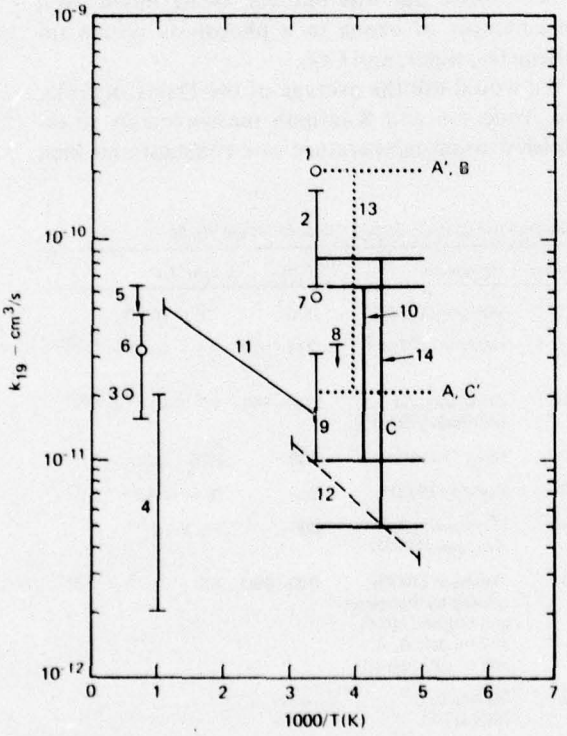

Experimental data (1–8) and reviews (9–14)

Symbol	Reference	T (K)	k (cm^3 s)
1	Hochanadel et al. (1972)	298	2×10^{-10}
2	DeMore and Tschuikow-Roux (1974)[b]	300	$6-16 \times 10^{-11}$
3	Friswell and Sutton (1972)[c]	2000	2×10^{-11}
4	Tröe (1969)[c]	1000	$2-20 \times 10^{-12}$
(Not plotted)	Hack et al. (1975)[d]	298	$\leq 3 \times 10^{-11}$
5	Glänzer and Tröe (1975)[d]	1250–1800	6.6×10^{-11}
6	Dixon-Lewis et al. (1974)[e]	1300–1600	$(3 \pm 1.5) \times 10^{-11}$
(Not plotted)	Kaufman (1964); review based on Foner and Hudson (1962)	300	$\geq 1 \times 10^{-11}$
7	Burrows et al. (1977)	300	5.1×10^{-11}
8	Chang and Kaufman (1977)	–	$\leq 3.5 \times 10^{-11}$
9	Kaufman (1975)	300	$1-3 \times 10^{-11}$
10	DeMore and Watson (1976)	200–300	$1-6 \times 10^{-11}$
11	Lloyd (1974)	300–1000	$8.3 \times 10^{-11} e^{-500/T}$
12	Nicolet (1970)[e]	–	$3 \times 10^{-12} T^{1/2} e^{-500/T}$
13	H.S. Johnston in Hampson and Garvin (1974)	200–300	$2-20 \times 10^{-11}$
14	Duewer (this work)	200–300	5×10^{-12} to 8×10^{-11}
(Not plotted)	Hudson (1977), Stolarski (1977)	–	3×10^{-11}

[a]Several problems with this measurement have been discussed in the reviews of Lloyd (1974) and Kaufman (1975) and in Hamilton (1975).

[b]Ratio measurement. Actual measurement covered the range 273–342 K and gave a temperature-dependent rate. Slanting lines give these values for various assumed values of the other rates in the ratio.

[c]High-temperature experiment, indirect determination.

[d]Indirect determination based on an analysis of the HO_2 + NO system.

[e]As quoted by Baulch et al. (1972).

Figure 9 **Summary of available data for k_{19} ($HO + HO_2 \rightarrow H_2O + O_2$).**

for the rate constant in the range of 3×10^{-12} to 5×10^{-11} (Kaufman 1975). Further, the observed stratospheric OH concentrations (Anderson, private communication, 1975) are very difficult to support in models using the faster rate coefficients for this reaction.

None of the above arguments is conclusive. Chemical theory has difficulty in predicting slow, nearly temperature-independent rate coefficients for simple reactions such as that for

$$OH + HNO_3 \rightarrow H_2O + NO_3$$

$$(k_{21} \approx 8.9 \times 10^{-14} \text{ cm}^3/\text{s})$$

and must be used with some caution. The stratospheric models may be in error in other ways; thus they do not provide a conclusive test of the HO_x sink rates.

We note that, as was discussed earlier, kinetic complications in the reaction system of Hochanadel et al. (1972) have been identified by Hamilton (1975) and Kaufman (1974), and the data analysis of Hochanadel used parameters at values not currently accepted (Lloyd 1974). Dixon-Lewis et al. (1974) make similar criticisms of the analysis used by Friswell and Sutton (1972). Thus, those experiments should be used with even more caution than the other indirect measurements. The data of DeMore and Tschuikow-Roux (1974) were taken in the form of the ratio

$$R_2 = \frac{k_{19} \cdot k_{14}}{k_{12} \cdot k_{18}}.$$

This ratio can also be calculated from the various models. If this is done, we find that the experimental temperature dependence for the ratio has the opposite sign from the temperature dependence that can be deduced from the models unless k_{19} has a significant activation energy or there are substantial errors in the activation energies used for the other rate coefficients. None of the models agrees with this ratio over a very extended temperature range. The analysis of Johnston and Nelson (1977) indicates that heterogeneous reactions may account for much of the discrepancy in the room-temperature values for this ratio, but not for the differences in activation energy.

In our concerted variations of rate constants, where k_{18} and k_{19} were varied in the same sense, and k_{12} (which appears to be relatively well established) was either held constant or varied in the same sense as k_{14} (and oppositely to k_{18} and k_{19}), we found that models A and A′ of Duewer et al. (1977b) are the extreme models, A′ being in approximate agreement with the experiment near 300 K, while B and C′ are fairly close to the extrapolated data near 250 K, and A and C intercept the extrapolated experimental curve near 180–200 K.

It is troubling that the models, especially model A, are as far from this experiment as they are. However, the experimental ratio was indirectly determined and may be seriously affected by heterogeneous processes. Although, to first order, this ratio was free of the identified systematic error that appeared in the ratio of k_{14} to $(k_{18})^{1/2}$ from the same work, the data analysis was such as to potentially magnify errors in the directly determined quantities. Further, if the ratio determined by DeMore and Tschuikow-Roux (1974) is correct, then an appreciable activation energy for k_{19}, a very strong negative activation energy for k_{18}, or a large error in the ratio of k_{14} to $(k_{18})^{1/2}$ (R_1) is implied.

Finally, we note that in their recent recommendations to NASA, W. B. DeMore and K. Watson (private communication, 1976) recommended the use of values in the range of $1–6 \times 10^{-11}$ cm^3/s for k_{19}.

Because of the indirect nature of the various experiments and the apparent incompatibility of the results of various workers, we have been guided primarily by the rates of similar reactions and by theoretical considerations and secondarily by the observed concentrations of stratospheric OH. We consider 5×10^{-12} to 8×10^{-11} cm^3/s to be the plausible range of values for k_{19}, with $k = 2 \times 10^{-11}$ cm^3/s a likely value.*

Reaction 26. $HO_2 + NO \rightarrow NO_2 + HO$

This reaction couples the NO_x and HO_x cycles. It reduces the efficiency of both cycles, especially in the lower stratosphere where NO_2 is usually photolyzed.

The available data are summarized in Fig. 10. All of the data are obtained by indirect methods,† and we find no clear basis for deciding which are the most reliable measurements.

*The NASA panel recommendation (Hudson 1977) of 3×10^{-11} seems as reasonable as our use of 2×10^{-11}.

†The recent measurement of Howard and Evenson (1977), 8×10^{-12} at 300 K, was directly determined and seems substantially more plausible than any other published measurement of this quantity. Moreover, several other unpublished determinations of this rate constant have been made recently which seem to lie in the range 8×10^{-12} to 1×10^{-11}. Thus we would accept Howard and Evenson's room-temperature rate constant and speculate that the temperature dependence would be in the range $+200/T$ to $-800/T$, with $-500/T$ a plausible value.

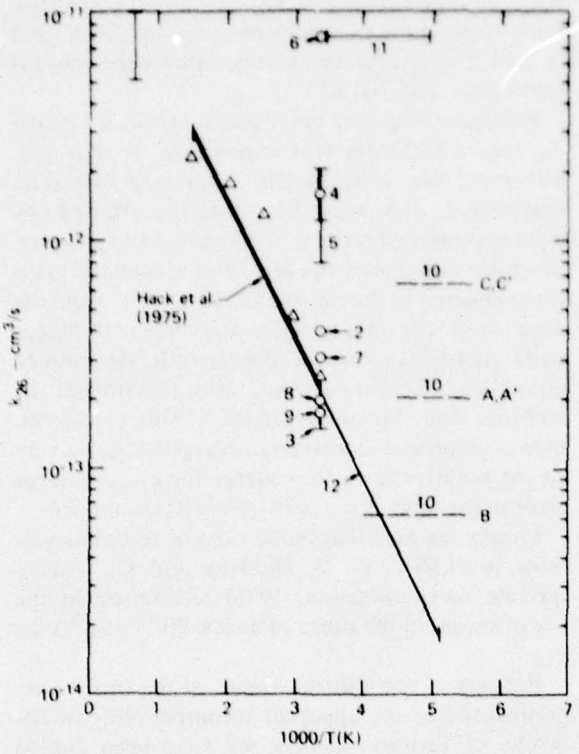

Experimental data (Δ, 1–6) and reviews (7–12)

Symbol	Reference	T (K)	k (cm^3 s)
Δ	Hack et al. (1975)	298–666	$2 \times 10^{-11} e^{-1200/T}$
1	Glänzer and Troe (1975)	1250–1810	5×10^{-12}
2	Payne et al. (1973)	300	4×10^{-12}
3	Simonaitis and Heicklen (1973)	300	1.5×10^{-13}
4	Cox (1975)	298	1.6×10^{-12}
5	Simonaitis and Heicklen (1976)	298	1.0×10^{-12}
6	Howard and Evenson (1977)	298	8×10^{-12}
7	Baulch et al. (1973)	300	3×10^{-13}
8	Hampson and Garvin (1974)	300	2×10^{-13}
9	Lloyd (1974)	300	1.7×10^{-13}
10	Models (this work)	—	—
11	Hudson (1977)	200–300	9×10^{-12}
12	Stolarski (1977)	200–300	$2 \times 10^{-11} e^{-1200/T}$

Figure 10. **Summary of available data for k_{20} ($HO_2 + NO \xrightarrow{M} NO_2 + HO$).**

We note that the newer data suggest that the room-temperature rate constant was underestimated by Hampson and Garvin, but that the reaction may have a significant temperature dependence. As a result, we believe that the uncertainty factor applied might have been increased, but that the range considered is appropriate for stratospheric conditions.

Reaction 20. $OH + NO_2 \rightarrow HNO_3$

This reaction reduces the effect of both NO_x and HO_x on ozone by tying up both species in the relatively inert species HNO_3. Further, it catalyzes HO_x destruction through the reaction

$$OH + HNO_3 \xrightarrow{M} H_2O + NO_3 \quad .$$

Reaction 20 is dependent on both temperature and pressure, and the pressure dependence is a function of the identity of the third body M. As a result of this we have chosen to present the data in the form given in Fig. 11. The altitude dependence portrayed does not pertain to actual measurements at various altitudes, but rather to measurements at various temperatures and pressures interpolated or extrapolated to the conditions of the U.S. Standard Atmosphere. There are other pertinent measurements, including recent work (e.g.: Davis 1974; P. Atkinson, private communication, 1976). However, most of that work does not cover stratospheric temperatures, is not compatible with the data presentation adopted, and is not included in Fig. 11. The data of the various workers do form a reasonably consistent set of measurements. However, as is evident in Fig. 11, for the conditions of the lower stratosphere the data of Anastasi et al. (1976) fall somewhat outside the expected error range quoted by Hampson and Garvin. In this range the curve quoted from Anastasi et al. is an interpolation from the data, but the Hampson and Garvin recommendation is based on a substantial extrapolation. The two expressions agree in the range of 30–45 km, where both are interpolating functions. In order to cover the full range of our model, 0–55 km, we fit the primary data of Anastasi et al. to the expression

$$k = \frac{2.76 \times 10^{-13}\, e^{880/T} \cdot M}{1.16 \times 10^{18}\, e^{222/T} + M} \quad .$$

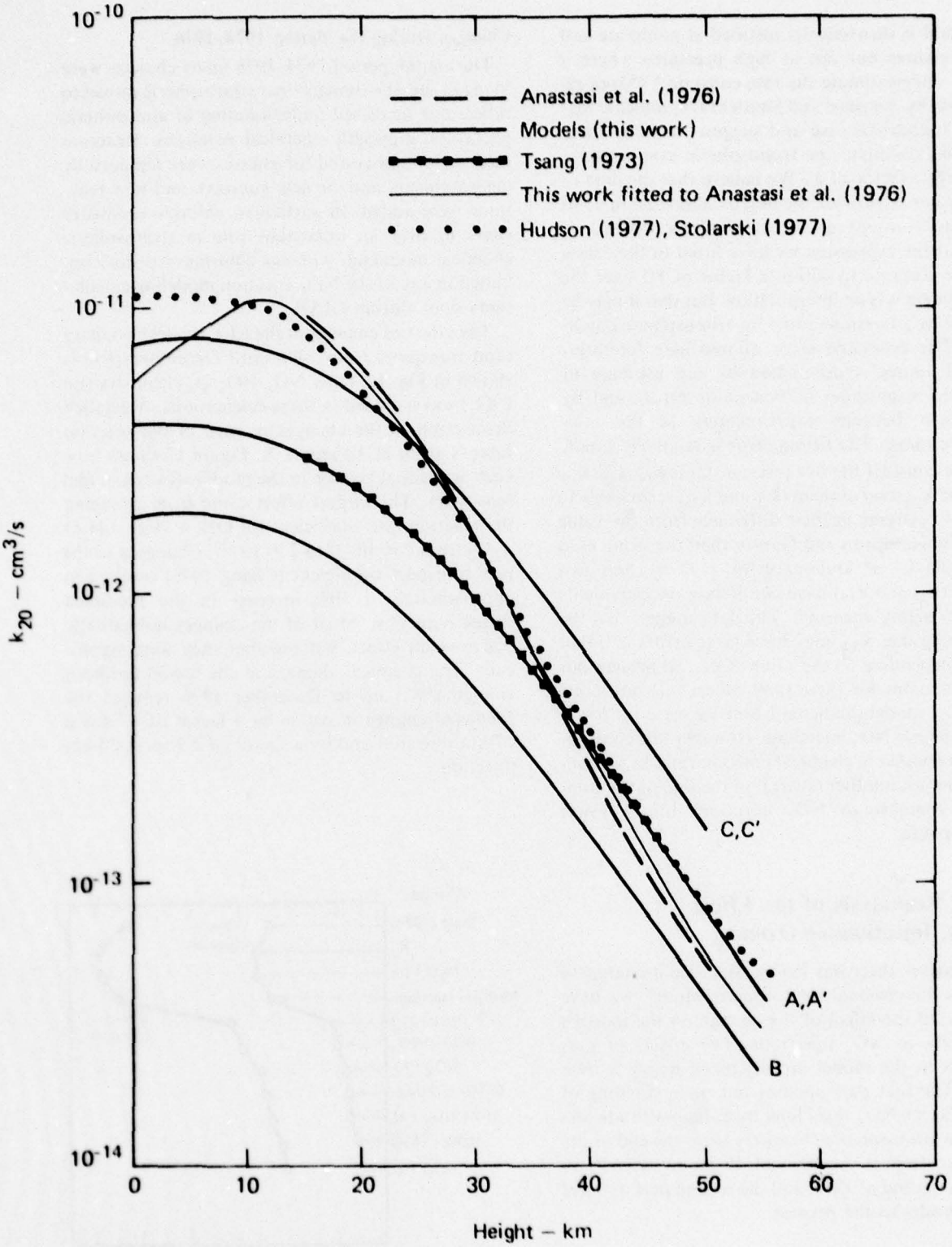

Figure 11. **Summary of available data for k_{20} ($OH + NO_2 \xrightarrow{M} HNO_3$).**

This form is theoretically justified at moderate and low pressures but not at high pressures where it should underestimate the rate constant.* (More recent data by Anastasi and Smith (1976) indicate that this is indeed the case and suggest that our curve may underestimate the tropospheric rate constant by nearly a factor of 2.) We believe that the data of Anastasi et al. provide the best available estimate of this rate constant under stratospheric conditions and that the expression we have fitted to their data may be accurate to within a factor of 1.5 over the range where it is an interpolation, but that it may be in error by a factor of 2 to 3 for tropospheric conditions. The estimated error quoted here for interpolated values is dominated by our estimate of plausible magnitudes of systematic errors and by differences between experimenters in the low-pressure range. The fitting error is relatively small.

If we consider the five rate constants k_{14}, k_{18}, k_{19}, k_{20}, and k_{26}, two of them (k_{20} and k_{26}) seem likely to be more extreme in their difference from the value given by Hampson and Garvin than the value used in model C′ of Duewer et al. (1977b), and two others (k_{18} and k_{19}) have conflicting measurements and are highly uncertain. The data suggest that the *remaining one, k_{14}, may have large errors in either* sense, depending on the value of k_{18}. At present our best estimates for these (and other) rate constants lead to a model-predicted ozone increase for lower stratospheric NO_x injections. However, the continuing uncertainty in chemical reaction rates leaves ample room for another reversal of the sign of the computed response to NO_x injections in the lower stratosphere.

2.3 A Reanalysis of the Effect of NO_x Injections on Ozone

Whenever there has been a significant change in the one-dimensional stratospheric model, we have reanalyzed the effect of the change on the model's sensitivity to NO_x injections. The effects of past changes in the model are discussed below in two parts. The first part updates our understanding of the effect of NO_x injections from high-altitude aircraft on stratospheric chemistry from the end of the Climatic Impact Assessment Program (CIAP) in 1974 to the end of 1976, and the second part updates these results to the present.

*The NBS group has recommended a complex expression for this rate coefficient that has been accepted by the NASA panel (Hudson 1977). At present we would accept that expression.

Changes During the Period 1974–1976

During the period 1974–1976 many changes were made in the one-dimensional stratospheric model to reflect our increased understanding of atmospheric processes, especially chemical reactions. Reaction rates were remeasured (or guesses were replaced by measurements and/or new guesses), and new reactions were added. In particular, chlorine chemistry came to play an important role in stratospheric chemical modeling, whereas chlorine was not contained in any of the NO_x injection modeling calculations done during CIAP.

The effect of changes in the LLL model chemistry (and transport) from 1974 until December 1976 is shown in Fig. 12. Only NO_x-HO_x-O_x chemistry (no ClO_x) was included in these calculations. A detailed description of the changes in each of the reaction rates is given in Appendix A. Figure 12 shows how each sequential change in the model affected model sensitivity. The largest effect came from changing the reaction rate coefficient for $OH + HO_2 \rightarrow H_2O + O_2$ from 2×10^{-10} to 2×10^{-11}. Changing to the new transport coefficient (Chang 1976) resulted in approximately a 10% increase in the predicted ozone reduction. Most of the changes individually *had a small effect*, but together they were significant. The chemical changes in the model (without changing K_z) up to December 1976 reduced the predicted change in ozone by a factor of 4.7 for a 17-km injection and by a factor of 2.9 for a 20-km injection.

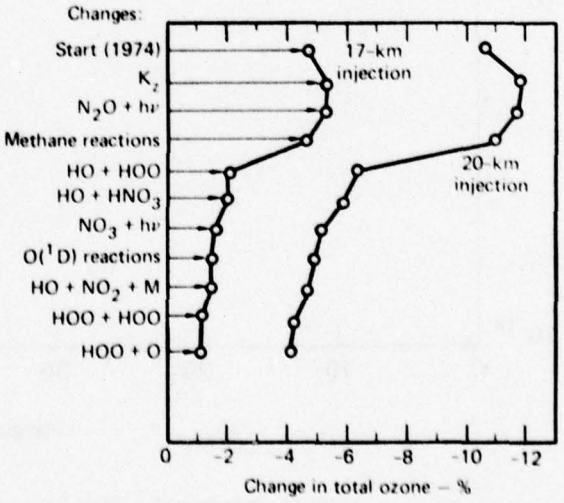

Figure 12. **Effects of changes in model assumptions (ordinate) on calculated change in total ozone (abscissa) for an injection of 2.46×10^9 kg/yr of NO_x at altitudes of 17 and 20 km.**

Since Molina and Rowland (1974) first noted the potential effect of the chlorofluoromethanes (CFMs), $CFCl_3$ and CF_2Cl_2, on the stratospheric ozone, much effort has been given to determining the effect of chlorine species such as Cl, ClO, HCl, $ClONO_2$, etc. on stratospheric chemistry. The 1976 calculations predicted a background concentration of ClO_x (Cl + ClO + HCl) in the natural stratosphere of 1 ppb resulting from CH_3Cl and CCl_4 without any CFMs. With the addition of CFMs, we calculated approximately 1.5 ppb stratospheric ClO_x for current levels of $CFCl_3$ and CF_2Cl_2, 2 ppb ClO_x for predicted 1990 levels of CFMs due to constant production beyond 1973, and 4 ppb at steady state (100–200 years).

We made a series of calculations to determine the effect of various background levels of ClO_x on the predicted ozone reduction due to NO_x injection. As an initial condition for the calculations, a background steady-state atmosphere containing various levels of ClO_x (1, 2, or 4 ppb) was derived, then the model was calculated to steady state with NO_x aircraft emissions of 2000 molecules/cm^3·s as NO_2 injected into a 1-km-thick layer centered at various altitudes (9, 13, 17, or 20 km). These calculations were carried out with the Chang (1976) and the Hunten (1975) K_z profiles. The results are summarized in Table 1.

For stratospheric injections of NO_x (at 17 and 20 km), increasing the background levels of ClO_x decreases the magnitude of the ozone reduction. The effect of the ClO_x background is substantial, even leading to a net ozone increase for a 17-km NO_x injection with a ClO_x background of about 4 ppb. The changes in total ozone are small for tropospheric injections of NO_x. The results for injections at 9 km should be considered to be within the "noise," since these changes are the net result of ozone reduction above about 20 km and ozone production below 20 km. Because the model uses fixed boundary conditions and incorporates rainout processes for NO_2 and HNO_3, a large effect should not be expected from a 9-km injection. The change in total ozone is basically linear with NO_x injection rate using the Chang (1976) K_z profile but not with the Hunten K_z profile.

Calculations were also made for an NO_x-HO_x-O_x atmosphere using an FAA estimate of 1990 aircraft emissions. The model input used is shown in Table 2. With the Chang (1976) K_z profile there was a net increase in total ozone of 0.15% after the first year, which reduced to a steady-state net increase of 0.02% after the tenth year. With the Hunten K_z profile, a 0.20% increase in total ozone after one year reduced to 0.04% at steady state.

Changes Since 1976

Since the end of 1976 there have been a number of changes to the stratospheric model including changes in chemical rate coefficients and improvements in the representation of physical processes, such as including multiple scattering in the photodissociation rate calculation. The changes in model chemistry up to June 1977 were based upon the Hudson (1977) reevaluation of chemical rate data (see Table A-1 in Appendix A). These changes led to an increase in the ozone reduction estimates due to an NO_x injection of 2000 molecules cm^{-3}·s as NO_2 at either 17 or 20 km. The most significant change since December 1976 was a new measurement of the reaction rate for $NO + HO_2 \rightarrow NO_2 + OH$ by Howard and Evenson (1977). Using a direct measurement technique, laser magnetic resonance, they measured this reaction rate to be roughly 30 times faster than previously thought. The effect that this one change in a chemical rate measurement has on the model is shown in Table 3. With the Chang (1976) K_z profile, there is a reversal in the sign of the ozone change such that aircraft emissions in the lower stratosphere cause an increase in total ozone. With the Hunten K_z profile, there is an ozone decrease for a 20-km injection but an ozone increase for a 17-km injection.

Figures 13 and 14 show the effect the change in the $HO_2 + NO$ rate has on model-derived species concentrations. The new faster rate has a large impact on stratospheric constituents such as NO (as

Table 2. **Estimated 1990 aircraft emissions used in the LLL 1-D model.**

Altitude (km)	Emissions (kg NO_2/yr)
6	5.857×10^7
7	1.171×10^8
8	1.932×10^8
9	4.364×10^8
10	7.645×10^8
11	7.627×10^8
12	3.410×10^8
13	4.859×10^7
14	1.155×10^7
15	1.180×10^7
16	2.098×10^7
17	2.354×10^7
18	1.515×10^7
19	4.739×10^6

Table 3. **The effect on model sensitivity of changing the rate coefficient for the reaction $NO + HO_2 \rightarrow NO_2 + OH$. Old rate = 2.0×10^{-13}, new rate = 4.28×10^{-11} exp (−500/T) (Howard and Evenson 1977).**

K_z profile	NO_x injection altitude (km)	Change in O_3 (%)		Change in NO_x (%)	
		Old rate	New rate	Old rate	New rate
Chang (1976)	20	−4.79	0.55	46.7	47.9
	17	−1.31	1.96	27.3	27.8
Hunten (1975)	20	−10.8	−6.90	96.2	97.1
	17	−4.35	0.83	61.4	62.3

much as a factor of 3 lower concentration at 15 km) and OH (a factor of 2 larger concentration at 15 km). Other species more indirectly related to the reaction of HO_2 + NO, such as ClO and $ClONO_2$, are also strongly affected by the new rate.

There is now a nonlinear relationship between the magnitude of the NO_x injections and the predicted change in total ozone. This is illustrated in Fig. 15 for 17- and 20-km injection altitudes. Note that doubling the rate of an NO_x injection does not result in doubling the change in ozone as was found during CIAP. Depending on the magnitude of the injection, either a new increase or decrease of total ozone results.

The change in the local ozone concentration is shown in Fig. 16 for three different NO_x injection rates at 20 km. There is a net production of O_3 in the lower stratosphere and net destruction in the upper stratosphere. It is the summing of these two effects that determines whether a net increase or decrease in total ozone is calculated. Therefore, while there may be no net change in total ozone for a specific NO_x injection, there may be large predicted local ozone changes in the stratosphere. Such

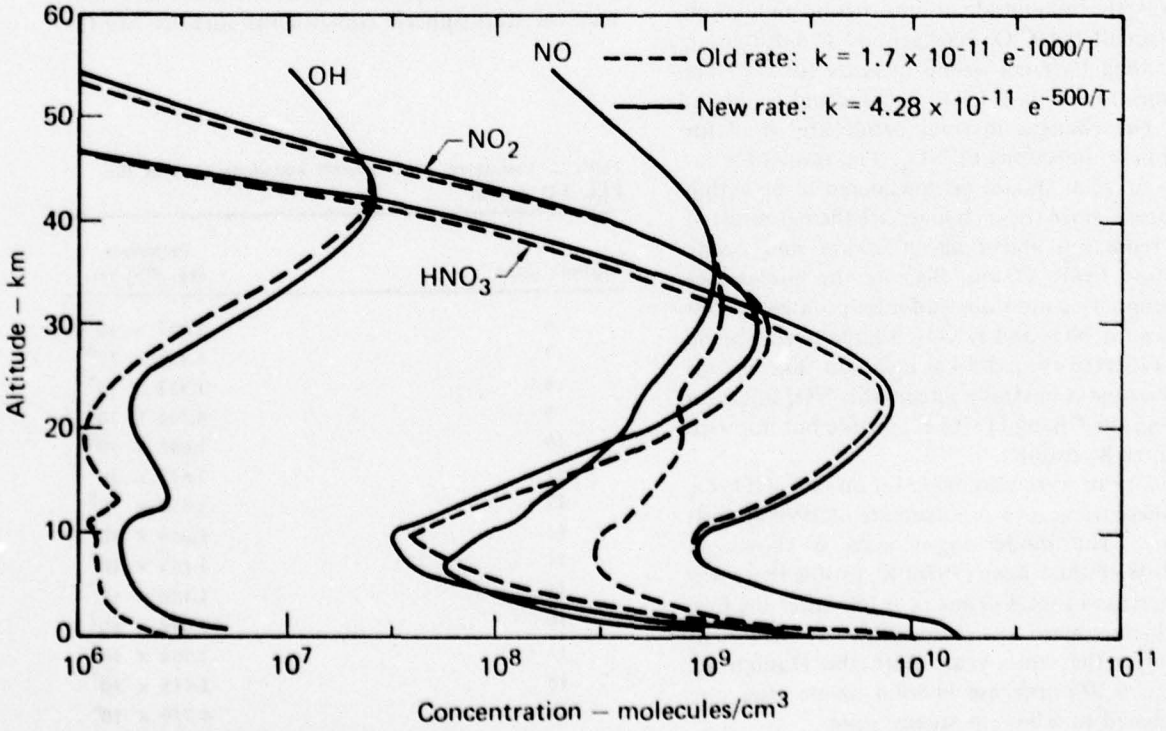

Figure 13. **Effect of the change in the HO_2 + NO reaction rate on model-derived concentrations of HNO_3, NO_2, OH, and NO. New rate is based on Howard and Evenson (1977).**

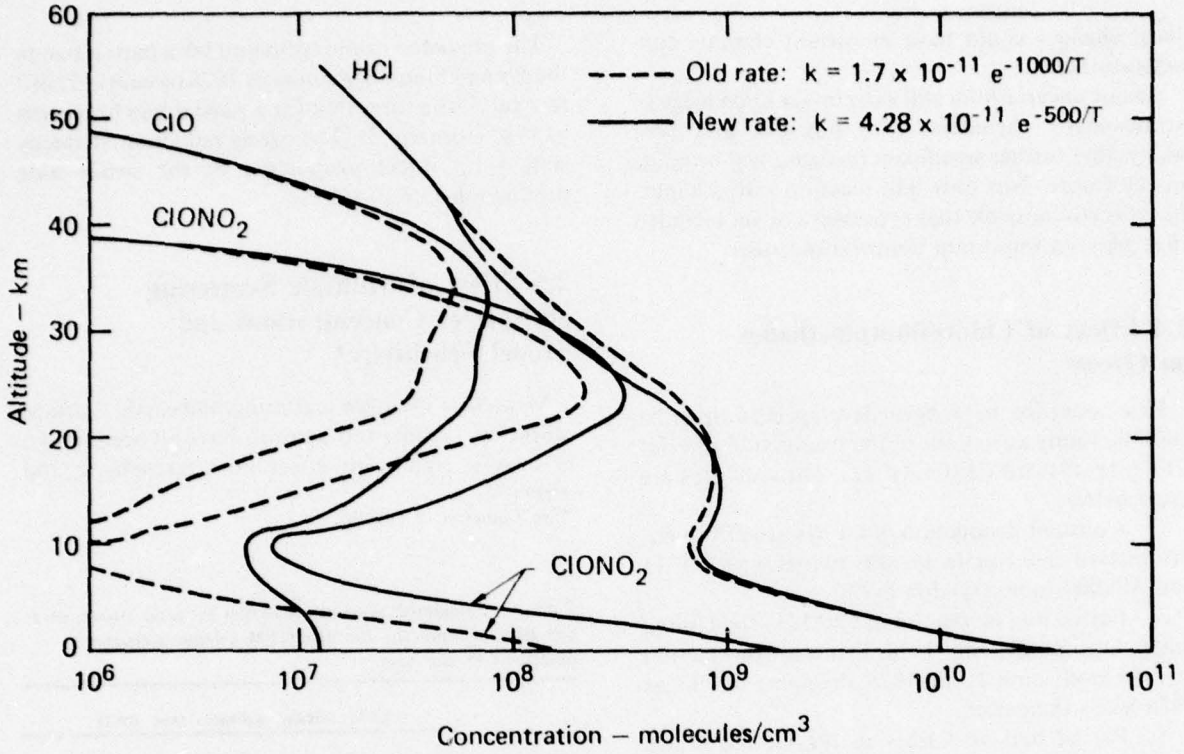

Figure 14. **Effect of the change in the HO_2 + NO reaction rate on model-derived concentrations of HCl, ClO, and $ClONO_2$.**

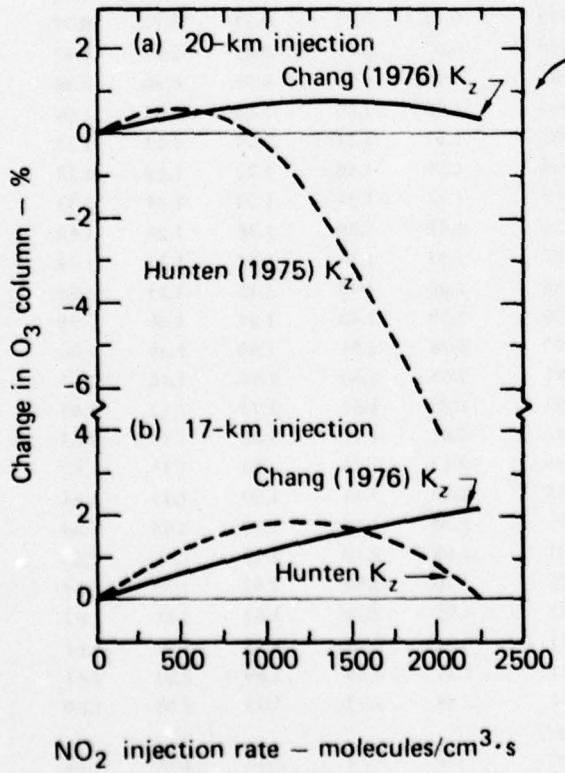

Figure 15. **Calculated change in the ozone column at steady state as a function of NO_x injection rate (as NO_2) for injection altitudes of 17 and 20 km. An injection rate of 2000 molecules/cm^3·s in a hemispheric shell 1 km thick corresponds to an annual injection rate of 1.23×10^9 kg/yr.**

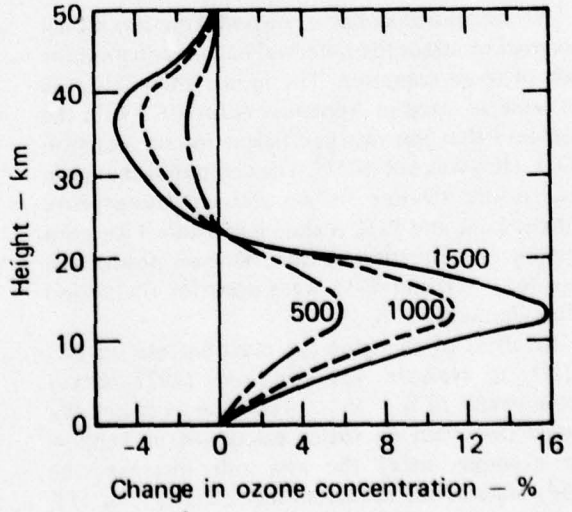

Figure 16. **Calculated change in the local ozone concentration versus height for NO_x injection rates of 500, 1000, and 1500 molecules/cm^3·s in a 1-km-thick layer centered at 20 km.**

local changes could have important climatic considerations.

Major uncertainties still exist in our knowledge of stratospheric chemistry. It is possible, and even likely, that further significant revisions will be made in the future. Not only will reaction rates change, but it is still possible that processes not yet included may play an important contributing role.

2.4 Effect of Chlorofluoromethanes on Ozone

Five scenarios have been developed to describe possible future variations in the production rates of $CFCl_3$ (F-11) and CF_2Cl_2 (F-12). The scenarios are listed below:

1. Constant production of CFMs at 1975 levels. Production rate equals 347,000 tonnes/yr for F-11 and 415,000 tonnes/yr for F-12.*

2. Partial ban on the use of CFMs in the United States beginning 1 July 1978. Constant production at 1975 levels until 1 July 1978, dropping to 70% of 1975 levels thereafter.

3. Partial ban on CFMs in the United States beginning 1 July 1980. Same as scenario 2 except reduction beginning 1 July 1980.

4. Partial ban by the United States and several other countries concurrently on 1 July 1980. Constant production at 1975 levels until 1 July 1980, then dropping to 33% of 1975 levels.

5. Technical breakthrough allowing a drastic reduction in CFM production in 1984. Constant production at 1975 levels until 1 July 1984, dropping to 20% of 1975 levels thereafter.

The one-dimensional transport-kinetics model was used to assess the potential ozone reduction for each of these scenarios. The model chemistry was the same as listed in Appendix A for 1977 with the exception that the rate coefficient for the reaction $NO + HO_2$ was 6×10^{-13}. The computed change in total ozone relative to an ambient atmosphere without F-11 and F-12 is shown in Table 4 for each scenario as a function of time. Known production rates for F-11 and F-12 were used for the period before January 1976.

The effect of changing the reaction rate for $NO + HO_2$ to Howard and Evenson's (1977) recent measurement of 8×10^{-12} would be to essentially double the effect on ozone calculated in Table 4. For example, using the new rate increases the steady-state ozone reduction for scenario 1 to 15% as compared with the 7.9% shown in Table 4.

*One tonne = 1 metric ton = 10^3 kg.

The predicted ozone reduction for a partial ban in the United States beginning in 1978 (scenario 2) differs very little from that for a partial ban beginning in 1980 (scenario 3). The ozone reduction at steady state is in direct proportion to the steady-state production rate of CFMs.

2.5 Effect of Multiple Scattering on Species Concentrations and Model Sensitivity*

Molecular multiple scattering, the earth's surface reflection, clouds, and aerosols have all been shown to have a significant effect on stratospheric and

*See Luther et al. (1977b).

Table 4. **Calculated percent reduction in total ozone as a function of time for the five CFM release scenarios described in the text.**

	CFM release scenario (see text)				
Year	1	2	3	4	5
1976	0.48	0.48	0.48	0.48	0.48
1977	0.58	0.58	0.58	0.58	0.58
1978	0.68	0.68	0.68	0.68	0.68
1979	0.77	0.77	0.77	0.77	0.77
1980	0.87	0.87	0.87	0.87	0.87
1981	0.96	0.95	0.96	0.96	0.96
1982	1.06	1.03	1.05	1.05	1.06
1983	1.17	1.11	1.14	1.13	1.17
1984	1.24	1.18	1.22	1.19	1.24
1985	1.33	1.24	1.29	1.24	1.33
1986	1.42	1.30	1.36	1.28	1.42
1987	1.52	1.36	1.42	1.31	1.49
1988	1.60	1.42	1.48	1.33	1.54
1989	1.69	1.48	1.54	1.36	1.58
1990	1.78	1.54	1.60	1.38	1.60
1991	1.86	1.60	1.66	1.40	1.62
1992	1.95	1.65	1.71	1.42	1.63
1993	2.04	1.71	1.76	1.44	1.63
1994	2.12	1.76	1.82	1.45	1.64
1995	2.20	1.81	1.87	1.47	1.64
1996	2.28	1.87	1.92	1.48	1.64
2001	2.68	2.12	2.17	1.56	1.64
2011	3.40	2.58	2.63	1.70	1.63
2021	4.05	2.98	3.03	1.81	1.62
2031	4.61	3.34	3.38	1.92	1.61
2041	5.11	3.65	3.69	2.01	1.61
2051	5.54	3.93	3.95	2.09	1.60
Steady state	7.94	5.55	5.55	2.55	1.53

tropospheric radiative intensities at photodissociative wavelengths. The importance of molecular scattering and surface albedo and their effect on atmospheric photodissociation rates have been discussed by Luther and Gelinas (1976). Parameterizations of the effect of multiple scattering on photodissociative flux densities have been included in one-dimensional transport-kinetics models by Crutzen and Isaksen (1976), Callis et al. (1976), Ashby (1976), and Kurzeja (1976). Crutzen and Isaksen (1976) use a two-flux approximation to account for the direct and scattered radiation. Callis et al. (1976), using a detailed solar radiation model, compute correction factors which are then applied to the photodissociative rates computed assuming a purely absorbing atomic and molecular atmosphere. The correction factors vary with altitude for each photodissociative reaction, and they are assumed to be unaffected by changes in atmospheric composition.

We have assessed in detail the effect of including molecular multiple scattering and surface reflection in the transport-kinetics model on ambient species concentration profiles and on model sensitivity to perturbations affecting stratospheric ozone. The effect of multiple scattering was incorporated into the photodissociation rate calculation by applying correction factors to the short-wave fluxes used in the pure absorption calculation (the method is described in detail below). Calculations were made with the 1977 model chemistry listed in Table A-1 of Appendix A with the exception of a few rates indicated in Table 5. Calculations were later repeated using NASA recommendations (Hudson 1977) and Howard and Evenson's (1977) new measurement of the rate for $NO + HO_2$. These changes are listed in Table 5.

The solution of the one-dimensional purely absorbing radiative transfer equation at a particular altitude z_p, solar zenith angle θ_0, and atmospheric composition $\{N_A\}$ is given by

$$F_\lambda(z_p, \theta_0, \{N_A\}, t) = F_\lambda(\infty) \times \exp[-\tau_\lambda(z_p, \theta_0, \{N_A\}, t)] \quad . \tag{5-1}$$

Table 5. **Reaction rate coefficients used in the latest calculations. See Table A-1 for other reactions.**

Reaction	Old rate (used in first calculation)	New rate (used in second calculation)
$O_3 + NO \rightarrow NO_2 + O_2$	$2.3 \times 10^{-12} \exp(-1450/T)$	$2.1 \times 10^{-12} \exp(-1450/T)$
$O_3 + OH \rightarrow HO_2 + O_2$	$1.6 \times 10^{-12} \exp(-1000/T)$	$1.5 \times 10^{-12} \exp(-1000/T)$
$O_3 + HO_2 \rightarrow OH + 2O_2$	$1.0 \times 10^{-13} \exp(-1250/T)$	$7.3 \times 10^{-14} \exp(-1225/T)$
$O + HO_2 \rightarrow OH + O_2$	3.0×10^{-11}	3.5×10^{-11}
$HO_2 + HO_2 \rightarrow H_2O_2 + O_2$	$1.7 \times 10^{-11} \exp(-500/T)$	2.5×10^{-12}
$HO_2 + OH \rightarrow H_2O + O_2$	2.0×10^{-11}	3.0×10^{-11}
$NO + HO_2 \rightarrow NO_2 + OH$	$1.7 \times 10^{-11} \exp(-1000/T)$	8.0×10^{-12}
$N + O_3 \rightarrow NO + O_2$	$5.0 \times 10^{-12} \exp(-650/T)$	$2.0 \times 10^{-11} \exp(-1070/T)$
$O(^1D) + M \rightarrow O + M$	$2.0 \times 10^{-11} \exp(107/T)$	$2.2 \times 10^{-11} \exp(99/T)$[a]
$NO + ClO \rightarrow NO_2 + Cl$	2.2×10^{-11}	$1.0 \times 10^{-11} \exp(200/T)$
$ClO + ClO \rightarrow Cl + OClO$	$1.5 \times 10^{-13} \exp(-1238/T)$	$2.1 \times 10^{-12} \exp(-2200/T)$
$ClO + ClO \rightarrow 2Cl + O_2$	$4.5 \times 10^{-13} \exp(-1238/T)$	$5.0 \times 10^{-13} \exp(-1238/T)$[b]
$ClO + ClO \rightarrow Cl + ClO_2$	$9.0 \times 10^{-13} \exp(-1238/T)$	$1.0 \times 10^{-12} \exp(-1238/T)$
$OH + HCl \rightarrow H_2O + Cl$	$2.8 \times 10^{-12} \exp(-400/T)$	$3.0 \times 10^{-12} \exp(-425/T)$
$O + OClO \rightarrow ClO + O_2$	5.0×10^{-13}	$2.0 \times 10^{-11} \exp(-1100/T)$
$Cl + OH \rightarrow HCl + O$	$2.0 \times 10^{-12} \exp(-1878/T)$	$1.0 \times 10^{-11} \exp(-2970/T)$
$Cl + HNO_3 \rightarrow HCl + NO_3$	6.0×10^{-15}	$1.0 \times 10^{-11} \exp(-2170/T)$
$ClONO_2 + O \rightarrow ClO + NO_3$	$5.0 \times 10^{-12} \exp(-840/T)$	$3.0 \times 10^{-12} \exp(-808/T)$
$ClO + NO_2 \xrightarrow{M} ClONO_2$	$5.1 \times 10^{-33} \exp(1030/T)$	$\dfrac{3.3 \times 10^{-23} T^{-3.34}}{1 + 8.7 \times 10^{-9} T^{-0.6} M^{0.5}}$

[a] Differs from value given by Hudson (1977).

[b] No recommendation for this rate is given by Hudson (1977).

$F_\lambda\, d\lambda$ is the flux of photons in the wavelength interval $d\lambda$ about λ, and $F_\lambda(\infty)\, d\lambda$ represents the solar flux at the top of the atmosphere. The optical depth τ_λ is given by

$$\tau_\lambda\left(z_p,\theta_0,\{N_A\},t\right) \equiv \int_{z_p}^{\infty} \sum_A N_A(z,t)\ \sigma_T^A[\lambda,T(z)]\ \sec\ \theta_0(t)\ dz\ . \tag{5-2}$$

In Eq. (5-2) the summation on A includes all atmospheric absorbers, each having number density $N_\lambda(z,t)$ and a total absorption cross section $\sigma_T^\lambda[\lambda,T(z)]$. Most generally, $\sigma_T^\lambda[\lambda,T(z)]$ is a function of the temperature $T(z)$.

The photodissociation rate for transforming species i to species j is denoted by

$$J_{i\to j}(z_p,\theta_0,t)\ N_i(z_p,t)\ ,$$

where

$$J_{i\to j}(z_p,\theta_0,t) \equiv \int_{\text{all }\lambda} \sigma_D^i[j,\lambda,T(z_p)]\ F_\lambda(z_p,\theta_0,\{N_A\},t)\ d\lambda\ . \tag{5-3}$$

The microscopic photodissociation cross section $\sigma_D^i[j,\lambda,T(z_p)]$ is often written in terms of the quantum yield $Q_\lambda(i\to j)$ as

$$\sigma_D^i[j,\lambda,T(z_p)] \equiv \sigma_T^i[\lambda,T(z_p)]\ Q_\lambda(i\to j)\ . \tag{5-4}$$

It should be noted that significant uncertainties remain in the data used to calculate the photodissociation coefficients in the models. For example, major uncertainties remain in the branching of O_3 photolysis near 310 nm to either $O(^3P)$ or $O(^1D)$, in the branching and quantum yield for NO_3 photolysis, and in the methodology for calculating the photolysis of species having banded or line absorption-cross-section structures, such as O_2 or NO.

When molecular multiple scattering and surface albedo are included in the radiative transfer calculation, Eq. (5-1) is no longer the solution of the radiative transfer equation. However, the flux in the direct solar beam F_λ^s is given by an equation similar to (5-1):

$$F_\lambda^s(z_p,\theta_0,\{N_A\},t) = F_\lambda(\infty) \times \exp[-\tau_\lambda^s(z_p,\theta_0,\{N_A\},t)]\ , \tag{5-5}$$

where the optical depth along the slant path, τ_λ^s, is given by

$$\tau_\lambda^s\left(z_p,\theta_0,\{N_A\},t\right) \equiv \int_{z_p}^{\infty} \sum_A N_A(z,t)\ \sigma_T^A[\lambda,T(z)]\ \sec\ \theta_0(t)\ dz + \int_{z_p}^{\infty} \sum_i N_i(z,t)\ \sigma_R^i(\lambda)\ \sec\ \theta_0(t)\ dz\ . \tag{5-6}$$

In (5-6) the summation on i includes all atmospheric species, and σ_R^i is the Rayleigh-scattering cross section for species i. $F_\lambda^s(z_p,\theta_0,\{N_\lambda\},t)$ in (5-5) differs from $F_\lambda(z_p,\theta_0,\{N_\lambda\},t)$ as defined by (5-1) in that attenuation due to both absorption and scattering is included in (5-5), whereas only absorption is included in (5-1).

The photodissociation coefficient also depends upon the scattered (diffuse) radiation given by

$$J_{i\to j}(z_p,\theta_0,t) \equiv \int_{\text{all }\lambda} \sigma_D^i[j,\lambda,T(z_p)] \times \left[F_\lambda^s(z_p,\theta_0,N_A,t) + \int_{4\pi} I_\lambda(z_p,\omega)\ d\omega\right] d\lambda\ , \tag{5-7}$$

where I_λ is the specific intensity of the diffuse radiation and ω is the solid angle. Including the effect of molecular multiple scattering and surface albedo in the calculation is simply expressed by changing the value of F_λ appearing in (5-3). For clarity we define

$$F_\lambda^{MS}(\text{multiple scattering}) \equiv F_\lambda^s\left(z_p,\theta_0,\{N_A\},t\right) + \int_{4\pi} I_\lambda(z_p,\omega)\ d\omega\ . \tag{5-8}$$

Henceforth, F_λ^{PA} (pure absorption) will refer to the flux defined by (5-1). Aside from substituting F_λ^{MS} in place of F_λ^{PA} in (5-3), all other aspects of the photodissociation rate calculation are the same as for the purely absorbing molecular atmosphere.

The effect of multiple scattering was incorporated into the photodissociation rate calculation by applying correction factors to the flux F_λ used in the pure absorption calculation. These correction factors, which are given by the ratio $F_\lambda^{MS}/F_\lambda^{PA}$, were computed for the unperturbed species profiles using the same detailed solar radiation model as Luther and Gelinas (1976). A separate factor was computed for each of the 44 levels and for each of the 148 wavelength intervals between 133 and 735 nm. Different sets of correction factors were computed for each assumed value of surface albedo A_s using a solar zenith angle of 45°.

Correction factors for a solar zenith angle of 45° are qualitatively similar to, although somewhat larger than, those computed by Luther and Gelinas (1976) for $\theta = 60°$. The correction factors are nearly constant with height above 20 km, but they may vary significantly with height in the region below 20 km, which is where most scattering events occur.

Including multiple scattering in the photodissociation rate calculation affects the photodissociation coefficients, the ambient species concentration profiles, and the model sensitivity to perturbations by NO_x and ClX pollutants. Each of these effects is discussed separately below.

Photodissociation Coefficients

Table 6 compares photodissociation coefficients for pure absorption and for multiple scattering computed for the same ambient model atmosphere. These coefficients were computed for a solar zenith angle of 45° and a surface albedo of 0.25. For reactions with strong absorption at wavelengths less than 290 nm, multiple scattering has the most significant effect on the photodissociation coefficients below 25 km. The coefficients are changed only slightly above 25 km. Reactions with strong absorption at wavelengths greater than 290 nm show enhancement at all altitudes due to multiple scattering. At altitudes above 10 km, including multiple scattering increases the photodissociation rates by a factor of 1.27–1.46 for O_3, 1.56–1.64 for NO_2, 1.23–1.67 for $ClNO_2$, 1.07–1.65 for $ClONO_2$, and 1.33–1.60 for OClO. There is less than a 7% change in the photodissociation rates above 30 km for O_2, HNO_3, H_2O_2, HO_2, ClO, CF_2Cl_2, and $CFCl_3$. At lower altitudes there is significant enhancement for several of these species due to multiple scattering. For example, at 10 km the photodissociation rate is increased by a factor of 1.59 for HNO_3, 1.59 for H_2O_2, and 1.46 for ClO.

Species Concentration Profiles

The concentration profiles for selected O_x, HO_x, and ClX species are shown in Figs. 17–20 for the ambient atmosphere prior to inclusion of multiple scattering. These figures define the reference conditions for assessing the fractional change in concentration caused by multiple scattering.

The changes in concentration of chemical species due to multiple scattering relative to the pure absorption calculation for a surface albedo of 0.25 are shown in Figs. 21–24. Figure 21 shows the effect of multiple scattering on O_x species concentrations. The large percentage increase in $O(^1D)$ near 10 km occurs where the ambient concentration is very small; nevertheless, it has a significant effect on atmospheric chemistry. The increases in $O(^3P)$ and $O(^1D)$ in the 20-to-30-km region are due to increased photolysis of O_3. Because of differences in ambient concentrations, a small percentage decrease in O_3 causes large percentage increases in the other species. The increase in $O(^3P)$ near 40 km is due primarily to increased photolysis of NO_2. Ozone at this height is increased largely as a result of the reduction in the efficiency of the NO_x catalytic destruction cycle caused by the increased rate of NO_2 photolysis. The ratio of column-integrated total O_3 computed with multiple scattering to that computed with pure absorption is 0.90.

Figure 22 shows the effect of multiple scattering on HO_x species. Increased OH below 30 km results from increased rates for the reaction $HNO_3 \xrightarrow{h\nu} OH + NO_2$ and $H_2O_2 \xrightarrow{h\nu} 2OH$. Since the concentration of H_2O_2 below 35 km is much larger than that of the other hydrogen oxide species, a small percentage decrease in H_2O_2 can cause a much larger percentage change in OH and HO_2, as evidenced near 10 km. The increase in $O(^1D)$ leads to an increase in the production rate of HO_x by $O(^1D) + H_2O \rightarrow 2OH$, yet there is actually a decrease in HO_x in the region around 10 km. This occurs because conversion of H_2O_2 to 2OH by photolysis substantially increases the HO_x destruction rate through the reactions $OH + HO_2 \rightarrow H_2O + O_2$ and $OH + H_2O_2 \rightarrow H_2O + HO_2$.

Figure 23 shows the effect of multiple scattering on NO_x species. Because the NO_2 photolysis rate is increased, the concentration of NO and the ratio NO/NO_2 are both increased at all altitudes. There is very little HNO_3 above 30 km, so NO_2 decreases in this region because of increased photolysis. Below 30 km, NO_2 increases because of increased photolysis of HNO_3, which is the most plentiful NO_x species in this region.

Table 6. Comparison of photodissociation rates calculated with and without multiple scattering. The values correspond to a solar zenith angle of 45° and half-sun to account for day-night averaging.

Reaction	Altitude (km)	J_{PA} (s^{-1})	J_{MS} (s^{-1})	J_{MS}/J_{PA}
$O_3 + h\nu \rightarrow O(^3P) + O_2$	40	2.74×10^{-4}	3.49×10^{-4}	1.27
	30	2.40×10^{-4}	3.18×10^{-4}	1.33
	20	2.06×10^{-4}	2.95×10^{-4}	1.43
	10	2.01×10^{-4}	2.94×10^{-4}	1.46
$O_3 + h\nu \rightarrow O(^1D) + O_2$	40	9.10×10^{-4}	9.09×10^{-4}	1.00
	30	5.30×10^{-5}	5.30×10^{-5}	1.01
	20	7.49×10^{-6}	9.66×10^{-6}	1.29
	10	5.44×10^{-6}	8.26×10^{-6}	1.52
$O_2 + h\nu \rightarrow O + O$	40	3.01×10^{-10}	3.01×10^{-10}	1.00
	30	1.83×10^{-11}	1.74×10^{-11}	0.95
	20	5.73×10^{-14}	4.42×10^{-14}	0.77
	10	7.64×10^{-20}	8.91×10^{-20}	1.17
$NO_2 + h\nu \rightarrow NO + O$	40	4.97×10^{-3}	7.73×10^{-3}	1.56
	30	4.85×10^{-3}	7.67×10^{-3}	1.58
	20	4.74×10^{-3}	7.74×10^{-3}	1.63
	10	4.72×10^{-3}	7.74×10^{-3}	1.64
$HNO_3 + h\nu \rightarrow OH + NO_2$	40	3.50×10^{-5}	3.51×10^{-5}	1.00
	30	4.66×10^{-6}	4.54×10^{-6}	0.97
	20	3.25×10^{-7}	4.54×10^{-7}	1.40
	10	2.61×10^{-7}	4.16×10^{-7}	1.59
$H_2O_2 + h\nu \rightarrow 2OH$	40	2.11×10^{-5}	2.14×10^{-5}	1.01
	30	3.79×10^{-6}	4.07×10^{-6}	1.07
	20	1.30×10^{-6}	1.85×10^{-6}	1.42
	10	1.10×10^{-6}	1.75×10^{-6}	1.59
$HO_2 + h\nu \rightarrow OH + O$	40	6.50×10^{-5}	6.49×10^{-5}	1.00
	30	3.35×10^{-6}	3.19×10^{-6}	0.95
	20	1.05×10^{-8}	8.08×10^{-9}	0.77
	10	1.55×10^{-14}	1.81×10^{-14}	1.17
$ClONO_2 + h\nu \rightarrow ClO + NO_2$	40	2.21×10^{-4}	2.37×10^{-4}	1.07
	30	5.09×10^{-5}	6.83×10^{-5}	1.34
	20	3.41×10^{-5}	5.46×10^{-5}	1.60
	10	3.28×10^{-5}	5.40×10^{-5}	1.65
$ClNO_2 + h\nu \rightarrow Cl + NO_2$	40	6.03×10^{-4}	7.42×10^{-4}	1.23
	30	3.41×10^{-4}	4.89×10^{-4}	1.43
	20	2.73×10^{-4}	4.46×10^{-4}	1.63
	10	2.64×10^{-4}	4.42×10^{-4}	1.67
$OClO + h\nu \rightarrow ClO + O(^1D)$	40	2.27×10^{-3}	3.02×10^{-3}	1.33
	30	1.53×10^{-3}	2.29×10^{-3}	1.50
	20	1.40×10^{-3}	2.23×10^{-3}	1.59
	10	1.39×10^{-3}	2.23×10^{-3}	1.60
$ClO + h\nu \rightarrow Cl + O$	40	1.61×10^{-3}	1.62×10^{-3}	1.01
	30	1.77×10^{-4}	1.78×10^{-4}	1.01
	20	2.37×10^{-5}	2.86×10^{-5}	1.21
	10	1.57×10^{-5}	2.29×10^{-5}	1.46

Table 6. (continued)

Reaction	Altitude (km)	J_{PA} (s^{-1})	J_{MS} (s^{-1})	J_{MS}/J_{PA}
$CF_2Cl_2 + h\nu \rightarrow 2Cl$	40	5.12×10^{-7}	5.14×10^{-7}	1.00
	30	6.17×10^{-8}	5.83×10^{-8}	0.94
	20	1.92×10^{-10}	1.45×10^{-10}	0.76
	10	1.09×10^{-16}	1.28×10^{-16}	1.17
$CFCl_3 + h\nu \rightarrow 2.5\ Cl$	40	4.39×10^{-6}	4.40×10^{-6}	1.00
	30	5.20×10^{-7}	4.94×10^{-7}	0.95
	20	1.79×10^{-9}	1.36×10^{-9}	0.76
	10	1.53×10^{-15}	1.78×10^{-15}	1.16

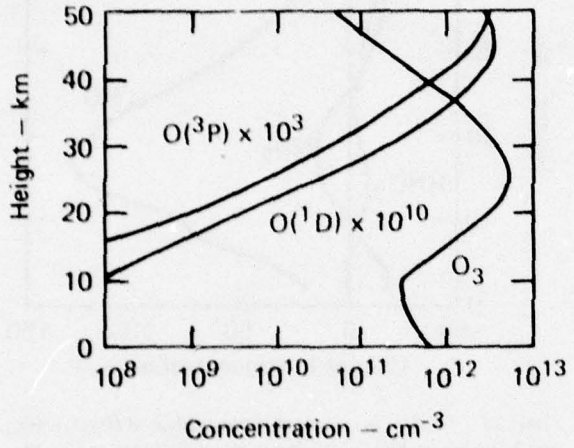

Figure 17. **Calculated concentration profiles for $O(^3P)$, $O(^1D)$, and O_3 for the ambient atmosphere, without multiple scattering.**

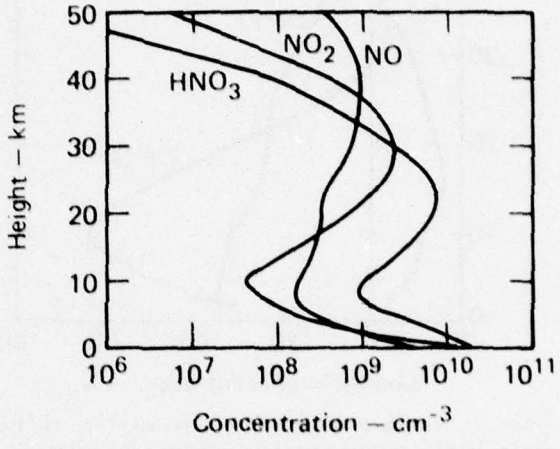

Figure 19. **Calculated concentration profiles for HNO_3, NO_2, and NO for the ambient atmosphere, without multiple scattering.**

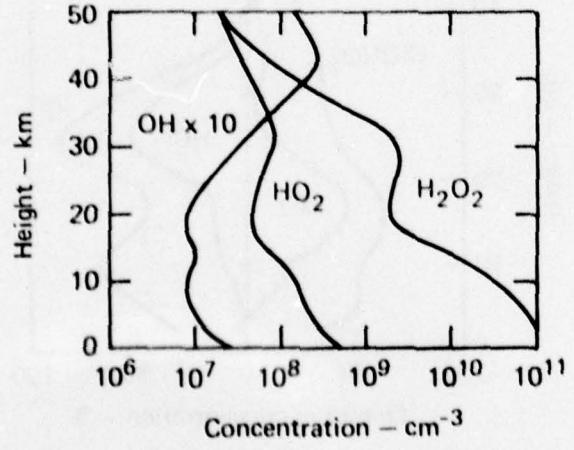

Figure 18. **Calculated concentration profiles for OH, HO_2, and H_2O_2 for the ambient atmosphere, without multiple scattering.**

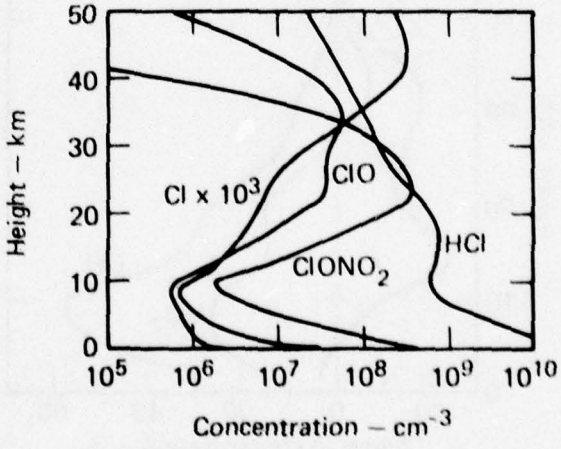

Figure 20. **Calculated concentration profiles for Cl, ClO, $ClONO_2$, and HCl for the ambient atmosphere, without multiple scattering.**

Multiple scattering has a large effect on NO_2 photolysis but a negligible effect on HNO_3 above 30 km (see Table 6). The reduction in HNO_3 above 30 km, therefore, is due to a decrease in the HNO_3 production rate brought about primarily by the decrease in NO_2. The percentage decrease in NO_2 is greater than the increase in OH, consequently there is a net decrease in the rate of the reaction $OH + NO_2 \rightarrow HNO_3$. The ratio of total column abundance computed with multiple scattering to that computed with pure absorption is 0.94 for NO_2 and 1.36 for NO.

The effect of multiple scattering on species containing chlorine is shown in Fig. 24. The concentration of $ClONO_2$ is reduced 35–45% between 20 and 30 km, which is the region of its maximum concentration. Photolysis of $ClONO_2$ affects several other chlorine-containing species through a complex chain of reactions. Certain key reactions are

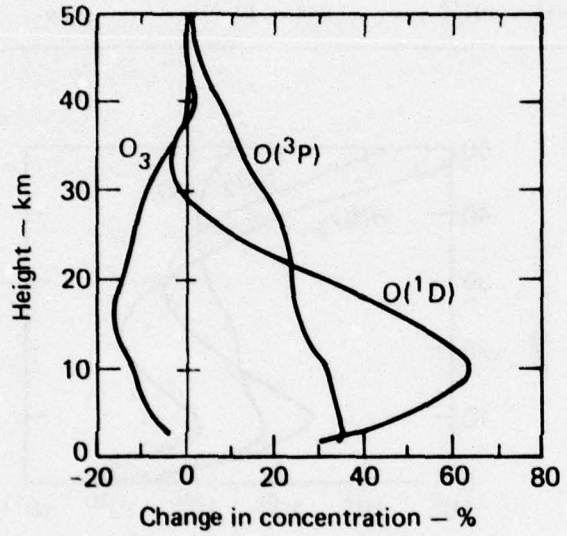

Figure 21. **Changes in calculated concentrations of O_3, $O(^3P)$, and $O(^1D)$ when multiple scattering is included (compare Fig. 17).**

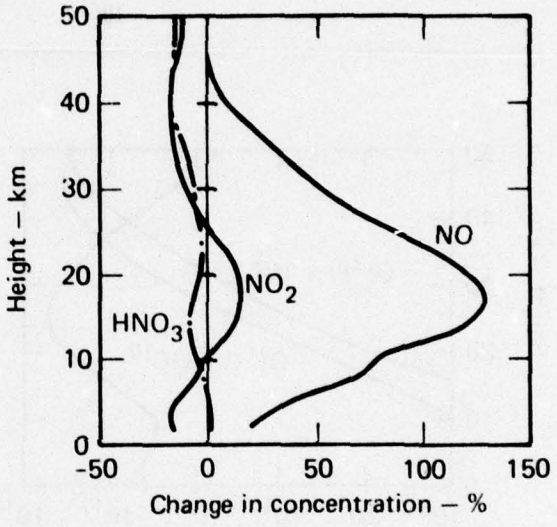

Figure 23. **Changes in calculated concentrations of HNO_3, NO_2, and NO when multiple scattering is included (compare Fig. 19).**

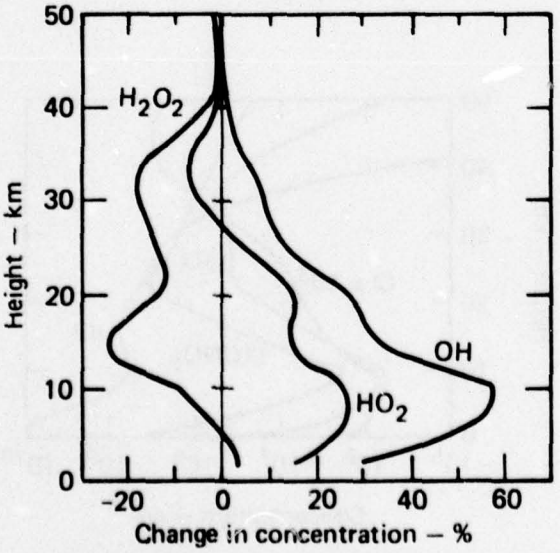

Figure 22. **Changes in calculated concentrations of H_2O_2, HO_2, and OH when multiple scattering is included (compare Fig. 18).**

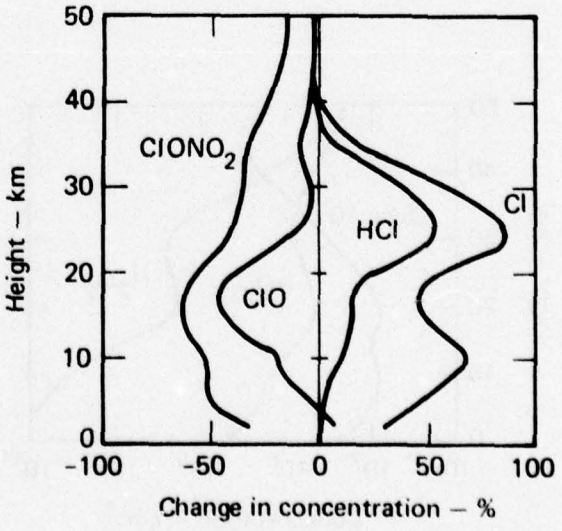

Figure 24. **Changes in calculated concentrations of $ClONO_2$, ClO, HCl, and Cl when multiple scattering is included (compare Fig. 20).**

$$ClONO_2 \xrightarrow{h\nu} ClO + NO_2 ,$$

$$ClO + NO \rightarrow Cl + NO_2 ,$$

$$Cl + CH_4 \rightarrow HCl + CH_3 .$$

The peak concentration of $ClONO_2$ occurs near 25 km, so photolysis of $ClONO_2$ acts as a strong source of ClO in this region. The large increase in NO between 20 and 30 km tends to shift ClO to Cl, leading to a net decrease in ClO in this region and an increase in Cl. This leads to an increase in HCl production through reaction of Cl with CH_4. The decrease in $ClONO_2$ above 40 km occurs because of the effect of decreased NO_2 on the $ClONO_2$ production rate ($ClO + NO_2 \rightarrow ClONO_2$).

Model Sensitivity

In addition to affecting the concentration of many species in the model, multiple scattering affects the model sensitivity to perturbations. This was tested for an NO_x perturbation and a CFM perturbation. The NO_x perturbation was an injection of NO_x at a rate of 1000 molecules/cm^3·s as NO_2 over a 1-km-thick layer centered at 20 km. The change in total ozone at steady state is shown in Table 7 for both the pure absorption and the multiple scattering calculations. The ratio of the percent change in ozone with multiple scattering to the percent change with pure absorption, R = MS/PA, is also presented in Table 7. Including multiple scattering has very little effect on the model sensitivity to an NO_x injection at 20 km (R = 1.01) in spite of significant differences in the ambient species profiles. Increasing the surface albedo from 0.25 to 0.75 also has a very small effect on the model sensitivity (R = 1.03). Consequently, the choice of A_s used in the photodissociation rate calculations is not a critical factor in NO_x perturbation studies which include multiple scattering where one is primarily interested in the change in total ozone. It should be noted, however, that the choice of A_s significantly affects the photodissociation rates and the ambient species profiles (see Luther and Wuebbles 1976 for details).

The effect of variations in model chemistry on the above results was tested first by varying the reaction rate for $OH + HO_2 \rightarrow H_2O + O_2$, then by making the changes listed in Table 5. A recent measurement by Burrows et al. (1977) gives a value of 5.1×10^{-11} for the rate coefficient of $OH + HO_2$. Chang and Kaufman (1977) report an upper limit of 5×10^{-11} for the rate coefficient, whereas their experimental results are best fitted by using a value of 2×10^{-11} (Chang and Kaufman 1977). The calculations described above were repeated using a value of 5.1×10^{-11}, and the results are presented in Table 7. Changing this rate coefficient significantly increases the ozone reduction due to this NO_x perturbation, but there is no significant change in R (MS/PA).

When the new rate coefficients listed in Table 5 were incorporated into the model, the effect of the NO_x injection changed from a reduction to an increase in total ozone. Including multiple scattering in this case significantly enhanced the ozone increase. The change in ΔO_3 due to including multiple scattering, however, is small compared to the change in ΔO_3 resulting from changing the model chemistry.

For the CFM perturbation, we consider the steady-state ozone reduction due to CFMs at the 1975 release rate, which is assumed to be 290 kilotonnes/yr for $CFCl_3$ and 425 kilotonnes/yr for CF_2Cl_2. Results for both the pure absorption and multiple scattering calculations are presented in Table 8. For the CFM perturbation, including multiple scattering increases the ozone reduction by a factor of 1.16 for a surface albedo of 0.25. As in the case of the NO_x perturbation, changing the surface albedo has little effect on the change in total ozone, e.g., the ozone reduction increases by a factor of

Table 7. **Change in total ozone due to an NO_x injection of 1000 molecules/cm^3·s as NO_2 over a 1-km-thick layer centered at 20 km. R is the ratio ΔO_3 (multiple scattering)/ΔO_3 (pure absorption).**

Case	ΔO_3 (%)	R
(a) OH + HO_2 rate coefficient = 2×10^{-11}:		
Pure absorption	-2.34	–
Multiple scattering, A_s = 0.25	-2.36	1.01
Multiple scattering, A_s = 0.75	-2.40	1.03
(b) OH + HO_2 rate coefficient = 5.1×10^{-11}:		
Pure absorption	-3.44	–
Multiple scattering A_s = 0.25	-3.50	1.02
(c) Rate changes given in Table 5:		
Pure absorption	-0.07	–
Multiple scattering, A_s = 0.25	0.39	1.9[a]

[a]Ratio is not meaningful for such small quantities.

1.17 relative to the pure absorption calculation using a surface albedo of 0.75. When the rate coefficient for OH + HO_2 is increased to 5.1×10^{-11}, the ozone reduction with multiple scattering increases by a factor of 1.22 (Table 8) relative to the pure absorption calculation.

Using the rate coefficients in Table 5 approximately doubles the predicted ozone reduction due to CFMs. In this case, including multiple scattering still causes a significant increase in ΔO_3 (i.e., R = 1.21).

The effect of multiple scattering on species concentration profiles illustrates the importance of including multiple scattering when comparing model-derived concentration profiles with observational data. For the cases studied, the effect on model sensitivity of including multiple scattering ranged from no change in ΔO_3 compared to the pure absorption calculation to a significant increase in ΔO_3 depending upon the model chemistry. The change in ΔO_3 due to multiple scattering, however, was small compared to the change in ΔO_3 resulting from varying chemical reaction rates.

Table 8. **Change in total ozone due to CFMs at the 1975 release rate. R is the ratio ΔO_3(multiple scattering)/ΔO_3 (pure absorption).**

Case	ΔO_3 (%)	R
(a) OH + HO_2 rate coefficient = 2×10^{-11}:		
Pure absorption	-6.31	–
Multiple scattering, A_s = 0.25	-7.31	1.16
Multiple scattering, A_s = 0.75	-7.41	1.17
(b) OH + HO_2 rate coefficient = 5.1×10^{-11}:		
Pure absorption	-3.86	–
Multiple scattering, A_s = 0.25	-4.70	1.22
(c) Rate changes given in Table 5:		
Pure absorption	-11.95	–
Multiple scattering, A_s = 0.25	-14.42	1.21

2.6 Effect of Changes in Stratospheric Water Vapor on Ozone Reduction Estimates *

The potential threat to the earth's ozone layer of supersonic transports' engine effluents and chlorofluoromethanes has received a great deal of attention. Early estimates of the potential ozone reduction considered NO_x or CFM pollutants alone. However, recent assessments have also considered the possibility of a simultaneous change in stratospheric water-vapor abundance (Liu et al. 1976, Duewer et al. 1977b). Both of these studies showed that increased water vapor caused enhanced ozone reduction for the then accepted rate coefficients.

The H_2O emission index (1.3 kg/kg fuel) is much larger than the NO_x emission index (0.018 kg/kg fuel) for SSTs (Grobecker et al. 1974). An annual fuel consumption rate of 10^{11} kg/yr for a fleet of SSTs at a cruise altitude of 20 km would increase the stratospheric water-vapor burden approximately 15% (Grobecker et al. 1974, p. 52). Changes in atmospheric composition due to stratospheric perturbations might affect stratospheric water-vapor abundance indirectly by changing the temperature of the tropical tropopause. Since the saturation vapor pressure of H_2O doubles for a rise of 4 K in tropopause temperature (Ellsaesser 1974, Liu et al. 1976), this could have a larger effect than the direct injection of water vapor in the stratosphere.

The most thorough study to date of the effect of changes in water vapor abundance on the estimated ozone reduction by NO_x and CFM pollutants is that of Liu et al. (1976), who used a one-dimensional transport-kinetics model for their calculations. Imposing an increase in the water-vapor mixing ratio of 1 ppmv at the tropopause caused an additional reduction in total ozone of 0.3–1.0% (from their Fig. 12) for an NO_x perturbation and 0.4–1.4% (from their Fig. 5) for a CFM perturbation; the range cited reflects variation of the reaction rate for OH + $HO_2 \rightarrow H_2O + O_2$ between 2×10^{-10} and 2×10^{-11} cm^3/s. The largest sensitivity to changes in water vapor abundance was associated with the slow rate for this reaction. Although the change in stratospheric water-vapor abundance was postulated to be due to a change in tropopause temperature, the temperature profile was fixed, and the effect of changes in temperature on chemical reaction rates was not included in their calculations. We

*See Luther and Duewer (1977).

have expanded upon the work of Liu et al. (1976) by including temperature changes in our calculations.

In order to include the effect of changes in temperature, we used the one-dimensional transport-kinetics model coupled with a stratospheric radiative transfer model. The transport-kinetics model used in this study included multiple scattering in the photodissociation rate calculation assuming a surface albedo of 0.25. Calculations were made using the model chemistry listed in Table A-1 of Appendix A and the old rates listed in Table 5, then the calculations were repeated using the new rates listed in Table 5.

A stratospheric radiative transfer model (Luther et al. 1977a) is used to compute the temperature profile above 12 km. The temperature profile below 12 km is specified. The model includes solar absorption and long-wave interaction by O_3, H_2O, and CO_2 along with solar absorption by NO_2. The radiative transfer model is the same as Ramanathan's (1974) except that we have added solar absorption by NO_2. There are several differences between this model and Ramanathan's latest model (Ramanathan 1976), as described in detail in his paper.

We assume that the change in surface temperature is negligible. The change in surface temperature associated with a 10% reduction in ozone due to CFMs at a tropospheric concentration of approximately 2 ppb was computed to be 0.3 K or less by Ramanathan (1975) and by Reck (1976). Ozone reductions up to 30% due to NO_x injections were computed to cause a change of less than 0.1 K in surface temperature by Ramanathan et al. (1976). Neglecting changes in surface temperature of this magnitude has no significant effect on the results.

The tropospheric distribution of H_2O is based on Mastenbrook (1974). The stratospheric mixing ratio of H_2O is assumed to be 4.3 ppmv. Liu et al. (1976) computed the stratospheric distribution of H_2O by specifying the mixing ratio at the tropopause and assuming that methane oxidation increases the water content of the upper stratosphere. Their calculations showed that changing the water-vapor mixing ratio at the tropopause by some amount ΔH_2O resulted in the same change in mixing ratio at altitudes up to 50 km. Above 50 km, the change in local H_2O mixing ratio was less than ΔH_2O at the tropopause. In our calculations, when the stratospheric water-vapor mixing ratio is changed, the same ΔH_2O is applied at all altitudes above 13 km, thus leading to a change in stratospheric water-vapor abundance similar to that of Liu et al. (1976).

Large-scale dynamical processes are neglected in the determination of the temperature profile. These processes have a significant effect on the temperature profile near the tropopause. For our application here, the ability of the model to compute the *change* in temperature is more important than the particular ambient temperature profile. Since changes in atmospheric dynamics brought about by changes in temperature structure and in the radiation balance are not included in the model (or any other transport-kinetics model at the present time), there may be significant errors in the predicted temperature change in the lower stratosphere. Consequently, in discussing the results, we want to emphasize their qualitative nature rather than the quantitative details.

NO_x Injection

The effect of a change in stratospheric water vapor on total ozone was computed for cases with and without a simultaneous NO_x injection in order to test the sensitivity of the results to the magnitude of the NO_x perturbation. We consider an NO_x injection rate of 1000 molecules/cm^3·s as NO_2 over a 1-km-thick layer centered at 20 km, which is a larger injection rate than that used by Liu et al. (1976). Calculations were first performed using the fixed ambient-temperature profile in order to verify qualitatively the results obtained by Liu et al. (1976), then the calculations were repeated with temperature feedback included. The results using the Chang (1976) diffusion coefficients are presented in Fig. 25, which shows the change in total ozone at steady state as a function of the change in stratospheric water vapor mixing ratio. This calculation did not include the recent changes in chemistry listed in Table 5.

With no change in H_2O, this NO_2 injection causes a reduction in total ozone of 2.25% with a fixed temperature profile and 2.03% with temperature feedback. Temperature feedback, therefore, has approximately a 10% restoring effect on the change in total ozone, which is consistent with our earlier results (Luther et al. 1977a).

The results using a fixed temperature profile are similar to those of Liu et al. (1976) for the slow reaction rate of OH + HO_2. The slope of ΔO_3 versus ΔH_2O is -0.42%/ppmv (at $\Delta H_2O = 0$) with the NO_x injection and -0.64%/ppmv with no NO_x injection as compared to Liu et al.'s value of -1.0% ppmv, thus our model is less sensitive to changes in water vapor abundance. The results also demonstrate that the model sensitivity depends upon the amount of NO_x present. Since the eddy diffusion profile affects the background NO_x, the results can be expected to depend also upon the eddy diffusion profile used in the calculation.

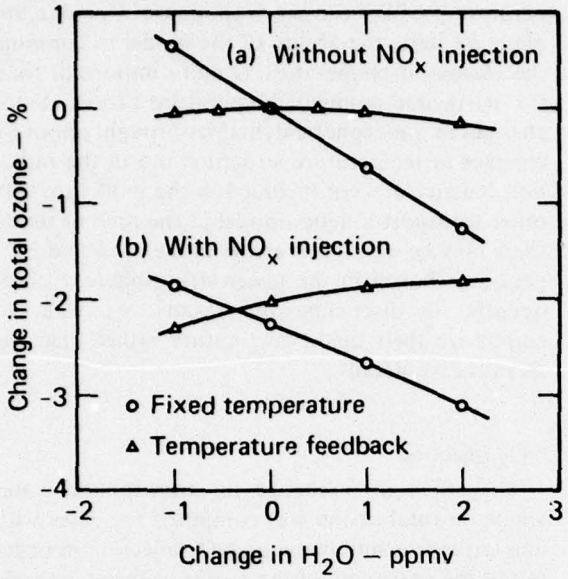

Figure 25. **Change in total ozone vs change in water-vapor mixing ratio above 13 km, computed using the Chang (1976) K_z profile with and without an NO_x injection of 1000 molecules/cm^3·s of NO_2 over a 1-km-thick layer centered at 20 km: (a) without NO_x injection, (b) with NO_x injection.**

When temperature feedback is included, the results change dramatically. An increase in stratospheric water vapor now causes less reduction in total ozone, the slope being 0.21%/ppmv for this NO_x injection. With no NO_x injection, the model is virtually insensitive to changes in water vapor.

An analysis of the effect of changes in water vapor with fixed temperature is helpful in showing why temperature feedback has such a significant effect. Profiles of the change in ozone concentration due to the NO_x injection at 20 km are shown in Fig. 26a for various values of ΔH_2O. Destruction of odd oxygen is dominated by HO_x reactions in the regions 10–20 km and 40–50 km. In the 10-to-20-km region, odd-oxygen destruction is dominated by the reactions

$$OH + O_3 \rightarrow HO_2 + O_2 \ . \qquad (6\text{-}1)$$

$$HO_2 + O_3 \rightarrow OH + 2O_2 \qquad (6\text{-}2)$$

$$(\text{net: } 2O_3 \rightarrow 3O_2) \ .$$

whereas in the 40-to-50-km region the dominant reactions are

$$O + OH \rightarrow O_2 + H \ . \qquad (6\text{-}3)$$

$$H + O_2 \rightarrow HO_2 \ . \qquad (6\text{-}4)$$

$$HO_2 + O \rightarrow OH + O_2 \qquad (6\text{-}5)$$

$$(\text{net: } 2O \rightarrow O_2) \ .$$

Increasing the water-vapor mixing ratio increases the ozone destruction rate in these regions because HO_x increases (Fig. 26a). Although relatively large percentage changes occur in the ozone concentration above 40 km, these changes make a relatively small contribution to the change in total ozone because of the small O_3 concentration above 40 km.

The NO_x catalytic cycle dominates odd oxygen destruction in the middle stratosphere. Increased HO_x decreases ozone destruction in the 25-to-35-km region because of two processes. First, more NO_x is converted to HNO_3 by the reaction $NO_2 + OH$, thus inhibiting the NO_x catalytic cycle. Secondly, increased HO_x leads to interference with NO_x cycle destruction of odd oxygen through the reactions

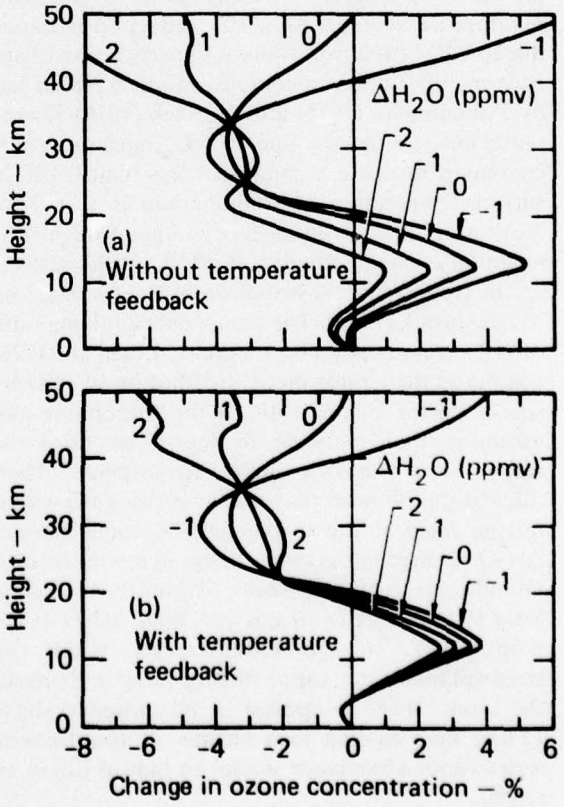

Figure 26. **Change in ozone concentration vs height due to the NO_x injection of Fig. 25, calculated for several values of ΔH_2O, with and without temperature feedback.**

$$HO_2 + NO \cdot NO_2 + OH \qquad (6\text{-}6)$$

$$NO_2 \cdot NO + O \qquad (6\text{-}7)$$

$$(\text{net: } HO_2 \cdot OH + O) .$$

Since the rate of destruction of odd oxygen depends upon the amount of HO_x and NO_x in this region, the effect of changing the water-vapor mixing ratio will depend to some extent upon the magnitude of the NO_x injection.

Similar results for the calculation including temperature feedback are shown in Fig. 26b. Comparing Figs. 26a and 26b, we see in the latter less sensitivity to changes in water vapor above 40 km and in the region 10–20 km. However, the sensitivity is enhanced in the region 25–35 km. In order to demonstrate the effect of changes in water vapor and temperature on ozone more clearly, we introduce the quantity $DO_3(z)$ which is defined by

$$DO_3(z) = \frac{\Delta[O_3]_z}{O_3 \text{ (column)}} , \qquad (6\text{-}8)$$

where $\Delta[O_3]_z$ is the change in local ozone concentration, and O_3(column) is the unperturbed total ozone. The function $DO_3(z)$ represents the contribution per unit altitude to the change in total ozone. The change in total ozone is therefore given by the integral

$$\Delta O_3 = \int_0^{z_{max}} DO_3(z)\, dz . \qquad (6\text{-}9)$$

In other words, the area under the curve of $DO_3(z)$ versus z equals ΔO_3. In order to extract the contribution to DO_3 due expressly to changes in water-vapor mixing ratio, we introduce the expression $\Delta DO_3(H_2O)$, which is defined by

$$\Delta DO_3(H_2O) = DO_3(\Delta H_2O) - DO_3(\Delta H_2O = 0) , \qquad (6\text{-}10)$$

where $\Delta DO_3(H_2O)$ is a function of altitude (z), although the z dependence is not indicated. This function is plotted for several values of ΔH_2O in Fig. 27a for the case with fixed temperature and in Fig. 27b for the case with temperature feedback. Those regions in which changes in water vapor either increase or decrease ozone are clearly apparent. With fixed temperature the greatest contribution to the change in total ozone comes from the change in ozone concentration in the region 10–25 km, whereas with temperature feedback the greatest contribution comes from changes in the region 20–30 km. These differences are related to the sensitivity of various reaction rates to changes in temperature.

The changes in temperature due to the NO_x injection at 20 km along with changes in water-vapor mixing ratio are shown in Fig. 28. With no change in water vapor, NO_x injection causes a temperature increase in the vicinity of the tropopause (15 km) and a temperature decrease above 21 km. Increasing the water-vapor mixing ratio now decreases the temperature by varying amounts at all altitudes above 13 km. The ozone destruction reactions have positive activation energies, thus they are slowed when the temperature is decreased. In contrast, ozone production is a photolytic process nearly independent of temperature.

Reactions (6-1) and (6-2) have relatively high activation energies. Consequently, they are very sensitive to temperature change. As shown in Fig. 27, the ozone destruction due to enhanced water vapor in the region 10–20 km is greatly reduced due to the temperature decrease. The NO_x catalytic reactions, which dominate ozone destruction in the region 20–40 km, have moderate activation energies. Therefore, the decrease in ozone destruction in this region (which appears as enhanced ozone production in Fig. 27) is also significant, but it is not as large as in the region 10–20 km. Reactions (6-3), (6-4), and (6-5) have very low activation energies, so the region 40–50 km is least sensitive to changes in temperature.

The increase in stratospheric water vapor is postulated upon the assumption of an increase in the tropopause temperature. The calculation indeed shows (Fig. 28) an increase in temperature at the altitude of the tropopause (15 km) for $\Delta H_2O = 0$, which occurs because of increased solar absorption by NO_2 (Luther et al. 1977a). As ΔH_2O increases, the temperature at this level decreases, which is a negative feedback process limiting the change in H_2O. The tropopause temperature might also be affected by changes in surface temperature resulting from increased stratospheric water vapor, but this effect has not yet been included in the calculation. In order to accurately estimate the expected change in the temperature of the tropical tropopause and the change in the stratospheric water-vapor mixing ratio, we would need a multidimensional model

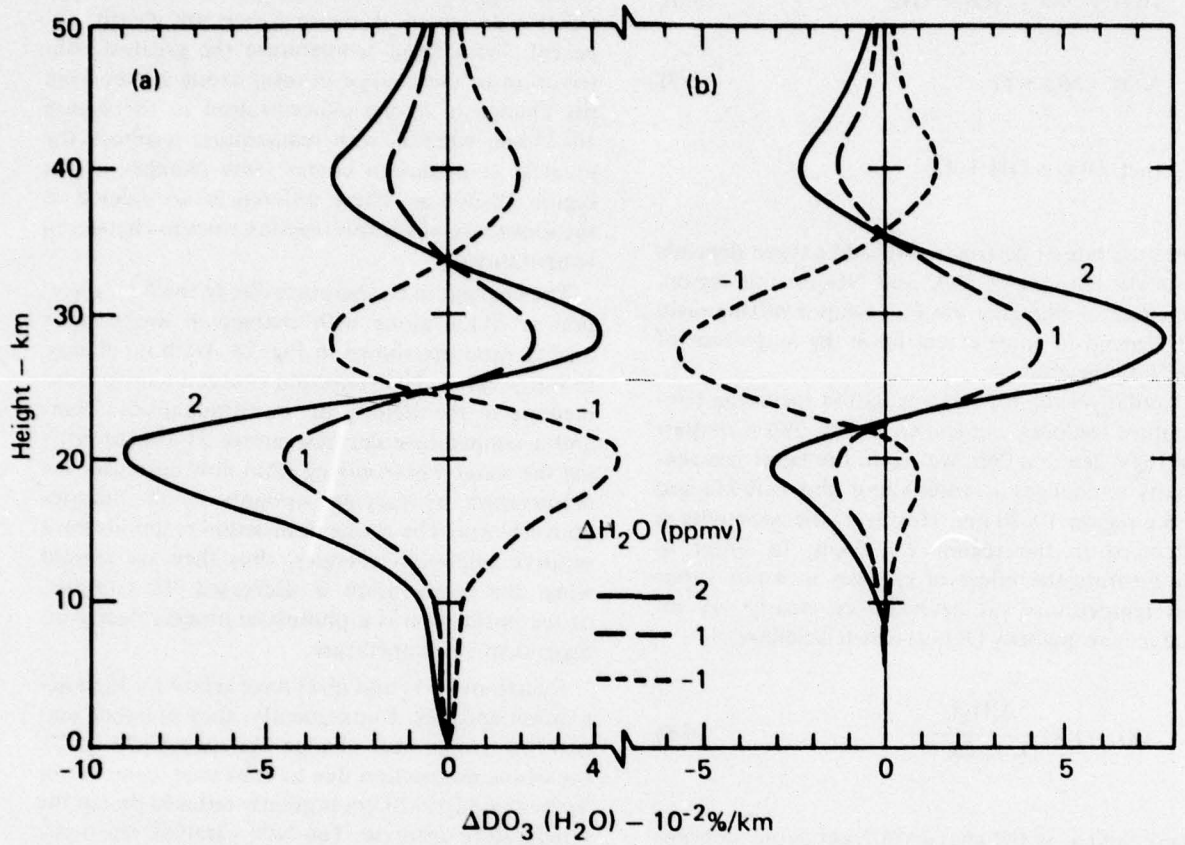

Figure 27. **Calculated profiles of $DO_3(H_2O)$ corresponding to various values of ΔH_2O using the Chang (1976) K_z profile for the case of the NO_x injection of Fig. 25: (a) with fixed temperature, (b) with temperature feedback.**

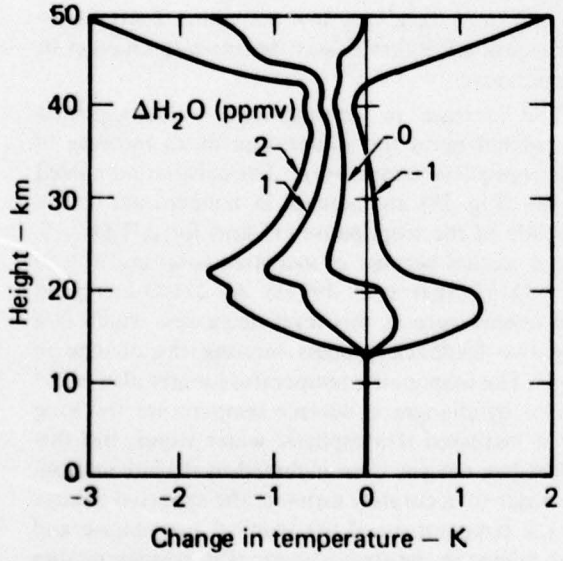

Figure 28. **Calculated changes in temperature for the stratosphere perturbed by the NO_x injection of Fig. 25.**

capable of computing changes in dynamics (transport) and temperature. This entails predicting changes in the mean and eddy components of the circulation as well as changes in the energy and moisture budgets. The one-dimensional calculation is useful in that it qualitatively demonstrates that large changes in stratospheric water vapor are unlikely.

In order to test the degree to which these results might be model-dependent, we repeated the calculations using the Hunten K_z profile; the results are shown in Fig. 29. The model sensitivity to changes in water-vapor mixing ratio without an NO_x injection is nearly the same using the Hunten K_z profile as it was using the Chang (1976) K_z profile (Fig. 25). The slope of ΔO_3 versus H_2O is -0.75%/ppmv with no temperature feedback as compared with -0.64%/ppmv using the Chang K_z profile. When temperature feedback is included, the slope is nearly zero. However, with the NO_x injection, the model sensitivity changes significantly. First, the ozone

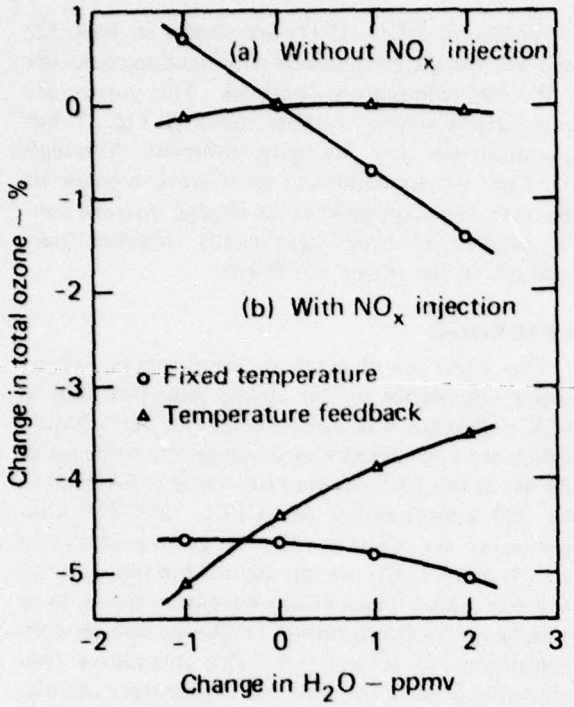

Figure 29. **Change in total ozone vs change in water-vapor mixing ratio above 13 km computed using the Hunten (1975) K_z profile: (a) without NO_x injection, (b) with the NO_x injection of Fig. 25.**

reduction with no change in H_2O using a fixed temperature profile is considerably larger with the Hunten K_z profile: 4.66% as compared to 2.25%. Second, the slopes of the curves are changed dramatically. The amount of ozone reduction due to an increase in H_2O is reduced for the fixed-temperature calculation (the slope is -0.07%/ppmv as compared with -0.42%/ppmv previously). For the calculation with temperature feedback, the reduction in ΔO_3 due to increased H_2O is further enhanced (the slope is 0.63%/ppmv as compared with 0.21%/ppmv previously). Thus, the choice of the K_z profile and the magnitude of the NO_x injection significantly affect the sensitivity to changes in H_2O.

Profiles of $\Delta DO_3(H_2O)$ are shown in Figs. 30a and 30b for the calculations with fixed temperature and with temperature feedback, respectively. The results are qualitatively similar to those in Fig. 27, but there are some quantitative differences. The ozone production (or destruction, depending upon the sign of ΔH_2O) in the region 20–35 km approximately balances the ozone destruction (production) in the region 10–20 km for the fixed-temperature calculation using the Hunten K_z profile, whereas the lower region is dominant using the Chang K_z profile. Above 35 km, the curves are virtually unchanged. The ozone production (destruction) in the region 20–35 km using the Hunten K_z profile shows

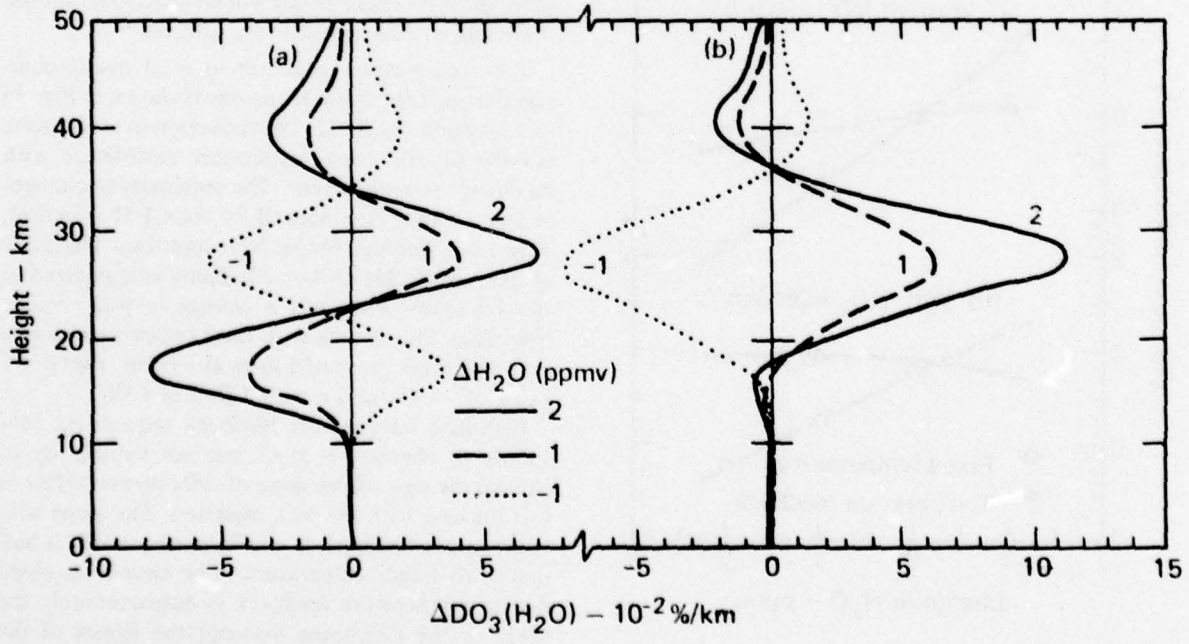

Figure 30. **Calculated profiles of $DO_3(H_2O)$ corresponding to various values of ΔH_2O using the Hunten (1975) K_z profile for the case of the NO_x injection of Fig. 25: (a) with fixed temperature, (b) with temperature feedback.**

more enhancement with temperature feedback than when the Chang K_z profile is used.

The ozone production in the region 20–35 km associated with an increase in H_2O is the net result of competing processes, some which tend to increase ozone and some which tend to destroy ozone. The net result is sensitive to the HO_x and NO_x abundances, which are affected by the diffusion coefficient profile, key reaction rates such as $OH + HO_2$ and $HO_2 + NO$, and the magnitude of the NO_x injection. Because of uncertainties in these quantities, there is a significant uncertainty in the quantitative results in the region 20–35 km of Figs. 27 and 30. These figures, however, illustrate the significant effect which changes in temperature have on the chemistry in the region below 35 km.

The computed change in total ozone due to a change in water-vapor mixing ratio using the chemical rates listed in Table 5 and the Chang K_z profile is shown in Fig. 31. Although the model sensitivity to a stratospheric NO_x injection with $\Delta H_2O = 0$ has changed from a decrease in total ozone to an increase, the effect on ozone of changing water-vapor abundance is nearly unchanged. Compared to Fig. 25, the curves are displaced, but the slopes of the curves are changed only slightly.

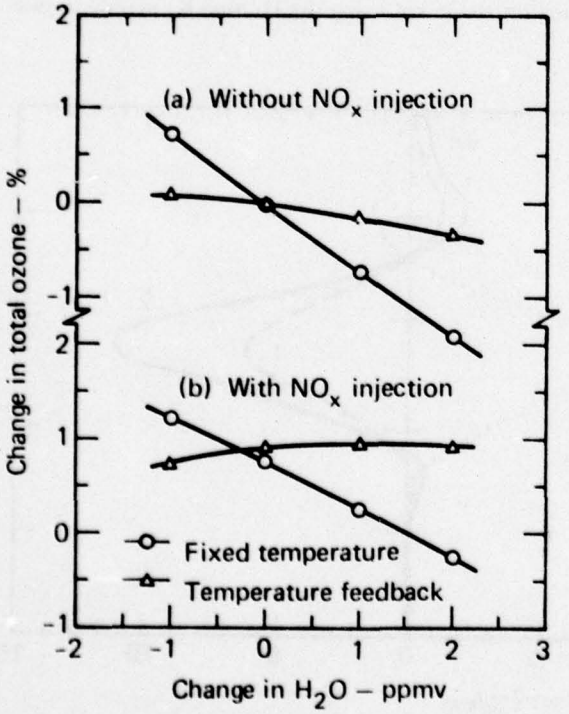

Figure 31. **Change in total ozone vs change in water-vapor mixing ratio above 13 km computed using the new rate coefficients in Table 5: (a) without NO_x injection, (b) with NO_x injection of Fig. 25.**

Profiles of $\Delta DO_3(H_2O)$ are shown in Figs. 32a and 32b for the calculations with fixed temperature and with temperature feedback. The curves are qualitatively similar to those shown in Fig. 27, but quantitatively they are quite different. Although there are similar regions of local ozone increase or decrease, the magnitude of the change in ozone concentration has been significantly affected, particularly in the region 25–35 km.

CFM Release

The effect of changes in stratospheric water-vapor abundance on the ozone reduction due to ClX pollutants was also tested. The perturbation which we considered was a steady-state release of CFMs at the 1975 release rate, which is assumed to be 290 kilotonnes/yr for $CFCl_3$ and 425 kilotonnes/yr for CF_2Cl_2. The long-wave effects of $CFCl_3$ and CF_2Cl_2 are not included in the radiative transfer model. These effects have been shown to be significant by Ramanathan (1976) for species concentrations of several ppb. This introduces considerable uncertainty into the temperature calculation in the region 15–25 km for the perturbed stratosphere. The effect of changes in water vapor abundance on total ozone is not altered since the incremental change in temperature due to ΔH_2O is not changed significantly. There will be an effect, however, on the ozone reduction for the temperature feedback calculation with $\Delta H_2O = 0$. The curve of ΔO_3 versus ΔH_2O will be displaced, but the slope will not be significantly affected.

The steady-state reduction in total ozone computed using the Chang K_z profile is shown in Fig. 33 as a function of ΔH_2O. The reduction in total ozone is 6.9% for the fixed-temperature calculation with no change in water vapor. The sensitivity to changes in water vapor is enhanced by the CFM injection, unlike our findings for an NO_x injection. The slope of ΔO_3 versus ΔH_2O is –1.2%/ppmv as compared to –0.64%/ppmv with only a change in water vapor (Fig. 25a). Our results with fixed temperature agree very well with those of Liu et al. (1976), who got a value of –1.4%/ppmv with 1 ppb of ClX.

Including temperature feedback reduces the sensitivity to changes in H_2O, but not sufficiently to change the sign of the slope of ΔO_3 versus ΔH_2O as was the case with the NO_x injection. The slope with temperature feedback is –0.6%/ppmv, which is half that with fixed temperature. The change in slope due to temperature feedback is approximately the same as the difference between the slopes of the curves in Fig. 25b.

Figure 34 shows the change in ozone concentration versus height for the fixed-temperature and

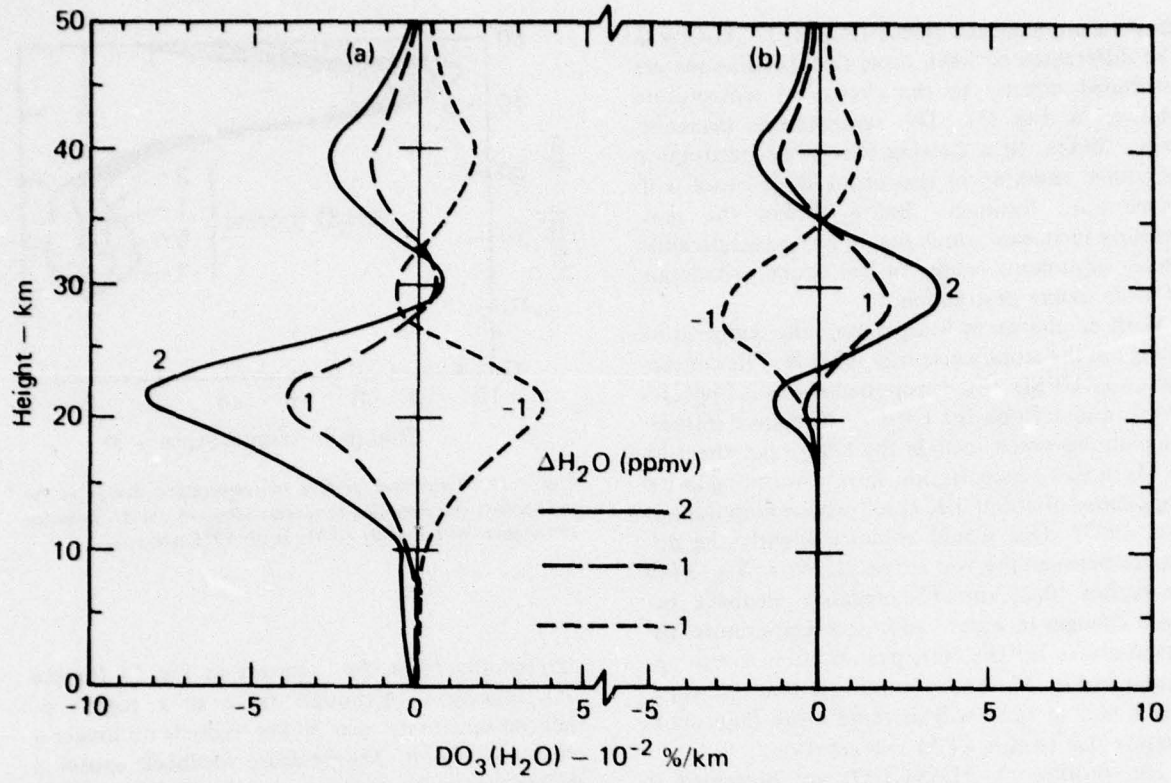

Figure 32. Calculated profiles of $DO_3(H_2O)$ corresponding to various values of ΔH_2O using the new rate coefficients given in Table 5, for the case of the NO_x injection of Fig. 25: (a) with fixed temperature, (b) with temperature feedback.

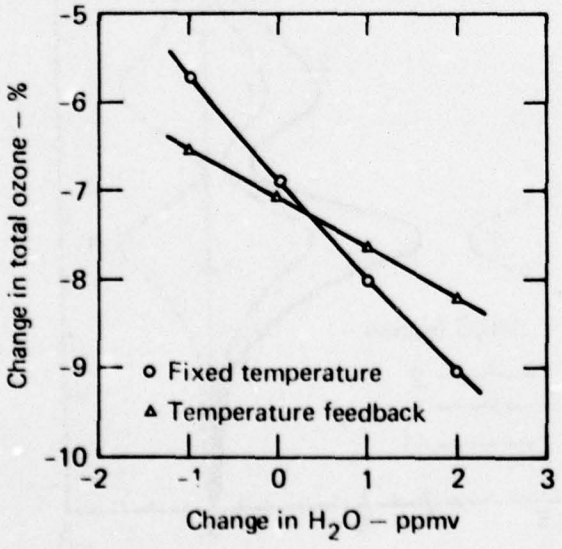

Figure 33. Change in total ozone at steady state vs change in water-vapor mixing ratio above 13 km, computed using the Chang (1976) K_z profile and assuming the 1975 CFM release rate.

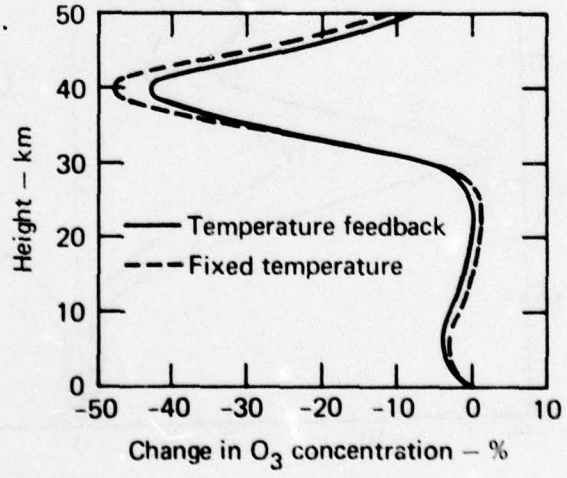

Figure 34. Change in ozone concentration at steady state with height, computed using the 1975 CFM release rate and assuming $\Delta H_2O = 0$.

temperature-feedback calculations with $\Delta H_2O = 0$. The differences between these two calculations are attributed directly to the change in temperature (shown in Fig. 35). The temperature decreases above 30 km, thus slowing the ozone destruction reactions, resulting in less ozone destruction with temperature feedback. Below 30 km the temperature increases, which (again using an activation energy argument) results in less ozone production or more ozone destruction.

With no change in water vapor, the temperature change at the tropopause was -0.03 K. The concentration of CFMs at the tropopause was 0.7 ppb for $CFCl_3$ and 1.7 ppb for CF_2Cl_2. Radiative transfer calculations which include the long-wave effect on CFMs at this concentration show a warming at the tropopause of about 1 K (Liu, private communication, 1977). This would enhance slightly the difference between the two curves shown in Fig. 34 in the region 10–20 km. The negative feedback between changes in water vapor and temperature discussed above for the NO_x perturbation is also apparent in Fig. 35, thus it is unlikely that the water-vapor mixing ratio will increase more than about 1 ppmv due to this CFM perturbation.

The profiles of $\Delta DO_3(H_2O)$ are presented in Fig. 36 for the CFM perturbation. The results differ

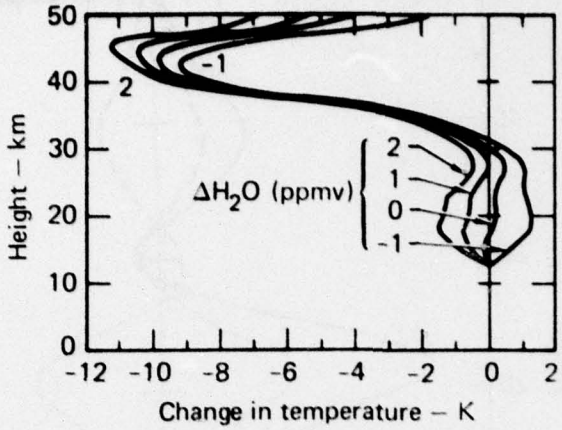

Figure 35. **Calculated profiles of temperature change in the stratosphere corresponding to various values of ΔH_2O, assuming stratosphere perturbed by CFMs at the 1975 release rate.**

significantly from those shown in Fig. 27 for the NO_x injection. Although there is a region of reduced sensitivity near 30 km, there is no longer a crossover region. Temperature feedback causes a shift in sensitivity similar to that for the NO_x perturbation case. For smaller CFM release rates, there is

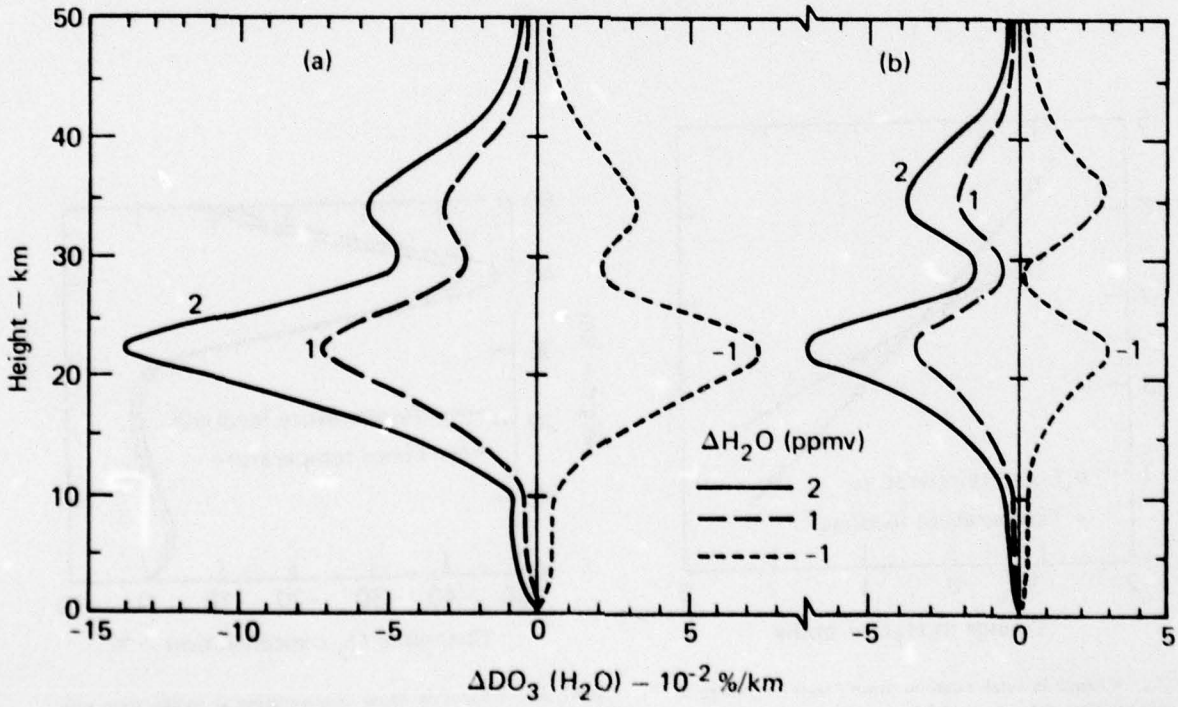

Figure 36. **Calculated profiles of $DO_3(H_2O)$ corresponding to various values of ΔH_2O using the Chang (1976) K_z profile for the case of CFMs at the 1975 release rate: (a) with fixed temperature, (b) with temperature feedback.**

a crossover similar to Fig. 27, which illustrates the dependence upon the magnitude of the CFM perturbation.

The effect of changes in water vapor is somewhat different for the CFM perturbation because of the importance of the reaction

$$OH + HCl \rightarrow H_2O + Cl \qquad (6\text{-}11)$$

Although increased HO_x in the lower atmosphere tends to increase O_3 due to conversion of NO_x to HNO_3 and production of odd oxygen through reactions (6-6) and (6-7), it also releases more free chlorine through reaction (6-11) which tends to enhance the ozone reduction. The results depend upon the magnitude of the CFM perturbation because of its effect on the concentration of HCl. Again, we are seeing in Fig. 36 the net effect of many competing processes.

In analyzing the effect of changes in water vapor on the ozone profile, we found that the region between 10 and 35 km was most sensitive. In the 25-to-35-km region, an increase in H_2O may either increase ozone or decrease ozone depending upon the *concentrations of* NO_x *and* Cl; the larger the NO_x perturbation, the more H_2O tends to decrease ozone.

The results depend quantitatively upon the reaction rates and the K_z profile used for the calculation. Because of uncertainties in these quantities, the qualitative nature of the results should be emphasized rather than their quantitative nature. The change in O_3 depends upon the net effect of several competing mechanisms, particularly in the region 25–35 km. In spite of significant changes in model chemistry, the calculations still indicate that changes in stratospheric water vapor would have much less effect on total ozone than originally estimated by Liu et al. (1976).

2.7 Effect of Past Atmospheric Nuclear Tests on Ozone *

It was suggested by Foley and Ruderman (1973) that the atmospheric nuclear tests of the late 1950s and early 1960s should have caused a stratospheric ozone depletion of more than 10% if then current models of the effect of NO_x on stratospheric ozone were correct. However, their analysis failed to consider the difference in effect to be expected from a pulse injection of NO_x in contrast to the effect of a continuous NO_x source. In 1973 Chang and Duewer calculated the effect on ozone of the nuclear tests (using a production of NO_x/megaton yield about half that used by Foley and Ruderman), and obtained a calculated northern-hemisphere ozone reduction of roughly 4% for 1963. It was concluded that the calculated reduction was not inconsistent with the observed variability of atmospheric ozone as analyzed by Johnston et al. (1973).

In the intervening years, significant changes have occurred in the formulation of the model and in the experimental values of rate constants used as model input. Also, substantially more analysis of the ozone record has been carried out. We will discuss the effect several of these advances have had on the computed effect of the atmospheric nuclear test series on stratospheric ozone and some implications for models of the stratosphere.

Several workers have investigated the problem of NO_x production from a nuclear fireball (see Table 9). The most recent and comprehensive investigations are those of Gilmore (1975) and COMESA (1975). As can be seen in Table 9, these two studies are in good agreement as to their estimates for the total NO_x produced by a nuclear explosion. However, the COMESA study included an estimate of loss of NO_x from the rising debris cloud (i.e., 20%). In this work we accept the COMESA estimate of the total NO_x injection per megaton, but we note that this value should be considered uncertain by roughly $\pm 50\%$.

A related question concerns the yields of the various nuclear weapons. Table 10 gives several published estimates of the total yield for the period of active testing. In this work we have followed the procedure of taking unclassified qualitative yield descriptions and assigning them quantitative values consistent with other available data. Our integrated yield estimate for the period 1961–62 is consistent with the estimates given by COMESA (1975) and Foley and Ruderman (1973), but roughly 10% larger than those cited by Johnston et al. (1976) and Seitz et al. (1968).

A few nuclear devices were exploded in or above the stratosphere, generating clouds that stabilized in or above the mesosphere. These tests may have created more NO_x/megaton than low-altitude tests, because a low-density fireball can be expected to depart from equilibrium composition at a higher temperature than a higher density fireball. Thus, it might be argued (Hampson 1977) that these devices could have produced a very high yield of NO at altitudes of 70–200 km. However, in that altitude range NO_x has a lifetime on the order of a day (Gerard and Barth 1977), and it is unlikely that any

*See Chang et al. (1977).

significant fraction of NO_x produced at high altitudes reached the stratosphere. Further, while energetic particles escaping from a high-altitude fireball might produce NO_x in the stratosphere, it is unlikely that this process had a significant effect on the yields of NO_x summed over all tests.

The model perturbations are small enough that model response to variation of the total NO_x injection is approximately linear for most chemistries. Thus if a readjustment of the NO_x yield should be dictated by future work, our computed ozone perturbations would, to a fair approximation, scale linearly.

A more difficult point concerns the altitude of injection. Foley and Ruderman (1972) gave a parameterization for the top and bottom of the stabilized cloud versus device yield:

$$CT = 21.64Y^{(0.2)} ,$$

$$CB = 13.41Y^{(0.2)} ,$$

where

CT = cloud top (km) ,

CB = cloud bottom (km) ,

Y = yield (megatons TNT equivalent) .

This parameterization was largely based on direct observations of United States tests (Peterson 1970); it was only inferred to be valid for the Soviet tests.

Seitz et al. (1968) estimated cloud tops and bases from measurements of the radioactive debris a few days after the 1961–1962 tests. Very few of the

Table 9. **Estimates of NO produced per megaton (Mt) of nuclear-explosive yield.**

Source	Estimated NO production (10^{32} molecules/Mt)
Zeldovich and Razier (1967)	0.5
Foley and Ruderman (1972)	0.3–1.5
Johnston et al. (1973)	0.17–1.0
Chang and Duewer (1973)	0.5
Goldsmith et al. (1973)	1.0
Gilmore (1975)	0.4–1.5 (0.9)
COMESA (Goldsmith et al.) (1975)	0.6–1.1 (0.84)
COMESA (after allowance for disentrainment) (1975)	0.5–0.9 (0.67)
This work uses	0.67

Table 10. **Estimates of approximate total yields (in megatons (Mt)) of high-yield[a] atmospheric nuclear tests by year.**

	COMESA (1975)	Foley and Ruderman (1973)	Johnston et al. (1976)	Seitz et al. (1968)	This work
Pre-1956	61.6	62	–	–	–
1956	26.0	26	–	–	20
1957	13.5	} 85	–	–	16
1958	61.9		–	–	58
1959	0	0	–	–	0
1960	0	0	–	–	0
1961	120.6	} 340	99.7	97	119
1962	213.5		204	206	216
1963	–	–	–	–	–
1964	–	–	–	–	–
1965	–	–	–	–	–
1966	1.4	–	–	–	–
1967	3.5	–	–	–	–
1968	7.6	–	–	–	–
1969	3.0	–	–	–	–
1970	6.1	–	–	–	–
Total 1961–62	334	340	304	303	335
Total 1956–62	435	451	–	–	429

[a]Tests having a yield of 1 Mt or greater (1 Mt = 4.2×10^{15} joules).

debris measurements extended above 24 km, and the cloud tops of most of the higher yield tests were not directly measured. When samples were taken near 30 km shortly after a high yield test, the cloud top was estimated to be above 30 km; however, when no data above 24 km were available, a cloud top near 24 km was assumed (Seitz et al. 1968). From an analysis of the ratio of ^{14}C to ^{90}Sr, Telegadas and List (1969) concluded that the very large Soviet test of October 1961 probably stabilized almost entirely above the region examined by Seitz et al.

The parameterization of Foley and Ruderman (1973), which we used in earlier reports (Chang and Duewer 1973, MacCracken and Chang 1975), may overestimate the height of stabilization since it is based almost exclusively on data from the tropics. However, the stabilization heights quoted by Seitz et al. may generally underestimate the stabilization altitude of the debris from Soviet tests. Figure 37 presents the stabilization estimates from the two different methodologies.

When we used the Foley and Ruderman (1973) parameterization, we assumed the injection to result in a uniform increase in concentration between cloud top and cloud bottom. When we used Seitz et al.'s (1968) injection altitudes we assumed that it was appropriate to adjust the injection to a constant height above the tropopause corrected to mid-latitude conditions (Johnston et al. 1976). Thus, we increased CT and CB by 4 km for polar tests and reduced them by 2 km for tropical tests. We believe that these procedures provide approximate upper and lower bounds for the stabilization altitudes of the test debris. As we will show (Fig. 38 and Table 11), the computed ozone reductions in the peak year (1963) are larger by about 1–2% (of total O_3) when we use the Foley and Ruderman (1973) expression than when we use the Seitz et al. (1968) stabilization altitudes.

In all calculations the injection was assumed to be mixed throughout the northern hemisphere, and no further dilution was considered. Mixing into the southern hemisphere might have reduced the NO_x perturbation by 15–25% in 1963–64 (Johnston et al. 1976).

Johnston et al. (1973) analyzed the global ozone record for 1960–1970 and found a statistically insignificant decrease of 2.2% for 1960–1962 followed by a statistically significant increase of 3.7% for

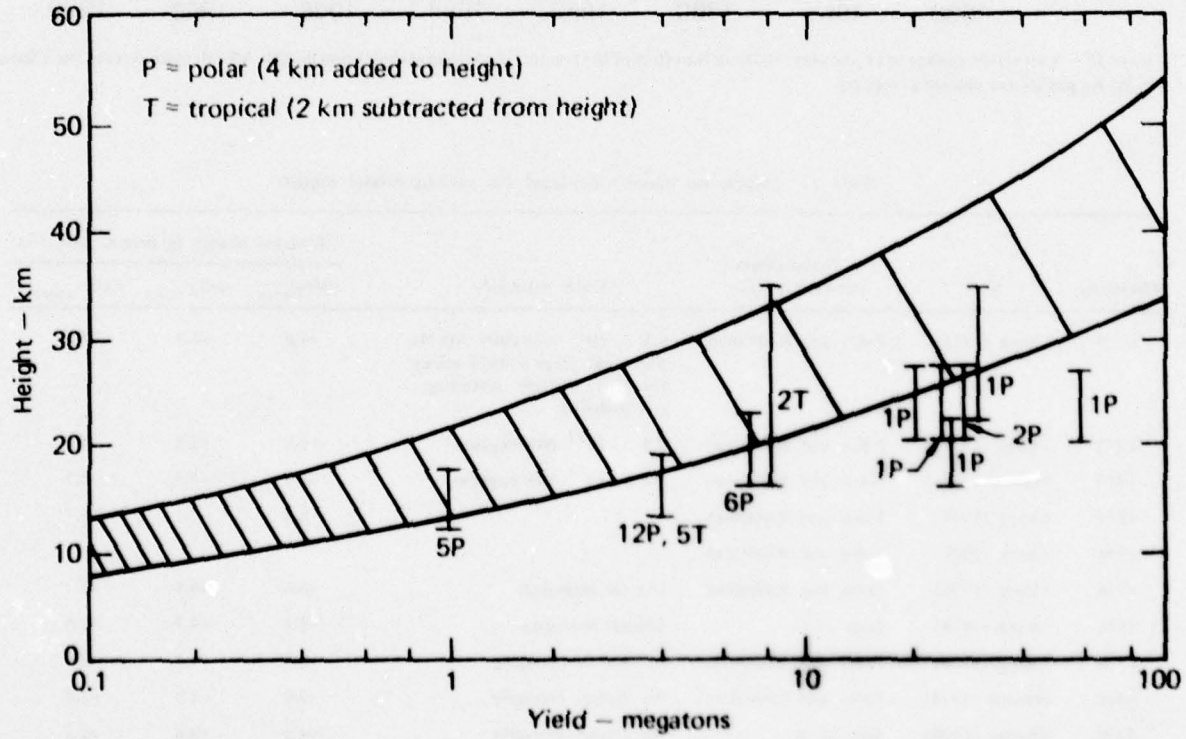

Figure 37. **Cloud top and base elevations vs yield. The curves defining the shaded area give the cloud top and base according to the parameterization of Foley and Ruderman (1973). The vertical bars extend from cloud base to top for the data cited by Seitz et al. (1968) after adjustment to height above a variable tropopause as discussed in the text. The number of tests for a particular yield at high latitudes (P) and low latitudes (T) is also given for the data of Seitz et al.**

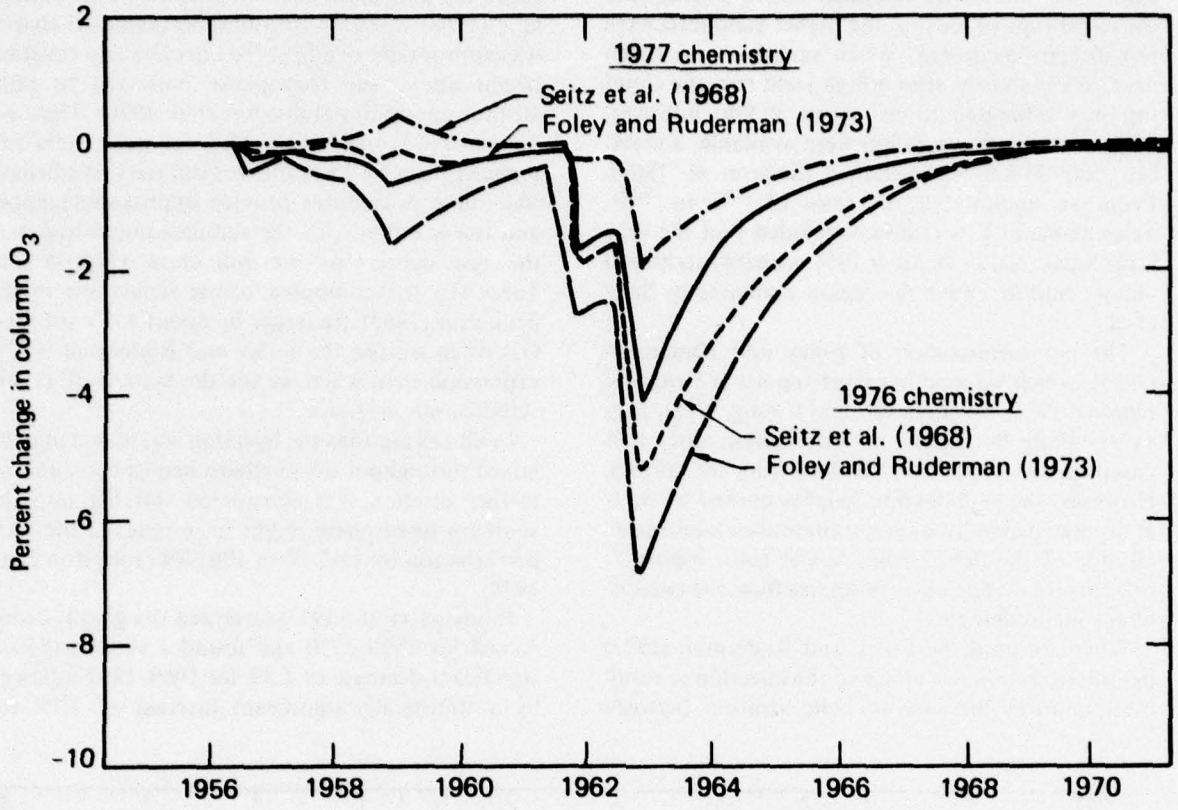

Figure 38. Calculated change in O_3 vs year, showing the effect of the treatment of cloud stabilization height. All calculations used the Chang (1976) K_z profile and diurnal averaging.

Table 11. Effects on ozone calculated for various model inputs.

Chemistry	K_z	Stabilization parameterization	Other variations	Calculated change in ozone, ΔO_3 (%)		
				$(\Delta O_3)_{max}$	$(\Delta O_3)_{1963}$	$(\Delta O_3)_{1964}$
1973	Chang (1974)	Foley and Ruderman	0.5×10^{31} molecules NO/Mt, Bates and Hays (1967) values for N_2O, multiple scattering not included	-5.0	-4.0	-3.3
1973	Chang (1974)	Foley and Ruderman	0.5×10^{31} NO/megaton	-4.8	-3.8	-3.1
1973	Hunten (1975)	Foley and Ruderman	0.5×10^{31} NO/megaton	-5.3	-4.5	-3.9
1974	Chang (1974)	Foley and Ruderman	–	-8.2	-7.1	-6.2
1974	Chang (1976)	Foley and Ruderman	–			
1976	Chang (1976)	Foley and Ruderman	Diurnal averaging	-6.8	-4.5	-2.7
1976	Chang (1976)	Seitz et al.	Diurnal averaging	-5.1	-4.3	-2.6
1976	Chang (1976)	Foley and Ruderman	No diurnal averaging	-6.1	-4.2	-2.6
1976	Hunten (1975)	Foley and Ruderman	No diurnal averaging	-5.0	-3.9	-2.8
1976	Change (1976)	Seitz et al.	No diurnal averaging	-4.3	-3.8	-2.5
1977	Chang (1976)	Foley and Ruderman	Diurnal averaging	-4.2	-3.0	-1.4
1977	Chang (1976)	Seitz et al.	Diurnal averaging	-1.9	-1.5	-0.8
1977	Hunten (1975)	Seitz et al.	Diurnal averaging	-1.8	-1.4	-0.7

1963–1970. They viewed this increase as consistent with recovery from an ozone depletion of "a few percent" induced by the nuclear tests. The same data have been analyzed by several other authors (Komhyr et al. 1971, Angell and Korshover 1973, 1976, Goldsmith et al. 1973, COMESA 1975, London and Kelley 1974). Most of these more recent analyses agree in finding the observations less consistent with a nuclear test series effect. Angell and Korshover (1976) note that apparent ozone minima occurred in 1960 and 1962, whereas the major nuclear tests occurred in the autumns of 1961 and 1962 so that any predicted depletions would be expected in 1962 and 1963. When the effects of the quasi-biennial ozone variations were allowed for, Angell and Korshover (1976) concluded that any ozone reductions caused by the nuclear test series must have been less than 1–2%; this is consistent with COMESA (1975), which concluded that any nuclear test series effects were not detectable in the ozone record. In our discussion we will accept Angell and Korshover's analysis with the reservation that if an effect is calculated to have a sufficiently long time constant, the gradual increase in ozone found during the middle and late 1960s (Johnston et al. 1973, Angell and Korshover 1973, 1976) might be consistent with a slightly larger perturbation.

The model chemistry used in our 1973 calculation contained 33 reactions of HO_x, NO_x, and O_x, with rate constants based primarily on Garvin and Gevantman (1972). These are given in Table A-1 of Appendix A as 1973 chemistry.

When the CIAP calculations were carried out (1974) we incorporated the 41 reactions listed as 1974 chemistry in Table A-1. Most rate constants were taken from Garvin and Hampson (1974).

Our 1976 chemistry (Table A-1) incorporated ClO_x reactions and was nearly the same as that used in the National Academy of Sciences CFM report (National Research Council 1976). Most of the rate constants were derived from Hampson and Garvin (1975), but several had been revised to reflect 1975 or 1976 measurements (National Research Council 1976, DeMore et al. 1977). Our 1977 chemistry (Table A-1 of Appendix A) contains the same reactions as our 1976 chemistry, but several rate constants have been adjusted to reflect recent evaluations (DeMore et al. 1977, Watson 1977) and measurements (Howard and Evenson 1977, Burrows et al. 1977, Chang and Kaufman 1976). As we will show, the predicted effect of the nuclear test series is quite sensitive to model chemistry. For this study the model contained about 1.3 ppb of ClO_x from CH_3Cl and CCl_4, but chlorofluoromethanes were neglected.

The 1973 model (Chang and Duewer 1973) did not include rainout processes. All subsequent models included rainout losses below 8 km using rates of $2.31 \times 10^{-6}\ s^{-1}$ for HNO_3, HCl, and ClO (for models including chlorine chemistry) and 1.16×10^{-6} for NO_2. The major effect of rainout is to uncouple surface boundary conditions for NO_x and ClX from stratospheric and upper tropospheric concentrations. Calculated stratospheric perturbations are not strongly sensitive to the precise rainout rates chosen.

The model uses fixed concentration boundary conditions at the surface (Chang et al. 1974). For versions incorporating rainout, the model stratosphere has significant sensitivity to the boundary conditions for only N_2O, CH_4, CH_3Cl, and CCl_4. The 1973 model was also influenced by the surface boundary conditions for NO, NO_2, and HNO_3, which produced a nearly uniform 3.7 ppb NO_x mixing ratio in the troposphere. In models treating rainout processes, the NO_x mixing ratio in the upper troposphere is dependent on K_z but is smaller than 0.1 ppb.

In our 1973 calculation, we neglected multiple scattering effects and diurnal variation of species concentrations, and we used then current values for the N_2O photodissociation cross sections (Bates and Hays 1967). In all of the current calculations we used Johnston and Selwyn (1975) photodissociation cross sections for N_2O. The 1974 and 1976 models approximated diurnal variations in solar flux by using one-half the noontime photodissociation rates. The chlorine nitrate formation rate was adjusted to be consistent with a fully diurnal calculation for the 1976 model. The 1977 model averages reaction rates at each level over a diurnal cycle (Chang et al. 1977). Limited calculations were made using the 1976 chemistry and diurnal averaging. The 1976 and 1977 models included multiple scattering effects (Luther et al. 1977b).

The response of the model is little affected by the change in N_2O absorption cross sections or multiple scattering (together they resulted in a 0.2% change in total ozone for a calculated maximum depletion of roughly 5% using the 1973 chemistry). The incorporation of diurnal averaging of reaction rates increased the ozone depletion for 1977 chemistry by about 0.5 to 1% of total ozone when the Seitz injection scheme was used (see Table 10).

We considered the effects of different K_z choices by performing calculations using the Chang (1974), Chang (1976), and Hunten (1975) K_z profiles. The Chang (1974) K_z profile was used in the earlier work by Chang and Duewer (1973). Only the recovery time had a strong sensitivity to K_z (see Fig. 39 and Table 10).

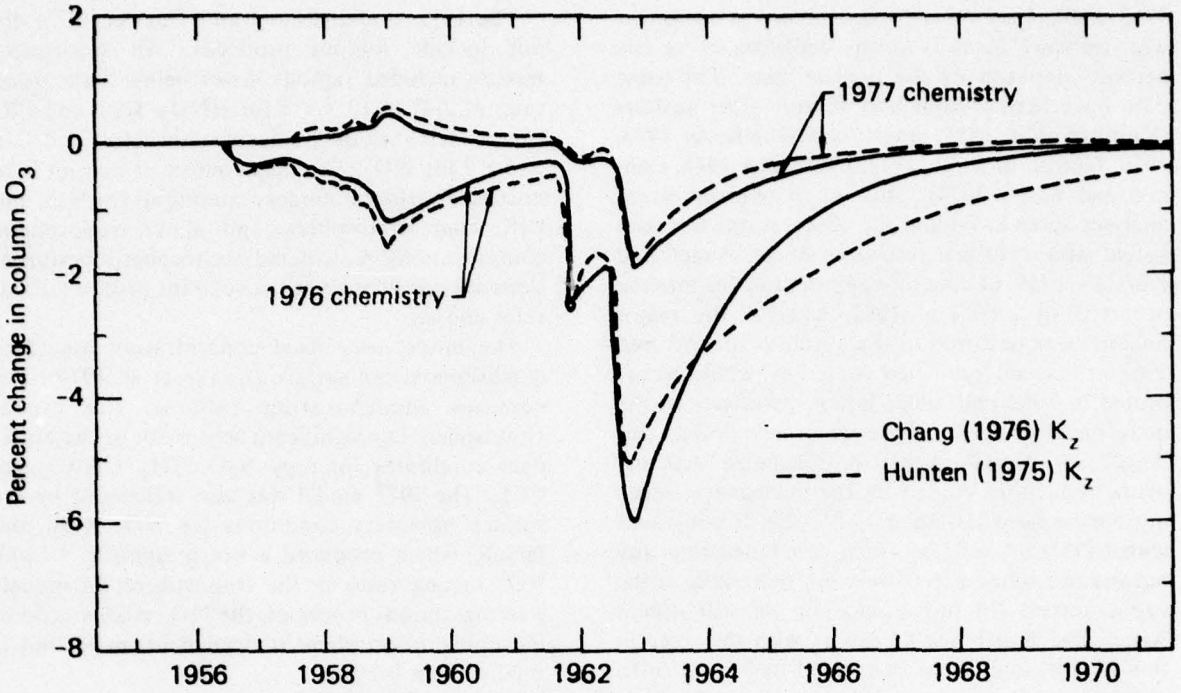

Figure 39. **Calculated change in O_3 vs year for two K_z profiles. Upper curves use the 1977 chemistry and diurnal averaging. Lower curves use the 1976 chemistry without diurnal averaging.**

Calculations were carried out using the Foley and Ruderman stabilization parameterization for 1973, 1974, 1976, and 1977 chemistries. The Chang (1976) K_z was used with the 1974, 1976, and 1977 chemistries, the Chang (1974) K_z was used with the 1973 and 1974 chemistries, and the Hunten (1975) K_z was used with the 1973, 1976, and 1977 chemistries. The Seitz et al. (1968) stabilization estimates were considered using 1976 and 1977 chemistries with the Chang (1976) K_z and 1977 chemistry with the Hunten (1975) K_z.

In the calculation of the nuclear test series effects, the total NO_x injection is determined by the device yield and is independent of K_z. Further, most of the injection occurred over a fairly short time; therefore, unlike SST calculations, ΔNO_x is nearly independent of K_z. As Fig. 39 and Table 11 show, for the cases considered, the ozone depletions in 1963–64 were weakly dependent on K_z. For pre-1977 model chemistries, there is a substantial difference in recovery time, based on the effective removal rate of excess stratospheric NO_x. For the 1977 model chemistry the apparent recovery time is initially determined by the rate of vertical redistribution of the injection, although at later times recovery is controlled by the rate of removal of excess NO_x from the stratosphere. In no case would the choice of K_z alone cause the calculation to conflict with observation.

As shown in Fig. 38 and Table 11, the procedure used to estimate the stabilization altitude has a significant effect on the calculation. However, for the model chemistries studied, the differences in the effects computed using these two stabilization estimates were less dramatic than the differences between model computations using different chemistries (Fig. 40).

The estimated stabilization heights for the polar tests remain a significant source of uncertainty in the calculations. For reasons discussed above, we find the published information ambiguous and somewhat unsatisfactory. The two methods of estimation used provide a probable upper and lower bound to the true stabilization heights, but the Foley and Ruderman parameterization should be the more nearly accurate of the two. Chang (1975) and Mahlman (1977) have discussed the information available from tracer calculations based on ^{14}C and ^{90}Sr. At present, we will note that these results further strengthen the need to accept the uncertainty in cloud stabilization heights as inherent uncertainties in such analyses.

The model representation of atmospheric chemistry has evolved substantially since early 1973,

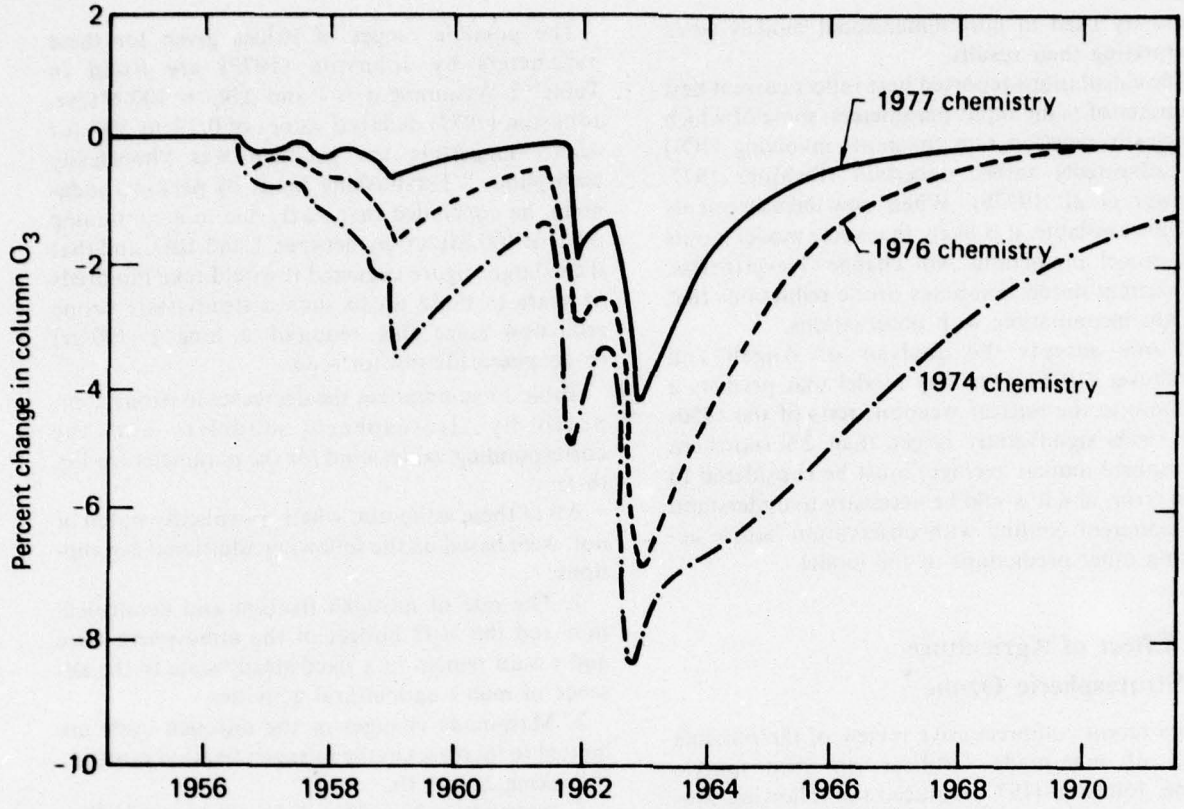

Figure 40. **Calculated change in O_3 vs year for three different chemistries. All calculations used the Foley and Ruderman (1973) stabilization parameterization.**

and the effect of the most recent changes has been dramatic. With our 1977 chemistry, when the Seitz et al. (1968) stabilization height estimates are used, we compute ozone increases from the 1950s tests and less than 2% ozone reductions at all times. When the Foley and Ruderman (1973) stabilization height estimates are used, we compute ozone decreases for all years during the period of active atmospheric testing, and the reductions calculated for 1963 (3% annual average ozone reduction in the northern hemisphere) are still larger than is easily consistent with observation. However, the source term consists of pulse injections primarily at high latitudes, most of them in a period of about 4 months in late 1962. Thus, at least for the several months before horizontal mixing in the northern hemisphere should have been complete, the one-dimensional approximation is expected to be poor and to overestimate the ozone depletions (Bauer and Gilmore 1975). Therefore, it would appear that our current results may be comparable to the upper limit permitted by the observations. A two-dimensional model calculation of the weapons tests would be useful in this regard.

It should be noted that the problems related to high-latitude injection of NO_x are also present in calculations of the effects of SST flight since more than half of projected SST emissions occur north of 50° (Oliver et al. 1977). Thus, many of the potential sources of error introduced by the use of one-dimensional models in the calculation of the test series effects also exist for calculations of SSTs. Two- or three-dimensional calculations of both effects are to be desired, but present multidimensional models are relatively expensive to run, and the rapid evolution of model chemistry may act to discourage extensive calculations since further substantial evolution of model chemistry seems very likely. The major changes in model chemistry—the changes that most strongly affect model sensitivities—have been in the treatment of reactions that affect HO_x species or link NO_x to minor species other than odd oxygen, rather than in the major catalytic odd-oxygen destruction cycles involving NO_x (see also Duewer et al. 1977b). Because this secondary chemistry has such a strong effect on one-dimensional model sensitivity to NO_x injection, one must closely examine the representation of the

chemistry used in multidimensional models when interpreting their results.

The calculations reported here reflect current best estimates of many input parameters, some of which (especially reaction rate constants involving HO_2) are admittedly rather uncertain (DeMore 1977, Duewer et al. 1977b). When new measurements become available, it is likely that some model inputs and model predictions will change. Nevertheless, our current model computes ozone reductions that are not incompatible with observations.

If one accepts the analysis of Angell and Korshover (1976), then any model that predicts a response to the nuclear weapons tests of the 1950s and 1960s significantly larger than 2% (northern hemisphere annual average) must be considered to be in error, and it would be necessary to understand this apparent conflict with observation before accepting other predictions of the model.

2.8 Effect of Agriculture on Stratospheric Ozone *

In a recent comprehensive review of the possible effect of man-made fertilizer on stratospheric ozone, Johnston (1977) deduced the following simple steady-state model for the percentage decrease in ozone, $-\Delta O_3$ (%), in terms of the increment in nitrogen fixation due to man, ΔN_f (Mt of N/yr) †:

$$-\Delta O_3 = \alpha\beta\gamma\tau\Delta N_f/N_2O_a \quad . \qquad (8\text{-}1)$$

The remaining variables are defined as follows:

- α = the fraction of denitrified nitrogen released to the atmosphere as N_2O,
- β = the fraction of ΔN_f that will be denitrified within a few decades, i.e., immediately or after one or more passes through living organisms, as opposed to the fraction $1 - \beta$ which will be transferred to long-lived ($\geq$1000 yr) oceanic or lithospheric reservoirs of fixed nitrogen,
- γ = the ratio of the percentage decrease in the O_3 column to the percentage increase in stratospheric NO_x ($NO + NO_2$),
- τ = the tropospheric lifetime of N_2O in years,
- N_2O_a = the unperturbed atmospheric burden of N_2O (Mt of N).

The possible ranges of values given for these parameters by Johnston (1977) are listed in Table 12. Assuming $\beta = 1$ and $\Delta N_f = 100$ Mt/yr, Johnston (1977) deduced values of 0.2% to 50% for $-\Delta O_3$, suggesting the problem was "hopelessly amorphous." Establishing limits by personal judgment, he concluded that $-\Delta O_3$ due to a continuing ΔN_f of 100 Mt/yr lay between 1 and 10%, and that if the larger figure occurred it would take hundreds of years to build up to such a steady-state ozone reduction since this required a long (~100-yr) tropospheric lifetime for N_2O.

Table 13 summarizes the decreases in ozone computed by stratospheric modelers and the corresponding values used for the parameters in Eq. (8-1).

All of these estimates, whether explicitly stated or not, were based on the following additional assumptions:

1. The rate of nitrogen fixation and denitrification and the N_2O budget of the atmosphere were and would remain in a fixed steady state in the absence of man's agricultural activities.
2. Man-made changes in the nitrogen cycle are limited to increases in the nitrogen fixation rate (i.e., to making $\Delta N_f > 0$).
3. Increases in N_f ($\Delta N_f > 0$) will have no effect on the remaining parameters α, β, γ, and τ.

The available observational data tend to support the conclusion of Crutzen and Ehhalt (1977): "for millions of years the rate of denitrification must, therefore, on the average, have equalled the rate of nitrogen fixation on earth." But this leaves unconsidered man-made effects on the biosphere other than increased nitrogen fixation plus secondary changes in α, β, γ, and/or τ which may result from any disturbance of the equilibrium or steady-state natural nitrogen cycle.

Table 12. **Possible ranges of parameter values as given by Johnston (1977).**

Parameter	Possible range of values
α	0.025–0.1 (land) 0–1 (ocean) 0.025–0.4 (global)
β	0.01–0.75, probable average 0.1–0.15
γ	1/5 (modification to 1/3 or 1/8 considered possible)
τ	5–160 yr
N_2O_a	1300 Mt N
ΔN_f	160–650 Mt N/yr

*See Ellsaesser (1977c).

† 1 Mt = 10^6 tonnes = 10^9 kg in this usage; not to be confused with the megaton of nuclear explosive yield, which is the equivalent of the explosive energy of a million tons of chemical high explosive.

Table 13. Summary of computed decreases in O_3 due to use of nitrogen fertilizer and values of relevant parameters used.

Computed decrease in O_3, $-\Delta O_3$ (%)	Reference	Parameter			
		α	β	τ	ΔN_F (Mt)
19	Vupputuri (1974)	(Doubled N_2O_a).			
20 (by 2025)	McElroy (1974, 1975, 1976)	0.08	1	20	200
20 (by 2025)	McElroy et al. (1976)	0.23	1	20	200
8 (by 2100) 14 steady state	Crutzen (1975)	0.04	1	100–160	200
1.7	Crutzen (1976) (by 2025)	0.07	1	10	200
4.3		0.2	1	10	200
9.5		0.5	1	10	200
6.7		0.2	1	20	200
1 (by 2025) 4 (by 2050)	Liu et al. (1976)	?	1	20	40 in 1974, +6%/yr
1.6	Sze and Rice (1976) (by 2025)	0.26	0.1	20	200
5		0.26	0.25 (0.35 after 2000)	20	200
9		0.26	0.6	20	200
6	NRC (1976)	(Doubled N_2O_a).			
1–15 (200 yr for maximum)	Crutzen and Ehhalt (1977)	0.05–0.2	0.33	10–160	40–200

Johnston (1977) reported that the environmental conditions favoring denitrification were:

1. Saturation of soils with water.
2. Absence of oxygen.
3. Availability of organic matter for microbial consumption.

While not clarified by Johnston (1977), it appears likely that these factors favoring denitrification will lead to a larger β since a larger portion of N_F will presumably be denitrified before it has a chance to move into a long-lived reservoir, and vice versa. The environmental conditions favoring a large α were given by Johnston (1977) as:

1. Low temperature.
2. Low pH.
3. Marginal anaerobic conditions.

All three of these conditions were also cited as leading "to a low rate of denitrification." While also not addressed by Johnston (1977), it nevertheless appears likely that the latter effect may predominate, leading to a lower rate of N_2O production. That is, if the fraction $1 - \beta$ of N_F moving into long-lived oceanic and lithospheric reservoirs depends on the length of time N_F remains in the soil, then these factors favoring a large α by slowing denitrification might also lead to a smaller β and to no change or even a decrease in the product, $\alpha\beta$, or fraction of ΔN_F (or $N_F + \Delta N_F$) converted to N_2O within the "short" recycle time of a few decades. According to McElroy (1976), "denitrification can take place to a significant extent only in media with pH larger than about 5.5."

While little quantitative information is available, it is well known that man, since taking up agriculture, has induced large-scale changes on the biosphere other than those resulting from the application of fertilizer. These include:

1. Increasing soil oxygen by: (a) loosening and turning the soil to produce increased aeration, (b) treatments to improve porosity and drainage, (c) reducing competitive oxygen demand from root growth through spacing of monocultured plants, elimination of competing plants or weeds, and fallowing.

2. Reducing oxygen-excluding soil moisture by: (a) increasing runoff through removal of plant

cover, (b) reducing water-retaining topsoil and humus through erosion and oxidation and non-return of plant debris, (c) measures to improve percolation and/or drainage wherever water stagnation restricts plant growth.

3. Reducing the volume of organic material or culture medium for soil bacteria as indicated in 2(b) above.

4. Increasing soil pH by: (a) loss of humus which is rich in organic acids, (b) accumulation of alkali metals through salination in most areas placed under irrigation, (c) deliberate use of lime, etc.

5. Decreasing the natural equilibrium level of N_f in the biosphere through clearing of forests and shrubs and actions in 2(b) above. For example, Soderland and Svensson (1976) estimated global soil nitrogen loses due to agricultural activities at 6,000–13,000 Mt N. (This should be compared with the estimates for N_f, or total global annual fixation rates, of 160–650 Mt N/yr (Johnston 1977) and 230–400 Mt N/yr (Crutzen and Ehhalt 1977).)

Initial appraisals of each of these anthropogenic effects suggest that, except for the increase in pH, each should have tended to decrease the rate at which N_2O is produced. Increased oxygenation, decreased organic material, and reduced water saturation all appear to operate directly to reduce the rate of denitrification and thus would appear to allow the fixed nitrogen more time to find its way into the long-lived oceanic and lithospheric reservoirs, thereby decreasing β. In addition, except insofar as they tend to increase "marginal anaerobic conditions," each of these would have tended to reduce α. Reducing the biospheric store of fixed nitrogen would not disturb any of the quantities in Johnston's (1977) simple model but would disturb the assumed steady state on which it is based. That is, the natural rate of production of N_2O can hardly remain unchanged if the accumulated fixed nitrogen in the biosphere from which it is formed is suddenly reduced. If the fixed nitrogen lost during the early years of cultivation were denitrified with no change in the preexisting steady-state product, $\alpha\beta$, then it should have caused a temporary increase in the rate of N_2O production before the decrease set in. However, it appears more likely that most of this fixed nitrogen entered the long-lived oceanic and lithospheric reservoirs and that nearly all of it (rather than the normal $1 - \beta$ fraction of it) will undergo the long-term ($\geq$1000 yr) cycle of denitrification as opposed to the short-term (few decades) cycle. As indicated below, the effect of any significant increase in pH is less clear.

Another point which appears to have been overlooked in previous analyses of this problem is the manner and locale in which man's additions of fixed nitrogen to the biosphere are made. Fertilizer is added almost exclusively to well-drained and well-aerated soils, i.e., to those which do not provide the anaerobic conditions required for denitrification until the nitrogen has moved deep enough to be below the humus or organic material which denitrifying bacteria require as a culture medium. Further, mass applications of fixed nitrogen tend to be in the reduced rather than the oxidized state. While reduced nitrogen will generally be readily oxidized by nitrifying bacteria in the soil, the fact of its being oxidized indicates soil conditions which are aerobic rather than anaerobic and thus unfavorable for denitrification, at least at that specific location and time. This suggests that most of man's additions of fixed nitrogen to the soil will be taken up by plants or move into the long-lived oceanic and lithospheric reservoirs. That portion taken up by plants may be returned to the soil, burned, or wind up as sewer sludge, feedlot manure, and/or landfill. All of these would appear to lead to lower than the natural values of the product, $\alpha\beta$. Detailed quantitative analyses will be required to reach a firm conclusion as to whether the fraction converted to N_2O is greater or less than the product $\alpha\beta$ for the assumed preindustrial steady state. Initial indications are that it is somewhat less and that, until the long-lived oceanic and lithospheric reservoirs are brought into a new equilibrium, man's effect on N_2O production will be such as to cause a decrease.

Other factors have been raised which bear on this problem, but they appear to be minor (as yet) compared with those considered above. Man is also contributing to nitrogen fixation through combustion (20 Mt N/yr), ammonia production (17 Mt N/yr), and direct output of N_2O by coal combustion (now estimated at 2.2 Mt N/yr) and auto exhaust; these latter two may become important in the future (Crutzen and Ehhalt 1977). McElroy (1976) has suggested that man's injection of sulfur and nitrogen compounds (air pollution) into the atmosphere is causing a decrease in the pH of precipitation, which in turn will cause a decrease in the environmental pH of denitrifying bacteria and thus an increase in α and N_2O production. As of now this can be considered no more than interesting speculation. Decreases in the pH of precipitation have been reported in only restricted areas of the globe, and past data for establishing trends in these areas are fragmentary at best. Soil scientists have measured pH profiles in the solums of many soils. In the podzols typical of timbered regions such as New England and Scandinavia where increasing

acidity of precipitation has been claimed, measured pH values range from 3.1 to 5.5 (Bailey 1945). The low pH's, the date of observation (1923–1935), and the fact that pH not uncommonly decreased with depth suggest that soil acidity is being controlled by factors other than the pH of precipitation. Even more critical is the fact that low pH reduces the overall rate of denitrification at the same time as it increases α. Note that all of the pH's for podzols reported by Bailey (1945) were at and below the 5.5 cutoff at which denitrification becomes insignificant according to McElroy (1976) and thus presumably unresponsive to further decrease in pH.

This admittedly qualitative analysis suggests that man's modifications of spaceship Earth may have already led to a decrease in the production of N_2O, and that this decrease, if real, is likely to continue at least until man's contributions of fixed nitrogen to the long-term oceanic and lithospheric reservoirs lead to a new global equilibrium between nitrogen fixation and denitrification. At present we have almost no information on which to estimate the rate of N_2O production that will occur when the new equilibrium is established.

Our current understanding of the chemistry of the O_3 layer suggests that any decrease in N_2O production should be followed within a few years by an increase in the depth of the O_3 layer. This should result from a decline in N_2O_a, the atmospheric burden and concentration of N_2O, causing a decrease in the rate of transport of N_2O to the stratosphere where a small fraction of it (1–5%) is oxidized to NO, a catalytic destroyer of O_3. The recent faster rate determined by Howard and Evenson (1977) for the $NO + HO_2$ reaction is not expected to change this picture qualitatively but will, presumably, reduce γ of Eq. (8-1).

Available data on the trend in tropospheric concentrations of N_2O are very confusing (Pierotti and Rasmussen 1976, Johnston 1977, Crutzen and Ehhalt 1977) and are of little help in resolving this question at present. They suggest abrupt increases in N_2O between 1967 and 1968 and again in recent years. However, the differences in N_2O concentrations indicated by the different sets of measurements are mainly such as to cast doubt upon the accuracy of the measurements themselves. Total ozone measurements are a bit more encouraging. They suggest, if anything, an increase in total ozone since measurements were first made in the early 1920s and particularly since the significant increase in the number of observing stations which began about 1955 (Christie 1973, London and Kelley 1974, Angell and Korshover 1973, 1976).

2.9 Global Tropospheric OH Distributions *

The research for this study was first carried out using 1976 chemistry. There have subsequently been new measurements of some of the chemical rates important to tropospheric OH (see Section 2.10 for further details). Since we expect these changes to have a potentially significant effect on the magnitude and latitudinal variation of the theoretically derived OH concentrations, we are in the process of rederiving the global OH distribution. However, we do not expect the changes to have a large enough impact on the results to invalidate the qualitative features of the global OH distributions. The effect of changes in various parameters on model sensitivity is discussed later in this section under the heading "New 1-D Model Results." The methodology of the derivation as described will not be affected by these changes in model chemistry.

Global OH Distribution

The importance of the hydroxyl free radical in tropospheric photochemistry has been suggested by numerous authors (Levy 1971, Crutzen 1974, Warneck 1974, 1975, Wofsy 1976, and Davis and Klauber 1975). Among the important trace gases whose chemistry is now believed to be influenced by the hydroxyl species are carbon monoxide, methane, sulfur dioxide, nitrogen dioxide, hydrogen sulfide, and a wide variety of higher-molecular-weight hydrocarbons. On the global scale, assignment of the role of OH in defining trace gas chemistry is predicated on knowing the variability of the OH radical as a function of season, altitude, latitude, and time of day. The variability in the concentration of the OH radical is in large part a result of the nature of the formation process, i.e.,

$$O_3 + h\nu \rightarrow O(^1D) + O_2 ,$$

$$O(^1D) + M \rightarrow O(^3P) + M ,$$

$$O(^1D) + H_2O \rightarrow 2OH .$$

Important loss processes include its reaction with both CO and CH_4. For a complete listing of the key reactions used in the following model calculations see the 1976 chemistry shown in Table A-1 of Appendix A.

Assuming the hydroxyl radical has a short tropospheric chemical lifetime, we expect that the

*See Chang, Wuebbles, and Davis (1977).

tropospheric OH concentration is highly variable and is almost totally controlled by local variables such as H_2O, O_3, CO, CH_4, $O(^1D)$, solar radiation, temperature, and others. Consequently, an accurate determination of tropospheric OH concentrations will require the detailed modeling of both tropospheric chemistry and dynamics. An alternative to this would be the utilization of many of the currently available measurements which are determined by real tropospheric dynamic transport. Insofar as the hydroxyl radicals are always in kinetic equilibrium with the governing variables listed above, and these variables are in turn based on observation, we suggest that the quasi-equilibrium hydroxyl radical concentrations represent a reasonable approximation to physical reality.

If the global distribution of species important to OH are known, then a series of local quasi-equilibrium calculations can be used to determine a global representation of the OH distribution. The model can thus account for the effect of dynamic transport through the specific concentrations of the important species at all latitudes. Vertical profiles of temperature, water vapor, carbon monoxide, ozone, and methane were specified in the model, and were varied with latitude and season according to available measurements. The temperature and water-vapor data are from Louis (1974) and Oort and Rasmussen (1971), respectively. The global CO distributions are those of Seiler (1974). The ozone latitudinal and altitudinal global distributions are from Dütsch (1969), and the surface concentrations of O_3 are assumed fixed at the values of Pruchniewicz (1973). The vertical CH_4 distribution is that reported by Ehhalt (1974).

To demonstrate the validity of the quasi-equilibrium approach, typical calculated lifetimes for OH and HO_x ($OH + HO_2 + H_2O_2$) are shown in Table 14 as a function of altitude, latitude, and season. For OH, the longest lifetime shown is 6.0 seconds, which occurs during the winter at 30°S and 10 km altitude. It should be noted, however, that near 0° latitude at 10 km, the lifetime is approximately 4–5 seconds. The small change in lifetime with latitude primarily reflects the change in CO concentration. Substantial change in lifetime would not be expected at still higher latitudes in the winter southern hemisphere where OH concentrations are decreasing rapidly (Fig. 41). The lifetime of HO_x is shown to fall in the range $1–8 \times 10^{-4}$ seconds. These lifetimes, although considerably longer than that for OH, are still quite short when compared to those for meridional and vertical transport.

The calculation procedure used in this study was a modified version of a one-dimensional time-dependent model using the above-mentioned fixed variables. The model normally calculates the concentrations of 15 different trace species. While a number of these had fixed concentrations in this study, others important to the OH distribution have not been measured in sufficient detail. Their concentrations were calculated within the model, utilizing the variations in solar zenith angle, temperature, and concentrations of specified species to determine their distributions. Species such as N_2O, NO, NO_2, HNO_3, and H_2O_2 have fixed concentrations at the surface, which basically define their tropospheric profiles. These fixed boundary conditions were not varied with latitude and season in the calculations. Heterogeneous removal processes for NO_2, HNO_3, and H_2O_2 were included in the model by assuming a constant decay rate below 8 km with an assumed lifetime of 10 days for NO_2 and 5 days for HNO_3 and H_2O_2. Reaction rates in the model were based on the evaluated rates as given in Hampson and Garvin (1975). Also, the chain of reactions resulting from the oxidation of methane is likely to result in the production of several HO_x molecules (Crutzen and Isaksen 1975). However, the reaction mechanism is still not fully established and needs further analysis. We have assumed in this study that each CH_3 molecule produced from CH_4 results in

Table 14. Some estimated tropospheric chemical lifetimes for HO_x ($HO_2 + H_2O_2 + OH$) and OH.

Species	Altitude (km)	Lifetime (seconds) at latitude of:		
		30° N (summer)	0°	30° S (winter)
HO_x	1	1.5×10^{-4}	1.5×10^{-4}	3.7×10^{-4}
	5	3.3×10^{-4}	3.6×10^{-4}	6.9×10^{-4}
	10	4.8×10^{-4}	4.7×10^{-4}	7.6×10^{-4}
OH	1	1.0	1.3	3.7
	5	1.7	2.2	3.5
	10	4.6	4.7	6.0

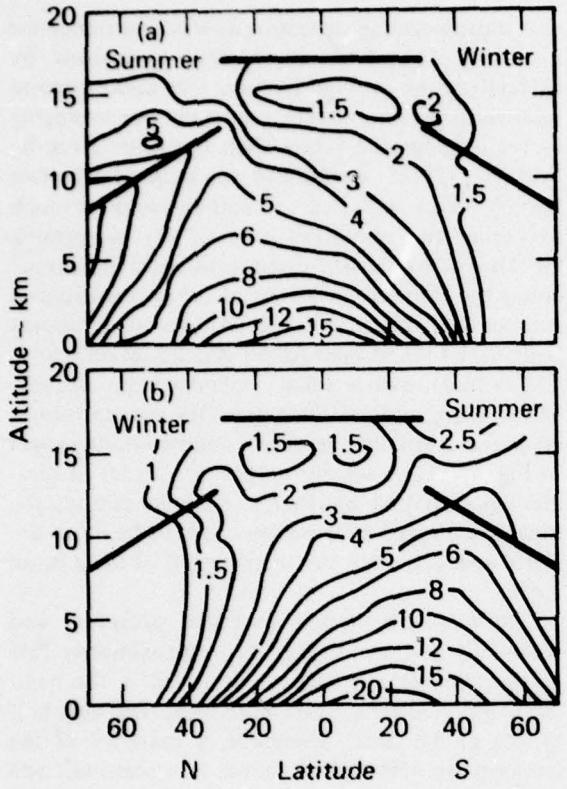

Figure 41. **Calculated global variations in tropospheric OH concentrations. Values are at local noon, heavy lines represent average tropopause altitude.**

the formation of two HO_2 molecules. We have based this on the examination of a 16-step mechanism for methane oxidation. However, because of uncertainties in reaction rates, it is still not clear exactly how many HO_x molecules result from this series of reactions.

Model sensitivity to the fixed surface concentrations of some of the less well measured species has been studied. Surface concentrations of NO_2 and NO are important in this study because of their central role in determining the OH concentration through the reactions

$$OH + NO_2 + M \rightarrow HNO_3 + M \ , \qquad (9\text{-}1)$$

$$HO_2 + NO \rightarrow OH + NO_2 \ . \qquad (9\text{-}2)$$

The relative loss rate of HO_2 through reaction (9-2) and the reaction $HO_2 + HO_2 \rightarrow H_2O_2 + O_2$ determines the effectiveness of CO *as a net sink for OH* through the cycle

$$OH + CO \rightarrow H + CO_2 \ , \qquad (9\text{-}3)$$

$$H + O_2 + M \rightarrow HO_2 + M \ , \qquad (9\text{-}4)$$

$$HO_2 + NO \rightarrow OH + NO_2 \ , \qquad (9\text{-}5)$$

$$HO_2 + HO_2 \rightarrow H_2O_2 + O_2 \ . \qquad (9\text{-}6)$$

With high NO concentration, reaction (9-3) no longer represents a major sink for OH radicals. In our calculations, we used fixed surface concentrations of 0.4 ppb for NO_2 and 0.17 ppb for NO. These concentrations were low enough that our results for OH were not very sensitive to further decreases in concentration. For example, decreasing NO and NO_2 by a factor of 20 resulted in less than a 3% change in OH concentrations. However, larger surface concentrations for NO and NO_2 would increase the sensitivity sharply. For example, increasing the NO and NO_2 concentrations by a factor of 5 (to 2.0 ppb for NO_2) resulted in approximately a 40% increase in tropospheric OH concentrations. This clearly points to the need for better NO_x measurements in the troposphere. Furthermore, insofar as the local NO_x concentration is also dependent upon the heterogeneous removal rates of HNO_3 and NO_2, a careful quantification of global rainout would be desirable. We have also noted a high level of model sensitivity to the lower boundary condition of H_2O_2, and this is being studied in greater detail. We would recommend strongly some measurement of tropospheric H_2O_2 in the near future.

Vertical OH distributions corresponding to local noon were computed for every ten degrees of latitude from 70°N to 70°S for the summer and winter seasons, and the results are shown in Fig. 41. The highest OH concentrations occurred in regions of high solar insolation where $O(^1D)$ concentrations are highest. The lack of symmetry between the northern and southern hemispheres for the same season (Fig. 41) occurs because of the differences in CO concentrations between hemispheres (approximately a factor of 3 more CO in the northern hemisphere according to Seiler (1974)).

In order to compare these results with the autumn noon measurements of Davis et al. (1976), we averaged the summer and winter values. The resulting OH distribution is in good agreement with the available measured values. For 7 km at 32°N, Davis et al. found $(3.5 \pm 2.3) \times 10^6$ molecules/cm^3, whereas the model result was 3.2

$\times 10^6$. For 7 km and 11.5 km at 21°N, the observed values were respectively $(9.1 \pm 3.2) \times 10^6$ and $(4.9 \pm 2.0) \times 10^6$, whereas the model results were 4.2×10^6 and 3.2×10^6. The concentrations corresponding to local noon in Fig. 41 were then utilized as the initial condition in a diurnal calculation of the OH distribution. Examples of the diurnal results are shown in Fig. 42. In general, OH concentrations reach a peak at local noon, when $O(^1D)$ concentration is highest, and rapidly decrease at sunset due to loss mechanisms that continue while production mechanisms have stopped.

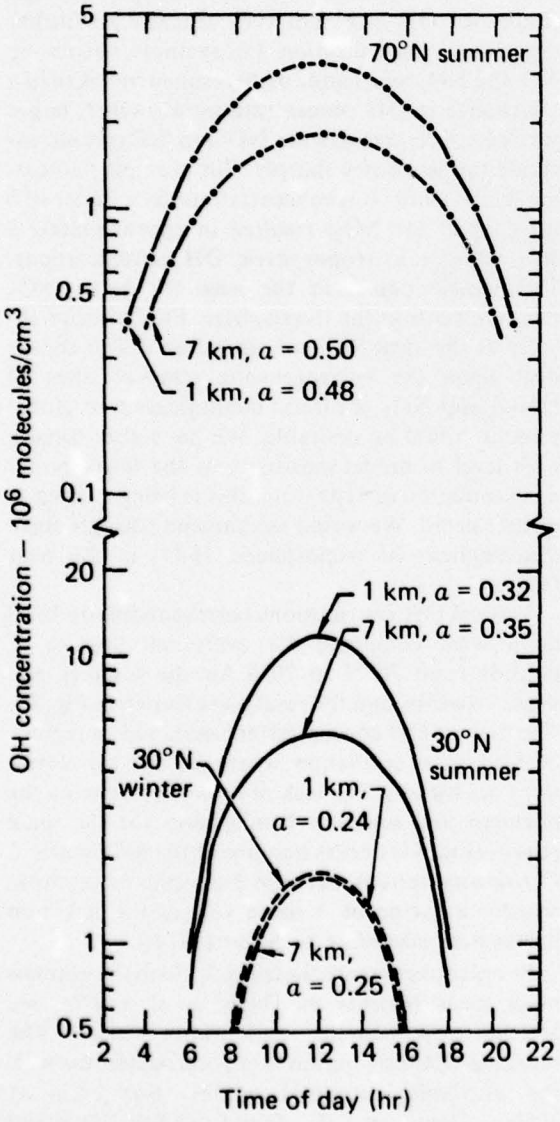

Figure 42. **Examples of the time and spatial variations in the diurnal OH distribution.**

A diurnal averaging factor, α, was determined for each of the calculated diurnal variations by calculating the average 24-hour OH concentration relative to the noon value. Generally our averaging factor is somewhat larger than the value given by Warneck (1975). We believe this is due to the fact that Warneck obtained the scaling factor through averaging the photolysis rate of O_3 in forming $O(^1D)$ while ours is a direct result taking into account the diurnal variations of other trace species such as NO, NO_2, HO_2, etc. Values of α ranging from 0.22 to 0.50 were found depending on season and latitude, with a small dependence on altitude. Multiplying α times the noon OH concentrations gives the diurnally averaged concentrations shown in Fig. 43. Since smaller values of α occur in summer equatorial regions than in the polar regions, the diurnal-averaged distribution tends to be more uniform spatially than the distribution of local noon values.

The OH distribution averaged diurnally and seasonally is shown in Fig. 44. Approximately 75% of the tropospheric OH is contained in the band 30°S–30°N, although this band comprises only half of the global area. Therefore, a majority of the tropospheric OH will be found, in a seasonal- and diurnal-averaged sense, within the equatorial region; 97% of it is contained between 60°S and 60°N. Integrating the diurnal- and seasonal-averaged concentrations of OH in Fig. 44 results in a tropospheric average OH concentration of 1.68×10^6 molecules/cm^3.

It is also interesting to note the clear presence of the tropopause in these results (Figs. 41, 43, and 44). This is expected in that the initial data such as temperature, water vapor, ozone, and carbon monoxide all exhibit distinct transitions between the troposphere and stratosphere. The preservation of such transition regions in the computed OH distribution is indirect evidence on the meaningfulness of this modeling procedure.

New 1-D Model Results

Recent remeasurements of the reaction rates for NO + HO_2 and OH + CO (a large pressure dependence was noted) have led to significant changes in the model chemistry. The net result of these model changes is that the tropospheric average OH concentration computed with our one-dimensional model is now 1.28×10^6 molecules/cm^3 as compared to the previous value of 1.7×10^6 molecules/cm^3. Table 15 shows the sensitivity of the tropospheric average OH to changes in various parameters within the one-dimensional model. Note that the sensitivity to NO and NO_2 is much greater

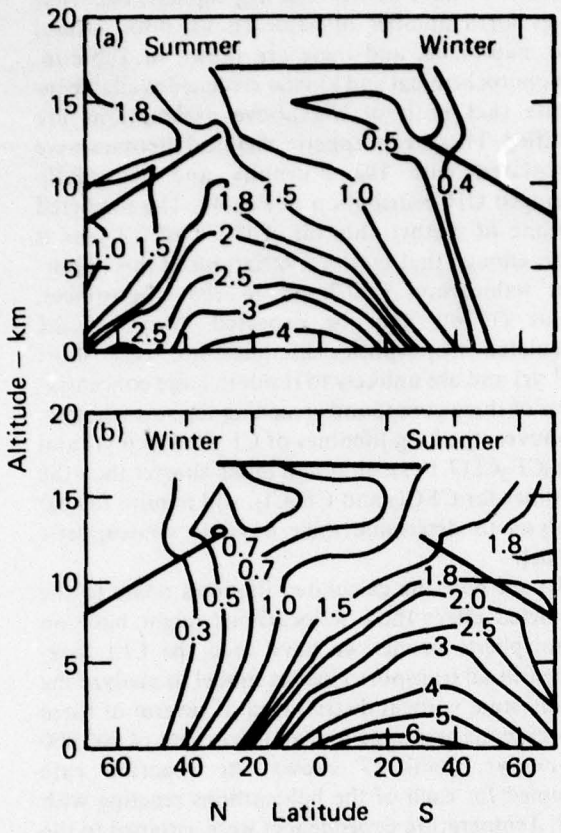

Figure 43. **Calculated diurnally averaged global OH distribution. Heavy lines represent average tropopause altitude.**

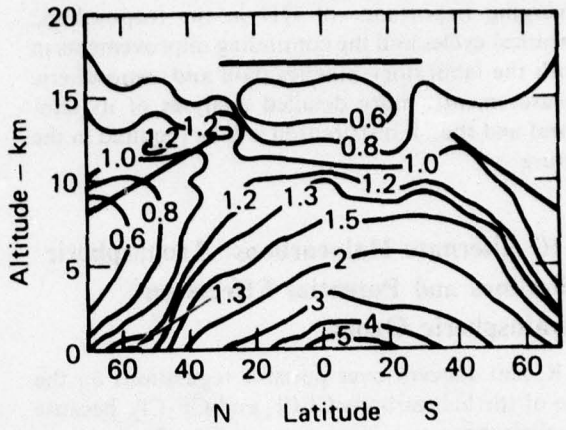

Figure 44. **Seasonally and diurnally averaged global OH distribution. Heavy lines represent average tropopause altitude.**

than that found previously. The present values from the one-dimensional model compare very closely to those found at midlatitudes in the global distribution derivation. Therefore, although the latitudinal distribution would be affected, a recalculation of the global OH distribution should not result in large differences in average tropospheric OH from the previous assessment.

Utilizing observational data for the key parameters to determine tropospheric OH, we have calculated a global distribution that agrees well with the available but limited measured data. We have also identified some of the major uncertainties in the determination of global OH distribution, such as the lack of measurements of H_2O_2 and HO_2, the lack of global tropospheric data on NO_x, and the uncertainty in the production mechanisms of HO_x from hydrocarbons. In addition, it should be noted that neglected processes such as a net source or sink of HO_x from nonmethane hydrocarbons may play an important role in the determination of a global

Table 15. **Sensitivity of calculated average tropospheric OH to changes in various parameters within the one-dimensional model.**

Case	Average OH calculated (molecules/cm^3)
Ambient atmosphere	1.28×10^6
Change NO_x boundary conditions—less NO_x (NO from 0.1 to 0.067 ppb, NO_2 from 0.25 to 0.1 ppb)	1.05×10^6
Change NO_x boundary conditions—more NO_x (NO to 0.17 ppb, NO_2 to 0.4 ppb)	1.5×10^6
$HO_2 + NO$ rate = 6×10^{-13} rather than 8×10^{-12}	0.4×10^6
Pressure dependence of CO + OH not included	1.9×10^6
Methane cycle produces 1 HO_2 rather than 2 HO_2	1.1×10^6
H_2O_2 photolysis cutoff at 254 nm rather than 315 nm	0.7×10^6

tropospheric OH distribution. Because of the emerging importance of OH in the tropospheric chemical cycles and the continuing improvements in both the laboratory kinetics data and atmospheric measurements, more detailed analyses of its temporal and spatial distribution will be required in the future.

2.10 Alternate Halocarbons: Tropospheric Lifetimes and Potential Effects on Stratospheric Ozone

Recent concern over possible regulations on the use of the halocarbons $CFCl_3$ and CF_2Cl_2, because of their potential impact on stratospheric ozone (National Research Council 1976, Hudson 1977), has prompted consideration of potential replacement compounds. The prime reason for the accumulation of $CFCl_3$ and CF_2Cl_2 in the troposphere and eventually the stratosphere is their inertness. Consequently, in seeking alternate halocarbons, we consider it a desirable characteristic that they be degraded in the troposphere. For many of the potential substitutes, reaction with OH radicals appears to be the principal mode of degradation in the troposphere. Given a tropospheric distribution of OH, we can estimate the tropospheric chemical lifetimes.

The tropospheric chemical lifetime τ for the reaction OH + X with reaction rate K can be specified by

$$\frac{1}{\tau} = \frac{\int_V K[X]\,[OH]\,dV}{\int_V [X]\,dV}$$

where [ ] is concentration and V is volume, indicating integration over the whole troposphere. If we assume that the species X is uniformly mixed in the troposphere, then

$$\frac{1}{\tau} = \frac{\int_V K[OH]\,\rho\,dV}{\int_V \rho\,dV}$$

where ρ is air density.

Assuming that the reaction with OH is the rate-determining step for the overall degradation process, we have determined tropospheric residence times for a number of halocarbons, both natural and man-made, and these are shown in Table 16. All photochemical and kinetic evidence available indicate that both of the above assumptions are justified. These tropospheric chemical lifetimes were calculated with the diurnally and seasonally averaged OH distribution in Fig. 44. The predicted lifetime of methyl chloride, CH_3Cl, of 0.4 year is short enough that seasonal variations of this important halocarbon (~0.7 ppb in the troposphere, Davis (1976)) may be expected. Most of the calculated tropospheric lifetimes are very short (≤1 yr) and are unlikely to result in large concentrations of these compounds reaching the stratosphere. However, the long lifetimes of CF_2ClH (4.6 yr) and CH_3CF_2Cl (7.1 yr), although much shorter than the lifetimes for $CFCl_3$ and CF_2Cl_2, will require further analysis to determine their possible stratospheric impact.

To see how the calculated lifetimes relate to the predicted effect these halocarbons might have on stratospheric ozone, we have used the LLL one-dimensional transport-kinetics model to analyze the steady-state vertical distribution of several of these halocarbons assuming a production rate of 500,000 tonnes/yr. Table 17 shows the reaction rate assumed for each of the halocarbons reacting with OH. Temperature dependences were assigned to the rate coefficients for CF_3CH_2Cl, CF_3CL_2H, and CF_3CFClH on the basis of a comparison with the reaction rates of similar reactions as measured by Davis (1976).

Figure 45 shows the absorption cross sections used for the five halocarbons tested. These cross

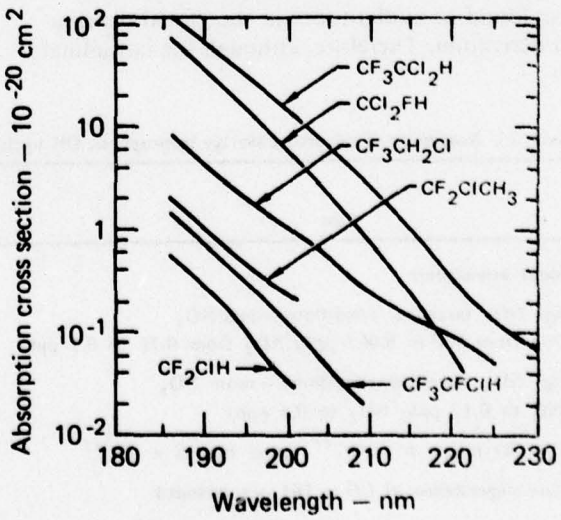

Figure 45. **Absorption cross sections used for the five halocarbons tested.**

Table 16. Estimated tropospheric chemical lifetimes (τ) of halocarbons.[a]

Species	Designation	τ (yr)	Rate data
CH_3Cl	–	0.4	Davis (1976)[b]
CH_2Cl_2	–	0.2	Davis (1976)[b]
CCl_3H	–	0.2	Davis (1976)[b]
CH_3Br	–	0.5	Davis (1976)[b]
C_2Cl_4	–	0.2	Davis (1976)[b]
CH_3CCl_3	FC-31	1.4	Howard and Evenson (1976)[c]
CH_2ClF	FC-31	1.5	Davis (1976)
CF_3Cl_2H	FC-123	0.6	Howard and Evenson (1976)
CCl_2FH	FC-21	0.6	Howard and Evenson (1976)
CCl_2FH	FC-21	0.7	Davis (1976)
CF_3CFClH	FC-124	1.3	Howard and Evenson (1976)
CF_3CH_2Cl	FC-133a	1.5	Howard and Evenson (1976)
CF_2ClH	FC-22	4.5	Howard and Evenson (1976)
CF_2ClH	FC-22	4.6	Davis (1976)
CF_2ClCH_3	FC-142b	5.4	Howard and Evenson (1976)
CF_2ClCH_3	FC-142b	7.1	Davis (1976)

[a]These lifetimes are based on the 2-D OH distribution computed in Section 2.9.

[b]Temperature-dependent rate data.

[c]Room-temperature measurements.

Table 17. The reaction rates of halocarbons with OH assumed in investigating the effects of the calculated halocarbon lifetimes (Table 16) on the predictions of stratospheric ozone (see Table 18).

Reaction	Rate coefficient	Source
$CF_3CH_2Cl + OH$	$5.9 \times 10^{-13} \exp(-1200/T)$	Based on Howard and Evenson (1976)
$CF_3Cl_2H + OH$	$1.24 \times 10^{-12} \exp(-1056/T)$	Based on Howard and Evenson (1976)
$CF_2ClH + OH$	$9.5 \times 10^{-13} \exp(-1577/T)$	Davis (1976)
$CF_3CFClH + OH$	$5.25 \times 10^{-13} \exp(-1191/T)$	Based on Howard and Evenson (1976)
$CF_2ClCH_3 + OH$	$1.14 \times 10^{-12} \exp(-1750/T)$	Davis (1976)

sections are based on unpublished data by Witt and Silver (private communication, 1977). All chlorine atoms in a molecule were assumed to be released when it reacted.

The change in total ozone computed at steady state is shown in Table 18 for each of the halocarbons. The predicted change in total ozone was small for all of the halocarbons tested, ranging from –0.13% for CF_3Cl_2H to –0.40% for CF_2ClCH_3. These are to be contrasted to the –9.3% change in total ozone predicted for CF_2Cl_2 assuming the same production rate to steady state of 500,000 tonnes/yr. As shown in Table 18, changing the boundary conditions for NO and NO_2

Table 18. **Calculated change in total ozone due to a steady-state release of halocarbons at a rate of 500,000 tonnes/yr. Results are given for two different average tropospheric OH concentrations.**

Species	Change in total ozone (%) assuming:	
	OH = 1.28×10^6 cm^{-3}	OH = 1.05×10^6 cm^{-3}
CF_3CH_2Cl (FC 133a)	−0.19	−0.21
CF_3Cl_2H (FC-123)	−0.13	−0.14
CF_2ClH (FC-22)	−0.36	−0.40
CF_3CFClH (FC-124)	−0.17	−0.18
CF_2ClCH_3 (FC-142b)	−0.40	−0.43

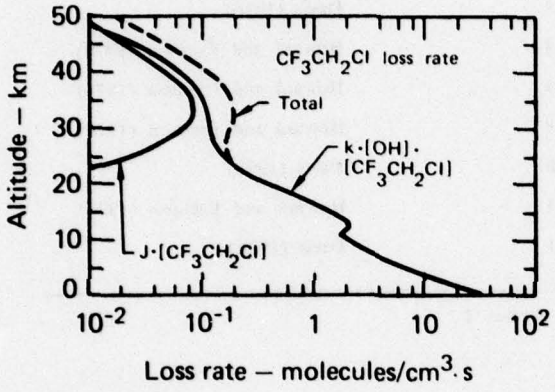

Figure 46. **Calculated loss rate with altitude for CF_3CH_2Cl (FC-133). Both photochemical (J) and two-molecule chemical-kinetics (k) reactions are plotted.**

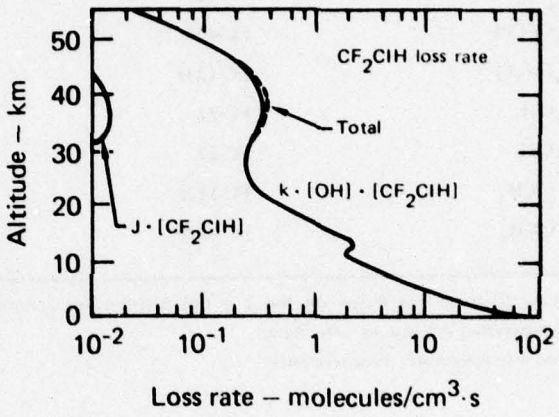

Figure 48. **Calculated loss rate with altitude for CF_2ClH (FC-22).**

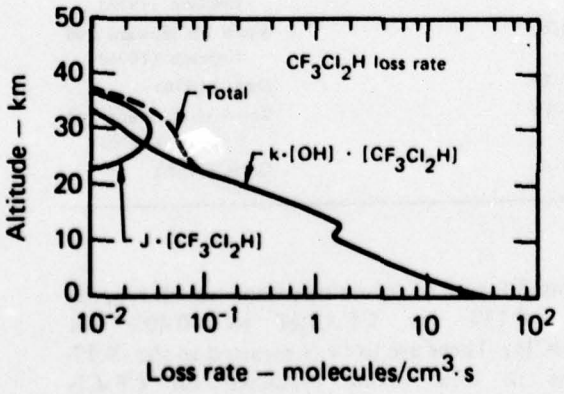

Figure 47. **Calculated loss rate with altitude for CF_3Cl_2H (FC-123).**

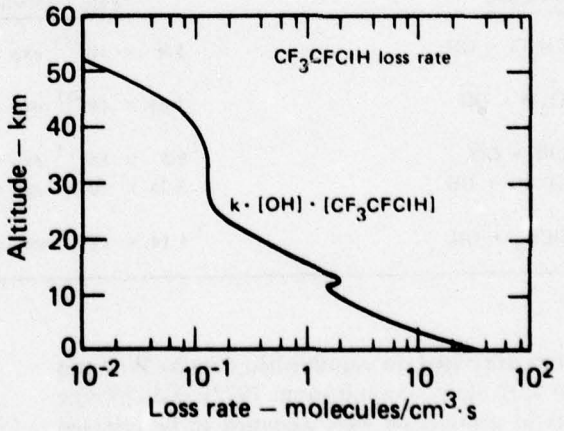

Figure 49. **Calculated loss rate with altitude for CF_3CFClH (FC-124).**

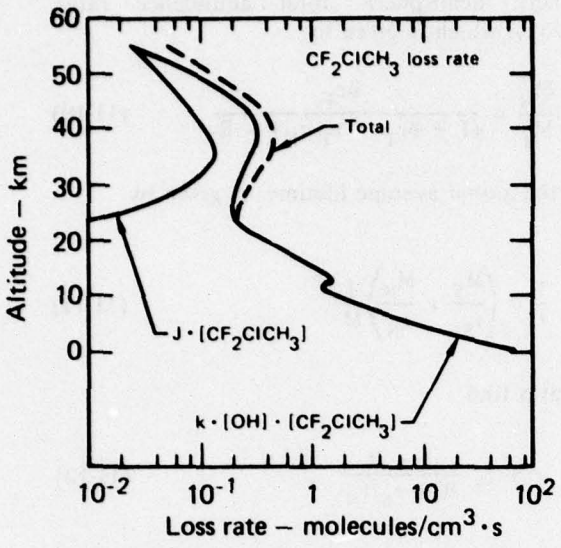

Figure 50. **Calculated loss rate with altitude for CF_2ClCH_3 (FC-142b).**

(see Table 15) so as to reduce the average tropospheric OH to 1.05×10^6 molecules/cm^3 has very little effect on the predicted ozone perturbation.

Figures 46–50 show the calculated loss rates versus altitude for each of the halocarbons. In each case, most of the loss occurs in the troposphere or lower stratosphere where very little of the released chlorine is capable of reaching altitudes important to the chlorine-ozone catalytic cycle. On the other hand, most of the CF_2Cl_2 is destroyed in the upper stratosphere, with very little being destroyed in the troposphere or lower stratosphere.

2.11 Analysis of Global Budgets of Halocarbons

A two-box model provides a framework within which one may examine the consistency of atmospheric data concerning the abundance and hemispheric ratio of man-made halocarbons and their release rate data. The continuity equations that constitute the model relate the hemispheric abundances (north and south) to the anthropogenic release rates, the chemical removal rates, and the interhemispheric transport time. Given the usually representative exponentially increasing release rates, the solutions of the two-box model are no more complicated than those of the simple one-box model, but they add considerable insight into the adequacy and deficiencies of these simple analysis techniques. By accounting for the two hemispheric abundances separately, it is possible to check the internal consistency of hemispheric data and global averages.

The continuity equations for the abundance of a given trace species in each hemisphere may be written

$$\frac{dM_N}{dt} = S_N - \frac{1}{\tau_N} M_N - \frac{1}{\tau_T} (M_N - M_S) . \quad (11\text{-}1)$$

$$\frac{dM_S}{dt} = S_S - \frac{1}{\tau_S} M_S + \frac{1}{\tau_T} (M_N - M_S) . \quad (11\text{-}2)$$

where

M_N, M_S = the total hemispheric abundances (north and south),

S_N, S_S = the hemispheric release rates,

τ_N, τ_S = the chemical removal rates,

τ_T = the interhemispheric mixing time.

Following the pattern of historical release data, the release rate in the northern hemisphere is taken to be equal to a simple exponential function,

$$S_N = ae^{bt} , \quad (11\text{-}3)$$

and the southern hemispheric release rate is assumed to equal zero. The solutions for (11-1) and (11-2) are

$$M_N(t) = \alpha_0 e^{bt} + \alpha_1 \exp(-\lambda_1 t) + \alpha_2 \exp(-\lambda_2 t) . \quad (11\text{-}4)$$

$$M_S(t) = \beta_0 e^{bt} + \beta_1 \exp(-\lambda_1 t) + \beta_2 \exp(-\lambda_2 t) . \quad (11\text{-}5)$$

where

$$\alpha_0 = \frac{a\tau_T(1 + b\tau_T + \tau_T/\tau_S)}{(1 + b\tau_T + \tau_T/\tau_S)(1 + b\tau_T + \tau_T/\tau_N) - 1} ,$$

$$\alpha_1 = -\alpha_0 - \alpha_2 ,$$

$$\alpha_2 = \frac{\alpha_0(1/\tau_N + 1/\tau_T - \lambda_1) - \beta_0/\tau_T}{\lambda_1 - \lambda_2} ,$$

$$\beta_0 = \frac{a\tau_T}{(1 + b\tau_T + \tau_T/\tau_S)(1 + b\tau_T + \tau_T/\tau_N) - 1} ,$$

$$\beta_1 = \alpha_1\tau_T(1/\tau_N + 1/\tau_T - \lambda_1) ,$$

$$\beta_2 = \alpha_2\tau_T(1/\tau_N + 1/\tau_T - \lambda_2) ,$$

$$\lambda_{1,2} = \frac{1}{2}\left[(1/\tau_S + 1/\tau_N + 2/\tau_T) \pm \left[\left(1/\tau_N - 1/\tau_S\right)^2 + 4/\tau_T^2\right]^{1/2}\right] . \quad (11\text{-}6)$$

and we have assumed $M_N = M_S = 0$ at $t = 0$. A similar solution may be found for the case in which S_N varies exponentially, as in (11-3), with different rates, b, over different time periods.

The total cumulative amount of gas released into the atmosphere at any given time t is

$$M_T = \frac{a}{b}(e^{bt} - 1) . \quad (11\text{-}7)$$

For sufficiently long times ($bt >> 1$), the ratio of the total atmospheric abundance, $M = M_S + M_N$, to the total released is approximately constant,

$$\frac{M}{M_T} = \frac{b\tau_S}{1 + b\tau_S - \frac{1}{1 + R}(1 - \tau_S/\tau_N)} , \quad (11\text{-}8)$$

where R is the hemispheric ratio of abundances, M_S/M_N. This formula reduces to the formula derived for the one-box model in the case $\tau_S = \tau_N$ (compare Singh 1977). To the same order of approximation, the ratio R is further related to the parameters τ_S and τ_T according to

$$R = \frac{M_S}{M_N} = \frac{1}{1 + b\tau_T + \tau_T/\tau_S} , \quad (11\text{-}9)$$

from which τ_T may be easily deduced from a knowledge of the hemispheric abundance ratio for a gas with a fairly long lifetime (see next subsection). For our further discussion we introduce the northern hemispheric total abundance ratio, M_N/M_T, which is given by

$$\frac{M_N}{M_T} = \frac{b\tau_T}{(1 + b\tau_T + \tau_T/\tau_N) - R} , \quad (11\text{-}10)$$

and the global average lifetime, τ, given by

$$\frac{1}{\tau} = \left(\frac{M_S}{\tau_S} + \frac{M_N}{\tau_N}\right)\frac{1}{M} . \quad (11\text{-}11)$$

We also find

$$\tau = \tau_S \frac{1 + R}{R + \tau_S/\tau_N} . \quad (11\text{-}12)$$

If $\tau = \tau_S = \tau_N$ (e.g., F-11 and F-12), we have from Eq. (11-8)

$$\frac{\Delta\tau}{\tau} = -\frac{\Delta b}{b}$$

$$= \frac{\Delta(M/M_T)}{(M/M_T)}\left[1 + \frac{M/M_T}{(1 - M/M_T)}\right] .$$

Consequently, if one deduces the atmospheric lifetime from the real release rate coefficient b and the measured global abundance ratio, M/M_T, the percent variation in τ is only directly proportional to the percent variation in b but may have a very strong dependence on the variations in M/M_T. If M/M_T is in the range of 0.8 to 0.9 as is observed for the long-lived halocarbons, the amplification factor on the variation of the atmospheric lifetime is in the range of 5 to 10. Thus, a 5% uncertainty in the global abundance ratio M/M_T for F-11 or F-12 will lead to 25% to 50% error in the deduced lifetime for these trace species. A large number of very accurate measurements with good global coverage would be required to establish the abundance ratio M/M_T to better than 5%. Thus it is nearly impossible to conclusively detect the existence or nonexistence of the so-called "hidden tropospheric sinks" for long-lived halocarbons through global budget analysis (see the second subsection following for further discussion).

For shorter-lived species we may hope to derive a more meaningful lifetime from a budget analysis. It is important, however, in this case to use the two-box model to check the atmospheric data for consistency with the analysis. If τ_T and b are known, Eqs. (11-9) and (11-10) provide a clear test for this

purpose. While the lifetime analysis for shorter-lived species is still highly sensitive to uncertainties in R and M_N/M_T if varied separately, the field of possible variations is reduced with the two-box model since both R and M_N/M_T must be consistent with a single interhemispheric mixing time, τ_T.

We have framed our two-box model discussion in terms of the parameters M_N/M_T and R because we believe that their determination from atmospheric data should be relatively more accurate than the determination of either hemispheric abundance separately. The determination of R should be less sensitive than that of either M_N or M_S to any possible systematic instrumental bias present in the measurements. The use of M_N/M_T is preferable to the use of M/M_T because the relative error for M_N should be smaller than the relative error for M. This follows because of the better latitudinal coverage in the northern hemisphere and the larger magnitude of local concentrations. For the gases discussed below, R and M_N/M_T were calculated assuming a constant mixing ratio equal to that obtained for a particular observation above 20° latitude in the northern hemisphere and below 30° latitude in the southern hemisphere (Rasmussen 1977), and assuming a linearly decreasing concentration from 20°N to 30°S. The mixing ratio was constant throughout the troposphere, whose vertical extent was taken equal to 16 km from 30°N to 30°S, and decreased linearly from a value equal to 13 km at 30°N and 30°S to 8 km at the poles. The concentration in the stratosphere was taken equal to zero, except for the species with known long tropospheric lifetimes.

Application to Freon-11

As shown in Fig. 51, we obtain a good fit to the release rate data for F-11 using the exponential function given in Eq. (11-3), for the periods 1958–1965, 1965–1973, 1973–1974, and 1974–1977, with the following parameters:

a	b	Period
28.0	0.19	1958–1965
106	0.13	1965–1973
314	0.032	1973–1974
324	−0.025	1974–1977

The formulas (11-9) and (11-10) relating M_N/M_T and R to τ_N, τ_S, and τ_T should be applicable for data obtained before 1975 if we use b = 0.13. Data obtained after early 1975 must be analyzed using the full time-dependent solution given by (11-4) and (11-5), since a new steady state for M_N/M_T and R would take several years to develop (see Fig. 54). Unfortunately, as discussed below, not many measurements for F-11 are available for the period before 1975.

Figure 52 shows how the solutions for the interhemispheric mixing time, τ_T, and atmospheric lifetime, τ, depend on the parameters M_N/M_T and R in the case $\tau_S = \tau_N$. Large values for the ratio R are consistent with short mixing times; large values for M_N/M_T are consistent with long atmospheric lifetimes. The dependence of the lifetime on M_N/M_T is quite sensitive to values of M_N/M_T near the physical upper limit,

$$M_N/M_T = \frac{1}{1+R} \quad (\text{as } \tau_S = \tau_N \to \infty) .$$

This is illustrated further in Fig. 53, and we may conclude that, as already mentioned, a very high level of accuracy in the data for the hemispheric abundance is required in order to derive a reliable estimate for the lifetime of long-lived species (i.e., F–11 and F-12). For example, Fig. 53 shows that M_N/M_T would need to be known to better than 6% in order to conclusively show that the lifetime for

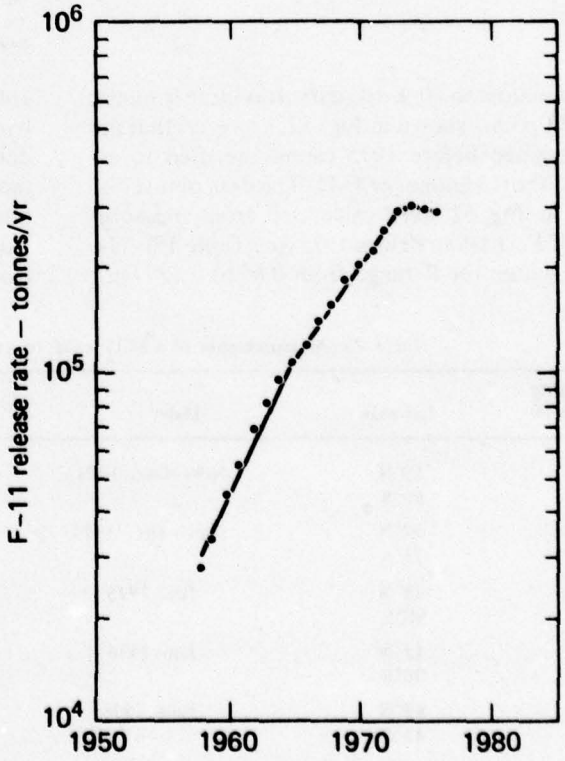

Figure 51. **Release rate of F-11 (Freon 11). Data points were taken from Hudson (1977) and Van Horn (1977). The straight lines correspond to the fit obtained using the parameters for Eq. (11-3) given in the text.**

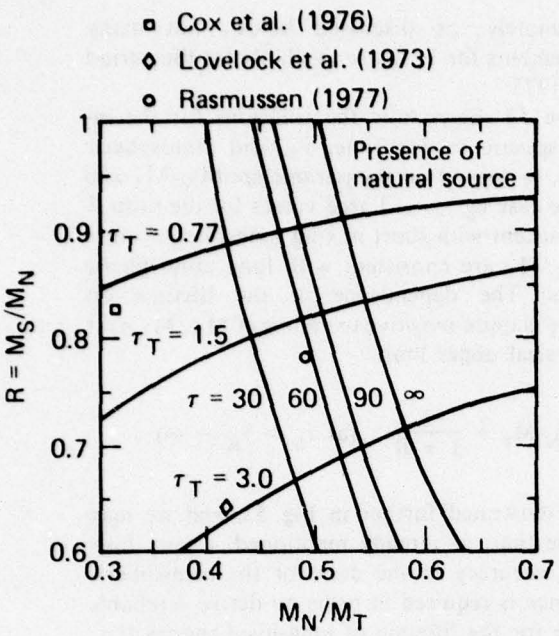

Figure 52. **Relationship between the F-11 hemispheric ratio of abundances, $R = M_S/M_N$, the northern hemispheric abundance ratio, M_N/M_T, the interhemispheric mixing time, τ_I, and the chemical removal time, τ, for the two-box model with $\tau = \tau_S = \tau_N$. The units for τ and τ_I are years.**

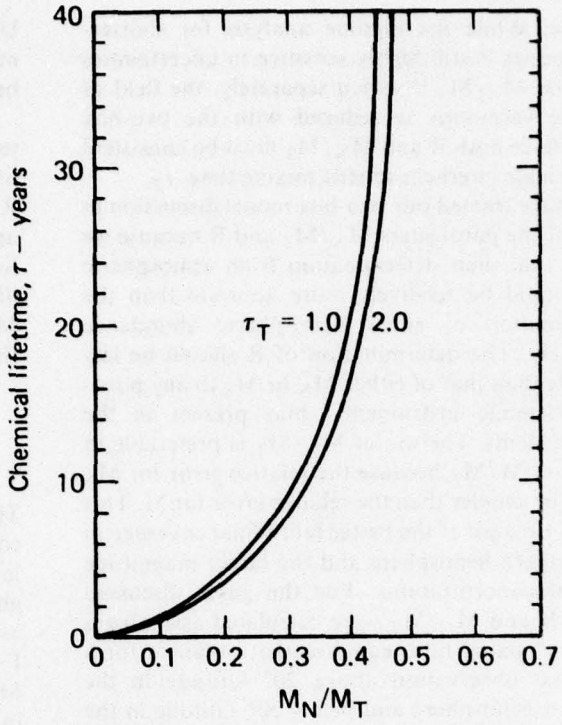

Figure 53. **Sensitivity of the derived atmospheric lifetime of F-11 to changes in the abundance ratio M_N/M_T for the case $\tau = \tau_S = \tau_N$ for two values of the interhemispheric mixing time τ_I (in years).**

F-11 was equal to 30 ± 10 years. It is clear from the scatter of points shown in Fig. 52, however, that the data obtained before 1975 cannot be used to establish a short lifetime for F-11. The data points displayed in Fig. 52 were calculated from measurements of F-11 taken before 1975 (see Table 19). The derived values for R range from 0.65 to 0.82. They are consistent with transport times in the range from 0.94 to 3.0 years. The measured total abundance ratios, M_N/M_T, are also widely scattered and range from 0.31 to 0.49. The concentrations reported by Rasmussen (1977) appear to be most consistent with the 60-year lifetime for F-11 determined from atmospheric models (National Research

Table 19. **Measurements of $CFCl_3$ used to calculate data points of Fig. 52.**

F-11 mixing ratio (ppt)[a]	Latitude	Date	R	M_N/M_T	Reference
70	50°N	Nov.–Dec. 1971	0.640	0.417	Lovelock et al. (1973)
38	60°S				
79.8	52°N	Sept.–Dec. 1974	0.824	0.313	Cox et al. (1976)
61.7	33°S				
125	43°N	Jan. 1975	0.782	0.489	Rasmussen (1977)
90	90°S				
138	43°N	Jan. 1976	0.860	0.489	Rasmussen (1977)
113	90°S				
143	43°N	June 1976	0.903	0.483	Rasmussen (1977)
125	43°S				
154	43°N	Jan. 1977	0.822	0.493	Rasmussen (1977)
127	90°S				

[a]Parts per trillion (10^{12}).

Council 1976). His measured interhemispheric ratio, 0.78, would imply an interhemispheric mixing time of 1.9 years.

Since 1975 the value for R derived from atmospheric measurements has apparently increased. As shown in Fig. 54 the growth in R is consistent with the decreasing rate for the release of F-11 (Fig. 51). A very rapid growth of R, as suggested by the data shown in Fig. 54, is not consistent with the two-box time-dependent model. As shown in Fig. 54 the calculated rise in R after 1975 increases more rapidly for longer interhemispheric mixing times. If the interhemispheric transport time were longer than two years, a rapid rise could be explained, but then the calculated absolute value of R would be substantially less than that required by the data. Since there were very few measurements taken before 1975, conclusions based on the rate of growth for R are risky. We therefore take 1 yr $< \tau_T <$ 2 yr as an acceptable range for the interhemispheric transport time (compare Czeplack and Junge 1973).

Application to CH_3CCl_3

The time history for the release of methylchloroform is shown in Fig. 55 along with the exponential release rate we used for Eq. (11-3). The data shown in Fig. 55 do not correspond precisely to the single exponential growth rate chosen, but the solutions for R and M_N/M_T are very stable to changes in the parameter b used in Eq. (11-3). We have verified numerically that the change in b could be as large as 50% lasting over 3-year periods without causing the solution for R and M_N/M_T to change by more than 5%.* We may therefore use Eqs. (11-9) and (11-10) in what follows.

Table 20 presents the data for CH_3CCl_3 and the calculated values for R and M_N/M_T. In order to compare these values with the two-box theory, we must specify one of the three parameters τ_S, τ_N, or τ_T, or introduce another relationship. CH_3CCl_3 is removed in the troposphere by reaction with OH, and the average abundance of OH in each hemisphere is not expected to be the same since higher concentrations of CO in the north should cause a lower OH concentration (Wofsy 1976). Current models suggest there should be about a 25% variation in the average concentration for OH between the hemispheres. In what follows we therefore assume $\tau_S = 0.75\tau_N$, although the conclusions drawn are not very sensitive to the precise value used for the ratio of the removal rates.

Figure 56 shows the values for R and M_N/M_T from Table 20 plotted on a graph which relates these parameters for several values of τ_T, with $\tau_S = 0.75\tau_N$. Also shown are the values derived using a constant tropospheric mixing ratio in each

*This conclusion was based on the use of τ_T = 1.5 years.

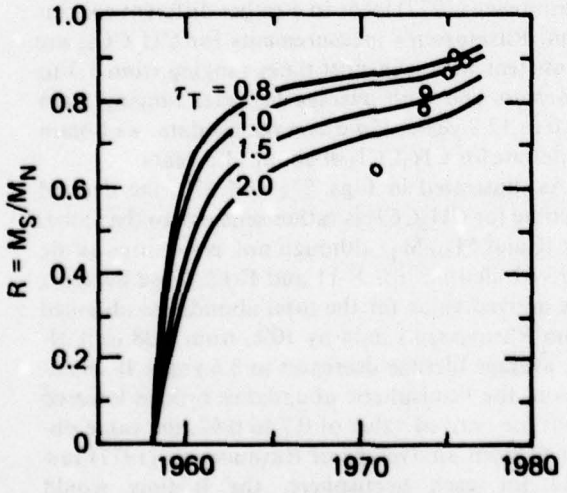

Figure 54. **Growth in the F-11 hemispheric abundance ratio, R = M_S/M_N, for the release data shown in Fig. 51, for four values of the interhemispheric mixing time τ_T (in years). Data points are taken from Table 19 and refer to the measurements of Lovelock et al. (1973), Cox et al. (1976), and Rasmussen (1977).**

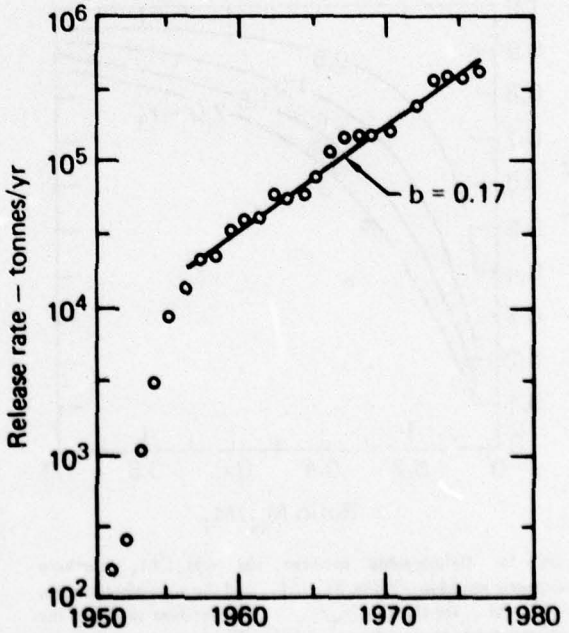

Figure 55. **Release rate of CH_3CCl_3. Data points were taken from Neely and Plonka (1977). The straight line corresponds to the fit obtained with b = 0.17 in Eq. (11-3).**

Table 20. **Measurements of CH_3CCl_3 mixing ratios.**

CH_3CCl_3 mixing ratio (ppt)[a]	Latitude	Date	R	M_N/M_T	Reference
64.8	52°N	Sept.–Dec. 1974	0.503	0.285	Cox et al. (1976)
24.4	35°S				
90	47°N	Jan. 1975	0.686	0.403	Rasmussen (1977)
54	90°S				
98	47°N	Jan. 1976	0.672	0.376	Rasmussen (1977)
57	78°S				
109	43°N	June 1976	0.743	0.389	Rasmussen (1977)
73	43°S				
110	47°N	Jan. 1977	0.716	0.364	Rasmussen (1977)
70	90°S				

[a]Parts per trillion (10^{12}).

hemisphere equal to the value measured in each hemisphere. For Rasmussen's (1977) data, the more carefully derived hemispherical abundances are consistent with an average interhemispheric transport time of 1.5 years. This is easily within the range of acceptable values for τ_T derived from the budget for the more extensively measured F-11. The interhemispheric transport time derived from the raw abundance data is 2.11 years, somewhat longer than that considered appropriate.

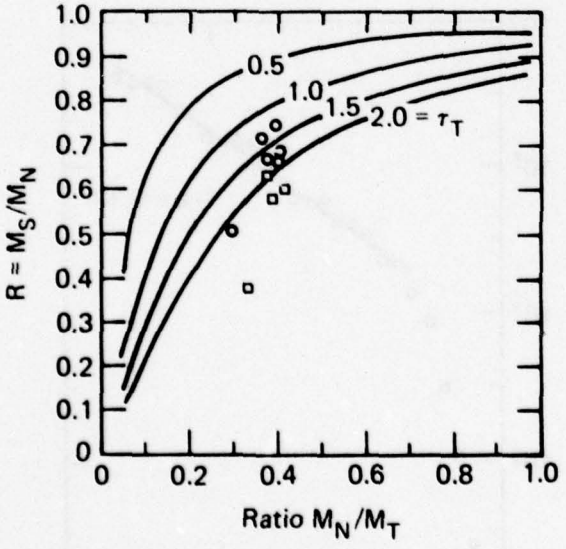

Figure 56. **Relationship between the CH_3CCl_3 northern hemispheric abundance ratio, M_N/M_T, and the hemispheric ratio, $R = M_S/M_N$, for the case $\tau_S/\tau_N = 0.75$, for four values of the interhemispheric mixing time τ_T (years). The circle data points are measurements by Cox et al. (1976), the square points by Rasmussen (1977) (see Table 20).**

Even for the adjusted values, the earliest measurements (Cox et al. 1976) appear not to be consistent with interhemispheric mixing times that are less than about two years. This conclusion remains true unless the removal rate in the southern hemisphere is more than two times faster than that in the north, a condition that is not presently supported by two-dimensional models for the tropospheric OH abundance (Wofsy 1976, Chang et al. 1977). Using the data measured by Cox et al. (1976) and assuming the northern hemispheric removal rate is 25% slower than that in the south, we derive a transport time equal to 2.3 years and an average atmospheric lifetime for CH_3CCl_3 equal to about 4.5 years. This same analysis applied to the measurements made by Rasmussen (1977) leads to a rather different conclusion. Rasmussen's measurements for CH_3CCl_3 are consistent with transport times ranging from 1.3 to 1.8 years and with average lifetimes ranging from 10.0 to 12.8 years. If we average his data, we obtain a lifetime for CH_3CCl_3 of about 11.3 years.

As illustrated in Figs. 57a and 57b, the derived lifetime for CH_3CCl_3 is rather sensitive to the values for R and M_N/M_T, although not as sensitive as the derived lifetimes for F-11 and F-12. If we decrease the derived value for the total abundance obtained from Rasmussen's data by 10%, from 0.38 to 0.34, the average lifetime decreases to 8.6 years. If, in addition, the hemispheric abundance ratio is lowered from the derived value of 0.7 to 0.62, the value obtained from an average of Rasmussen's (1977) raw data for each hemisphere, the lifetime would decrease to 7.6 years. This again illustrates the high level of sensitivity to uncertainties in the atmospheric data.

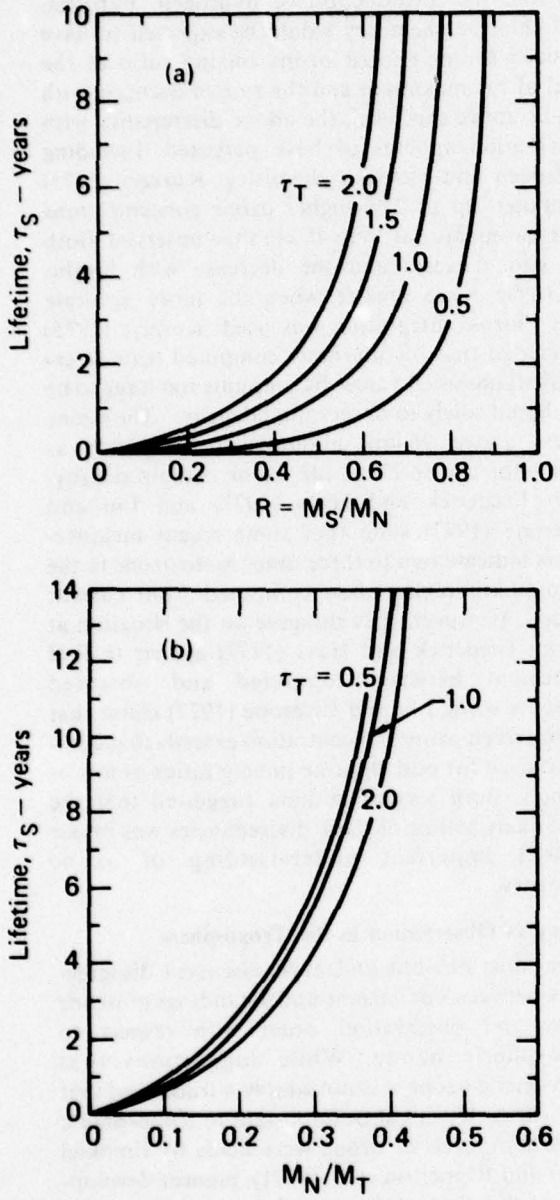

Figure 57. (a) Sensitivity of the CH_3CCl_3 derived southern hemispheric lifetime, τ_S, to the hemispheric abundance ratio, $R = M_S/M_N$, for the case $\tau_S/\tau_N = 0.75$, for four values of the interhemispheric mixing time τ_T (years). (b) Sensitivity of τ_S to the northern hemispheric abundance ratio, M_N/M_T, for the same conditions as in (a).

The 11.3-year average lifetime for CH_3CCl_3 derived above is not consistent with the lifetime derived using the OH concentrations from a one-dimensional chemical model. In order to obtain a lifetime for CH_3CCl_3 consistent with the values derived from the two-box model, the diurnally and vertically averaged tropospheric OH concentration in the one-dimensional model would have to be lowered from the current value of 8.0×10^5 molecules/cm^3 to 2.5×10^5.*

It is not likely that the entire tropospheric OH concentration from the one-dimensional model is a factor of 3 too high since the calculated noontime OH concentrations near 7 km and 11 km are already somewhat lower than the values measured by Davis et al. (1976). If the entire tropospheric OH column were adjusted downward in order to calculate a longer lifetime for CH_3CCl_3, the concentrations near 7 km and 11 km would be at least a factor of 5 smaller than those measured by Davis et al. (1976). While Davis's measurements might be somewhat higher than the appropriate noontime global background values at those altitudes, it is difficult to imagine local perturbations which might increase OH by a factor of 5. The model results for OH above 7 km are therefore probably fairly reliable. In any case, any adjustment for OH above 5 km has very little effect on the calculated lifetime for CH_3CCl_3, since the concentration for CH_3CCl_3 decreases exponentially with the air density. The major contribution to the chemical removal of CH_3CCl_3 comes from the OH molecules near the earth's surface. This is also the region where complex processes that are not accounted for by current models may cause large variations in the density of OH. In order to increase the calculated lifetime for CH_3CCl_3 from the one-dimensional model by a factor of 3, the OH concentrations below 4 km would have to decrease by about a factor of 3.

The requirement for a large change in the concentration of OH near the surface would be reduced somewhat if the global abundance for CH_3CCl_3 were actually smaller than the values derived above. It is clear that a better understanding of the chemical balances in the lower troposphere is needed. More latitudinal coverage in the measurements of CH_3CCl_3 and more measurements of the OH concentration in the lower troposphere are highly desirable.

2.12 A Review of Ozone Theory and Observational Data †

Until recently, attempts to validate ozone models have been restricted to comparisons within the stratosphere and primarily to total column depths and vertical profiles of measurable species. For 1-D

*With the cross sections for photolysis of H_2O_2 of Molina and Molina (private communication, 1977) the average OH concentration in our model increases to 1.25×10^6 molecules/cm^3. Compare Section 2.9.

†See Ellsaesser (1976b).

(one-dimensional) models such comparisons have been ambiguous at best due to the large seasonal and latitudinal variations and the paucity of observational data even for ozone and particularly so for all other trace species. Duewer et al. (1977b) demonstrated that comparison of computed and observed species profiles within the stratosphere is currently inadequate to determine a choice between ensembles of reaction rates producing drastically different sensitivities to stratospheric injection of oxides of nitrogen. In addition, with the recent development of several 2-D stratosphere models, it has become apparent that by a judicious choice of transport prescription it is possible to match latitudinal and seasonal variations in total ozone with various representations of stratospheric chemistry. Accordingly, it now appears that validation of the chemistry of the stratospheric ozone layer can best be done outside the stratosphere, or at least outside the middle and lower stratosphere where species concentrations depend more on transport than on photochemical equilibrium. That is, the most sensitive regions for validating ozone chemistry by comparison with observations appear to be above 35 km, where photochemical equilibrium is believed to be least disturbed by transport, and in the troposphere where we have the most observational data.

A review of comparisons which have been made in these regions indicates some remaining flaws or uncertainties in our current understanding of the chemistry of the ozone layer. Prechlorine models typically computed a maximum ozone mixing ratio exceeding that observed and a decrease in ozone concentration with height ($-\partial[O_3]/\partial z$) above this altitude more rapid than observed. This in turn led to computation of lower ozone concentrations than observed in the upper stratosphere and lower mesosphere.

Theory vs Observation Above Ozone Maximum

Dütsch and Ginsburg (1969) and Dütsch (1971) pointed out that with a pure oxygen atmosphere and Chapman chemistry, $-\partial[O_3]/\partial z$ is determined by the temperature dependence (or activation energy) of the ratio of the reaction rate k_2 for ozone formation ($O + O_2 + M \rightarrow O_3 + M$) to the rate k_3 for ozone destruction ($O + O_3 \rightarrow 2O_2$) and the temperature lapse rate in the stratosphere. They obtained the best fit to available ozone observations by assuming no temperature dependence for this ratio, a surprising result since 1800 K (i.e., $k_2/k_3 \approx e^{1800/T}$) was the smallest value they ever found reported from laboratory results at that time. (The currently accepted temperature dependence for this ratio is $e^{2810/T}$ (Hampson and Garvin 1975).)

While the introduction of hydrogen, nitrogen, and chlorine chemistry would be expected to have reduced the computed ozone mixing ratio at the level of the maximum and the rate of decrease with height above this level, the above discrepancy with observation appears to have persisted. Including hydrogen and nitrogen chemistry, Kurzeja (1975) computed up to 25% higher ozone concentrations over the equator at 35 to 45 km than observed. Both the ozone excess and the decrease with height, $-\partial[O_3]/\partial z$, were greater when the more accurate fully diurnal integration was used. Kurzeja (1975) concluded that his diurnally computed ozone "exceed[ed] observed values by amounts too large to be attributed solely to observational error." The ozone excess above 26 km amounted to as much as 30 m·atm·cm or 9% of the ozone column density. Both Frederick and Hays (1977) and Liu and Cicerone (1977) state that some recent measurements indicate two to three times more ozone in the 50-to-60-km region than computed from current models. However, they disagree on the situation at 40 km; Frederick and Hays (1977) appear to find agreement between computed and observed amounts while Liu and Cicerone (1977) claim that the observed ozone concentration exceeds that computed even for odd chlorine mixing ratios as low as 2.3 ppb. Both sets of authors suggested that the most likely source of these discrepancies was in our present imperfect understanding of ozone chemistry.

Theory vs Observation in the Troposphere

The most obvious and most discussed disagreements between our current understandings of ozone theory and observation occur with respect to tropospheric ozone. While suggestions that tropospheric ozone was not simply a tracer and that photochemistry might be important to tropospheric (nonurban) levels of ozone were made by Frenkiel (1955) and Ripperton et al. (1971), pioneer development of the photochemistry of tropospheric ozone and particularly of the methane cycle is generally attributed to Crutzen (1973) and Johnston and Quitevis (1974). Papers by Levy (1972, 1973), Wofsy et al. (1972), and Chameides and Walker (1973, 1976) are also relevant.

Crutzen's (1972, 1973) early work in this area led to estimates of tropospheric ozone production which exceeded the estimates of stratospheric injection and boundary-layer destruction rates of $(5.6 \pm 1.8) \times 10^{10}$ molecules/cm^2·s (Fabian and Pruchniewicz 1977) by more than 10-fold. Crutzen (1973) cautioned against accepting his results because of their apparent conflict with the observational evidence. Using more recent reaction rates

and lower concentrations of odd nitrogen, Crutzen (1974b) calculated net tropospheric (lowest 2 km) ozone production rates of $(-1.2 \text{ to } +2.6) \times 10^{11}$ molecules/cm^2·s for the reaction schemes considered. While inferring that tropospheric ozone was not chemically inert, he could not decide whether there is net destruction or production, "due to insufficient knowledge of some essential chemical processes" (Crutzen 1974b). In a still later study Fishman and Crutzen (1976), using 0.2 ppb of NO_2, arrived at a net ozone column production rate of 5×10^{10} molecules/cm^2·s, a rate regarded as "significant compared with...estimates of downward ozone flux from the stratosphere and photochemical column destruction rates." They concluded that it is "difficult to explain the observed tropospheric ozone profiles" and hypothesized "therefore, that catalytic ozone-producing mechanisms are operative in the troposphere in addition to those...considered" or "that the rate coefficients which govern ozone production are substantially larger than assumed."

Johnston and Quitevis (1974), using Crutzen's (1973) photochemistry, determined the crossover altitude as 13 km at which the "standard" NO_x profile switches from net destruction of ozone in the stratosphere to net production of ozone at lower levels via the "methane smog cycle." Their Fig. 13 indicates a net ozone column production below 13 km of about 10^{11} molecules/cm^2·s. Since then the crossover altitude for NO_x net production of ozone has been pushed above 13 km by Hidalgo and Crutzen (1976), Duewer et al. (1976), and Widhopf et al. (1977).

From their calculations Chameides and Walker (1973, 1976) concluded that tropospheric ozone is near a state of photochemical equilibrium (i.e., not transport-dominated). Serious conflicts between their results and observational data were cited by Fabian (1974), Chatfield and Harrison (1976), and Fabian and Pruchniewicz (1977). A reexamination of the tropospheric ozone budget by Chameides and Stedman (1977), in the light of revised reaction rates and lower observed concentrations of odd nitrogen, concluded "that at mid-latitudes photochemistry acts primarily as an ozone sink."

A recent more complete tropospheric model by Stewart et al. (1977), using more recent reaction rates, obtained results differing from previous models in several respects. One of their more interesting findings was that ozone did not increase monotonically with NO_x but rather exhibited a maximum for $[NO_x] \approx 0.5$ ppb. Although they could choose an NO_x concentration that would produce an ozone level near that observed, over most of the range of likely NO_x amounts the computed ozone concentration was much less than that observed. They concluded that "photochemical activity alone cannot account for observed [tropospheric] values of ozone and many other important species."

In addition to the dramatic evolution in model results reviewed above, all recent investigators have concluded that tropospheric ozone is photochemically active; except for very specific profiles of NO_x, they compute ozone production or destruction rates which exceed or are a significant fraction of the rates (generally considered to be identical) at which ozone enters the troposphere from the stratosphere and at which it is destroyed at the earth's surface. Thus, unless the observational data have been misinterpreted, there appear to be serious errors in our understanding of ozone chemistry in the troposphere. It appears unlikely that correction of such errors would leave our computations of stratospheric ozone unchanged.

The Importance of Transport

Transport has long been recognized to be the overriding controlling mechanism for many types of variations revealed by the ozone data. The list of variations begun by Chamberlain and Leovy (1975) has been expanded upon and now includes:

1. Seasonal variation. Total ozone has long been known to have a seasonal variation with maxima occurring in winter to spring and minima in summer to fall. Photochemistry alone would predict a maximum in summer and a minimum in winter.

2. Latitudinal variation. Minima in total ozone occur near the equator and maxima occur poleward of 55° latitude.

3. Biennial oscillation. Ozone observations generally reveal an oscillation with an amplitude of about 5% which in low latitudes is in phase with the quasi-biennial oscillation in the 50-mbar zonal wind over Panama. The oscillation shows an increasing phase lag with latitude but little change in the percentage amplitudes (Wilcox et al. 1977).

4. Day-to-day local variations. Day-to-day variations of total ozone correlated with the passage of synoptic systems have long been recognized.

5. Longitudinal variations. As with synoptic variations, changes in vertical motion patterns and heights of the tropopause induced by the semistationary long-wave patterns of the general circulation are accompanied by primarily longitudinal variations in total O_3. In addition, longitudinal variations in total ozone in the tropics have been ascribed to large-scale cells of ascending and descending motion induced by continent and

ocean contrasts in surface heating and topographic uplift.

6. Northern hemisphere total ozone increase of 5 to 11% from 1957 to 1970. Unless this change can be related to the parallel increase in stratospheric water vapor (Harries 1976), this increase, which is apparently restricted to the northern hemisphere (London and Kelley 1974), cannot be explained by photochemistry alone. Ellsaesser (1976c) proposed that this increase was due to a progressive weakening of Hadley-cell-driven exchange between stratosphere and troposphere evidenced by the weakening and virtual disappearance of the Junge layer in 1971, the Sahelian drought, and the lowering and warming of the tropical tropopause reported by Angell and Korshover (1974).

7. Hemispheric variation. Most investigators have concluded that mean annual total O_3 is less over the southern hemisphere than over the northern. London (1975), for the period July 1957 to June 1970, reported values of 282 and 292 m·atm·cm, respectively. From IRIS data for April through July 1969, Lovill (private communication, 1977) obtained 303 and 318 m·atm·cm, and from Nimbus BUV* data for April 1970 through April 1971, Heath (1974) reported mean hemispheric values of 301 and 314 m·atm·cm.

Stratospheric Odd-Nitrogen Budgets

Tables 21 and 22 summarize a review of stratospheric odd-nitrogen budgets determined from theoretical work and from observational data. It is apparent that the theoretical work reveals an uncertain consensus that N_2O produces approximately 80% of the odd nitrogen in the stratosphere and cosmic rays account for most of the remainder. While the N_2O production rate shows a fairly strong mode near 9×10^7 molecules/cm^2·s, the range is 20-fold, extending from 2×10^7 to 40×10^7. Additional sources that have been proposed (other than cosmic rays) include:

1. Downward transport from the thermosphere, particularly during the polar night.
2. Oxidation of NH_3.
3. Upward transport of NO_2 from the troposphere.
4. Other hypothesized but unidentified sources.

On the other hand, estimates of odd-nitrogen turnover rates in the range $4.4–50 \times 10^7$ molecules/cm^2·s have been obtained using the same types of vertical transport used in models and basing the results at least partially on observational data such as the stratospheric profiles of HNO_3 and N_2O. Only estimates made using stratospheric profiles based on the filter collections of HNO_3 by Lazrus and Gandrud (1974) provide numbers ($4.4–12.4 \times 10^7$) close to the mode of the theoretical estimates (11×10^7). All other estimates derived from observed profiles of HNO_3 and N_2O are 2-to-5-fold larger than the theoretical estimates. Since there are reasons to believe that the filter collections by Lazrus and Gandrud (1974) are underestimates, this seems to suggest rather strongly that current models are underestimating the odd-nitrogen budget of the stratosphere. This is a conclusion also reached by Ackerman (1975) and COMESA (1975).

2.13 Effect of Receiver Orientation on Erythema Dose

Because reductions in total ozone would permit greater amounts of ultraviolet (uv) radiation to reach the surface of the earth (Cutchis 1974, Halpern et al. 1974), a number of studies have been performed with the goal of assessing biological sensitivity to ozone-induced changes in uv radiation (National Research Council 1973). One branch of these studies has been concerned with the impact of increased uv radiation on human beings, the principal effects being increased occurrence of skin cancer (Urbach 1969, Giese 1968) and increased vitamin D production (Leach et al. 1976). One approach has been to correlate skin cancer incidence data directly with ozone layer thickness. The possible influence of such factors as duration of sunlight, clothing and exposure habits, and optical path length have been considered (McDonald 1971, van der Leun and Daniels 1975). Another approach has been to explicitly consider the dose of uv radiation received as a function of ozone amount and other climatic variables (Green and Mo 1975). The radiation dose is then related to cancer incidence after weighting by a wavelength-dependent function accounting for variation in radiation efficacy. This second approach, though less direct, is appealing because the mechanism of cancer production is more fully represented in it, and it allows for experimentation with combinations of independent variables outside the rather narrow range of reliable observation.

As the first step in this approach, Green and coworkers developed a semiempirical model for

*BUV is the abbreviation for the backscatter ultraviolet sensor carried on the Nimbus satellite.

Table 21. Estimates of production rates for exotic sources of stratospheric NO_x.

Source	Reference	Production rates: 10^{15} molecules/cm² per event or year	Production rates: 10^{32} molecules per event or year	Remarks
Solar-proton PCAs (latitude 65° or higher)	Zinn and Sutherland (1975)	20	96	Four equal events of 11 May–17 July 1959, computed by L. M. Jones.
	Crutzen et al. (1975)	2	14	12–16 Nov. 1960 event.
		0.6	4	2–5 Sept. 1966 event.
		6	40	2–10 Aug. 1972 event.
Galactic cosmic rays (GCRs), mean and solar-cycle amplitude	Warneck (1972)	0.22	11	Reported as global mean of 0.07×10^8 cm²·s, 0.33 NO per ion pair.
	Nicolet and Peetermans (1972)	0.16–1.6	–	Reported as latitudinal range of 0.05–0.5 $\times 10^8$/cm²·s.
	Johnston (1974a)	–	(?) ~4	Reported as solar-cycle double amplitude of 8×10^{32}, approx 17 SSTs or 50 Concordes.
	Ruderman and Chamberlain (1975)	1.4 ± 0.21	9.8 ± 1.5	Reported as 0.45 $\times 10^8$/cm²·s ±15% for high latitudes.
	Nicolet (1975a)	1.57 ± 0.31	10.8 ± 2.2	Reported as solar-cycle min and max of 0.4 and 0.6×10^8 cm²·s for lat. >60°.
		0.6 ± 0.13	30 ± 6.5	Global means from integrals of his Fig. 10.
	Crutzen et al. (1975)	1.5 ± 0.3	10.3 ± 2.6	Reported as 1.2–1.8 $\times 10^{15}$/cm²·s at lat. >60°.
Nuclear explosions (per Mt yield)	Bauer and Gilmore (1975)		0.17–2.5	Range of estimates in literature.
Oxidation of N_2O	Crutzen et al. (1975)	0.75–7.5	38–380	Range of estimates in literature.
Relativistic-electron-precipitation (REP) bremsstrahlung	Thorne (1977)	0.075	1.8	Columnar production given as 3×10^9 cm²·s "typically having a duration of a few hours," about half in stratosphere.

calculating uv radiation at the surface of the earth in the spectral region 280–340 nm (Green et al. 1974a,b, Mo and Green 1974). They have calculated erythema (sunburn) dose as a function of total ozone, solar zenith angle, latitude, season, and cloud amount. Their model was also used in the Climatic Impact Assessment Program's analysis of ozone depletion (Green et al. 1975).

One feature of this model, and of uv dosimetry in general (Berger et al. 1975), is that the receiver is assumed to be horizontal. The geometry of humans, however, is such that the majority of exposed skin would normally be in a nonhorizontal position. In fact, the horizontal projection of an upright person amounts to only a few percent of total surface area (Fanger 1970). This suggests that receiver orientation should be considered in the study of uv doses.

The effect of receiver orientation on incident solar radiation is routinely included in studies of building heating load (e.g., Kasuda 1973) and human comfort (Morgan 1972, Burt 1976). Orientation has also been investigated directly in connection with south-facing plane areas (Dave et al. 1975) and human beings (Terjung and Louie 1970) using

Table 22. **Available estimates of continuous natural stratospheric sources and sinks of odd nitrogen (10^8 molecules $cm^{-2} \cdot s$ averaged over the globe unless otherwise stated). Positive numbers imply sources; negative numbers, sinks.**

Source or sink	Reference	Magnitude	Remarks
Oxidation of N_2O by $O(^1D)$ in the stratosphere	Crutzen (1971)	0.29–1.5	Per Johnston (1972), not stated in report.
	McElroy and McConnell (1971)	0.2, 0.24, 0.63	Tropopause values (15 km) read from their Fig. 1b. Abstract cites ~0.2. Due to different diffusion profiles.
	Nicolet and Peetermans (1972)	0.5–2.5	Reported as 1.5 ± 1. Due to different diffusion and $O(^1D)$ profiles and zenith angles.
	Isaksen (1973a)	0.7, 1.0, 1.4	Winter, annual, and summer averages
	Isaksen (1973b)	1.2	computed from his Fig. 4. Quoted by Johnston (1974a) as 0.8–1.0.
	Brasseur and Cieslik (1973)	1.5, 4.0	Integrals computed from their Fig. 6 for two different diffusion profiles.
	McConnell and McElroy (1973)	0.3, 0.9	For two different diffusion profiles.
	McConnell (1973)	0.3, 0.9	Integrals computed from his Fig. 4 for two different diffusion profiles.
	Brasseur and Nicolet (1973)	0.5, 0.9, 1.4, 1.9	Integrals computed from their Table 1. Due to different diffusion and $O(^1D)$ profiles.
	McElroy et al. (1974)	0.819, 0.889	Due to reduced and normal O_3 profiles.
	Johnston (1974b)	~1	Based on first three estimates above.
	Crutzen et al. (1975)	0.25–2.5	Cited as range of first four estimates above.
	Duewer et al. (1976)	0.64, 0.98, 1.00, 1.53	Models B, A, A' and C', and C respectively. Due partly to rate for $N_2O + O(^1D)$ reaction.
	Duewer (1976)	0.92	Current LLL 1-D model with new Chang K_z profile and 20% increase in $O(^1D)$ quenching rate.
	Schmeltekopf et al. (1977a)	4.5	Observed N_2O profiles and Crutzen's (1973) 2-D model.
	Schmeltekopf et al. (1977b)	5.1	Observed N_2O profiles and Crutzen's (1973) 2-D model.
Oxidation of NH_3	McConnell and McElroy (1973)	−0.9, −0.5, 1.0	Source considered more likely.
	McConnell (1973)	−0.6, 0.6	—
	McElroy et al. (1974)	2.0	Integral computed from their Fig. 11.
Flux through stratopause	Crutzen (1971)	1.0	Tested in model.
	Nicolet and Peetermans (1972)	0.5	For $8 \times 10^8/cm^3$ (40 ppb) of NO at 80 km and maximum diffusion.
	McConnell and McElroy (1973)	0.15	Prescribed to model the possibility of significant high-latitude winter transport.
	McConnell and McElroy (1973)	−0.4, −0.2	Upward fluxes at 50 km from their Fig. 11.
	Brasseur and Nicolet (1973)	−0.1 to −0.02	Peak upward fluxes on their Fig. 24.

Table 22. (continued)

Source or sink	Reference	Magnitude	Remarks
Flux through stratopause (contd.)	Crutzen (1974a)	>0	Obtained from diffusion profile of Wofsy and McElroy (1973).
	Hesstvedt (1974)	>0	Downward-directed gradient in NO_y in high latitudes in winter.
	Johnston (1974b)	~0.1	Provided it is a source at all.
	Nicolet (1975b)	0	—
	Duewer et al. (1976)	−0.23	Model-computed photodissociation of NO in upper stratosphere.
	Zinn and Sutherland (1975)	<0	Upward gradient in model-computed mixing ratio at stratopause.
Flux through tropopause	Lazrus and Gandrud (1974)	−1.24 to −0.44	As HNO_3, based on measured HNO_3 and Krey and Krajewski's (1970) model.
	Ackerman (1975)	−0.8, −3, −5	As HNO_3; larger values would require NO source in addition to N_2O.
	Ackerman (1975)	>0	As NO_2, particularly in summer.
Galactic cosmic rays (GCRs)	Nicolet (1975a)	0.16, 0.24	Global mean solar cycle min and max, from integrals of his Fig. 10.
Net of all sources	Johnston (1974b)	1.0–2.0	Given as net effect of all natural sources.

the entire solar spectrum. The purpose of this work is to determine the significance of receiver orientation in the wavelength region responsible for sunburn and skin cancer. The effects on erythema dose are considered for different latitudes and seasons, and variations in total ozone and the erythema weighting curve are also included.

The procedure employed here involves using the Green model (Green et al. 1974a) to obtain total uv radiation ($Q_h + q_h$) as a function of wavelength λ and solar zenith angle θ. Valid for clear sky conditions, it is essentially a Beer-Bouguer formulation for both direct beam (Q_h) and diffuse (q_h) radiation. The latter is assumed to be isotropically distributed. These fluxes are determined using the relationships

$$Q_h(\theta,\lambda) = H(\lambda)\ V^2\ \exp[-A_t(\theta,\lambda)]\ \cos\theta \qquad (13\text{-}1)$$

and

$$q_h(\theta,\lambda) = H(\lambda)\ V^2\ \exp[-D_t(\theta,\lambda)]\ , \qquad (13\text{-}2)$$

where $H(\lambda)$ is the extraterrestrial solar irradiance at the mean earth-sun distance (taken from Howard et al. 1960). The symbol V, which does not appear in the Green model, is the ratio of the mean earth-sun distance to the earth-sun distance on a particular day. It thus allows for eccentricity in the earth's orbit, which causes variations in the extraterrestrial flux of about ±3.5%.

The terms A_t and D_t are optical thickness functions accounting for the presence of ozone (oz), air (a), and particulate matter (p); they are given by Green et al. (1974a):

$$A_t(\theta,\lambda) = w_{oz}k_{oz}\ \exp[-(\lambda - \lambda_0)/d]\ \mathrm{seq}(\theta,y_{oz}) + w_a k_a\left(\frac{\lambda_0}{\lambda}\right)^{\nu_a}\ \mathrm{seq}(\theta,y_a) + w_p k_p\left(\frac{\lambda_0}{\lambda}\right)^{\nu_p}\ \mathrm{seq}(\theta,y_p) \qquad (13\text{-}3)$$

and

$$D_t(\theta,\lambda) = K_{oz}\ \mathrm{seq}(\theta,q_1) \times \exp\left\{Kk_{oz}w_{oz} - \frac{(\lambda - \lambda_0)}{[\delta \cdot \mathrm{speq}(\theta)]}\right\} + K_{ap}\ \mathrm{seq}(\theta,q_2)\ , \qquad (13\text{-}4)$$

where

$$\text{speq}(\theta) = \left(1 - \frac{\sin^4\theta}{1.148}\right)^{-1/4} \qquad (13\text{-}5)$$

and

$$\text{seq}(\theta, y) = \left[1 - \frac{\sin^2\theta}{q}\right]^{-1/2}, \quad q = [1 + (y/R)]^2 . \qquad (13\text{-}6)$$

Values for the parameters appearing in (13-3) through (13-6) are the same as those published in the study by Green et al. (1974a). For the spectral region considered here, the total ozone optical depth w_{oz} is of special interest.

To calculate the direct-beam radiation incident on an inclined surface Q_p, it is necessary to replace θ in Eq. (13-1) with the angle between the position of the sun and a line normal to the surface (i):

$$Q_p(\theta, \lambda) = H(\lambda)\, V^2 \exp[-A_t(\theta, \lambda)] \cos i , \qquad (13\text{-}7)$$

where

$$\cos i = \cos\alpha \cos\theta + \sin\alpha \sin\theta \cos(a - a') . \qquad (13\text{-}8)$$

Here a' is the solar azimuth (relative to north), a is the azimuth of the receiver, and α is the angle of the receiver's inclination (relative to horizontal). For a horizontal receiver, $\alpha = 0$. Equations required to find θ and a' as a function of latitude, season, and time of day may be found in Dave et al. (1970), Sellers (1965), or the Smithsonian Meteorological Tables (List 1958). The last reference also contains tabulated values of V.

Diffuse radiation incident on an inclined surface has two components: that arriving from the sky as scattered radiation, q_s, and that reflected from the surface, q_g. Under the assumption of isotropic reflection and the earlier assumption of isotropic atmospheric scattering, these quantities are given by (Dave et al. 1970):

$$q_s(\theta, \lambda) = \frac{1}{2}\, q_h(\theta, \lambda)(1 + \cos\alpha) \qquad (13\text{-}9)$$

and

$$q_g(\theta, \lambda) = \frac{r}{2}\,[Q_\lambda(\theta, \lambda) + q_h(\theta, \lambda)] \times (1 - \cos\alpha) . \qquad (13\text{-}10)$$

The ground reflectivity r is small for surfaces other than snow and ice at uv wavelengths (Kondratyev 1973). A value of 0.1 was chosen here for r.

The sum $Q_p + q_s + q_g$ represents the total radiation incident per unit area on a plane inclined at an angle α and with azimuth a. Because radiation is not equally efficient at all wavelengths in producing a biologic response, one cannot integrate incident radiation directly over wavelength and obtain a meaningful measure of skin tissue insult. One must know the relative response of skin to uv radiation as a function of wavelength. In the case of sunburn the so-called action spectrum (or erythema efficiency) has been studied using uv lamps (e.g., Coblentz and Stair 1934, Magnus 1964, Cripps and Ramsay 1970) and can be represented by (Green et al. 1974b):

$$\epsilon(\lambda) = \left[4 \exp\left(\frac{\lambda - 297}{3.21}\right)\right] \times \left[1 + \exp\left(\frac{\lambda - 297}{3.21}\right)\right]^{-2} . \qquad (13\text{-}11)$$

The action spectrum for skin cancer in humans is not known; it is usually assumed to be the same as for erythema or similar to the DNA action spectrum (Setlow 1974).

Equations (13-8) through (13-11) may be used to calculate the instantaneous erythema dose for any time of day, date, latitude, ozone amount, and receiver position. In analyzing the effects of receiver orientation, we have numerically integrated over wavelength and time to produce daily erythema doses for northern hemisphere latitudes, assuming the receiver is stationary. Integrations were performed for the 15th day of each month using a time step of approximately 20 minutes. The total ozone was specified as a function of latitude for each month based on data from the Nimbus 3 satellite reported by Lovill (1972). Ozone reductions of 10 and 20% were also considered in the calculations.

To estimate the average dose for a population where there is random orientation (i.e., no preferred orientation), we made calculations while allowing the receiver to rotate 360° at each time step. Doses were computed at 20° intervals in the azimuth angle, and the average of these was used for integration. The inclination angle α was held fixed at values of 0, 45, and 90 degrees.

Figure 58 shows the daily total erythema dose for a rotated surface as a function of latitude for different ozone amounts and receiver inclinations for the 15th days of June, September, and December. Following the seasonal migration of solar declination, the peak daily erythema dose occurs in the latitude region 30–45°N in June and moves

southward to 0–20°N in September and to the southern hemisphere in December.

The relationship between dose magnitude and inclination is such that inclined surfaces generally receive less daily integrated dose than a horizontal surface at the same latitude. Exceptions to this occur in some low sun situations (large θ) where the dose on the inclined surface (e.g., $\alpha = 45°$) slightly exceeds that on the horizontal surface. This result is in contrast to the study of Dave et al. (1970) using the full solar spectrum where radiation on south-facing surfaces was shown to grow larger than that received by a horizontal surface near the poles. At the wavelengths contributing to erythema, the radiation is predominantly diffuse. Consequently, the angle of incidence does not exert as strong an influence as it would when the radiation is predominantly in the direct beam. For the isotropic model used here, the diffuse radiation flux incident on an inclined surface decreases with increasing angle of inclination (Eq. (13-9)) because as α increases less sky is visible to the inclined surface (e.g., the ratio is 1/2 for $\alpha = 90°$).

Figure 58 also indicates that daily erythema dose does not change uniformly with inclination angle. For example, at middle latitudes (30–50°N) for $\alpha = 45°$, the daily erythema dose ranges from 75 to 80% of the dose received by a horizontal surface depending upon month and latitude. For a vertical surface ($\alpha = 90°$), the daily erythema dose ranges from 25 to 50% of the dose received by a horizontal surface.

Variations in α also affect the latitudinal gradient of erythema dose. In June the largest changes in the latitudinal gradient occur at middle and low latitudes (Fig. 58a), with the smallest changes occurring poleward of 60°N. Increasing α decreases the latitudinal gradient poleward of the peak dose. In September the latitudinal gradient is almost unchanged at latitudes poleward of 50°N for $\alpha \leq 45°$, but the gradient is reduced by approximately a factor of 2 for $\alpha = 90°$. In December the latitudinal gradient is reduced only slightly for $\alpha \leq 45°$ in northern latitudes.

Figure 59 shows the percent change in erythema dose as a function of latitude for the rotated surface for reductions in total ozone of 10 and 20%. The maximum percent increase in daily erythema dose due to ozone reduction occurs at high latitudes where the average solar zenith angle is largest. The amplification factor on erythema dose (Δdose/ΔO_3) ranges from about 1.4 at low latitudes to over 3 at high latitudes (where the dose is small), the maximum value depending on season. Increasing α decreases the amplification factor at middle and low

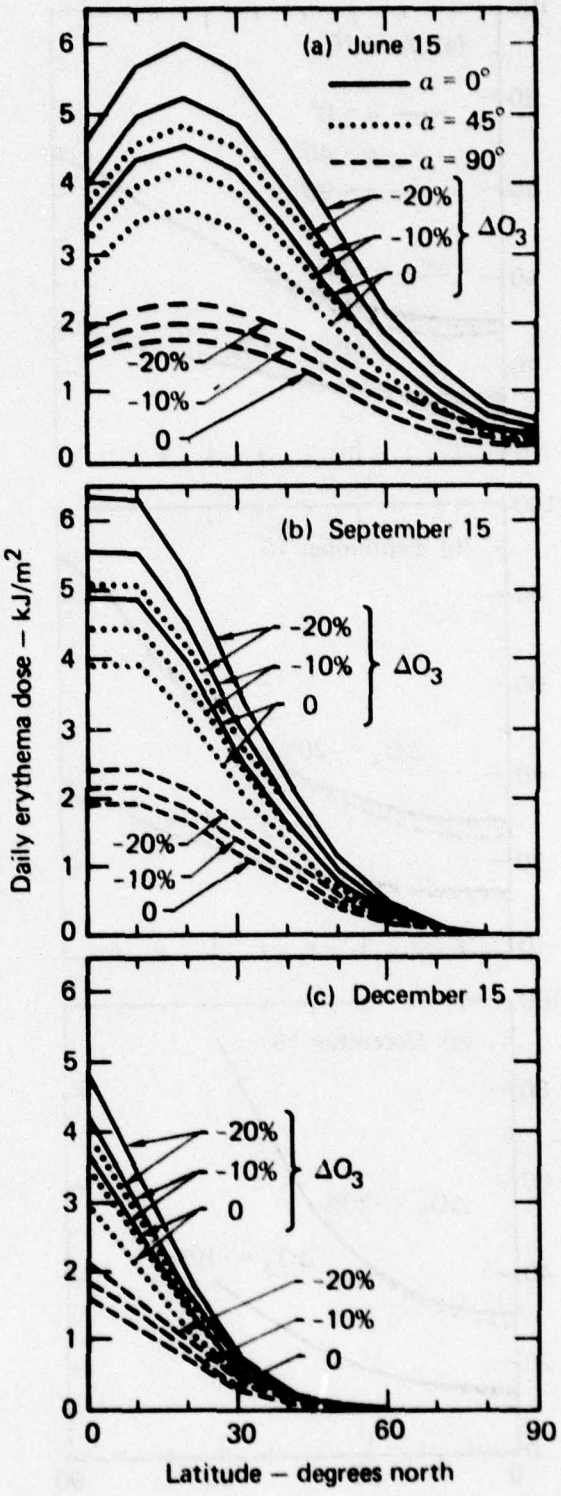

Figure 58. **Daily total erythema dose in the northern hemisphere for a rotated surface: (a) June 15, (b) September 15, (c) December 15.**

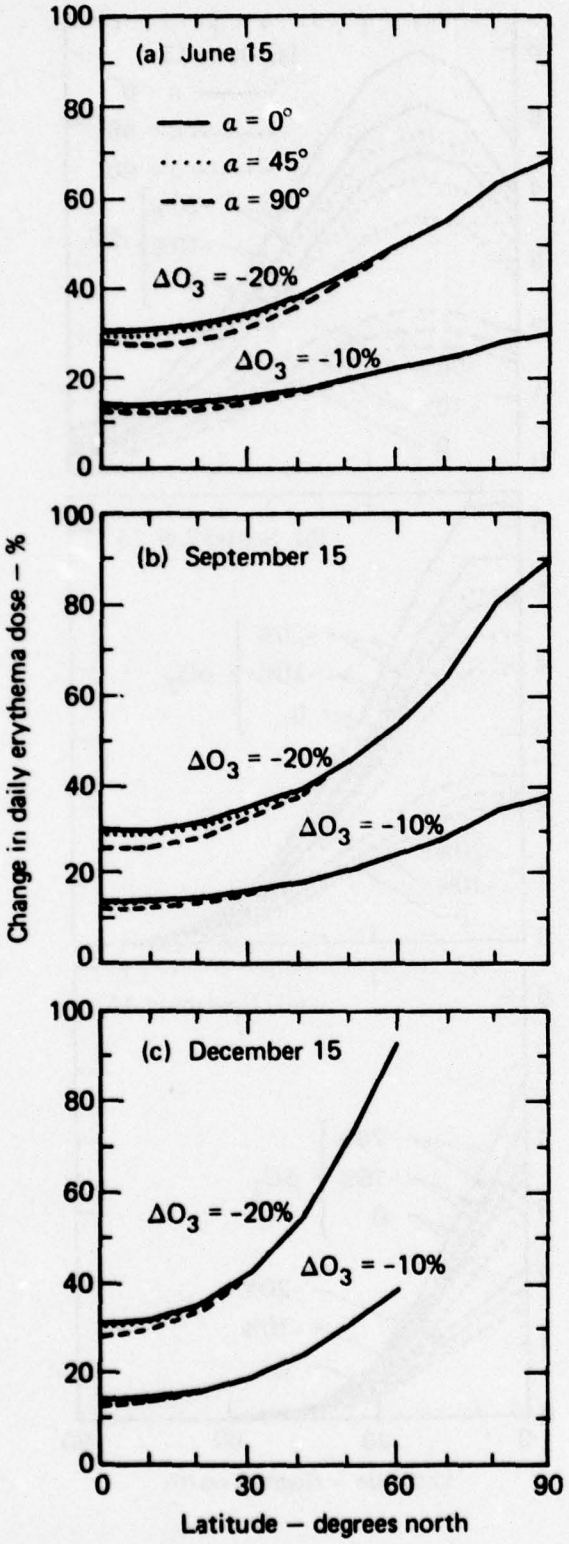

Figure 59. **Change in daily erythema dose for a rotated surface due to reductions in total ozone of 10 and 20%: (a) June 15, (b) September 15, (c) December 15.**

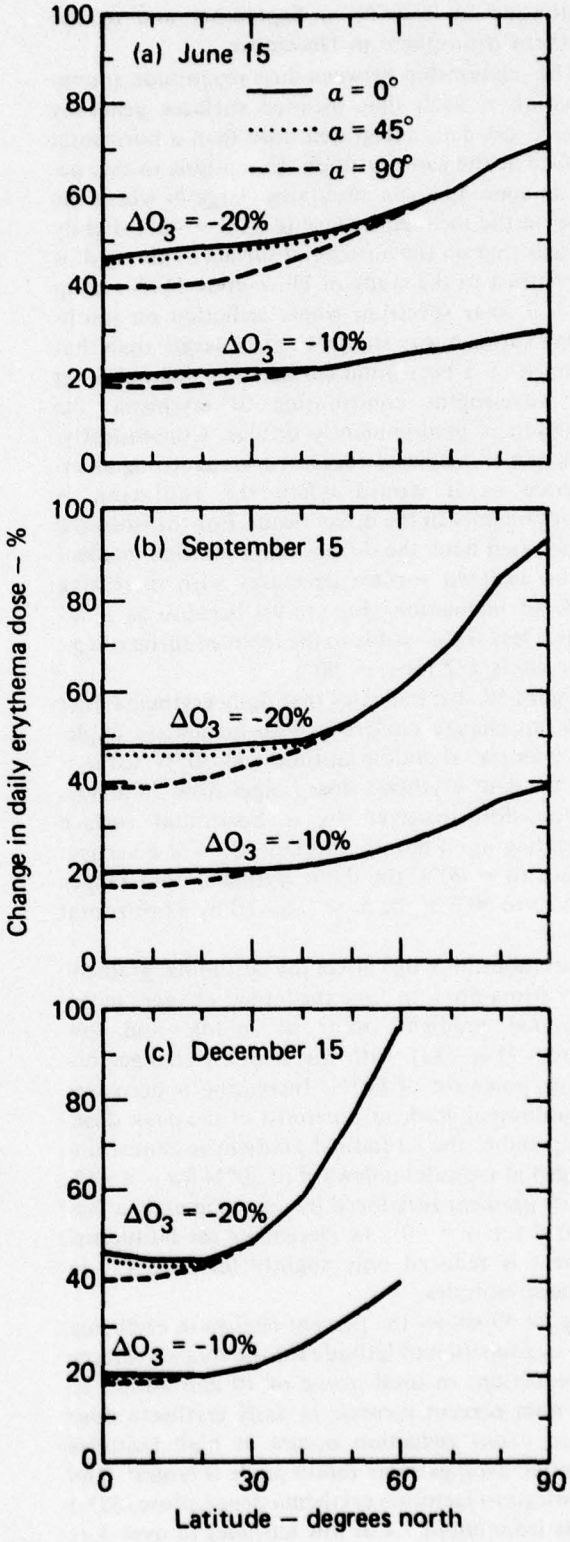

Figure 60. **Change in daily erythema dose for a rotated surface with the peak in the action spectrum shifted to 270 nm: (a) June 15, (b) September 15, (c) December 15.**

latitudes. This occurs because a change in ozone amount changes the partitioning of energy between the direct and diffuse flux components (see Eqs. (13-3) and (13-4)). In order for a change in partitioning to have an effect on the amplification factor, the direct and diffuse components must be roughly comparable in magnitude, which is only true for small zenith angles. Consequently, the greatest variation in amplification factor occurs at the latitude corresponding to solar declination.

As mentioned earlier, the action spectrum for skin cancer is an unknown function. However, van der Leun and Daniels (1975) argue that the peak in the action spectrum should occur near 270 nm. This is shifted considerably in wavelength from the location of the peak in the erythema action spectrum described by Eq. (13-11), which occurs at 297 nm. In order to test the sensitivity of dose to action spectrum position, the above calculations were repeated substituting 270 nm for 297 nm in Eq. (13-11). Aside from the expected decrease in dose magnitude, very little changed from the results obtained above. An important exception concerns the fractional change in dose produced by changing ozone amount, which is shown in Fig. 60. Dose amplification factors are significantly higher at middle and low latitudes where the dose is already highest for the action spectrum centered at the shorter wavelength. The minimum amplification factor is now about 2.0 compared with 1.4 for the results shown in Fig. 59. The reason for this increase is related to the ozone absorption cross section, which in the region near 300 nm is a rapidly decreasing function of wavelength. Shifting the action spectrum to shorter wavelengths, where the uv fluxes are more sensitive to variations in ozone amount, leads to larger amplification factors.

3. SATELLITE OZONE DATA: PROCESSING, ARCHIVING, AND ANALYSIS

3.1 Overview

Atmospheric total ozone has considerable temporal variability over a wide variety of geographical scales ranging from as large as the planetary scale to as small as the mesoscale (see e.g. Bojkov and Lovill 1969, Dobson et al. 1927, Dütsch 1969, Heath 1974, London 1963, Lovill 1969, 1970, Lovill and Miller 1968, Miller et al. 1976, Pittock 1971, and Reinking and Lovill 1971). These variations are postulated to be produced by a number of external as well as internal forcing functions. The effect of external mechanisms (such as sunspot intensity, solar proton events, and solar sector crossings) and internal mechanisms (for example, CFMs, aircraft effluents, volcanic effluents, and transport phenomena) are not well understood presently, due principally to the small total-ozone data set available since the establishment of the world total ozone surface network of Dobson observatories two decades ago. This surface network consists of fewer than 100 presently active total-ozone observatories, principally located in the northern hemisphere and on land masses. Clearly large voids remain in this "Dobson data" network over oceanic areas and in the southern hemisphere.

The advent of the meteorological satellite sensor in the early 1960s brought to the atmospheric sciences the first satellite ozone measurements in 1969. The measurements were taken by the Nimbus 3 and 4 spacecrafts' Infrared Interferometer Spectrometer (IRIS) and Backscatter Ultraviolet (BUV) sensors. Two years' worth of data taken by these sensors has been processed at the present time (Heath 1974, Lovill 1974, Prabhakara et al. 1971). The satellite IRIS sensor provided approximately 30 times as many total ozone observations in a day as the entire surface network could produce in the same time period. Moreover, the satellite data had none of the regional bias inherent in the surface network data (Reiter and Lovill 1974). The analysis of this satellite ozone data has given additional insight into the external and internal mechanisms mentioned earlier.

A new series of meteorological satellite sensors with ozone measurement capability was authorized for deployment in 1976 by the Department of Defense. The first of these sensors (termed a Multifilter Radiometer (MFR)) was launched in September 1976 and began transmission of meteorological data in March 1977.

The Satellite Ozone Analysis Center (SOAC) at Lawrence Livermore Laboratory was formed in August 1976. Its purpose is to produce total ozone data of high quality from measurements taken by the unique cross-track-scanning MFR sensor. This sensor permits areas as small as 39 km in diameter to be resolved for the first time with pole-to-pole coverage (Lovill et al. 1976). The increased data rate of this sensor enables 20 to 30 times as much ozone data to be obtained per day as was obtained by earlier satellite sensors. The initial SOAC effort is directed toward an analysis of the feasibility of obtaining useful data from the MFR ozone sensor. This feasibility study is scheduled for completion by June 1978.

The feasibility study will include a demonstration of the data-conversion technique, which is now being developed, and an assessment of the quality of the ozone data that results. To assess the quality of this satellite ozone data, we will compare it in detail with corresponding Dobson ozone data. We will also analyze the satellite ozone data to determine if it can be assimilated with other atmospheric data for a more complete understanding of the atmospheric general circulation and the delineation of anthropogenic and nonanthropogenic perturbations in the earth's atmosphere.

Data analysis beyond the feasibility study will be needed to show to what extent the SOAC MFR ozone sensor data are of use in (1) initializing numerical models, (2) long-term monitoring of global total ozone for trend analysis, (3) analysis of ozone variation at the meso-scale (which may be possible with the higher resolution of the MFR sensor), (4) analysis of the diurnal variability of total ozone (with a two-satellite ozone sensor system), and (5) integrating with studies under way by the World Meteorological Organization's Global Ozone Monitoring and Research Project (GORMP) and the United Nations Environmental Program's Global Environmental Monitoring (GEM).

The Defense Meteorological Satellite Program (DMSP) spacecraft with the MFR sensors are designed to provide water-vapor and temperature information to the Air Force Global Weather Central (AFGWC) for operational DOD meteorological commitments. After a storage period of less than 24 hours, these data are overwritten in the AFGWC data-base system by new data, and the old data would be lost if they were not archived by SOAC.

A memorandum of agreement was signed in 1976 between Lawrence Livermore Laboratory and the Department of Commerce's Environmental Data Service. Under this agreement the U.S. Air Force will furnish all available MFR data to SOAC. The data provided will be raw spectral radiance values with time and location identification. In addition to converting this raw data to ozone data, SOAC will also transmit the unchanged raw data to the National Climatic Center where it will be archived. From the derived ozone data SOAC will produce daily global total-ozone maps for the Air Force and NOAA.

The ultimate use of the data is to permit the national and international scientific communities to perform research directed toward a more complete understanding of the variability of the ozonosphere. The SOAC study contributes to this end by the integration of several tasks, described separately in the following sections. The SOAC operational plan, which describes the data flow beginning with the initial satellite sensor observation and terminating with the data dissemination and research objectives, is indicated in Fig. 61.

3.2 The Satellite Multifilter Radiometer (MFR) Sensor

SOAC receives spectral radiance data from the MFR sensors via a communication link that allows the satellite data to be telemetered to earth stations in the United States and then retransmitted to a telecommunication geosynchronous satellite, which in turn transmits to the Air Force Global Weather Central in Omaha, Nebraska. These data are then mailed to SOAC (Fig. 61) on magnetic tape.

The cross-track-scanning MFR returns 16 spectral radiance values: one radiance is located at 9.8 μm for ozone absorption, six are located in the 13-to-15-μm CO_2 band (selected for vertical temperature structure delineation), eight are located between 18 and 29 μm (selected for vertical and total water-vapor distribution), and one channel is at 12 μm for determination of the surface radiance. The channel spectral centers, widths, and noise equivalences are indicated in Table 23. Note that the noise-equivalent spectral radiance (NESR) for the 9.8-μm ozone measurement is only 0.05 erg/sec·cm^{-2}·sr·cm^{-1} (Nichols 1975).

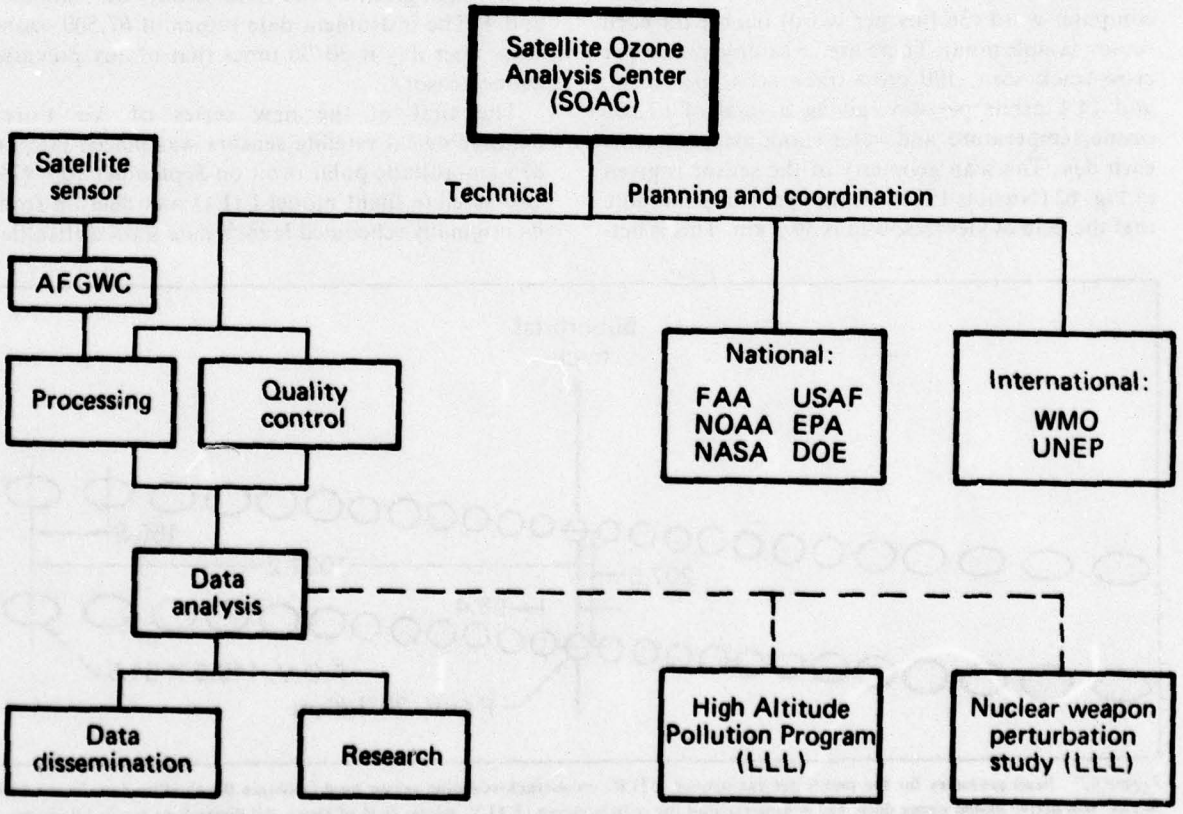

Figure 61 **Operational diagram for the Satellite Ozone Analysis Center (SOAC).**

Table 23. **The cross-track-scanning MFR sensor provides 16 channels of spectral radiance data: one channel for ozone (O_3) at 9.8 μm, one channel for the window at 12.0 μm, six CO_2 channels at 13.4 to 15.0 μm for delineation of the vertical temperature structure, and eight water-vapor channels at 18.7 to 28.3 μm. Tabulated below are the spectral centers, widths, and noise-equivalent spectral radiances (NESRs) for the 16 data channels.**

Channel No.	Species detected	Spectral center		Spectral width (cm^{-1})	NESR (10^{-7} W/cm^2·sr·cm^{-1})
		(μm)	(cm^{-1})		
1	O_3	9.8	1022	12.5	0.05
2	(Window)	12.0	835	8	0.11
3	CO_2	13.4	747	10	0.12
4	CO_2	13.8	725	10	0.11
5	CO_2	14.1	708	10	0.11
6	CO_2	14.4	695	10	0.10
7	CO_2	14.8	676	10	0.09
8	CO_2	15.0	668.5	3.5	0.30
9	H_2O	18.7	535[a]	16	0.15
10	H_2O	24.5	408.5	12	0.14
11	H_2O	22.7	441.5	18	0.09
12	H_2O	23.9	420	20	0.12
13	H_2O	26.7	374	12	0.18
14	H_2O	25.2	397.5	10	0.16
15	H_2O	28.2	355	15	0.25
16	H_2O	28.3	353.5	11	0.33

[a] This channel is not on the F1 MFR sensor.

The AFGWC provides the 16-channel digitized, calibrated, and earth-located data in an eight-computer-word (36 bits per word) packet for each sensor sample point. There are 25 sample points per cross-track scan, 190 cross-track scans per orbit, and 14.4 orbits per day, giving a total of 67,500 ozone, temperature, and water-vapor measurements each day. The scan geometry of the sensor is given in Fig. 62 (Nichols 1975). At the suborbit point note that the field of view resolved is 39.3 km. This is better earth resolution by factors of 3.8 and 2.4, respectively, than given by the IRIS sensors on Nimbus 3 and 4. The instrument data return of 67,500 ozone values per day is 20–30 times that of any previous ozone sensor.

The first of the new series of Air Force meteorological satellite sensors was placed into an 835-km-altitude polar orbit on September 10, 1976. The satellite flight model 1 (F1) was delayed from its originally scheduled launch date until difficulties

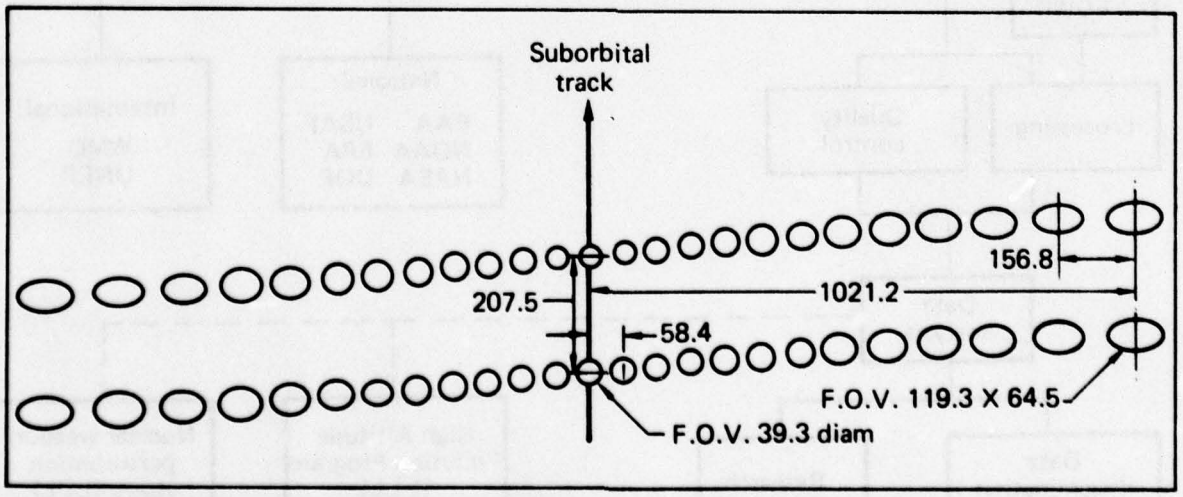

Figure 62. **Scan geometry for the multifilter radiometer (MFR) cross-track-scanning sensor used to obtain the satellite data from which SDAC will derive global ozone data. Earth projection of the scan is shown (F.O.V. means field of view). All dimensions are in kilometres.**

with the on-board computer and upper stage were alleviated. Prelaunch solar panel abnormalities during vibrational testing produced additional delay. The F1 vehicle achieved the predicted near-noon ascending orbit on September 10, but due to malfunction of an attitude-control gas valve within minutes after launch, the spacecraft began to spin about its vertical axis. The combined efforts of a USAF and industry team during the period from September 1976 to March 1977 produced a software telemetry command sequence that eventually permitted stabilization of the spacecraft and allowed data transmission on March 26, 1977. The F1 MFR sensor transmitted CO_2, H_2O, and O_3 data until September 1977, but postanalysis of the data stream indicated sensor degradation and CO_2 channel failure during the period July 15–29, 1977.

The F2 MFR sensor achieved an 835-km-altitude orbit on June 5, 1977. This sensor orbits with a view near the day-night terminator and a local early-morning ascending orbit. The first MFR data were transmitted from the sensor on July 11, 1977. An F3 MFR sensor will be launched in early 1978. It will be identical to those on the F1 and F2 satellites.

Figure 63 indicates the location of all cross-track-scan total ozone observations over the northern hemisphere taken by the F1 MFR on June 20, 1977. On this date approximately 31,000 observations were made over the northern hemisphere. This is 10% fewer observations than the theoretical maximum of 33,750 over a hemisphere. Note the high density of data over the polar region. It is theoretically possible to obtain 14 total ozone observations every 24 hours at the highest polar latitudes (an ozone observational rate of once per 1.7 hours). Figures 64 and 65 indicate the optical schematic of the sensor and the data flow, respectively (Nichols 1975). Note that the ozone channel at 1022 cm^{-1} makes six times as many observations as any of the other channels during a given atmospheric sounding.

3.3 Data Quality Control

A SOAC Satellite/Dobson Calibration Program to relate the SOAC satellite ozone data to the Dobson ozone data has been established to provide quality control for the satellite total-ozone observations. SOAC has carefully analyzed the data from the approximately 100 active Dobson stations in the world ozone network and from them has selected a high quality subset to participate in the quality control program. Thirty-three selected Dobson observatories have agreed to participate in the SOAC program (see Fig. 66). These stations were not selected for their geographical location, but on the basis of quality of observation. The Dobson-observatory geographical coverage extends from 90°S to 75°N (Fig. 66). The greatest data density is over North America, Europe, and in the Australian–New Zealand area. As many as five additional observatories may be added to our program

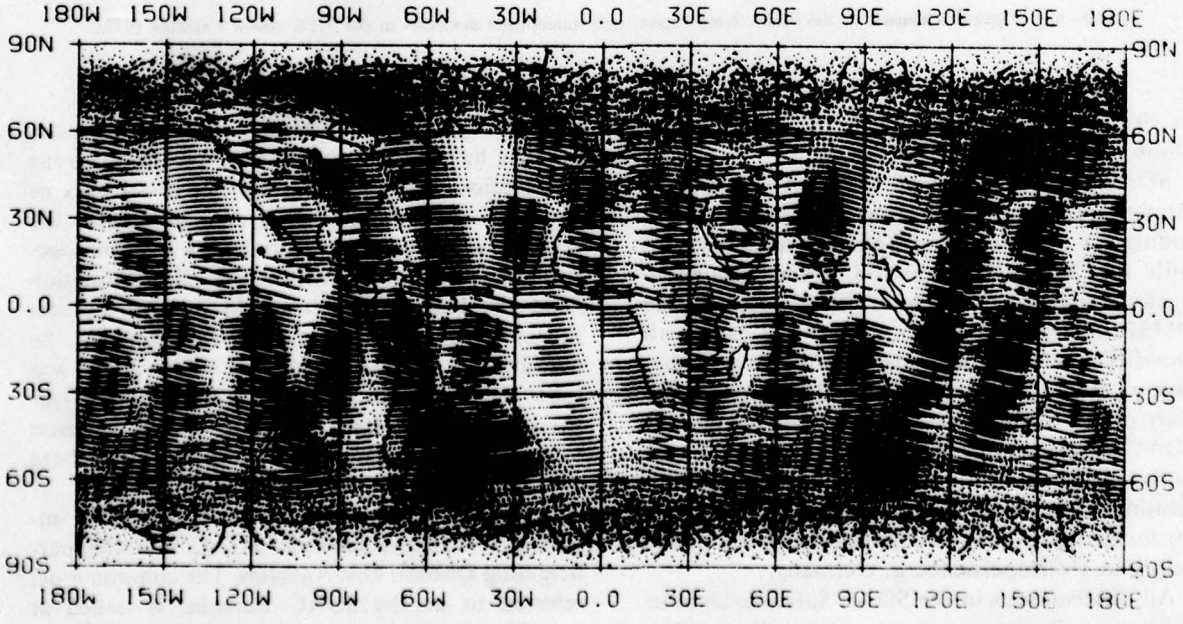

Figure 63. **Locations of total ozone observations in the northern hemisphere taken by the MFR on DMSP Satellite F1 on June 20, 1977.**

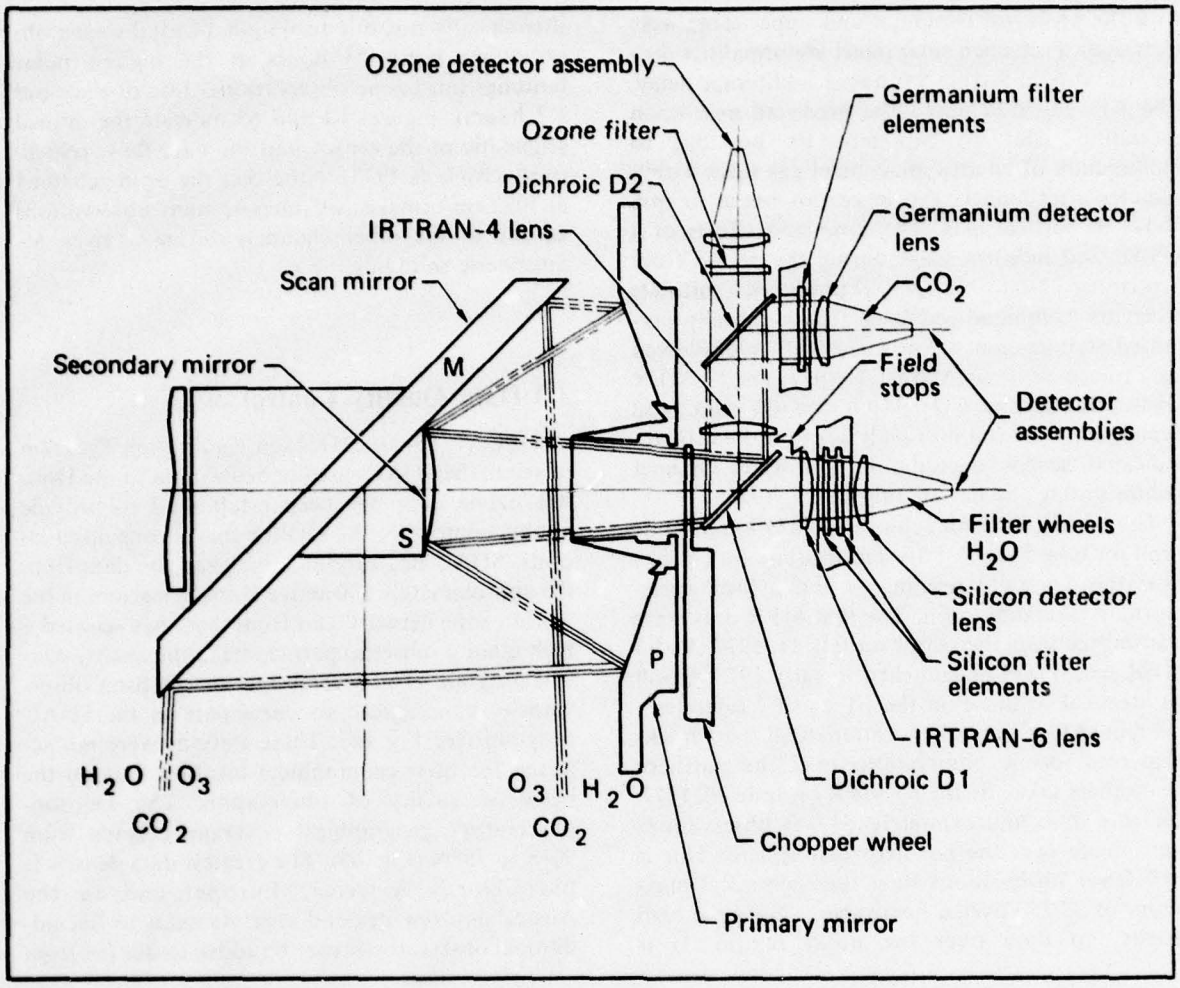

Figure 64. **Optical schematic of the ozone, temperature, and water-vapor detectors in the MFR sensor (Nichols 1975).**

in 1978, pending the results of the 1977 Boulder Dobson Intercomparison program.

SOAC has obtained NASA/NOAA software for satellite orbit prediction and has modified the coding for specific use. SOAC has an agreement with the NORAD (Colorado Springs) satellite-tracking facility to provide orbital elements of the DMSP satellites. These parameters are used with modified prediction software to produce a prediction of the daily passage of the MFR sensor over each of the Dobson stations participating in the SOAC program. An example of the prediction sent to the participating stations is shown in Fig. 67, indicating the overhead passage time of the MFR sensor for each day of the month for the Dobson observatory in Hohenpeissenberg, Germany.

All observatories in the SOAC Satellite/Dobson Calibration Program network receive the satellite prediction times at monthly intervals. These observatories have agreed to transmit their total ozone observations at weekly intervals by either telex or air mail. An example of the type of observation taken at a typical observatory by the Dobson spectrophotometer can be seen in Fig. 68. Information from the Hohenpeissenberg observatory includes the total ozone amount (in units of m·atm·cm), the background against which the observation was taken, the specific uv wavelength, and the optical air mass. These data from the global SOAC Dobson network are integrated into the SOAC data base continually.

A communique was begun in August 1977 initiating a dialogue between SOAC and the participating Dobson observatories. The communique, referred to as the SOAC Bulletin, is issued at monthly intervals and provides a frequent update to

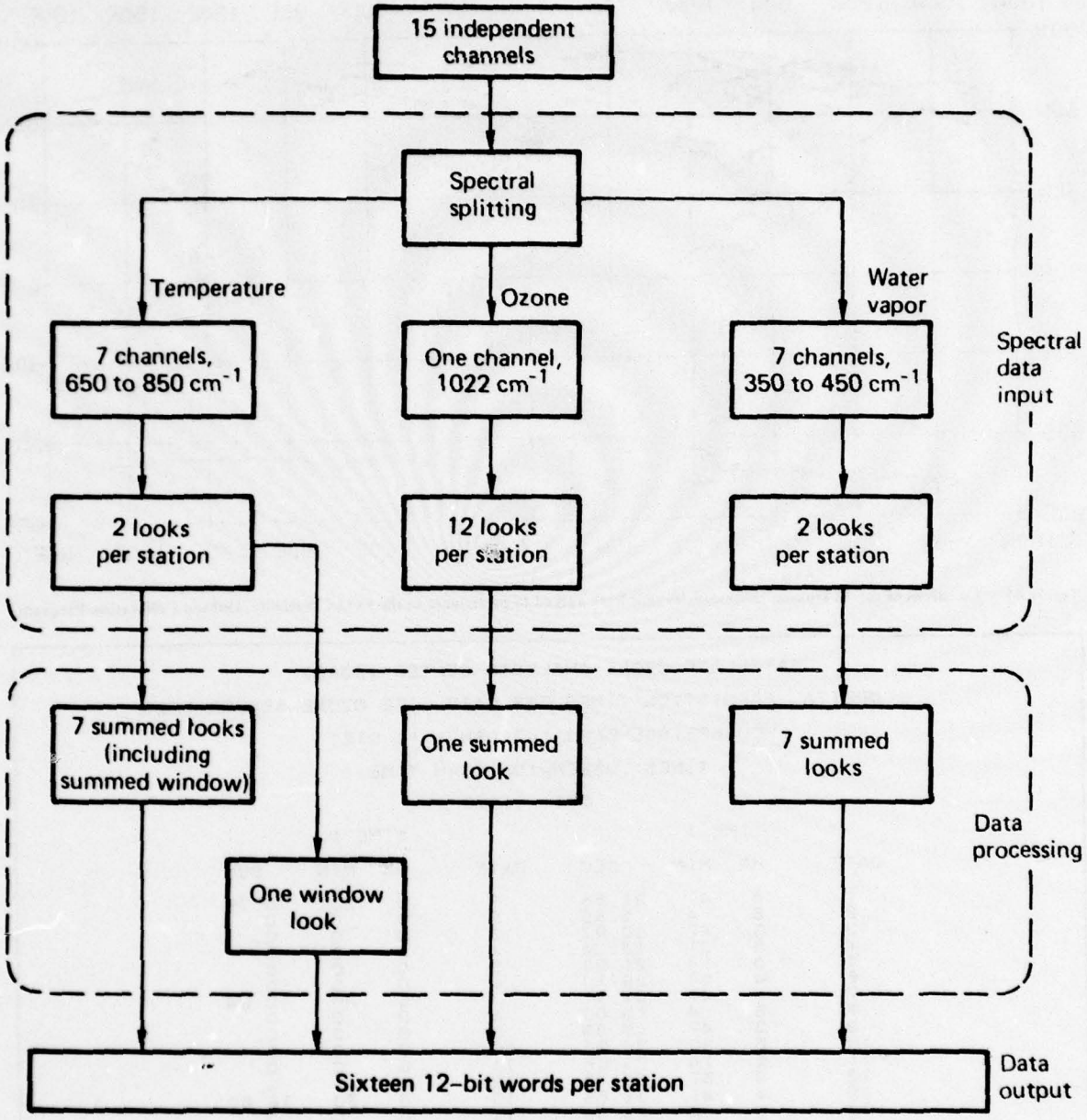

Figure 6.5 **Flow diagram for data from the ozone, temperature, and water-vapor detectors in the MFR sensor (Nichols 1975).**

those in the ozone community interested in learning of research at SOAC and those individuals outside of SOAC interested in communicating their recent results or comments on programs. As an example, the September 1977 SOAC Bulletin was used in part by the World Meteorological Organization (WMO) to communicate to the community the stations that participated in the Dobson intercomparison tests. These instruments were designated in August 1977 as area secondary-standard instruments by the International Ozone Commission (IOC), and the WMO in the SOAC Bulletin urged that all Dobson spectrophotometers not participating in the intercomparison should calibrate against the secondary instruments as soon as possible.

In addition to the special Dobson observations taken at the participating observatories, a smaller set of observatories has agreed to launch ozonesondes simultaneous with the passage of the MFR sensor. The first of these simultaneous

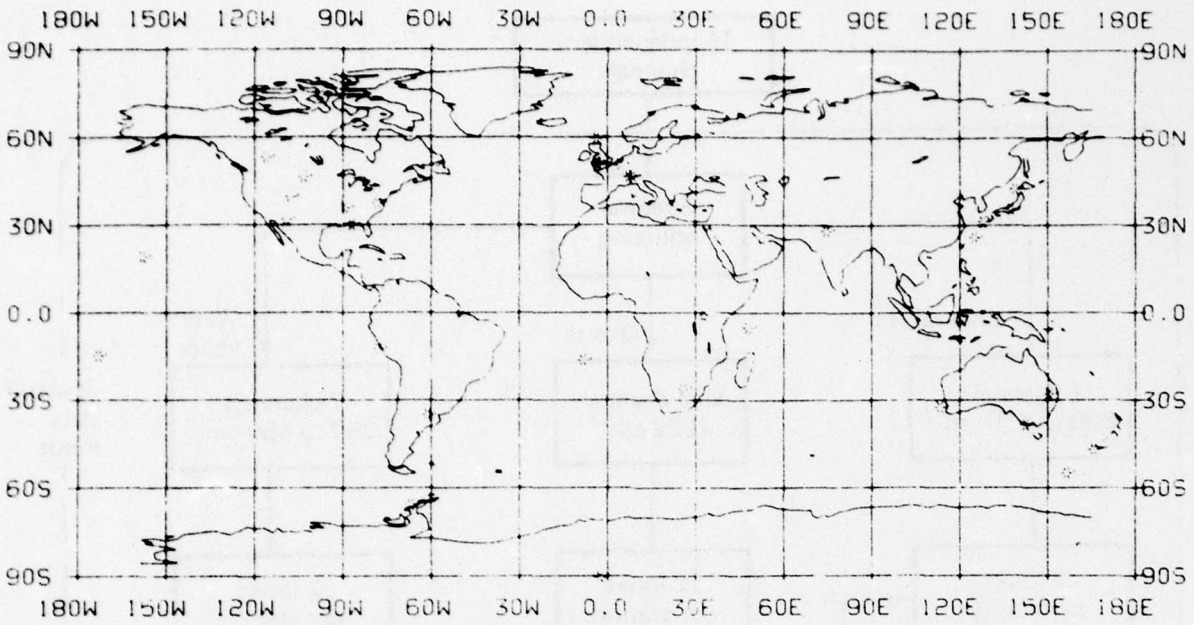

Figure 66 **Locations of the 33 Dobson observatories that have agreed to participate in the SOAC Satellite/Dobson Calibration Program.**

SATELLITE OZONE ANALYSIS CENTER (SOAC)

ORBITAL PREDICTION TIMES FOR SATELLITE OZONE SENSOR (F2)

HOHENPEISSENBERG (47 08N - 11 01E)

TIMES: GREENWICH MEAN TIME

OCT 1977

	TIME 1				TIME 2		
DATE	HR	MIN	SEC	DATE	HR	MIN	SEC
1	4	41	21.86	1	6	20	0.79
2	6	4	5.89	2	0	0	0.
3	5	47	10.97	3	0	0	0.
4	5	31	16.04	4	0	0	0.
5	5	14	21.08	5	0	0	0.
6	4	57	26.10	6	0	0	0.
7	4	41	31.11	7	6	20	10.04
8	6	4	15.03	8	0	0	0.
9	5	47	19.99	9	0	0	0.
10	5	30	24.94	10	0	0	0.
11	5	14	29.88	11	0	0	0.
12	4	57	34.79	12	0	0	0.
13	4	41	39.68	13	6	20	18.60
14	6	4	23.48	14	0	0	0.
15	5	47	28.33	15	0	0	0.
16	5	30	33.17	16	0	0	0.
17	5	14	37.99	17	0	0	0.
18	4	57	42.79	18	0	0	0.
19	4	41	47.57	19	6	20	26.49
20	6	4	31.25	20	0	0	0.
21	5	47	35.99	21	0	0	0.
22	5	30	40.72	22	0	0	0.
23	5	14	45.43	23	0	0	0.
24	4	57	50.11	24	0	0	0.
25	4	41	54.79	25	6	20	33.69
26	6	3	38.34	26	0	0	0.
27	5	47	42.97	27	0	0	0.
28	5	30	47.58	28	0	0	0.
29	5	14	52.18	29	0	0	0.
30	4	57	56.76	30	0	0	0.
31	4	42	1.31	31	6	20	40.21

Figure 67 **Example of the predictions supplied to each participating Dobson observatory of the times when the satellite will be overhead. This printout shows the predicted passage times for DMSP Satellite F1 over the Dobson observatory in Hohenpeissenberg, German, for the month of October 1977.**

MONTH	YEAR			HOHENPEISSENBERG	
8	1977			DOBSON NR. 104	
DAY	TIME (GMT)	TOTAL OZONE	OBS KIND	WAVE-LENGTH	AIR MASS
26	10.28	334	O	C	1.382
26	10.30	326	O	AD	1.380
26	10.34	326	O	C	1.376
26	10.36	327	O	AD	1.374
26	10.38	326	O	C	1.373
26	10.40	326	O	AD	1.371
26	10.42	326	O	C	1.370
26	10.44	326	O	AD	1.368
27	10.10	332	O	C	1.404
27	10.12	331	O	AD	1.407
27	10.14	334	O	C	1.404
27	10.16	331	O	AD	1.401
27	10.18	334	O	C	1.398
27	10.20	331	O	AD	1.395
27	10.22	333	O	C	1.394
27	10.24	330	O	AD	1.392
27	10.26	333	O	C	1.390
27	10.28	329	O	AD	1.388
27	10.30	332	O	C	1.386
27	10.32	327	O	AD	1.384
29	12.13	292	O	C	1.308
29	12.15	301	O	AD	1.310
29	12.17	290	O	C	1.313
29	12.19	300	O	AD	1.315
29	12.21	292	O	C	1.318
29	12.23	301	O	AD	1.321
29	12.25	291	O	C	1.324
29	12.27	300	O	AD	1.327
29	12.35	293	O	C	1.340
29	12.37	302	O	AD	1.343
29	12.39	293	O	C	1.347
29	12.41	302	O	AD	1.351
30	9.22	299	O	C	1.408
30	9.24	302	O	AD	1.412
30	9.26	295	O	C	1.417
30	9.28	302	O	AD	1.421
30	9.30	296	O	C	1.407
30	9.32	303	O	AD	1.402
30	9.38	295	O	C	1.388
30	9.40	302	O	AD	1.385
30	9.42	293	O	C	1.379
30	9.44	302	O	AD	1.374
30	9.46	293	O	C	1.370
30	9.48	302	O	AD	1.366
31	8.32	315	O	C	1.636
31	8.34	313	O	AD	1.616
31	8.36	315	O	C	1.607
31	8.38	314	O	AD	1.597
31	8.40	316	O	C	1.588
31	8.42	314	O	AD	1.579

Figure 88 **Example of the Dobson spectrophotometer total-ozone observations to be used in the SOAC Satellite/Dobson Calibration Program. These observations were made at the Dobson observatory in Hohenpeissenberg, Germany, during the period August 26–31, 1977. (Retyped from computer output.)**

satellite MFR ozonesonde launches began in July 1977. This program has now expanded to other participating observatories.

The quality control program will compare the Dobson spectrophotometer total-ozone value with the satellite-derived total ozone value. Statistics will be built accompanying the wavelength type of observation and a set of such observations against the proximity of the satellite MFR field of view, the MFR observation angle, and other variables. This is the first time that satellite ozone-sensor calibration has been attempted on a global scale. It should answer many questions that have been raised in the past with regard to calibrating satellite ozone data against spectrophotometer observations not simultaneous in time or space. Most Dobson observations taken by the participating Dobson observatories are within five minutes of the satellite passage time. This precise time coincidence should allow most, if not all, of the 24-hour baroclinic vagaries to be eliminated.

3.4 MFR Data Processing

The processing of the MFR raw spectral data to a final total-ozone value requires progressive steps in the technique development phase. The first stage of development was to compare atmospheric gas transmittances determined from a random band model against calculations of high-resolution line-by-line integration. An example of the line-by-line

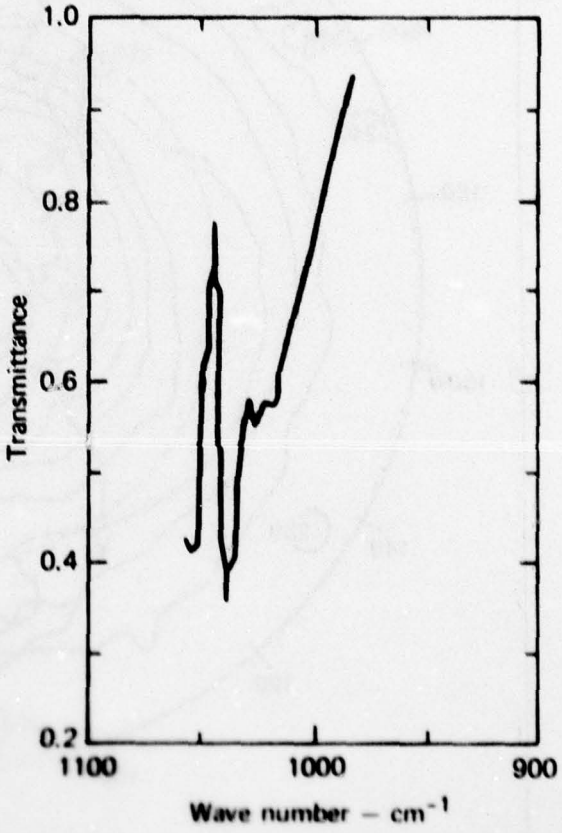

Figure 89 **Example of results calculated by high-resolution line-by-line integration. Triangular slit function smoothing was used on this calculation, which was centered about 1043 cm⁻¹.**

results is shown in Fig. 69. This is for a high-altitude, low-pressure case. Smoothing has been achieved using a triangular slit function. This phase of development determined which spectral intervals could be processed using the band model and which required the line-by-line integration technique.

The second stage of technique development was focused toward the selection of high-quality vertical ozone data, well distributed both by latitude and season. The selection was made, for example, from 12 ozonesonde soundings in Antarctica and 12 from Northern Canada (high-latitude cases), 12 ozonesonde soundings from Panama (tropical set), and 12 ozonesonde soundings from Hohenpeissenberg (middle-latitude location). These soundings are assimilated together and run against the band model and line-by-line calculations to produce a variety of multilevel, multilatitudinal models.

Approximately 6000 ozonesondes are archived in the SOAC data base. These consist of data from numerous observatories around the world that began taking vertical ozone soundings in the early 1960s. A large number of these soundings are utilized to generate statistics for regression and eigenvector analyses with various seasonally and latitudinally dependent distributions.

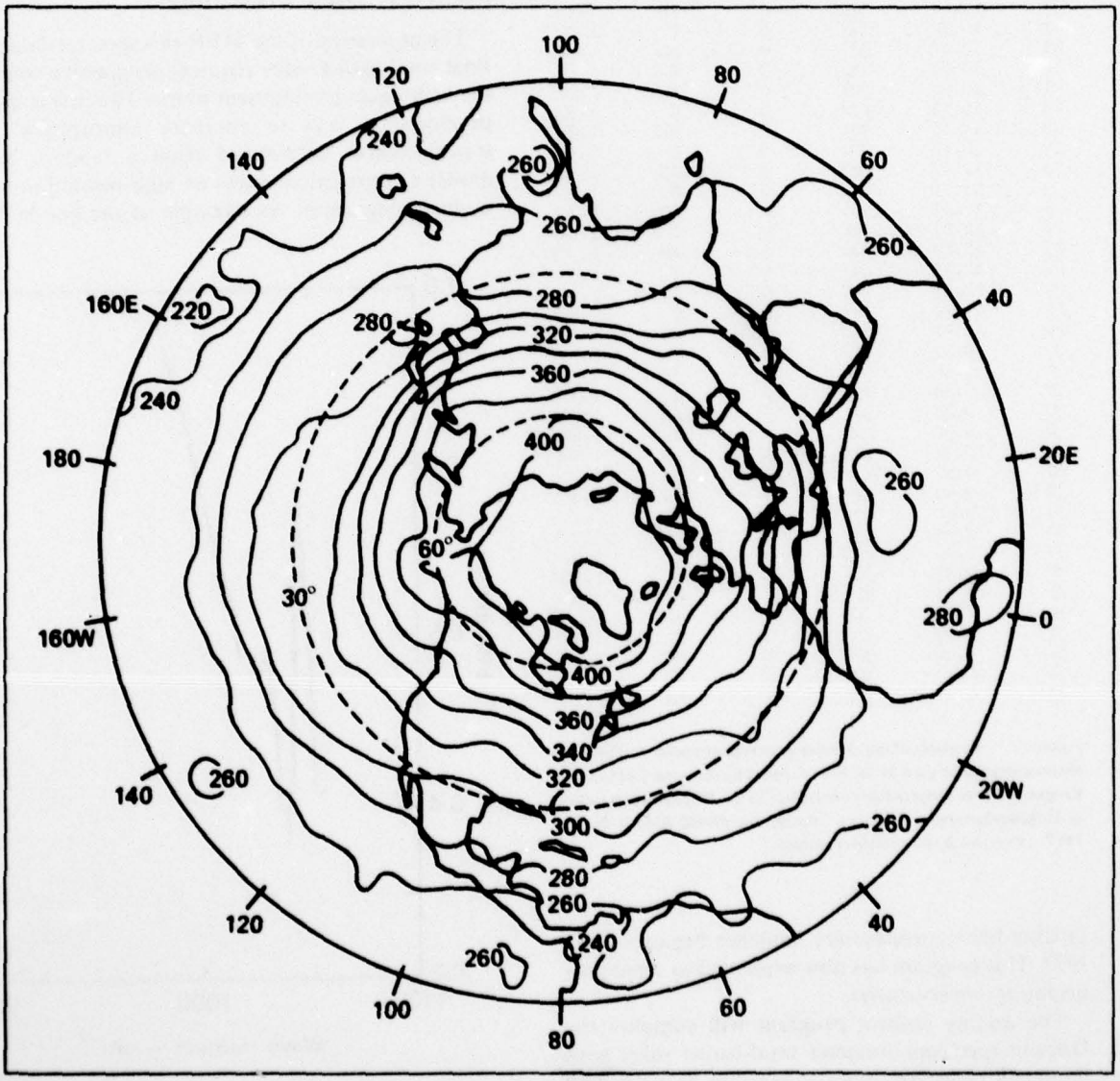

Figure 70 **The SOAC global ozone data will be presented in a form similar to the above plot, which shows the average distribution of total ozone from April 19 to July 21, 1969, for the northern hemisphere. Shading represents total ozone values less than 240 m-atm-cm (Lovill 1974).**

The final stage of the technique development will involve generation of large samples of simulated measurements for the desired MFR channels through the use of transmittances for individual profiles of atmospheric gases and temperature, and the development of the statistical regression equations relating the measurements to total ozone.

3.5 Data Analysis

A computer spline analysis will be performed on the approximately 68,000 final processed total-ozone values obtained daily. The data will be displayed in a graphical form similar to that shown in Fig. 70 and will also be tabulated in a global 2° grid. Processed ozone values with spatial and temporal locations will be available on tape to all interested agencies. A master software program is being written which will sequentially run the six programs involved in the data calibration, processing, quality control, and spline analyses in a production mode.

4. REFERENCES

Ackerman, M. (1975), "NO, NO_2 and HNO_3 Below 35 km in the Atmosphere," *J. Atmos. Sci.* **32**, 1649–1657.

Anastasi, C., P. P. Bemand, and I. W. M. Smith (1976), "Rate Constants for OH + NO_2 (+N_2) → HNO_3 (+N_2) Between 220 and 358 K," *Chem. Phys. Lett.* **37**, 370–372.

Anastasi, C., and I. W. M. Smith (1976), "Kinetics of the Reaction OH + NO_2 (+M) → HNO_3 (+M) Over a Wide Range of Temperature and Pressure," paper presented at 12th Conference on Photochemistry, Gaithersburg, Maryland, June 28 through July 1, 1976.

Angell, J. K., and J. Korshover (1973), "Quasi Biennial and Long-Term Fluctuations in Total Ozone," *Mon. Weather Rev.* **101**, 426–443.

Angell, J. K., and J. Korshover (1976), "Global Analysis of Recent Total Ozone Fluctuations," *Mon. Weather Rev.* **104**, 63–75.

Anderson, J. G., and F. Kaufman (1973), "Kinetics of the Reaction OH (v = 0) + O_3 → HO_2 + O_2," *Chem. Phys. Lett.* **19**, 483–486.

Ashby, R. W. (1976), *A Numerical Study of the Chemical Composition of the Stratosphere*, Ph.D. thesis, University of Wisconsin (University Microfilms No. 76-20653).

Bailey, E. H. (1945), "Hydrogen-Ion Concentration of the Important Soils of the United States in Relation to Other Profile Characteristics: II. Pedalfers and Soils Transitional Between Pedocals and Pedalfers," *Soil Sci.* **59**, 239–262.

Bates, D. R., and P. B. Hays (1967), "Atmospheric Nitrous Oxide," *Planet. Space Sci.* **15**, 189–197.

Bauer, E., and F. R. Gilmore (1975), "Effect of Atmospheric Nuclear Explosions on Total Ozone," *Rev. Geophys. Space Phys.* **13**, 451–457.

Baulch, D. L., D. D. Drysdale, D. G. Horne, and A. C. Lloyd (1972), *Evaluated Kinetic Data for High Temperature Reactions, Vol. 1: Homogeneous Gas Phase Reactions of the H_2–O_2 System* (Butterworths, London).

Baulch, D. L., D. D. Drysdale, and D. G. Horne (1973), *Evaluated Kinetic Data for High Temperature Reactions, Vol. 2: Homogeneous Gas Phase Reactions of the H_2–N_2–O_2 System* (Butterworths, London).

Berger, D., D. F. Robertson, and R. E. Davis (1975), "Field Measurements of Biologically Effective UV Radiation," Appendix D of Chapter 2 in *Impacts of Climatic Change on the Biosphere*, CIAP Monograph 5 (U.S. Department of Transportation, Washington, D.C.).

Bojkov, R. D., and J. E. Lovill (1969), "Comments on Berson's 'Spring Warming-Transfer Processes in the Lower Antarctic Stratosphere,'" *Tellus* **21**, 284.

Brasseur, G., and S. Cieslik (1973), "On the Behavior of Nitrogen Oxides in the Stratosphere," *Pure and Applied Geophysics (PAGEOPH)* **106–108**, 1431–1437.

Brasseur, G., and M. Nicolet (1973), "Chemospheric Processes of Nitric Oxide in the Mesosphere and Stratosphere," *Planet. Space Sci.* **21**, 939–961.

Broderick, A. J. (1977), "Stratospheric Effects from Aviation," paper presented at the AIAA/SAE 13th Propulsion Conference, Orlando, Florida, July 1977.

Burgess, R. H., and J. C. Robb (1957), "The Mercury-Photo-Sensitized Reaction of Hydrogen and Oxygen at Room Temperature," *Chem. Soc. Spec. Publ.* **9**, 167.

Burrows, J. P., G. W. Harris, and B. A. Thrush (1977), "Rates of Reaction of HO_2 with HO and O Studied by Laser Magnetic Resonance," *Nature* **267**, 233–234.

Burt, J. E. (1976), *Human Thermal Comfort in the U.S.*, M.A. thesis, University of California, Los Angeles, California.

Callis, L. B., R. E. Boughner, V. Ramanathan, and J. E. Nealy (1976), "Ozone: Effect of UV Variability and Stratospheric Coupling Mechanisms," paper presented at the International Joint Symposium on Atmospheric Ozone, Dresden, East Germany, August 9–17, 1976.

Chamberlain, J. S., and C. B. Leovy (1975), *The Stratosphere, 1975–1980*, Report of a Workshop, May 28–30, 1975, NASA Goddard Space Flight Center, Greenbelt, Maryland, pp. 44–48.

Chameides, W. L., and D. H. Stedman (1977), "Tropospheric Ozone: Coupling Transport and Photochemistry," *J. Geophys. Res.* **82**, 1787–1794.

Chameides, W. L., and J. C. G. Walker (1973), "A Photochemical Theory of Tropospheric Ozone," *J. Geophys. Res.* **78**, 8751–8760.

Chameides, W. L., and J. C. G. Walker (1976), "A Time-Dependent Photochemical Model for Ozone Near the Ground," *J. Geophys. Res.* **81**, 413–420.

Chang, J. S. (1974), "Simulations, Perturbations, and Interpretations," in *Proc. 3rd CIAP Conf.*, U.S. Department of Transportation, Cambridge, Mass., February 1974, DOT-TSC-OST-74-15, pp. 330–341.

Chang, J. S. (1975), "Uncertainties in the Validation of Parameterized Transport in 1-D Models of the Stratosphere," in *Proc. 4th CIAP Conf.*, U.S. Department of Transportation, Cambridge, Mass., DOT-TSC-OST-75-38, pp. 175–182.

Chang, J. S. (1976), eddy diffusion profile described in *High Altitude Pollution Program First Annual Report* [1976], Frederick M. Luther, principal investigator, Lawrence Livermore Laboratory, Livermore, Calif., UCRL-50042-76, p. 4 ff.

Chang, J. S. (1977), "Tropospheric Modeling," paper presented at the Gordon Conference on Environmental Sciences: Air, New Hampton, Virginia, August 15–19, 1977. (Chang was also chairman of the Stratospheric Session at this conference.)

Chang, J. S., and W. H. Duewer (1973), "On the Possible Effect of NO_x Injection in the Stratosphere Due to Past Atmospheric Nuclear Weapon Tests," paper presented at the AIAA/AMS Meeting, Denver, Colorado, June 1973. Lawrence Livermore Laboratory, Livermore, Calif., UCRL-74480 Preprint.

Chang, J. S., and W. H. Duewer (1977), "New Theoretical Estimate of the Effect of Past Nuclear Tests on Ozone," *EOS Trans. AGU* **58**(8), 689 (Abstract). Paper presented at the IAGA/IAMAP Joint Assembly, Seattle, Washington, August 22–September 3, 1977. Lawrence Livermore Laboratory, Livermore, Calif., UCRL-79302 Abstract.

Chang, J. S., W. H. Duewer, and D. J. Wuebbles (1977), "The Atmospheric Nuclear Tests of the 50's and 60's: A Significant Test of Ozone Depletion Theories," submitted to *J. Geophys. Res.* (September 1977). Lawrence Livermore Laboratory, Livermore, Calif., UCRL-80246 Preprint.

Chang, J. S., A. C. Hindmarsh, and N. K. Madsen (1974), "Simulation of Chemical Kinetics Transport in the Stratosphere," in *Stiff Differential Systems*, R. A. Willoughby, Ed. (Plenum, New York), pp. 51–65.

Chang, J. S., and F. Kaufman (1976), private communication cited by F. Kaufman in "The Ten Most Wanted Rate Constants in Stratospheric Chlorofluorocarbon Catalysis," paper by F. Kaufman and M. S. Zahniser presented at 172nd ACS Annual Meeting, San Francisco, Calif., August 29–September 3, 1976.

Chang, J. S., and F. Kaufman (1977), "Determination of an Upper Limit to the Rate Constant of the Reaction $OH + HO_2 \rightarrow H_2O + O_2$," paper presented at the AGU Spring Meeting, Washington, D.C., May 30–June 3, 1977.

Chang, J. S., and J. E. Penner (1977), "Analysis of Global Budgets of Halocarbons," paper presented at the IAGA/IAMAP Joint Assembly, Seattle, Washington, August 22–September 3, 1977. Lawrence Livermore Laboratory, Livermore, Calif., UCRL-79318 Abstract.

Chang, J. S., and D. J. Wuebbles (1976), "A Theoretical Model of Global Tropospheric OH Distribution," in Proceedings of the Joint AGU/AMS Symposium on the Non-Urban Tropospheric Composition, Hollywood, Florida, November 10–12, 1976. Lawrence Livermore Laboratory, Livermore, Calif., UCRL-78392 Preprint.

Chang, J. S., and D. J. Wuebbles (1977), "Fully Diurnal Averaged Model of the Stratosphere," paper presented at the IAGA/IAMAP Joint Assembly, Seattle, Washington, August 22–September 3, 1977. Lawrence Livermore Laboratory, Livermore, Calif., UCRL-79317 Abstract.

Chang, J. S., D. J. Wuebbles, and D. D. Davis (1977), "A Theoretical Model of Global Tropospheric OH Distribution," revision to paper presented at the Joint AGU/AMS Symposium on the Non-Urban Tropospheric Composition, Hollywood, Florida, November 10–12, 1976. Lawrence Livermore Laboratory, Livermore, Calif., UCRL-78392 Preprint Rev. 1 (1977).

Chatfield, R., and H. Harrison (1976), "Ozone in the Remote Troposphere: Mixing Versus Photochemistry," *J. Geophys. Res.* **81**, 421–423.

Christie, A. P. (1973), "Secular or Cyclic Changes in Ozone," *PAGEOPH* **106–108**, 1000–1009.

Coblentz, W. W., and R. Stair (1934), "Data on the Spectral Erythemic Reaction of the Untanned Human Skin to Ultraviolet Radiation," *U.S. Bureau of Standards J. Res.* **12**, 13–14.

COMESA (1975), *The Report of the Committee on Meteorological Effects of Stratospheric Aircraft (1972–1975)*, U. K. Meteorological Office, Bracknell.

Cox, R. A. (1975), "The Photolysis of Gaseous Nitrous Oxide: A Technique for Obtaining Kinetic Data on Atmospheric Photooxidation Reactions," *Int. J. Chem. Kinetics Symp. No. 1*, 379–398 (Proceedings of First Symposium on Chemical Kinetics Data for the Lower and Upper Atmosphere, published by Wiley, New York.)

Cox, R. A., R. G. Derwent, A. E. Eggleton, and J. E. Lovelock (1976), "Photochemical Oxidation of Halocarbons in the Troposphere," *Atmos. Environ.* **10**, 305–308.

Cripps, D. J., and C. A. Ramsay (1970), "Ultraviolet Action Spectrum with a Prism-Grating Monochromator," *Brit. J. Dermatol.* **82**, 584–592.

Crutzen, P. J. (1971), "Ozone Production Rates in an Oxygen-Hydrogen-Nitrogen Oxide Atmosphere," *J. Geophys. Res.* **76**(30), 7311–7327.

Crutzen, P. J. (1972), "SST's—A Threat to the Earth's Ozone Shield," *Ambio* **1**, 41–51.

Crutzen, P. J. (1973), "A Discussion of the Chemistry of Some Minor Constituents in the Stratosphere and Troposphere," *PAGEOPH* **106–108**, 1385–1399.

Crutzen, P. J. (1974a), "A Review of Upper Atmospheric Photochemistry," *Can. J. Chem.* **52**, 1569–1581.

Crutzen, P. J. (1974b), "Photochemical Reactions Initiated by and Influencing Ozone in Unpolluted Tropospheric Air," *Tellus* **26**, 47–57.

Crutzen, P. J. (1975), unpublished memorandum circulated in December 1975, cited by Johnston (1977).

Crutzen, P. J. (1976), "Upper Limits on Atmospheric Ozone Reductions Following Increased Application of Fixed Nitrogen to the Soil," *Geophys. Res. Lett.* **3**, 169–172.

Crutzen, P. J., and D. H. Ehhalt (1977), "Effects of Nitrogen Fertilizers and Combustion on the Stratospheric Ozone Layer," *Ambio* **6**, 112–117.

Crutzen, P. J., and I. S. A. Isaksen (1976), "The Impact of the Chlorocarbon Industry on the Ozone Layer," preprint submitted to *J. Geophys. Res.*

Crutzen, P. J., I. S. A. Isaksen, and G. R. Reid (1975), "Solar Proton Events: Stratospheric Sources of Nitric Oxide," *Science* **189**, 457–459.

Cutchis, P. (1974), "Stratospheric Ozone Depletion and Solar Ultraviolet Radiation on Earth," *Science* **184**, 13–19.

Czeplak, G., and C. E. Junge (1974), "Studies of the Interhemispheric Exchange in the Troposphere by a Diffusion Model," *Adv. Geophys.* **18B**, 57–72.

Dave, J. V., P. Halpern, and H. J. Myers (1975), *Solar Energy Incident Upon a South-Facing, Tilted, Flat Surface Under Cloudless Conditions*, IBM Palo Alto Scientific Center, Palo Alto, Calif., G320-3331.

Davis, D. D. (1974), *Absolute Rate Constants for Elementary Reactions of Atmospheric Importance: Results from the University of Maryland's Gas Kinetics Laboratory*, University of Maryland, Chemistry Department Report No. 1.

Davis, D. D., and G. Klauber (1975), "Gas-Phase Oxidation Mechanisms for the Molecule SO_2," *Int. J. Chem. Kinetics Symp. No. 1*, 543–556.

DeMore, W. B. (1973), "Rate Constants for the Reactions of Hydroxyl and Hydroperoxyl with Ozone," *Science* **180**, 735–737.

DeMore, W. B. (1975), "Rate Constant Ratio for the Reactions of OH with O_2 and CO," *Int. J. Chem. Kinetics Symp. No. 1*, 273–280.

DeMore, W. B., L. Stief, R. T. Watson, R. Hampson, D. Garvin, J. Margitan, M. Molmer, and D. Golder (1977), "Laboratory Measurements," in *Chlorofluoromethanes in the Stratosphere*, R. D. Hudson, Ed. (National Aeronautics and Space Administration, Greenbelt, Maryland), NASA Reference Publication 1010, pp. 1–50.

DeMore, W. B., and E. Tschuikow-Roux (1974), "Temperature Dependence of the Reactions of OH and HO_2 with O_3," *J. Phys. Chem.* **78**, 1447–1451.

Dixon-Lewis, G., J. B. Greenberg, and F. A. Goldsworthey (1974), "Reactions in the Recombination Region of Hydrogen and Lean Hydrocarbon Flames," *Proc. 15th Symposium on Combustion*, pp. 717–730.

Dobson, G. M. B., D. N. Harrison, and J. Lawrence (1926), "Measurements of the Amount of Ozone in the Earth's Atmosphere and Its Relation to Other Geophysical Conditions," *Proc. Roy Soc.* **A-110**, 660–693.

Duewer, W. H. (1976), private communication.

Duewer, W. H. (1977), "Evaluation of the Sums and Densities of Vibrational Energy Levels for Coupled Anharmonic Oscillator Models of Small Molecules and Some Implications for RRKM Calculations," paper presented at the 173rd National Meeting of the American Chemical Society, New Orleans, Louisiana, March 20–25, 1977. Lawrence Livermore Laboratory, Livermore, Calif., UCRL-78795 Abstract.

Duewer, W. H., D. J. Wuebbles, and J. S. Chang (1977a), "Effect of NO Photolysis on NO_y Mixing Ratios," *Nature* **265**, 523–525.

Duewer, W. H., D. J. Wuebbles, H. W. Ellsaesser, and J. S. Chang (1977b), "NO_x Catalytic Ozone Destruction: Sensitivity to Rate Coefficients," *J. Geophys. Res.* **82**, 935–942.

Duewer, W. H., D. J. Wuebbles, H. W. Ellsaesser, and J. S. Chang (1977c), "Authors Reply to Comment by Johnston and Nelson," *J. Geophys. Res.* **82**, 2599–2605.

Dütsch, H. U. (1969), "Atmospheric Ozone and Ultraviolet Radiation," in *World Survey of Climatology*, H. Landsberg, Ed. (Elsevier, Amsterdam), vol. 4.

Dütsch, H. U. (1971), "Photochemistry of Atmospheric Ozone," *Adv. Geophys.* **15**, 322.

Dütsch, H. U. (1973), "The Present Status of Ozone Research: Photochemistry and Observations," *Proc. 2nd CIAP Conf.* (U.S. Department of Transportation, Washington, D.C.), DOT-TSC-OST-73-4, pp. 106–113.

Dütsch, H. U., and Th. Ginsburg (1968), "Parametric Studies on Ozone Photochemistry," *Pure Appl. Geophys.* **72**, 204–213.

Ehhalt, D. H. (1974), "The Atmospheric Cycle of Methane," *Tellus* **26**, 58–70.

Ellis, J. S., and T. H. Vonder Haar (1977), "The Earth's Radiation Budget Sensitivity to Cloud Amount as Determined from Satellite Measurements," paper presented at the IAGA/IAMAP Joint Assembly, Seattle, Washington, August 22–September 3, 1977.

Ellsaesser, H. W. (1976a), "A Reassessment of Stratospheric Ozone: Credibility of the Threat," invited paper presented at the Environmental Health Sciences Symposium on SST Pollution and Skin Cancer, Hollywood, Florida, October 25–29, 1976. Lawrence Livermore Laboratory, Livermore, Calif., UCRL-78285 Preprint. Accepted subject to revision for publication in *Climatic Change*.

Ellsaesser, H. W. (1976b), "Ozone Destruction by Catalysis: Credibility of the Threat," paper presented at the Fall Annual Meeting of the American Geophysical Union, San Francisco, Calif., December 4–8, 1976. Lawrence Livermore Laboratory, Livermore, Calif., UCRL-78627 Preprint. Accepted subject to revision for publication in *Atmospheric Environment*.

Ellsaesser, H. W. (1976c), "The Increase in Total Ozone of the 1960's: Probable Cause," paper presented at the International Conference on the Stratosphere and Related Problems, Logan, Utah, September 15–17, 1976. Lawrence Livermore Laboratory, Livermore, Calif., UCRL-78408 Abstract.

Ellsaesser, H. W. (1977a), "Comments on 'Estimate of the Global Change in Temperature, Surface to 100 mb, Between 1958 and 1975,'" *Mon. Weather Rev.* **105**, 1200–1201.

Ellsaesser, H. W. (1977b), "Comments on 'The Distribution of Water Vapor in the Stratosphere,'" *Rev. Geophys. Space Phys.* **15**, 501.

Ellsaesser, H. W. (1977c), "Has Man Increased Stratospheric Ozone?" *Nature* **270**, 592–593.

Fabian, P. (1974), "Comments on 'A Photochemical Theory of Tropospheric Ozone' by W. L. Chameides and J. C. G. Walker," *J. Geophys. Res.* **79**, 4124–4125.

Fabian, P., and P. G. Pruchniewicz (1977), "Meridional Distribution of Ozone in the Troposphere and Its Seasonal Variations," *J. Geophys. Res.* **82**, 2063–2073.

Fanger, P. O. (1970), *Thermal Comfort* (Danish Technical Press, Copenhagen).

Fishman, J., and P. J. Crutzen (1976), "A Numerical Study of Tropospheric Photochemistry Using a One Dimensional Model," in Proceedings of the Joint AGU/AMS Symposium on the Non-Urban Tropospheric Composition, Hollywood, Florida, November 10–12, 1976.

Foley, H. M., and M. A. Ruderman (1972), *Stratospheric Nitric Oxide Production from Past Nuclear Explosions and Its Relevance to Projected SST Pollution*, Institute for Defense Analyses, JASON, Arlington, Virginia, Paper P-894, pp. 1–25.

Foley, H. M., and M. A. Ruderman (1973), "Stratospheric NO Production from Past Nuclear Explosions," *J. Geophys. Res.* **78**, 4441–4450.

Foner, S. N., and R. L. Hudson (1962), "Mass Spectrometry of the HO_2 Free Radical," *J. Chem. Phys.* **36**, 2681–2688.

Frederick, J. E., and P. B. Hays (1977), "The Need for a Revised Theory of Mesospheric Ozone," *EOS Trans. AGU* **58**(6), 462 (abstract).

Frenkiel, F. N. (1955), "Ozone Theory in the Troposphere," *J. Chem. Phys.* **23**, 2440.

Friswell, N. J., and M. M. Sutton (1972), "Radical Recombination Reactions in $H_2/O_2/N_2$ Flares: Participation of the HO Radical," *Chem. Phys. Lett.* **15**, 108–112.

Garvin, D., and T. H. Gevantman (1972), *Chemical Kinetics Data Survey. III. Selected Rate Constants for Chemical Reactions of Interest in Atmospheric Chemistry*, National Bureau of Standards, Washington, D.C., NBS Report 10867.

Garvin, D., and R. F. Hampson (1974), *Chemical Kinetics Data Survey. VII. Tables of Rate and Photochemical Data for Modeling of the Stratosphere*, National Bureau of Standards, Washington, D.C., NBSIR-74-430 (Revised).

Gelinas, R. J. (1974), *Summary of Radiative Data Used in LLL Atmospheric Physics Codes*, Lawrence Livermore Laboratory, Livermore, Calif., UCRL-74944 Rev. 4.

Gerard, J. C., and C. A. Barth (1977), "High Latitude Nitric Oxide in the Lower Thermosphere," *J. Geophys. Res.* **82**, 674–681.

Giese, A. C., Ed. (1968), *Responses of the Human Skin to Ultraviolet Light* (Academic Press, New York).

Gilmore, F. R. (1975), "The Production of Nitrogen Oxides by Low Altitude Nuclear Explosions," *J. Geophys. Res.* **80**, 4553–4554.

Glänzer, K., and J. Tröe (1975), "HO_2 Formation in Shock Heated HNO_3-NO_2 Mixtures," *Ber. Brunsenges Physik. Chem.* **79**, 465–569.

Goldsmith, P., A. F. Tuck, J. S. Foot, E. L. Simmons, and R. L. Newson (1973), "Nitrogen Oxides, Nuclear Weapon Testing, Concorde and Stratospheric Ozone," *Nature* **244**, 545–551.

Green, A. E. S., and J. Mo (1975), "Calculated Erythemal Radiation Doses," chapter 2.2.5 in *Impacts of Climatic Change on the Biosphere*, CIAP Monograph 5 (U.S. Department of Transportation, Washington, D.C.).

Green, A. E. S., J. Mo, and J. H. Miller (1974a), "A Study of Solar Erythema Radiation Doses," *Photochem. Photobiol.* **20**, 473–482.

Green, A. E. S., T. Sawada, and E. P. Shettle (1974b), "The Middle Ultraviolet Reaching the Ground," *Photochem. Photobiol.* **19**, 251–262.

Grobecker, A. J., S. C. Coroniti, and R. H. Cannon, Jr. (1974), *Report of Findings*, U.S. Department of Transportation, Washington, D.C., DOT-TSC-75-50.

Hack, W., K. Hoyermann, and H. G. Wagner (1975), "The Reaction NO + HO_2 → NO_2 + OH with OH + H_2O_2 → HO_2 + H_2O as a HO_2 Source," *Int. J. Chem. Kinetics Symp. No. 1*, 329–340.

Halpern, P., J. V. Dave, and N. Braslau (1974), "Sea-Level Solar Radiation in the Biologically Active Spectrum," *Science* **186**, 1204–1208.

Hamilton, E. J. (1975), "Water Vapor Dependence of the Kinetics of the Self-Reaction of HO_2 in the Gas Phase," *J. Chem. Phys.* **63**, 3682–3683.

Hampson, J. (1977), "A Model for Iterative Interaction Between Atmospheric Chemistry, Heating, and Circulation to Explain Perturbation of Weather and Climate by Solar Activity and Anthropogenic Change," paper presented at the IAGA/IAMAP Joint Assembly, Seattle, Washington, August 1977.

Hampson, R. F., and D. Garvin (1975), *Chemical Kinetic and Photochemical Data for Modeling Atmospheric Chemistry*, National Bureau of Standards, Washington, D.C., NBS Technical Note 866.

Harries, J. E. (1976), "The Distribution of Water Vapor in the Stratosphere," *Rev. Geophys. Space Phys.* **14**, 565–575.

Heath, D. F. (1974), "Recent Advances in Satellite Observations of Solar Variability and Global Atmospheric Ozone," in Proceedings of the International Conference on Structure, Composition and General Circulation of the Upper and Lower Atmospheres and Possible Anthropogenic Perturbations, Melbourne, Australia, January 14–15, 1974, pp. 1267–1291.

Hesstvedt, E. (1974), "Reduction of Stratospheric Ozone from High-Flying Aircraft, Studied in a Two-Dimensional Photochemical Model with Transport," *Can. J. Chem.* **52**(8), 1592–1598.

Hidalgo, H., and P. J. Crutzen (1976), "The Tropospheric and Stratospheric Composition Perturbed by NO_x Emissions of High Altitude Aircraft," in Proceedings of the Joint AGU/AMS Symposium on the Non-Urban Tropospheric Composition, Hollywood, Florida, November 10–12, 1976.

Hochanadel, C. J., J. A. Ghormley, and P. J. Ogren (1972), "Absorption Spectrum and Reaction Kinetics of HO_2 Radical in the Gas Phase," *J. Chem. Phys.* **56**, 4426–4432.

Howard, C. J., and K. M. Evenson (1977), "Laser Magnetic Resonance Study of HO_2 Chemistry," *EOS Trans. AGU* **58**(6), 464 (abstract).

Howard, J. N., J. I. F. King, and P. R. Gast (1960), "Thermal Radiation," chapter 16 in *Handbook of Geophysics* (Macmillan, New York).

Hudson, R. D., Ed. (1977), *Chlorofluoromethanes and the Stratosphere*, Goddard Space Flight Center, Greenbelt, Maryland, NASA Reference Publication 1010.

Hunten, D. M. (1975a), "Estimates of Stratospheric Pollution by an Analytic Model," *Proc. Nat. Acad. Sci. U.S.* **72**, 4711–4715.

Hunten, D. M. (1975b), "Vertical Transport in Atmospheres," in *Atmospheres of Earth and the Planets*, B. M. McCormac, Ed. (Reidel Publishing Co., Dordrecht, Netherlands).

Isaksen, I. S. A. (1973a), "The Production and Distribution of Nitrogen Oxides in the Lower Stratosphere," *PAGEOPH* **106–108**, 1438–1445.

Isaksen, I. S. A. (1973b), "Diurnal Variations of Atmospheric Constituents in an Oxygen-Hydrogen-Nitrogen-Carbon Atmospheric Model, and the Role of Minor Neutral Constituents in the Chemistry of the Lower Ionosphere," *Geophys. Norveg.* **30**(2), 1–63.

Johnston, H. S. (1974a), "Pollution of the Stratosphere," *Environ. Conservation* **1**(3), 163–176.

Johnston, H. S. (1974b), "Photochemistry in the Stratosphere with Applications to Supersonic Transports," *Acta Astron.* **1**, 135–156.

Johnston, H. S. (1977), "Analysis of the Independent Variables in the Perturbation of Stratospheric Ozone by Nitrogen Fertilizers," *J. Geophys. Res.* **82**, 1767–1772.

Johnston, H. S., D. Kattenhorn, and G. Whitten (1976), "Use of Excess Carbon 14 Data to Calibrate Models of Stratospheric Ozone Depletion by Supersonic Transports," *J. Geophys. Res.* **81**, 368–380.

Johnston, H. S., and H. Nelson (1977), "Comment on 'NO_x Catalytic Ozone Destruction: Sensitivity to Rate Coefficients,'" *J. Geophys. Res.* **82**, 2597–2598.

Johnston, H. S., and E. Quitevis (1974), "The Oxides of Nitrogen with Respect to Urban Smog, Supersonic Transports, and Global Methane," paper presented at National Congress of Radiation Research, Seattle, Washington, July 14–20, 1974.

Johnston, H. S., and G. S. Selwyn (1975), "New Cross Sections for the Absorption of Near-Ultraviolet Radiation by Nitrous Oxide (N_2O)," *Geophys. Res. Lett.* **2**, 549–551.

Johnston, H. S., G. Whitten, and J. Birks (1973), "Effects of Nuclear Explosions on Stratospheric Nitric Oxide and Ozone," *J. Geophys. Res.* **78**, 6107–6135.

Kasuda, T. (1973), *Heating and Cooling Loads Calculation Program (NBSLD)*, National Bureau of Standards, U.S. Department of Commerce, Washington, D.C.

Kaufman, F. (1975), "Hydrogen Chemistry: Perspective on Experiment and Theory," in *Atmospheres of Earth and the Planets*, B. M. McCormac, Ed. (Reidel Publishing Co., Dordrecht, Netherlands).

Komhyr, W. D., E. W. Barrett, G. Slocum, and H. K. Weickmann (1971), "Atmospheric Total Ozone Increase During the 1960's," *Nature* **233**, 390–391.

Kondratyev, K. Ya. (1973), *Radiation Characteristics of the Atmosphere and the Earth's Surface* (Amerind Publishing Co., New Delhi).

Kurylo, M. J. (1973), "Kinetics of the Reactions OH ($v = 0$) + $NH_3 \rightarrow H_2O + NH_2$ and OH ($v = 0$) + $O_3 \rightarrow HO_2 + O_2$ at 298°K," *Chem. Phys. Lett.* **23**, 467–471.

Kurzeja, R. J. (1975), "The Diurnal Variation of Minor Constituents in the Stratosphere and Its Effects on the Ozone Concentration," *J. Atmos. Sci.* **32**(5), 899–909.

Kurzeja, R. J. (1976), *The Production and Transport of Ozone and Other Minor Constituents in the Stratosphere*, Ph.D. thesis, Florida State University (University Microfilms No. 76-28636).

Lazrus, A. L., and B. W. Gandrud (1974), "Distribution of Stratospheric Nitric Acid Vapor," *J. Atmos. Sci.* **31**, 1102–1108.

Leach, J. F., A. R. Pingstone, K. A. Hall, F. J. Ensell, and J. L. Burton (1976), "Interrelation of Atmospheric Ozone and Cholecalciferol (Vitamin D_3) Production in Man," *Aviation Space Environ. Med.* (June 1976), 630–633.

Levy, H. (1971), "Normal Atmosphere: Large Radical and Formaldehyde Concentrations Predicted," *Science* **173**, 141–143.

Levy, H. (1972), "Photochemistry of the Lower Troposphere," *Planet. Space Sci.* **20**, 919–935.

Levy, H. (1973), "Photochemistry of Minor Constituents in the Troposphere," *Planet. Space Sci.* **21**, 575–591.

List, R. J. (1958), *Smithsonian Meteorological Table* (Smithsonian Institution Press, Washington, D.C.).

Liu, S. C., and R. J. Cicerone (1977), "Comparison of Theory and Measurements of Ozone Above 35 km," *EOS Trans. AGU* **58**(6), 462 (abstract).

Liu, S. C., R. J. Cicerone, T. M. Donahue, and W. L. Chameides (1976), "Limitation of Fertilizer Induced Ozone Reduction by the Long Lifetime of the Reservoir of Fixed Nitrogen," *Geophys. Res. Lett.* **3**, 157–160.

Liu, S. C., T. M. Donahue, R. J. Cicerone, and W. L. Chameides (1976), "Effect of Water Vapor on the Destruction of Ozone in the Stratosphere Perturbed by ClX or NO_x Pollutants," *J. Geophys. Res.* **81**, 3111–3118.

Lloyd, A. C. (1974), "Evaluated and Estimated Kinetic Data for Gas Phase Reactions of the Hydroperoxyl Radical," *Int. J. Chem. Kinetics* **6**, 169–228.

London, J. (1963), "The Distribution of Total Ozone in the Northern Hemisphere," *Beitrage zur Physik der Atmosphare* **26**, 254–263.

London, J. (1975), *The Global Distribution and Variations of Atmospheric Ozone*, Department of Astrogeophysics, University of Colorado, Boulder, Colorado, AD/A-019 501 (DOT-TST-76-12). Available from National Technical Information Service, Springfield, Virginia.

London, J., J. E. Frederick, and G. P. Anderson (1977), "Satellite Observations of the Global Distribution of Stratospheric Ozone," *J. Geophys. Res.* **82**, 2543–2556.

London, J., and J. Kelley (1974), "Global Trends in Total Atmospheric Ozone," *Science* **184**, 987–989.

Louis, J. F. (1974), *A Two-Dimensional Transport Model of the Atmosphere*, Ph.D. thesis, University of Colorado, Boulder, Colorado.

Lovelock, J. E., R. J. Maggs, and R. J. Wade (1973), "Halogenated Hydrocarbons in and Over the Atlantic," *Nature* **241**, 194–196.

Lovill, J. E. (1970), "Gravity Wave Measurements as Simultaneously Determined by Satellite, Ozone and Airplane," *Arch. Meteorol. Geophys. Bioklimatol. Ser. A* **19**, 13–28.

Lovill, J. E. (1974), "A Comparison of the Southern and Northern Hemisphere General Circulation Characteristics as Determined by Satellite Ozone Data," in Proceedings of the International Conference on Structure, Composition and General Circulation of the Upper and Lower Atmospheres and Possible Anthropogenic Perturbations, Melbourne, Australia, January 14–15, 1974, 340–359.

Lovill, J. E., and A. Miller (1968), "The Vertical Distribution of Ozone Over the San Francisco Bay Area," *J. Geophys. Res.* **73**, 5073–5079.

Lovill, J. E., T. J. Sullivan, and J. A. Korver (1976), "Measurement of Atmospheric Ozone by Satellite," in Proceedings of the Seventh Conference on Aerospace and Aeronautical Meteorology and Symposium on Remote Sensing from Satellites, Melbourne, Florida, November 16–19, 1976.

Luther, F. M. (1976a), "Relative Influence of Stratospheric Aerosols on Solar and Longwave Radiative Fluxes for a Tropical Atmosphere," *J. Appl. Meteorol.* **15**, 951–955.

Luther, F. M. (1976b), *High Altitude Pollution Program First Annual Report [1976]*, Lawrence Livermore Laboratory, Livermore, Calif., UCRL-50042-76.

Luther, F. M. (1977), "Effect of Multiple Scattering on Ozone Reduction by NO_x and CFM's," paper presented at the IAGA/IAMAP Joint Assembly, Seattle, Washington, August 22–September 3, 1977.

Luther, F. M., and W. H. Duewer (1977), "Effect of Changes in Stratospheric Water Vapor on Ozone Reduction Estimates," accepted for publication in *J. Geophys. Res.* Lawrence Livermore Laboratory, Livermore, Calif., UCRL-79660 Preprint.

Luther, F. M., and R. J. Gelinas (1976), "Effect of Molecular Multiple Scattering and Surface Albedo on Atmospheric Photodissociation Rates," *J. Geophys. Res.* **81**, 1125–1132.

Luther, F. M., and D. J. Wuebbles (1977), "Photodissociation Rate Calculations," paper presented at the NASA Workshop on CFM Assessment, Warrenton, Virginia, January 10–14, 1977. Lawrence Livermore Laboratory, Livermore, Calif., UCRL-78911 Preprint.

Luther, F. M., D. J. Wuebbles, and J. S. Chang (1977a), "Temperature Feedback in a Stratospheric Model," *J. Geophys. Res.* **82**, 4935–4942.

Luther, F. M., D. J. Wuebbles, W. H. Duewer, and J. S. Chang (1977b), "Effect of Multiple Scattering on Species Concentrations and Model Sensitivity," submitted to *J. Geophys. Res.* Lawrence Livermore Laboratory, Livermore, Calif., UCRL-79946 Preprint (August 1977).

MacCracken, M. C., and J. S. Chang, Eds. (1975), *A Preliminary Study of the Potential Chemical and Climatic Effects of Atmospheric Nuclear Explosions*, Lawrence Livermore Laboratory, Livermore, Calif., UCRL-51653 (April 1975).

Magnus, I. A. (1964), "Studies with a Monochromator in the Common Idiopathic Photodumatoses," *Brit. J. Dumatol.* **76**, 245–264.

Mahlman, J. P. (1977), "Application of General Circulation Models to Stratospheric Transport Problems," paper presented at the IAGA/IAMAP Joint Assembly, Seattle, Washington, August 22–September 3, 1977.

Mastenbrook, H. J. (1974), "Stratospheric Water Vapor Distribution and Variability," in Proceedings of the International Conference on Structure, Composition and General Circulation of the Upper and Lower Atmospheres and Possible Anthropogenic Perturbations, Melbourne, Australia, January 14–15, 1974, pp. 233–248.

McConnell, J. C. (1973), "Atmospheric Ammonia," *J. Geophys. Res.* **78**, 7812–7821.

McConnell, J. C., and M. B. McElroy (1973), "Odd Nitrogen in the Atmosphere," *J. Atmos. Sci.* **30**(8), 1465–1480.

McDonald, J. E. (1971), "Relationship of Skin Cancer Incidence to Thickness of Ozone Layer," *Congressional Record* **117** (March 19, 1971), 3493.

McElroy, M. B. (1974), testimony presented to the Committee on Interstate and Foreign Commerce, U.S. House of Representatives, Washington, D.C., December 11, 1974.

McElroy, M. B. (1975), testimony presented to the Committee on Aeronautical and Space Sciences, U.S. Senate, Washington, D.C., September 23, 1975.

McElroy, M. B., J. W. Elkins, S. C. Wofsy, and Y. L. Yung (1976), "Sources and Sinks for Atmospheric N_2O," *Rev. Geophys. Space Phys.* **14**, 143–150.

McElroy, M. B., and J. C. McConnell (1971), "Nitrous Oxide: A Natural Source of Stratospheric NO," *J. Atmos. Sci.* **28**(6), 1095–1098.

McElroy, M. B., S. C. Wofsy, J. E. Penner, and J. C. McConnell (1974), "Atmospheric Ozone: Possible Impact of Stratospheric Aviation," *J. Atmos. Sci.* **31**(1), 287–303.

Miller, A. J., R. M. Nagatani, K. B. Labitzke, E. Klinker, K. Rose, and D. F. Heath (1976), "Stratospheric Ozone Transport During the Mid-Winter Warming of December 1970–January 1971," in Proceedings of the Joint Symposium on Atmospheric Ozone, Dresden, 1976 (to be published).

Mo, J., and A. E. S. Green (1974), "A Climatology of Solar Erythema Dose," *Photochem. Photobiol.* **20**, 483–496.

Morgan, D. L. (1972), *Man-Environment Coupling: Physiologic Comfort of Man in an Urban Setting*, Ph.D. thesis, University of California, Davis, California.

National Research Council (1973), *Biological Impacts of Increased Intensities of Solar Ultraviolet Radiation*, NRC Environmental Studies Board, National Academy of Sciences, Washington, D.C.

National Research Council (1975a), *Environmental Impact of Stratospheric Flight*, National Academy of Sciences, Washington, D.C.

National Research Council (1975b), *Long-Term Worldwide Effects of Multiple Nuclear-Weapons Detonations*, National Academy of Sciences, Washington, D.C.

National Research Council (1976), *Halocarbons: Effects on Stratospheric Ozone*, NRC Panel on Atmospheric Chemistry, National Academy of Sciences, Washington, D.C.

Neely, W. B., and J. H. Plonka (1977), "An Estimation of the Time-Averaged Hydroxyl Radical Concentration in the Troposphere," Dow Chemical Company preprint.

Nichols, D. A. (1975), "DMSP Block 5D Special Meteorological Sensor H, Optical Subsystem," *Optical Eng.* **14**, 284–288.

Nicolet, M. (1964), "Reactions and Photochemistry of Atoms and Molecules," *Disc. Faraday Soc.* **37**, 7–20.

Nicolet, M. (1975a), "On the Production of Nitric Oxide by Cosmic Rays in the Mesosphere and Stratosphere," *Planet. Space Sci.* **23**, 637–649.

Nicolet, M. (1975b), "Stratospheric Ozone: An Introduction to Its Study," *Rev. Geophys. Space Phys.* **13**(5), 593–636.

Nicolet, M., and W. Peetermans (1972), "The Production of Nitric Oxide in the Stratosphere by Oxidation of Nitrous Oxide," *Ann. Epophys.* **28**(4), 751–762.

Normand, C. (1953), "Atmospheric Ozone and Its Upper-Air Circulation," *Quart. J. Roy. Meteorol. Soc.* **79**, 39–50.

Oliver, R. C., E. Bauer, H. Hidalgo, K. A. Gardner, and W. Uasylkiwskyj (1977), *Aircraft Emissions: Potential Effects on Ozone and Climate, a Review and Progress Report*, U.S. Department of Transportation, Washington, D.C., FAA-EQ-77-3 (March, 1977).

Oort, A. H., and E. M. Rasmusson (1971), *Atmospheric Circulation Statistics*, National Oceanic and Atmospheric Administration, NOAA Professional Paper 5.

Paukert, T. T., and H. S. Johnston (1972), "Spectra and Kinetics of the Hydroperoxyl Free Radical in the Gas Phase," *J. Chem. Phys.* **56**, 2824–2835.

Payne, W. A., L. J. Stief, and D. D. Davis (1973), "A Kinetics Study of the Reaction of HO_2 with SO_2 and NO," *J. Amer. Chem. Soc.* **95**, 7614–7619.

Peterson, K. R. (1970), "An Empirical Model for Estimating World-Wide Deposition from Atmospheric Nuclear Detonations," *Health Phys.* **18**, 357–378.

Pierotti, D., and R. A. Rasmussen (1976), "The Atmospheric Distribution of Nitrous Oxide," Proceedings of the Joint AGU/AMS Symposium on the Non-Urban Tropospheric Composition, Hollywood, Florida, November 10–12, 1976.

Pittock, A. B. (1971), "Synoptic Ozone Observations During the Passage of a Cyclonic Vertex," *Austr. Meteorol. Mag.* **19**(1), 1–11.

Prabhakara, C., V. V. Salomonson, B. J. Conrath, J. Steranka, and L. J. Allison (1971), "Nimbus III, IRIS Ozone Measurements over Southeast Asia and Africa During June and July 1969," *J. Atmos. Sci.* **28**, 828–831.

Pruchniewicz, P. G. (1973), "The Average Tropospheric Ozone Content and Its Variation with Season and Latitude as a Result of the Global Ozone Circulation," *Pure Appl. Geophys.* **106–108**, 1058–1073.

Ramanathan, V. (1974), "A Simplified Stratospheric Radiative Transfer Model: Theoretical Estimates of the Thermal Structure of the Basic and Perturbed Stratosphere," paper presented at the AMS/AIAA Second International Conference on the Environmental Impact of Aerospace Operations in the High Atmosphere, San Diego, Calif., July 8–10, 1974.

Ramanathan, V. (1975), "Greenhouse Effect Due to Chlorofluorocarbons: Climatic Implications," *Science* **190**, 50–51.

Ramanathan, V. (1976), "Radiative Transfer Within the Earth's Troposphere and Stratosphere: A Simplified Radiative-Convective Model," *J. Atmos. Sci.* **33**, 1330–1346.

Ramanathan, V., L. B. Callis, and R. E. Boughner (1976), "Sensitivity of Surface Temperature and Atmospheric Temperature to Perturbations in the Stratospheric Concentration of Ozone and Nitrogen Dioxide," *J. Atmos. Sci.* **33**, 1092–1112.

Rangarjan, S. (1969), "A Worldwide Anomaly in the Concentration of Ozone Above 80 km," *J. Atmos. Sci.* **26**, 613–616.

Rasmussen, R. A. (1977), personal communication.

Reck, R. A. (1976), "Atmospheric Temperature Calculated for Ozone Depletions," *Nature* **263**, 116–117.

Reed, R. J., and C. L. Vlcek (1969), "The Annual Temperature Variation in the Lower Tropical Stratosphere," *J. Atmos. Sci.* **26**, 163–167.

Reinking, R. F., and J. E. Lovill (1971), "A Comparison of Ice Nucleus and Ozone Concentrations in Stratospheric Air," *J. Atmos. Sci.* **28**, 812–816.

Reiter, E. R., and J. E. Lovill (1974), "The Longitudinal Movement of Stratospheric Ozone Waves as Determined by Satellite," *Arch. Meteorol. Geophys. Bioklimatol. Ser. A* **23**, 13–27.

Ripperton, L. A., H. Jeffries, and J. J. B. Worth (1971), "Natural Synthesis of Ozone in the Troposphere," *Environ. Sci. Technol.* **5**, 246–248.

Ruderman, M. A., and J. W. Chamberlain (1975), "Origin of the Sunspot Modulation of Ozone: Its Implications for Stratospheric NO Injection," *Planet. Space Sci.* **23**, 247–268.

Russell, E. W. (1973), *Soil Conditions and Plant Growth* (Longman, New York), 10th edition.

Schmeltekopf, A. L., E. E. Ferguson, P. D. Goldan, and J. R. McAfee (1977), "Stratospheric Measurements of N_2O, F_{11} and F_{12}," paper presented at IAGA/IAMAP Joint Assembly, Seattle, Washington, August 22–September 3, 1977.

Seiler, W. (1974), "The Cycle of Atmospheric CO," *Tellus* **26**, 116–135.

Sellers, W. D. (1965), *Physical Climatology* (University of Chicago Press, Chicago).

Seitz, H., B. Davidson, J. P. Friend, and H. W. Feely (1968), *Numerical Models of Transport Diffusion and Fallout of Stratospheric Radioactive Materials (Final Report on Project STREAK)*, USAEC Report NYO-3654-4.

Setlow, R. B. (1974), "The Wavelengths in Sunlight Effective in Producing Skin Cancer: A Theoretical Analysis," *Proc. Nat. Acad. Sci.* **71**, 3363–3366.

Simonaitis, R., and J. Heicklen (1973), "Reaction of HO_2 with O_3," *J. Phys. Chem.* **77**, 1932–1935.

Simonaitis, R., and J. Heicklen (1974), "The Reaction of HO_2 with NO and NO_2," *J. Phys. Chem.* **78**, 653–657.

Simonaitis, R., and J. Heicklen (1976), "Reactions of HO_2 with NO and NO_2 and of OH with NO," *J. Phys. Chem.* **80**, 1–7.

Singh, H. B. (1977), "Atmospheric Halocarbons: Evidence in Favor of Reduced Average Hydroxyl Radical Concentration in the Troposphere," *Geophys. Res. Lett.* **4**, 101–104.

Soderlund, R., and B. H. Svensson (1976), "The Global Nitrogen Cycle," *Ecol. Bull. (Stockholm)* **22**, 23–27.

Stewart, R. W., S. Hameed, and J. P. Pinto (1977), "Photochemistry of Tropospheric Ozone," *J. Geophys. Res.* **82**, 3134–3140.

Stolarski, R. S. (1977), private communication, a preliminary draft of the chemistry section of Hudson (1977).

Sze, N. D., and H. Rice (1976), "Nitrogen Cycle Factors Contributing to N_2O Production from Fertilizers," *Geophys. Res. Lett.* **3**, 343–346.

Telegadas, K., and R. J. List (1969), "Are Particulate Radioactive Tracers Indicative of Stratospheric Motions?" *J. Geophys. Res.* **74**, 1339–1350.

Terjung, W. H., and S. S-F. Louis (1970), "Potential Solar Radiation Climates of Man," *Ann. Assoc. Amer. Geographers* **60**, 481–500.

Thorne, R. M. (1977), "Energetic Radiation Belt Electron Precipitation: A Natural Depletion Mechanism for Stratospheric Ozone," *Science* **195**, 287–289.

Tröe, J. (1969), "Ultraviolet Spectrum and Reactions of HO_2 Radicals in the Thermal Decomposition of H_2O_2," *Ber. Bunsenges. Phys. Chem.* **73**, 946.

Tsang, W. (1923), "Comparison Between Experimental and Calculated Rate Constants for Dissociation and Combination Reactions Involving Small Polyatomic Molecules," *Int. J. Chem. Kinetics* **5**, 947–963.

Urbach, F., Ed. (1969), *The Biological Effects of Ultraviolet Radiation with Emphasis on the Skin* (Pergamon, Oxford).

U.S. Standard Atmosphere, 1976 (1976), U.S. Government Printing Office, Washington, D.C. See also *U.S. Standard Atmosphere, 1962*, and *U.S. Standard Atmosphere Supplements, 1966*.

van der Leun, J. C., and F. Daniels, Jr. (1975), "Biological Effects of Stratospheric Ozone Decrease: A Critical Review of Assessments," Appendix B, Chapter 7 of *Impacts of Climatic Change on the Biosphere*, U.S. Department of Transportation, Washington, D.C., CIAP Monograph 5.

Van Horn, J. C. (1977), personal communication.

Vupputuri, R. K. (1974), "The Role of Stratospheric Pollutant Gases (HO_2, NO_x) in the Ozone Balance and Its Implications for the Seasonal Climate of the Stratosphere," in *Proc. IAMAP/IAPSO First Special Assembly* (Atmospheric Environmental Service, Downsview, Ontario, Canada), vol. 2, pp. 905–931.

Warneck, P. (1972), "Cosmic Radiation as a Source of Odd Nitrogen in the Stratosphere," *J. Geophys. Res.* **77**, 6589–6591.

Warneck, P. (1974), "On the Role of OH and HO_2 Radicals in the Troposphere," *Tellus* **26**, 39–46.

Warneck, P. (1975), "OH Production Rates in the Troposphere," *Planet. Space Sci.* **23**, 1507–1518.

Watson, R. T. (1977), "Rate Constants of ClO_x of Atmospheric Interest," *J. Phys. Chem. Ref. Data* (in press).

Widhopf, G. F., L. Glatt, and R. F. Kramer (1977), "Results of Phenomenological Time-Dependent Two-Dimensional Photochemical Model of the Atmosphere," paper presented at AIAA 15th Aerospace Sciences Meeting, Los Angeles, Calif., January 24–26, 1977, AIAA paper 77-131.

Wilcox, R. W., G. D. Nostrom, and A. D. Belmont (1977), "Periodic Variations of Total Ozone and Its Vertical Distribution," *J. Appl. Meteorol.* **16**, 290–298.

Wofsy, S. C. (1976), "Interactions of CH_4 and CO in the Earth's Atmosphere," *Ann. Rev. Earth Planet. Sci.* **4**, 441–469.

Wofsy, S. C., J. C. McConnell, and M. B. McElroy (1972), "Atmospheric CH_4, CO and CO_2," *J. Geophys. Res.* **77**, 4477–4493.

Wuebbles, D. J. (1977), "Alternate Fluorocarbons: Tropospheric Lifetimes and Potential Effects on Stratospheric Ozone," paper presented at the IAGA/IAMAP Joint Assembly, Seattle, Washington, August 22–September 3, 1977, Lawrence Livermore Laboratory, Livermore, Calif., UCRL-79303 Abstract.

Wuebbles, D. J., and J. S. Chang (1975), "Sensitivity of Time-Varying Parameters in Stratospheric Modeling," *J. Geophys. Res.* **80**, 2637–2642.

Wuebbles, D. J., J. S. Chang, and W. H. Duewer (1977), "Effect of the SST in a Chlorinated Atmosphere," paper presented at the 173rd National Meeting of the American Chemical Society, New Orleans, Louisiana, March 20–25, 1977, Lawrence Livermore Laboratory, Livermore, Calif., UCRL-78803 Abstract.

Zeldovitch, Y., and Raizen, Y. (1967), *Physics of Shock Waves and High Temperature Phenomena* (Academic Press, New York), p. 565.

Zinn, J., and C. D. Sutherland (1975), *Stratospheric Chemistry Computation*, Los Alamos Scientific Laboratory, Los Alamos, New Mexico, LA-6111-M5.

APPENDIX A
CHANGES TO THE 1-D TRANSPORT-KINETICS MODELS

In the past year a number of changes have occurred in the series of theoretical models used at LLL to study tropospheric and stratospheric chemistry. These changes are discussed below.

1. Code Development

The 1-D transport-kinetics models for diurnal and time-dependent calculations have been redesigned to increase user efficiency. Whereas we formerly had to choose from one of three different codes to calculate an atmosphere, selecting the code according to the assumed level of chlorine in the atmosphere—zero chlorine, or background chlorine (due to CH_3Cl and CCl_4), or levels of chlorine predicted on the basis of prescribed growth rates for F-11 and F-12—we now have a single code that handles all three cases. The user decides at the beginning of a run which case to be used. I/O (input/output) efficiency was also improved in the redesigned code. These improvements have decreased the amount of user and computer time necessary to set up and perform a calculation.

In addition, a new code was developed which takes chemical equations and puts them into the forms required by the model. This code makes future changes to model chemistry much simpler.

2. Chemistry Changes

Table A-1 shows kinetic rate changes that have occurred in the past year as well as a comparison with the chemistry used in 1973 and 1974 (as discussed in Section 2.7 on the effect of past nuclear tests). One reaction presently included in recent model calculations (i.e., Section 2.9) is the pressure-dependent rate for $CO + OH \rightarrow CO_2 + H$, 7.3×10^{-33}. In addition, the absorption cross sections for H_2O_2 and HCl were modified to the recommended values in Hudson (1977).

3. Boundary Conditions

Due to changes in model chemistry (especially changes in rate coefficients for $HO_2 + NO$ and $CO + OH$), the lower boundary conditions for some of the species in the model have changed. New surface values (*in molecules/cm* ^{3}) *for some of the more important species are listed below:*

NO_2	2.3×10^9 (<0.1 ppb)
NO	9.0×10^8
OH	1.5×10^6
O_3	9.7×10^{11}
H_2O_2	7.0×10^{10}
HO_2	2.7×10^8
N_2O	8.2×10^{12}
HNO_3	1.6×10^{10}
CH_4	3.34×10^{13}
HCl	2.55×10^{10}

Heterogeneous removal of H_2O_2 at altitudes from the surface to 8 km with a lifetime of five days is now included in the model. Previously, such removal processes were included for only NO_2, HNO_3, and HCl.

4. Physical Improvements

Multiple scattering is now an integral part of the model and is included in all calculations. Diurnal averaging is also now included in the model as standard procedure for future calculations.

AD-A057 139 CALIFORNIA UNIV LIVERMORE LAWRENCE LIVERMORE LAB F/G 6/6
ANNUAL REPORT OF LAWRENCE LIVERMORE LABORATORY TO THE HIGH ALTI--ETC(U)
MAY 78 F M LUTHER DOT-FA76WA1-653

UNCLASSIFIED FAA-EQ-78-09 NL

2 OF 2
AD
A057 139

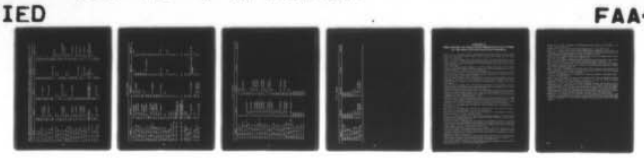

END
DATE
FILMED
9-78
DDC

Table A-1. Changes from 1973 through 1977 in chemical rate constants used in LLL computer simulations to study tropospheric and stratospheric chemistry. Asterisk (*) indicates multiple scattering effects are included, N.I. indicates the reaction is not included in the model. QJ's are photodissociation rate coefficients.

Reaction	Rate 1977	Rate 1976	Rate 1974	Rate 1973
$O_2 + h\nu \rightarrow O + O$	QJ(1)*	QJ(1)	Same	QJ(1) × 2
$O_3 + h\nu \rightarrow O + O_2$	QJ(2)*	QJ(2)	Same	QJ(2) × 2
$O_3 + h\nu \rightarrow O(^1D) + O_2$	QJ(3)*	QJ(3)	Same	QJ(3) × 2
$O + O_2 + M \rightarrow O_3 + M$	1.10×10^{-34} exp(510/T)	1.07×10^{-34} exp(510/T)	Same	Same
$O + O_3 \rightarrow 2O_2$	1.9×10^{-11} exp(−2300/T)	Same	Same	Same
$NO_2 + h\nu \rightarrow NO + O$	QJ(4)*	QJ(4)	Same	QJ(4) × 2
$O_3 + NO \rightarrow NO_2 + O_2$	2.1×10^{-12} exp(−1450/T)	9.0×10^{-13} exp(−1200/T)	Same	Same
$O + NO_2 \rightarrow NO + O_2$	9.1×10^{-12}	Same	Same	Same
$N_2O + h\nu \rightarrow N_2 + O(^1D)$	QJ(5)*	QJ(5)	Cross sections were larger	QJ(5) × 2 (larger cross sections)
$N_2O + O(^1D) \rightarrow N_2 + O_2$	5.5×10^{-11}	7×10^{-11}	1.1×10^{-10}	6.6×10^{-11}
$N_2O + O(^1D) \rightarrow 2NO$	5.5×10^{-11}	7×10^{-11}	1.1×10^{-10}	6.6×10^{-11}
$NO + h\nu \rightarrow N + O$	QJ(6)	QJ(6)	Same	QJ(6) × 2
$N + O_2 \rightarrow NO + O$	5.5×10^{-12} exp(−3220/T)	1.1×10^{-14} T exp(−3150/T)	Same	1.02×10^{-14} T exp(−3130/T)
$N + NO \rightarrow N_2 + O$	8.2×10^{-11} exp(−410/T)	2.7×10^{-11}	Same	5.1×10^{-11} exp(−170/T)
$O(^1D) + H_2O \rightarrow 2OH$	2.3×10^{-10}	2.1×10^{-10}	3.5×10^{-10}	2.8×10^{-10}
$O(^1D) + CH_4 \rightarrow OH + CH_3$	1.3×10^{-10}	Same	4.0×10^{-10}	2.4×10^{-10}
$HNO_3 + h\nu \rightarrow OH + NO_2$	QJ(7)*	QJ(7)	Same	QJ(7) × 2
$O_3 + OH \rightarrow HO_2 + O_2$	1.5×10^{-12} exp(−1000/T)	1.6×10^{-12} exp(−1000/T)	Same	1.3×10^{-12} exp(−956/T)
$O + OH \rightarrow O_2 + H$	4.2×10^{-11}	Same	Same	Same
$O_3 + HO_2 \rightarrow OH + 2O_2$	1.0×10^{-13} exp(−1250/T)	Same	Same	1.0×10^{-12} exp(−1875/T)
$O + HO_2 \rightarrow OH + O_2$	3×10^{-11}	Same	8×10^{-11} exp(−500/T)	1.0×10^{-11}
$H + O_2 + M \rightarrow HO_2 + M$	2.08×10^{-32} exp(+290/T)	Same	Same	1.1×10^{-32} exp(407/T)
$O_3 + H \rightarrow OH + O_2$	1.23×10^{-10} exp(−562/T)	Same	2.6×10^{-11}	2.6×10^{-11}
$HO_2 + HO_2 \rightarrow H_2O_2 + O_2$	1.7×10^{-11} exp(−500/T)	Same	3×10^{-11} exp(−500/T)	3×10^{-11} exp(−500/T)
$HO_2 + OH \rightarrow H_2O + O_2$	2×10^{-11}	Same	2×10^{-10}	2×10^{-10}
$OH + NO_2 + M \rightarrow HNO_3 + M$	Parameterization of Tsang et al. (1971)	$\frac{2.76 \times 10^{-13} \exp(880/T)}{1.166 \times 10^{18} \exp(222/T) + M}$	$\frac{4 \times 10^{-11}}{1.12 \times 10^{18} + M}$	$\frac{10^{-11}}{1.5 \times 10^{20} \exp(-750/T) + M}$
$OH + HNO_3 \rightarrow H_2O + NO_3$	8.9×10^{-14}	Same	1.3×10^{-13}	1.3×10^{-13}
$H_2O_2 + h\nu \rightarrow 2OH$	QJ(8)*	QJ(8)	Same	Same
$H_2O_2 + OH \rightarrow H_2O + HO_2$	1.0×10^{-11} exp(−750/T)	1.7×10^{-11} exp(−910/T)	Same	Same
$N_2 + O(^1D) + M \rightarrow N_2O + M$	3.5×10^{-37}	2.8×10^{-36}	Same	Same

Table A-1. (Continued)

Reaction	Rate 1977	Rate 1976	Rate 1974	Rate 1973
$N + NO_2 \rightarrow N_2O + O$	2×10^{-11} exp(−800/T)	1.4×10^{-12}	9×10^{-12}	9×10^{-12}
$NO + O + M \rightarrow NO_2 + M$	1.6×10^{-32} exp(+584/T)	3.96×10^{-33} exp(940/T)	Same	N.I.
$NO + HO_2 \rightarrow NO_2 + OH$	4.28×10^{-11} exp(−500/T)	2.0×10^{-13}	Same	N.I.
$H_2 + O(^1D) \rightarrow OH + H$	9.9×10^{-11}	2.9×10^{-10}	Same	N.I.
$OH + OH \rightarrow H_2O + O$	1.0×10^{-11} exp(−550/T)	Same	Same	N.I.*
$N + O_3 \rightarrow NO + O_2$	5×10^{-12} exp(−650/T)	5.7×10^{-13}	Same	N.I.*
$NO_2 + O_3 \rightarrow NO_3 + O_2$	1.2×10^{-13} exp(−2450/T)	Same	1.23×10^{-13} exp(−2470/T)	N.I.
$HO_2 + h\nu \rightarrow OH + O$	QJ(9)*	QJ(9)	N.I.	N.I.
$OH + CH_4 \rightarrow H_2O + CH_3$	2.36×10^{-12} exp(−1710/T)	Same	N.I.	N.I.*
$OH + OH + M \rightarrow H_2O_2 + M$	1.2×10^{-32} exp(900/T)	2.5×10^{-33} exp(2500/T)	N.I.	N.I.
$H_2O_2 + O \rightarrow OH + HO_2$	2.75×10^{-12} exp(−2125/T)	Same	N.I.	N.I.
$O + CH_4 \rightarrow OH + CH_3$	3.5×10^{-11} exp(−4550/T)	Same	N.I.	N.I.
$CO + OH \rightarrow H + CO_2$	1.4×10^{-13}	Same	N.I.	N.I.*
$O(^1D) + M \rightarrow O + M$	2.2×10^{-11} exp(+99/T)	2.2×10^{-11} exp(92/T)	5.85×10^{-11}	3.2×10^{-11}*
$NO_3 + h\nu \rightarrow NO_2 + O$	10^{-1}	10^{-1}	0.	0.
$NO_3 + h\nu \rightarrow NO + O_2$	4×10^{-2}	5×10^{-2}	1.	1.
$N + NO_2 \rightarrow 2NO$	N.I.	N.I.	6×10^{-12}	6×10^{-12}
$NO + NO_3 \rightarrow 2NO_2$	8.7×10^{-12}	N.I.	N.I.	N.I.
$NO_2 + O + M \rightarrow NO_3 + M$	1.0×10^{-31}	N.I.	N.I.	N.I.
$NO_2 + NO_3 \rightarrow NO + O_2 + NO_2$	2.0×10^{-13}	N.I.	N.I.	N.I.
$NO_2 + NO_3 + M \rightarrow N_2O_5 + M$	$\frac{2.92 \times 10^{-12}}{7 \times 10^{+21} \exp(-2670/T) + M}$	N.I.	N.I.	N.I.
$N_2O_5 + M \rightarrow NO_2 + NO_3 + M$	$\frac{6.0 \times 10^{+14} \exp(-1070/T)}{7.0 \times 10^{+21} \exp(-2670/T) + M}$	N.I.	N.I.	N.I.
$N_2O_5 + O \rightarrow 2NO_2 + O_2$	1.0×10^{-14}	N.I.	N.I.	N.I.
$N_2O_5 + H_2O \rightarrow 2HNO_3$	1.0×10^{-20}	N.I.	N.I.	N.I.
$N_2O_5 \rightarrow 2NO_2 + O$	QJ(10)*	N.I.	N.I.	N.I.
$Cl + O_3 \rightarrow ClO + O_2$	2.7×10^{-11} exp(−257/T)	2.97×10^{-11} exp(−243/T)	(No ClX reactions were included in 1973 or 1974 chemistries)	
$Cl + OClO \rightarrow 2ClO$	5.9×10^{-11}	Same	N.I.	N.I.
$Cl + O_2 + M \rightarrow ClO_2 + M$	N.I.	1.7×10^{-33} exp(300/T)	N.I.	N.I.
$Cl + CH_4 \rightarrow HCl + CH_3$	7.3×10^{-12} exp (−1260/T)	5.4×10^{-12} exp(−1133/T)	N.I.	N.I.

Table A-1. (Continued)

Reaction	Rate 1977	Rate 1976	Rate 1974	Rate 1973
$Cl + ClO_2 \rightarrow Cl_2 + O_2$	N.I.	5.0×10^{-11}		
$Cl + ClO_2 \rightarrow 2ClO$	N.I.	1.4×10^{-12}		
$Cl + NO + M \rightarrow ClNO + M$	N.I.	1.7×10^{-32} exp(553/T)		
$Cl + ClNO \rightarrow Cl_2 + NO$	N.I.	3.0×10^{-11}		
$Cl + NO_2 + M \rightarrow ClNO_2 + M$	6.9×10^{-34} exp(+2115/T)	Same		
$Cl + ClNO_2 \rightarrow Cl_2 + NO_2$	3×10^{-12}	Same		
$ClO + O \rightarrow Cl + O_2$	7.7×10^{-11} exp(−130/T)	5.3×10^{-11}		
$NO + ClO \rightarrow NO_2 + Cl$	2.2×10^{-11}	2.6×10^{-11} exp(−50/T)		
$ClO + O_3 \rightarrow ClO_2 + O_2$	1.0×10^{-12} exp(−4000/T)	1.0×10^{-12} exp(−2763/T)		
$ClO + O_3 \rightarrow OClO + O_2$	1.0×10^{-12} exp(−4000/T)	1.0×10^{-12} exp(−2763/T)		
$ClO + NO_2 + M \rightarrow ClONO_2 + M$	5.1×10^{-33} exp(+1030/T)	Same		
$ClO + ClO \rightarrow Cl + OClO$	2.1×10^{-12} exp(−2200/T)	2.0×10^{-12} exp(−2300/T)		
$ClO + ClO \rightarrow 2Cl + O_2$	1.5×10^{-12} exp(−1230/T)	2.0×10^{-13} exp(−1260/T)		
$HCl + O(^1D) \rightarrow Cl + OH$	1.4×10^{-10}	2×10^{-10}		
$OH + HCl \rightarrow H_2O + Cl$	3.0×10^{-12} exp(−425/T)	2×10^{-12} exp(−310/T)		
$O + HCl \rightarrow OH + Cl$	1.14×10^{-11} exp(−3370/T)	1.75×10^{-12} exp(−2273/T)		
$O + OClO \rightarrow ClO + O_2$	2×10^{-11} exp(−1100/T)	5.0×10^{-13}		
$NO + OClO \rightarrow NO_2 + ClO$	3.4×10^{-13}	Same		
$N + OClO \rightarrow NO + ClO$	6.0×10^{-13}	Same		
$H + OClO \rightarrow OH + ClO$	5.7×10^{-11}	Same		
$Cl + OH \rightarrow HCl + O$	1.0×10^{-11} exp(−2970/T)	2.0×10^{-12} exp(−1878/T)		
$Cl + HO_2 \rightarrow HCl + O_2$	3×10^{-11}	Same		
$Cl + HNO_3 \rightarrow HCl + NO_3$	1.0×10^{-11} exp(−2170/T)	4.0×10^{-12} exp(−1500/T)		
$ClONO_2 + O \rightarrow ClO + NO_3$	4.5×10^{-12} exp(−840/T)	Same		
$ClO_2 + HO_2 \rightarrow HCl + 2O_2$	N.I.	3.0×10^{-12}		
$CH_3Cl + OH \rightarrow Cl + H_2O + HO_2$	2.2×10^{-12} exp(−1142/T)	Same		
$CH_3Cl \rightarrow 2HO_2 + CO + Cl$	QCJ(1)*	QCJ(1)		
$HCl + h\nu \rightarrow H + Cl$	QCJ(2)*	QCJ(2)		
$ClONO_2 \rightarrow ClO + NO_2$	QCJ(3)*	QCJ(3)		
$ClO + h\nu \rightarrow Cl + O$	QCJ(4)*	QCJ(4)		
$ClO + h\nu \rightarrow Cl + O(^1D)$	QCJ(5)*	QCJ(5)		
$ClNO_2 + h\nu \rightarrow Cl + NO_2$	QCJ(7)*	QCJ(7)		

Table A-1. (Continued)

Reaction	Rate 1977	Rate 1976	Rate 1974	Rate 1973
$OClO + h\nu \rightarrow ClO + O(^1D)$	QCJ(8)	QCJ(8)		
$OClO + h\nu \rightarrow ClO + O$	QCJ(9)[a]	QCJ(9)		
$CF_2Cl_2 + h\nu \rightarrow 2Cl$	QCJ(10)[a]	QCJ(10)		
$CFCl_3 + h\nu \rightarrow 2.5Cl$	QCJ(11)[a]	QCJ(11)		
$CCl_4 + h\nu \rightarrow 2Cl$	QCJ(12)[a]	QCJ(12)		
$CFCl_3 + O(^1D) \rightarrow 2Cl$	2.3×10^{-10}	3.0×10^{-10}		
$CF_2Cl_2 + O(^1D) \rightarrow 2Cl$	2.0×10^{-10}	2.5×10^{-10}		
$Cl + H_2 \rightarrow HCl + H$	$4.7 \times 10^{-11}\ \exp(-2340/T)$	$5.7 \times 10^{-11}\ \exp(-2400/T)$		
$Cl + H_2O_2 \rightarrow HCl + HO_2$	$1.6 \times 10^{-12}\ \exp(-384/T)$	$1.0 \times 10^{-11}\ \exp(-810/T)$		

APPENDIX B
BIBLIOGRAPHY OF PUBLICATIONS PRODUCED IN LLL'S WORK ON THE HIGH ALTITUDE POLLUTION PROGRAM

Chang, J. S. (1977), "Tropospheric Modeling," paper presented at the Gordon Conference on Environmental Sciences: Air, New Hampton, Virginia, August 15–19, 1977. (Chang was also chairman of the Stratospheric Session at this conference.)

Chang, J. S., and W. S. Duewer (1977), "New Theoretical Estimate of the Effect of Past Nuclear Tests on Ozone," *EOS Trans. AGU* **58**(8), 689 (abstract). Paper presented at the IAGA/IAMAP Joint Assembly, Seattle, Washington, August 22–September 3, 1977. Lawrence Livermore Laboratory, Livermore, Calif., UCRL-79302 Abstract.

Chang, J. S., W. H. Duewer, and D. J. Wuebbles (1977), "The Atmospheric Nuclear Tests of the 50's and 60's: A Significant Test of Ozone Depletion Theories," submitted to *J. Geophys. Res.* (September 1977). Lawrence Livermore Laboratory, Livermore, Calif., UCRL-80246 Preprint.

Chang, J. S., and J. E. Penner (1977), "Analysis of Global Budgets of Halocarbons," paper presented at the IAGA/IAMAP Joint Assembly, Seattle, Washington, August 22–September 3, 1977. Lawrence Livermore Laboratory, Livermore, Calif., UCRL-79318 Abstract.

Chang, J. S., and D. J. Wuebbles (1976), "A Theoretical Model of Global Tropospheric OH Distribution," in Proceedings of the Joint AGU/AMS Symposium on the Non-Urban Tropospheric Composition, Hollywood, Florida, November 10–12, 1976. Lawrence Livermore Laboratory, Livermore, Calif., UCRL-78392 Preprint.

Chang, J. S., and D. J. Wuebbles (1977), "Fully Diurnal Averaged Model of the Stratosphere," paper presented at the IAGA/IAMAP Joint Assembly, Seattle, Washington, August 22–September 3, 1977. Lawrence Livermore Laboratory, Livermore, Calif., UCRL-79317 Abstract.

Chang, J. S., D. J. Wuebbles, and D. D. Davis (1977), "A Theoretical Model of Global Tropospheric OH Distribution," revision to paper presented at the Joint AGU/AMS Symposium on the Non-Urban Tropospheric Composition, Hollywood, Florida, November 10–12, 1976. Lawrence Livermore Laboratory, Livermore, Calif., UCRL-78392 Preprint Rev. 1 (1977).

Duewer, W. H. (1977), "Evaluation of the Sums and Densities of Vibrational Energy Levels for Coupled Anharmonic Oscillator Models of Small Molecules and Some Implications for RRKM Calculations," paper presented at the 173rd National Meeting of the American Chemical Society, New Orleans, Louisiana, March 20–25, 1977. Lawrence Livermore Laboratory, Livermore, Calif., UCRL-78795 Abstract.

Duewer, W. H., D. J. Wuebbles, and J. S. Chang (1977a), "Effect of NO Photolysis on NO_y Mixing Ratios," *Nature* **265**, 523–525.

Duewer, W. H., D. J. Wuebbles, H. W. Ellsaesser, and J. S. Chang (1977b), "NO_x Catalytic Ozone Destruction: Sensitivity to Rate Coefficients," *J. Geophys. Res.* **82**, 935–942.

Duewer, W. H., D. J. Wuebbles, H. W. Ellsaesser, and J. S. Chang (1977c), "Authors Reply to Comment by Johnston and Nelson," *J. Geophys. Res.* **82**, 2599–2605.

Ellis, J. S., and T. H. Vonder Haar (1977), "The Earth's Radiation Budget Sensitivity to Cloud Amount as Determined from Satellite Measurements," paper presented at the IAGA/IAMAP Joint Assembly, Seattle, Washington, August 22–September 3, 1977.

Ellsaesser, H. W. (1976a), "A Reassessment of Stratospheric Ozone: Credibility of the Threat," invited paper presented at the Environmental Health Sciences Symposium on SST Pollution and Skin Cancer, Hollywood, Florida, October 25–29, 1976. Lawrence Livermore Laboratory, Livermore, Calif., UCRL-78285 Preprint. Accepted subject to revision for publication in *Climatic Change*.

Ellsaesser, H. W. (1976b), "Ozone Destruction by Catalysis: Credibility of the Threat," paper presented at the Fall Annual Meeting of the American Geophysical Union, San Francisco, Calif., December 4–8, 1976. Lawrence Livermore Laboratory, Livermore, Calif., UCRL-78627 Preprint. Accepted subject to revision for publication in *Atmospheric Environment*.

Ellsaesser, H. W. (1976c), "The Increase in Total Ozone of the 1960's: Probable Cause," paper presented at the International Conference on the Stratosphere and Related Problems, Logan, Utah, September 15–17, 1976. Lawrence Livermore Laboratory, Livermore, Calif., UCRL-78408 Abstract.

Ellsaesser, H. W. (1977a), "Comments on 'Estimate of the Global Change in Temperature, Surface to 100 mb, Between 1958 and 1975,'" *Mon. Weather Rev.* **105**, 1200–1201.

Ellsaesser, H. W. (1977b), "Comments on 'The Distribution of Water Vapor in the Stratosphere,'" *Rev. Geophys. Space Phys.* **15**, 501.

Ellsaesser, H. W. (1977c), "Has Man Increased Stratospheric Ozone?" *Nature* **270**, 592–593.

Lovill, J. E., T. J. Sullivan, and J. A. Korver (1976), "Measurement of Atmospheric Ozone by Satellite," in Proceedings of the Seventh Conference on Aerospace and Aeronautical Meteorology and Symposium on Remote Sensing from Satellites, Melbourne, Florida, November 16–19, 1976.

Luther, F. M. (1976), "Relative Influence of Stratospheric Aerosols on Solar and Longwave Radiative Fluxes for a Tropical Atmosphere," *J. Appl. Meteorol.* **15**, 951–955.

Luther, F. M. (1977), "Effect of Multiple Scattering on Ozone Reduction by NO_x and CFM's," paper presented at the IAGA/IAMAP Joint Assembly, Seattle, Washington, August 22–September 3, 1977.

Luther, F. M., and W. H. Duewer (1977), "Effect of Changes in Stratospheric Water Vapor on Ozone Reduction Estimates," accepted for publication in *J. Geophys. Res.* Lawrence Livermore Laboratory, Livermore, Calif., UCRL-79660 Preprint (June 1977).

Luther, F. M., and D. J. Wuebbles (1977), "Photodissociation Rate Calculations," paper presented at the NASA Workshop on CFM Assessment, Warrenton, Virginia, January 10–14, 1977. Lawrence Livermore Laboratory, Livermore, Calif., UCRL-78911 Preprint.

Luther, F. M., D. J. Wuebbles, and J. S. Chang (1977a), "Temperature Feedback in a Stratospheric Model," *J. Geophys. Res.* **82**, 4935–4942.

Luther, F. M., D. J. Wuebbles, W. H. Duewer, and J. S. Chang (1977b), "Effect of Multiple Scattering on Species Concentrations and Model Sensitivity," submitted to *J. Geophys. Res.* Lawrence Livermore Laboratory, Livermore, Calif., UCRL-79946 Preprint (August 1977).

Wuebbles, D. J. (1977), Alternate Fluorocarbons: Tropospheric Lifetimes and Potential Effects on Stratospheric Ozone," paper presented at the IAGA/IAMAP Joint Assembly, Seattle, Washington, August 22–September 3, 1977. Lawrence Livermore Laboratory, Livermore, Calif., UCRL-79303 Abstract.

Wuebbles, D. J., J. S. Chang, and W. H. Duewer (1977), "Effect of the SST in a Chlorinated Atmosphere," paper presented at the 173rd National Meeting of the American Chemical Society, New Orleans, Louisiana, March 20–25, 1977. Lawrence Livermore Laboratory, Livermore, Calif., UCRL-78803 Abstract.

Wuebbles, D. J., J. S. Chang, and F. M. Luther (1976), "The Diurnal Model of Chlorine Chemistry in the Stratosphere," paper presented at the International Conference on the Stratosphere and Related Problems, Logan, Utah, September 15–17, 1976. Lawrence Livermore Laboratory, Livermore, Calif., UCRL-78454 Abstract.

WEC